

JOURNAL OF RESEARCH OF THE U.S. GEOLOGICAL SURVEY

NOVEMBER-DECEMBER 1978

VOLUME 6, NUMBER 6

*Scientific notes and summaries
of investigations in geology,
hydrology, and related fields*



U.S. DEPARTMENT OF THE INTERIOR



UNITED STATES DEPARTMENT OF THE INTERIOR

CECIL D. ANDRUS, Secretary

GEOLOGICAL SURVEY

H. William Menard, Director

For sale by Superintendent of Documents, U.S. Government Printing Office, Washington, DC 20402. Annual subscription rate, \$18.90 (plus \$4.75 for foreign mailing). Make check or money order payable to Superintendent of Documents. Send all subscription inquiries and address changes to Superintendent of Documents at above address.

Purchase single copy (\$3.15) from Branch of Distribution, U.S. Geological Survey, 1200 South Eads Street, Arlington, VA 22202. Make check or money order payable to U.S. Geological Survey.

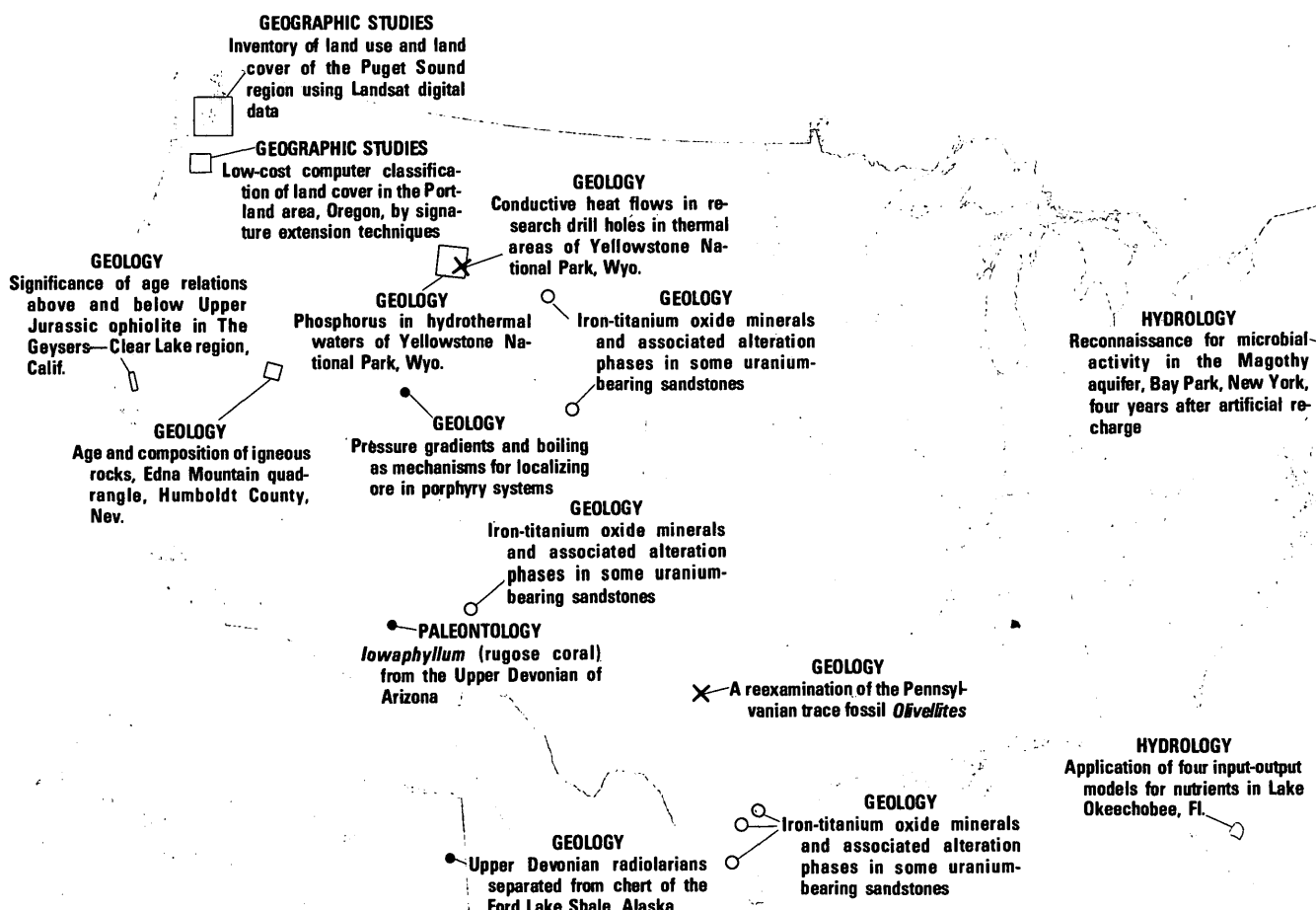
Library of Congress Catalog-card No. 72-600241.

The Journal of Research is published every 2 months by the U.S. Geological Survey. It contains papers by members of the Geological Survey and their professional colleagues on geologic, hydrologic, topographic, and other scientific and technical subjects.

Correspondence and inquiries concerning the Journal (other than subscription inquiries and address changes) should be directed to Janet S. Sachs, Managing Editor (Acting), Journal of Research, Publications Division, U.S. Geological Survey, 321 National Center, Reston, VA 22092.

Papers for the Journal should be submitted through regular Division publication channels.

The Secretary of the Interior has determined that the publication of this periodical is necessary in the transaction of the public business required by law of this Department. Use of funds for printing this periodical has been approved by the Director of the Office of Management and Budget through June 30, 1980.



GEOGRAPHIC INDEX TO ARTICLES

See "Contents" for articles concerning areas outside the United States and articles without geographic orientation.

IMPORTANT NOTICE

Publication of the Journal ceases with this issue. See Announcement section for details.

JOURNAL OF RESEARCH of the U.S. Geological Survey

Vol. 6 No. 6

Nov.-Dec. 1978

CONTENTS

SI units and Inch-Pound System equivalents-----	II
GEOLOGIC STUDIES	
Spectrophotometric determination of tungsten in rocks by using zinc-dithiol----- <i>Phillip Aruscavage and E. Y. Campbell</i>	697
Solubility of highly soluble salts in aqueous media—Part 1, NaCl, KCl, CaCl ₂ , Na ₂ SO ₄ , and K ₂ SO ₄ solubilities to 100°C----- <i>R. W. Potter II and M. A. Clyne</i>	701
Iron-titanium oxide minerals and associated alteration phases in some uranium-bearing sandstones----- <i>R. L. Reynolds and M. B. Goldhaber</i>	707
Significance of age relations above and below Upper Jurassic ophiolite in The Geysers-Clear Lake region, Calif----- <i>R. J. McLaughlin and E. A. Pessagno, Jr.</i>	715
Age and composition of igneous rocks, Edna Mountain quadrangle, Humboldt County, Nev----- <i>R. L. Erickson, M. L. Silberman, and S. P. Marsh</i>	727
Pressure gradients and boiling as mechanisms for localizing ore in porphyry systems----- <i>C. G. Cunningham</i>	745
Phosphorus in hydrothermal waters of Yellowstone National Park, Wyo----- <i>R. E. Stauffer and J. M. Thompson</i>	755
Conductive heat flows in research drill holes in thermal areas of Yellowstone National Park, Wyo----- <i>D. E. White</i>	765
Upper Devonian radiolarians separated from chert of the Ford Lake Shale, Alaska----- <i>B. K. Holdsworth, D. L. Jones, and Carol Allison</i>	775
A reexamination of the Pennsylvanian trace fossil <i>Olivellites</i> ----- <i>E. L. Yochelson and D. E. Schindel</i>	789
<i>Iowaphyllum</i> (rugose coral) from the Upper Devonian of Arizona----- <i>W. A. Oliver, Jr.</i>	797
GEOGRAPHIC STUDIES	
Inventory of land use and land cover of the Puget Sound region using Landsat digital data----- <i>Leonard Gaydos and W. L. Newland</i>	807
Low-cost computer classification of land cover in the Portland area, Oregon, by sig- nature extension techniques----- <i>Leonard Gaydos</i>	815
HYDROLOGIC STUDIES	
Application of four input-output models for nutrients in Lake Okeechobee, Fla----- <i>R. L. Miller</i>	821
Reconnaissance for microbial activity in the Magothy aquifer, Bay Park, New York, four years after artificial recharge----- <i>E. M. Godsy and G. G. Erhlich</i>	829
ANNUAL INDEX TO VOLUME 6	
Subject-----	837
Author-----	845
Recent publications of the U.S. Geological Survey-----	Inside of back cover

SI UNITS AND INCH-POUND SYSTEM EQUIVALENTS

[SI, International System of Units, a modernized metric system of measurement. All values have been rounded to four significant digits except 0.01 bar, which is the exact equivalent of 1 kPa. Use of hectare (ha) as an alternative name for square hectometer (hm^2) is restricted to measurement of land or water areas. Use of liter (L) as a special name for cubic decimeter (dm^3) is restricted to the measurement of liquids and gases; no prefix other than milli should be used with liter. Metric ton (t) as a name for megagram (Mg) should be restricted to commercial usage, and no prefixes should be used with it. Note that the style of meter² rather than square meter has been used for convenience in finding units in this table. Where the units are spelled out in text, Survey style is to use square meter]

SI unit	U.S. customary equivalent			SI unit	U.S. customary equivalent		
Length				Volume per unit time (includes flow)—Continued			
millimeter (mm)	=	0.039 37	inch (in)	decimeter ³ per second (dm^3/s)	=	15.85	gallons per minute (gal/min)
meter (m)	=	3.281	feet (ft)	=	543.4	buckets per day (bbl/d) (petroleum, 1 bbl=42 gal)	
kilometer (km)	=	1.094	yards (yd)	meter ³ per second (m^3/s)	=	35.31	feet ³ per second (ft^3/s)
	=	0.621 4	mile (mi)	=	15 850	gallons per minute (gal/min)	
	=	0.540 0	mile, nautical (nmi)				
Area				Mass			
centimeter ² (cm ²)	=	0.155 0	inch ² (in ²)	gram (g)	=	0.035 27	ounce avoirdupois (oz avdp)
meter ² (m ²)	=	10.76	feet ² (ft ²)	kilogram (kg)	=	2.205	pounds avoirdupois (lb avdp)
	=	1.196	yards ² (yd ²)	megagram (Mg)	=	1.102	tons, short (2 000 lb)
hectometer ² (hm ²)	=	0.000 247 1	acre		=	0.984 2	ton, long (2 240 lb)
	=	2.471	acres	Mass per unit volume (includes density)			
	=	0.003 861	section (640 acres or 1 mi ²)	kilogram per meter ³ (kg/m ³)	=	0.062 43	pound per foot ³ (lb/ft ³)
kilometer ² (km ²)	=	0.386 1	mile ² (mi ²)	Pressure			
Volume				kilopascal (kPa)	=	0.145 0	pound-force per inch ² (lbf/in ²)
centimeter ³ (cm ³)	=	0.061 02	inch ³ (in ³)	=	0.009 869	atmosphere, standard (atm)	
decimeter ³ (dm^3)	=	61.02	inches ³ (in ³)	=	0.01	bar	
	=	2.113	pints (pt)	=	0.296 1	inch of mercury at 60°F (in Hg)	
	=	1.057	quarts (qt)	Temperature			
	=	0.264 2	gallon (gal)	temp kelvin (K)	=	[temp deg Fahrenheit (°F) + 459.67]/1.8	
meter ³ (m ³)	=	0.035 31	foot ³ (ft ³)	temp deg Celsius (°C)	=	[temp deg Fahrenheit (°F) - 32]/1.8	
	=	35.31	feet ³ (ft ³)				
	=	1.308	yards ³ (yd ³)				
	=	264.2	gallons (gal)				
	=	6.290	barrels (bbl) (petro- leum, 1 bbl=42 gal)				
hectometer ³ (hm ³)	=	0.000 810 7	acre-foot (acre-ft)				
kilometer ³ (km ³)	=	810.7	acre-feet (acre-ft)				
	=	0.239 9	mile ³ (mi ³)				
Volume per unit time (includes flow)							
decimeter ³ per second (dm^3/s)	=	0.035 31	foot ³ per second (ft^3/s)				
	=	2.119	feet ³ per minute (ft^3/min)				

The policy of the "Journal of Research of the U.S. Geological Survey" is to use SI metric units of measurement except for the following circumstance:

When a paper describes either field equipment or laboratory apparatus dimensioned or calibrated in Inch-Pound System units and provides information on the physical features of the components and operational characteristics of the equipment or apparatus, then dual units may be used. For example, if a pressure gage is calibrated and available only in Inch-Pound System units of measure, then the gage may be described using SI units in the dominant position with the equivalent Inch-Pound System unit immediately following in parentheses. This also applies to the description of tubing, piping, vessels, and other items of field and laboratory equipment that normally are described in catalogs in Inch-Pound System dimensions.

S. M. LANG, Metrics Coordinator,
U.S. Geological Survey

Any use of trade names and trademarks in this publication is for descriptive purposes only and does not constitute endorsement by the U.S. Geological Survey.

SPECTROPHOTOMETRIC DETERMINATION OF TUNGSTEN IN ROCKS BY USING ZINC-DITHIOL

By PHILLIP ARUSCAVAGE and ESMA Y. CAMPBELL,
Reston, Va.

Abstract.—Tungsten is determined in 11 USGS standard rocks by a spectrophotometric procedure that measures the absorbance of the tungsten-dithiol complex. The results are compared with those obtained by other methods. After the samples are dissolved in HClO_4 and HF, the tungsten-dithiol complex is extracted into isoamyl acetate and then back-extracted into isoamyl acetate. The determination of 0.1 part per million in a 500-mg sample can be made routinely.

The determination of tungsten by colorimetric procedures is most often made by using the colored tungsten complexes formed with either thiocyanate (Fogg and others, 1970; Lillie and Greenland, 1973; Peng and Sandell, 1963) or dithiol (Chan and Riley, 1967; Stanton, 1970; North, 1956; Quin and Brooks, 1972; Hobart and Hurley, 1962; Short, 1951). The dithiol method is preferable because of its greater sensitivity for the determination of small amounts of tungsten in most rocks and because of the greater selectivity of the dithiol reagent for tungsten. However the procedures described for the determination of tungsten in rocks normally use dithiol as the final step after sometimes lengthy preliminary separations are performed and do not take advantage of this specificity.

In our procedure, after decomposition of the sample by HF- HClO_4 , tungsten is reacted with zinc-dithiol, and the colored complex is extracted by means of isoamyl acetate from approximately 10 N hydrochloric acid. The tungsten is then back-extracted by means of citric acid solution, reacted with additional zinc-dithiol, and reextracted from approximately 10 N hydrochloric acid into isoamyl acetate. By measuring the absorbance of the colored complex in a 5-cm cell, the determination can be made routinely down to 0.1 part per million in a 500-mg sample.

REAGENTS AND APPARATUS

Zinc-dithiol solution (2 percent w/v): Dissolve four pellets (about 1 g) of NaOH in 2 ml H_2O . Add

5 ml reagent-grade alcohol, 0.5 ml 97-percent thioglycollic acid, and 1 g zinc-dithiol. Stir to dissolve and make to 50 ml volume with 50-percent alcohol solution. Prepare fresh daily.

Citric acid solution (0.5 percent w/v): Dissolve 0.5 g citric acid in 100 ml 10-percent HCl.

Stannous chloride solution (30 percent w/v): Dissolve 300 g SnCl_2 in 1 L of concentrated HCl. Prepare fresh daily.

Fe solution (100 mg/ml): Dissolve 10 g Fe powder in concentrated HCl. Make to 100 ml in volumetric flask with concentrated HCl. No provision is made for keeping Fe reduced.

Perchloric acid (concentrated reagent grade).

Hydrofluoric acid (concentrated reagent grade).

Isoamyl acetate (technical grade).

Tungsten standard solution (100 ppm): Dissolve 0.0897 g reagent-grade $\text{Na}_2\text{WO}_4 \cdot 2\text{H}_2\text{O}$ in 500 ml H_2O .

The $\text{Na}_2\text{WO}_4 \cdot 2\text{H}_2\text{O}$ reagent was standardized gravimetrically by precipitation with cinchonine (Lundell and others, 1953, p. 689).

ANALYTICAL PROCEDURE

To 500 mg of powdered sample in a teflon beaker, add 1 ml HClO_4 , 10 ml HF, and 0.5 ml of Fe solution. Heat to dryness overnight on a hot plate at 125°C. Add 1 ml H_2O to the residue, swirl to loosen, add 25 ml 30-percent SnCl_2 solution, and heat 15 min at 100°C swirling occasionally to dissolve the residue. Add 1 ml zinc-dithiol solution, mix, and heat 30 min at 100°C. Transfer to a dry 60-ml separatory funnel and allow to cool 5 min. Add 5 ml isoamyl acetate and extract 4 min. Allow layers to separate 5 min, drain, and discard lower (aqueous) phase. Wash the stem of the separatory funnel thoroughly with H_2O . Add 2 ml citric acid solution and back-extract 3 min. Drain the aqueous phase into a test tube. Add 15 ml 30-percent SnCl_2 solution and 0.2 ml Fe solution to

the test tube and heat 10 min at 100°C in a hot-water bath. Add 1 ml zinc-dithiol solution, mix thoroughly, using a stirring rod, and heat 30 min at 100°C. Allow to cool 5 min, add 5.0 ml isoamyl acetate, and extract 1 min. Allow layers to separate 10 min. Transfer a portion of the organic layer to a 5-cm microcell, and read the absorbance at 640 nanometers against pure isoamyl acetate. Determine the amount of tungsten by comparison with standard solutions of tungsten (0.1–3.0 micrograms W) which have undergone the same procedures.

DISCUSSION AND RESULTS

The extraction and colorimetric determination of the tungsten-dithiol complex have been carried out under varying conditions. The reaction has been performed with and without the use of reducing agents in acids of differing strengths; the extraction has been performed with different organic solvents; and the determination has been made visually and spectrophotometrically. However, the specificity for tungsten has been shown to be greatest when the reaction take place in concentrated hydrochloric acid solution in the presence of strong reducing agents; for example, stannous chloride or titanous chloride solutions (Quin and Brooks, 1972; Stanton, 1970; Short, 1951).

Although one extraction of the tungsten-dithiol complex was sufficient for some acidic rocks such as RGM-1 and STM-1, preliminary work demonstrated that some mafic rocks, such as BCR-1 and W-1, gave high and irreproducible results. We found that the tungsten complex can be back-extracted readily from isoamyl acetate by using dilute citric acid solutions after which, reaction with additional zinc-dithiol and reextraction into isoamyl acetate removed the remaining interferences. Tests of the effect of 100 µg each of Cr, Co, Cu, Ni, and Mo and 3 mg each of Ti and Mn showed no interference on 1 µg W. Agreement of

the standard rock analyses with literature values confirms the freedom of interference in the method.

The extraction yields were tested by using radioactive ^{181}W and also by measuring the absorbance of spiked samples. Recoveries of 80–90 percent were found for all sample and standard solutions. The precision of the results for the standard rocks confirms the constancy of yields.

One milliliter of a 2-percent zinc-dithiol solution was required to achieve maximum sensitivity and complete reaction. The use of the Fe solution was found to be necessary for the complete reaction of the dithiol with tungsten in the second extraction where citrate is present. The Fe added before the first extraction was used mainly to provide a residue to ensure that the tungsten in the pure solution standards would be picked up from the teflon crucible after decomposition. The molar extinction coefficient is 22 100 under the conditions used.

The Beer-Lambert law is followed up to at least 3 µg W, the largest amount tested.

Table 1 shows the results of replicate analyses of nine standard rocks plus one each of G-1 and W-1 run in a random order. The relative standard deviation is less than 15 percent, except for GSP-1 (20 percent), even at the lowest levels of tungsten. The satisfactory agreement with literature values indicates that the method is free of interference and is accurate for the various types of rocks analyzed. However, the wide variation in reported tungsten content of these rocks indicates that much more work needs to be done before they can be considered as standards for tungsten determinations.

REFERENCES CITED

- Chan, K. M., and Riley, J. P., 1967, Determination of vanadium, molybdenum and tungsten in the new series of U.S. Geological Survey analyzed samples: Chem. Geology, v. 2, no. 2, p. 171–172.

TABLE 1.—Tungsten content, in parts per million, of USGS standard rocks
[Figures in parentheses indicate number of analyses]

Standard rock	This method	Mean	1	2	3	4	5	6
Granite G-1	0.44	—	0.40	—	1.31(2)	—	—	0.50
Granite G-2	0.26, 0.20, 0.24	0.23±0.03	.10±0.03(5)	0.04(3)	.00	0.4	—	—
Andesite AGV-1	0.73, 0.70, 0.77	.73±0.04	.57±0.07(5)	.45(3)	.63(2)	1.1	—	—
Granodiorite GSP-1	0.33, 0.48, 0.36	.39±0.08	.30±0.07(6)	.12(2)	.31(2)	.5	—	—
Quartz latite QLO-1	0.64, 0.66, 0.60	.63±0.03	.62	—	—	—	—	—
Syenite STM-1	3.82, 3.78, 3.76	3.78±0.03	3.8	—	—	—	4.1±0.5(14)	—
Mica schist SDC-1	0.88, 0.88, 0.92	.89±0.02	—	—	—	—	—	—
Diabase W-1	0.67	—	.58±0.10(5)	.38(3)	.45	—	—	.58
Rhyolite RGM-1	1.65, 1.86, 1.51	1.67±0.18	1.50±0.12(6)	—	—	—	1.8±0.5(9)	—
Basalt BCR-1	0.48, 0.54, 0.40	.47±0.07	.35±0.06(5)	.24(3)	.54(2)	.7	—	—
Basalt BHVO-1	0.30, 0.40, 0.35	.35±0.05	—	—	—	—	—	—

- Simon and Rollison (1975), neutron-activation analysis.
- Johansen and Steinnes (1970), neutron-activation analysis.
- Kawabuchi and Kuroda (1970), spectrophotometric analysis.

- Chan and Riley (1967), spectrophotometric analysis.
- Lillie and Greenland (1973). I.D.—spectrophotometric analysis.
- Hamaguchi and others (1962), neutron-activation analysis.

- Fogg, A. G., Marriott, D. R., and Burns, D. T., 1970, A review of procedures, pt. 1 of The spectrophotometric determination of tungsten with thiocyanate: *Analyst*, v. 95, 848-853.
- Hamaguchi, Hiroshi, Kuroda, Rokuro, Shimizu, Tsuneo, Tsukahara, Iwao, and Yamamoto, Ryuichi, 1962, Values for trace elements in G-1 and W-1 with neutron activation analysis, pt. 2, Mo, Sn, Ta, W: *Geochim. et Cosmochim. Acta*, v. 26, p. 503-505.
- Hobart, E. W., and Hurley, E. P., 1962, Spectrophotometric determination of molybdenum and tungsten in niobium with dithiol: *Anal. Chim. Acta*, v. 27, p. 144-152.
- Johansen, O., and Steinnes, Eiliv, 1970, Determination of Co, Cu, Fe, Ga, W, and Zn in rocks by neutron activation and anion-exchange separation: *Talanta*, v. 17, p. 407-414.
- Wawabuchi, Kazuaki, and Kuroda, Rokuro, 1970, Anion-exchange separation and spectrophotometric determination of molybdenum and tungsten in silicate rocks: *Talanta*, v. 17, p. 67-13.
- Lillie, E. G., and Greenland, L. P., 1973, Spectrophotometric determination of tungsten in rocks by an isotope dilution procedure: *U.S. Geol. Survey Jour. Research*, v. 1, no. 5, p. 555-558.
- Lundell, G. E. F., Bright, H. A., and Hoffman, J. I., 1953, *Applied inorganic analysis* (2d ed.): New York, John Wiley & Sons, 1034 p.
- North, A. A., 1956, Geochemical field methods for the determination of tungsten and molybdenum in soils: *Analyst (London)*, v. 81, p. 660-668.
- Peng, P. Y., and Sandell, E. G., 1963, Simultaneous spectrophotometric determination of tungsten and molybdenum with thiocyanate after α -benzoinoxime extraction: *Anal. Chim. Acta*, v. 29, p. 325-334.
- Quin, B. F., and Brooks, R. R., 1972, The rapid determination of tungsten in soils, stream sediments, rocks, and vegetation: *Anal. Chim. Acta*, v. 58, p. 301-309.
- Short, H. G., 1951, The determination of tungsten and molybdenum in titanium: *Analyst*, v. 76, p. 710-714.
- Simon, F. O., and Rollinson, C. L., 1975, Determination of tungsten in geologic materials by neutron activation analysis: *U.S. Geol. Survey Jour. Research*, v. 3, no. 4, p. 475-478.
- Stanton, R. E., 1970, The colorimetric determination of tungsten in soils, sediments, and rocks by zinc dithiol: *Australasian Inst. Mining and Metallurgy Proc.*, no. 236, p. 59-60.

SOLUBILITY OF HIGHLY SOLUBLE SALTS IN AQUEOUS MEDIA— PART 1, NaCl, KCl, CaCl₂, Na₂SO₄, and K₂SO₄ SOLUBILITIES TO 100°C

By ROBERT W. POTTER II and MICHAEL A. CLYNNE,
Menlo Park, Calif.

Abstract.—A modified visual method for determining the solubility of highly soluble salts in aqueous media up to 100° C is presented. The solubilities of NaCl, KCl, CaCl₂, Na₂SO₄, and K₂SO₄ were determined up to 100° C. The tabulated experimental data and the fitted equations describing the data indicate that the previous literature data for the solubility of these salts were generally high by 0.05 to 2.0 weight percent salt.

Recent models for calculating the solubility of salts in complex brines are based on the solubilities in the simpler binary (salt + H₂O) and ternary systems (2 salts + H₂O) (Wood, 1975, 1976). Models such as these are quite useful in studies of geothermal systems as well as hydrothermal ore-deposition systems. They can be used to predict scaling and salt deposition in turbines, heat exchangers, pipes, and so forth, and for modeling the first condensation of brine in a vapor-dominated geothermal system related to hydrothermal convection cells generated by an igneous intrusion. Such solubility models are also applicable to the study of salt-bearing fluid inclusions found in many ore deposits, notably porphyry copper deposits.

To apply these models, reliable solubility data for the simple binary and ternary systems are required, particularly at temperatures greater than 25°C. Wood (1976) primarily used the data of Linke (1965) at temperatures below 100°C, and he used the data of Potter, Babcock, and Brown (1975) between 100° and 200°C. The data of Linke (1965) for NaCl were derived from the classic study by the Earl of Berkeley (1904), and Linke's data for KCl were generated from the graphically smoothed data of several studies from 1865 to 1936. The precision of most of these data is on the order of ± 0.1 to ± 0.5 weight percent salt.

In view of the importance of solubility of the highly soluble salts in aqueous media to the understanding of the complex chemistry of hydrothermal systems and because of the precision of the available solubility

data, we have undertaken studies of the solubility of these salts. Potter, Babcock, and Brown (1977) have developed an indirect method for measuring the solubility of salts at temperatures in the range of 125° to 600°C. The extrapolation of these high-temperature data to lower temperatures proves difficult due to phase transitions in the salts as well as changes in the degree of ion association in the solution (for example, see Potter and others, 1977, with respect to KCl). Hence, a method was required to measure the solubilities of the salts at temperatures up to approximately 100°C. This paper reports on a modified visual method for determining solubilities and reports the measurements of the solubility in water of NaCl, KCl, CaCl₂, Na₂SO₄, and K₂SO₄ at temperatures up to 100°C.

EXPERIMENTAL METHOD

A review of the various methods employed for solubility studies of highly soluble salts was presented by Potter, Babcock, and Brown (1977). In light of the advantages and disadvantages discussed in that paper, we decided to adapt a visual method for determining solubilities at temperatures up to 100°C. The major problems to be overcome were sealing the system and overcoming density stratification.

The experimental apparatus used is illustrated in figure 1. Runs were conducted as follows:

1. A weighted amount of salt (± 0.001 g) was added to a weighed pyrex tube;
2. Water was added to the tube, and the amount of water was determined by subtracting the weight of the tube and salt without water from the weight with water, the stirrer was inserted, and a 0.6-cm layer of silicone oil was used to seal the tube and prevent evaporation;

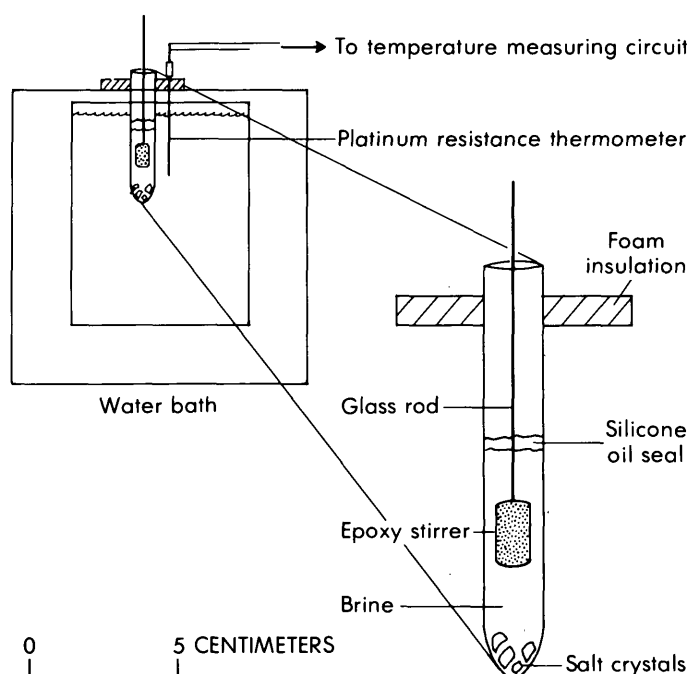


FIGURE 1.—Experimental apparatus used in this study.

3. The assembly was mounted in a water bath (25-L capacity) so that it could be viewed under strong illumination from the side, slowly heated, and agitated until the last crystal of salt dissolved.

The heating of the assembly was done incrementally and not in a continuous fashion. Initially, the increments were several degrees; however, as the amount of salt decreased, the increments were decreased to a few tenths of a degree. After each temperature increment, the system was allowed to reach thermal and chemical equilibrium (chemical equilibrium was assumed when the crystals stopped dissolving) before any new temperature increment. During this time, the assemblage was being vigorously agitated; however, during observation, the agitation was stopped. The temperature at which the last salt crystal disappeared was taken as the equilibrium temperature for the bulk composition in the tube. Experiments showed that 1 mg of salt could be easily seen with the unaided eye.

In early experiments, the platinum resistance thermometer was mounted inside the pyrex tube; however, the temperature difference between the inside thermometer and the one placed on the outside never exceeded 0.01°C over the temperature range of the study. Hence, the inside platinum resistance thermometer was abandoned, and the configuration shown in figure 1 was used for the majority of runs.

The effectiveness of the silicone oil seal was tested by repeated runs on the same assembly over a 48-hour

period. A slight but significant upward drift in the dissolution temperatures of 0.02°C was detected after 48 h. However, because all runs were completed within a few hours after the assembly was put together, the possible slow loss of water had an insignificant effect on the dissolution temperatures.

The precision of the method is affected by two parameters, the repeatability of the dissolution temperature and the accuracy with which the bulk composition of the salt plus water system was known. The repeatability of the dissolution temperature was checked by measuring the same assembly several times. In general, the dissolution temperature could be repeated between $\pm 0.05^{\circ}$ and $\pm 0.15^{\circ}\text{C}$ depending on the salt. (The temperature bath could be regulated over an 8-hour period to $+ 0.012^{\circ}\text{C}$, and the temperature read to $\pm 0.001^{\circ}\text{C}$ with a platinum resistance thermometer.) The salt charges weighed about 20 g; hence the uncertainties due to weighing errors were, at a maximum, on the order of 0.02 weight percent salt. To evaluate the combined effect of these two uncertainties, a series of runs with closely spaced compositions of NaCl and KCl was made. The results are illustrated in figure 2. Within the uncertainties of temperature and composition, the solubility data fit the experimentally determined curve. Using the degree of fit to a smooth curve, the estimated precision of the modified visual method is 0.03 to 0.05 weight percent salt at one standard deviation.

Some modifications of the basic method were required to handle salts with retrograde solubility such as Na_2SO_4 or extremely soluble and hydrated salts such as CaCl_2 . In the case of retrograde solubility, the dissolution temperatures were measured by cooling the bath until the last crystal of salt dissolved.

Salts other than CaCl_2 could be prepared as relatively stable anhydrous salts by the normal means of drying at 300°C and storing in a dessicator. However, this proved difficult for CaCl_2 , because weight changes could be noticed after a few minutes on the balance. To compensate for this problem, 500 g of 40 weight percent anhydrous CaCl_2 solution was prepared from $\text{CaCl}_2 \cdot 2\text{H}_2\text{O}$ and distilled water. Hence, the small weight gains due to the absorption of water had a negligible effect on the total concentration of CaCl_2 . Charges were prepared by using weighed amounts of the stock solution and $\text{CaCl} \cdot 2\text{H}_2\text{O}$. The uncertainty in the composition of the charges prepared in this fashion is estimated to be ± 0.05 weight percent anhydrous CaCl_2 .

For several runs, the heating was interrupted before the complete disappearance of the last salt crystal, and the assembly was then slowly cooled for a few degrees.

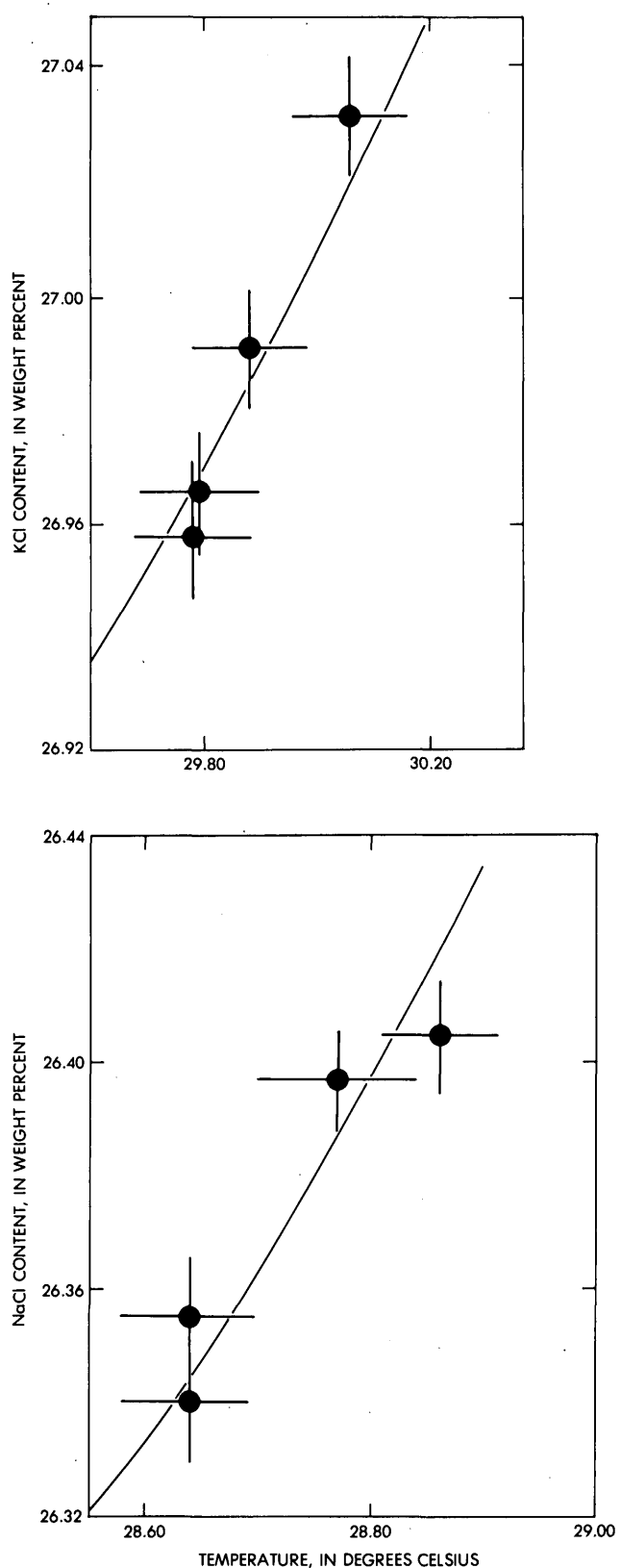


FIGURE 2.—Replicate solubility determinations on NaCl and KCl using different tubes compared with solubility curves determined in this study. Bars around dots indicate uncertainty.

The remaining crystal was then observed to increase in size. These observations support our contention that the crystals were indeed in equilibrium with the solution. However, once the last crystal dissolved, the solutions had to be significantly supercooled to induce crystallization.

EXPERIMENTAL RESULTS

The data obtained in this investigation are listed in

TABLE 1.—*Experimental data and regression coefficients*
[Concentrations are in weight percent anhydrous salt.
 $2\bar{\mu}_s$ = standard deviation]

Temperature (°C)	Experimental solution	Calculated solution	Temperature (°C)	Experimental solution	Calculated solution
¹ NaCl					
17.62	26.18	26.18	33.54	50.37	50.38
28.64	26.34	26.37	35.15	50.94	50.92
28.64	26.36	26.37	38.64	52.23	52.25
28.77	26.40	26.38	42.62	54.20	54.18
28.86	26.40	26.38	44.81	55.47	55.48
35.09	26.48	26.49			
39.90	26.59	26.57			
53.00	26.79	26.83			
59.78	27.01	26.97			
72.33	27.24	27.26			
80.87	27.49	27.48			
99.99	28.00	28.00			
⁵ CaCl ₂ ·4H ₂ O					
49.37			56.03	56.01	
61.81			56.85	56.87	
68.63			57.28	57.34	
85.85			58.69	58.68	
97.65			59.75	59.70	
⁶ CaCl ₂ ·2H ₂ O					
19.93	16.02	16.06			
22.56	19.01	18.90			
24.76	21.55	21.62			
25.77	22.99	22.97			
27.20	24.97	24.98			
28.62	27.06	27.08			
31.08	31.00	30.96			
31.69	31.85	31.97			
32.16	32.86	32.76			
32.27	32.90	32.94			
32.30	33.03	32.99			
⁷ Na ₂ SO ₄ ·10H ₂ O					
32.48	33.03	33.07			
34.26	32.90	32.89			
39.48	32.47	32.40			
42.85	32.15	32.11			
45.34	31.85	31.90			
48.81	31.55	31.63			
57.48	31.00	31.05			
57.55	31.14	31.04			
⁸ Na ₂ SO ₄					
63.62	30.68	30.70			
76.95	30.13	30.12			
93.30	29.73	29.73			

$$^1a_0 = 25.448, a_1 = 0.25541, a_2 = -0.033208, a_3 = 0.003322, 2\bar{\mu}_s = \pm 0.04.$$

$$^2a_0 = 8.062, a_1 = -0.78696, a_2 = 0.30789, a_3 = -0.014068, 2\bar{\mu}_s = \pm 0.02.$$

$$^3a_0 = 25.511, a_1 = 1.61803, a_2 = 0.446754, a_3 = -0.018428, 2\bar{\mu}_s = \pm 0.05.$$

$$^4a_0 = 1.783, a_1 = 28.92828, a_2 = -7.70073, a_3 = 0.726675, 2\bar{\mu}_s = \pm 0.19.$$

$$^5a_0 = -238.270, a_1 = 146.64404, a_2 = -25.46841, a_3 = 1.51148, 2\bar{\mu}_s = \pm 0.03.$$

$$^6a_0 = 39.17102, a_1 = 5.28050, a_2 = -0.623801, a_3 = 0.030331, 2\bar{\mu}_s = \pm 0.07.$$

$$^7a_0 = 43.728, a_1 = -18.1878, a_2 = 2.01989, a_3 = 0.149209, 2\bar{\mu}_s = \pm 0.11.$$

$$^8a_0 = 36.833, a_1 = 0.39342, a_2 = -0.28312, a_3 = 0.017218, 2\bar{\mu}_s = \pm 0.09.$$

table 1. To test the precision of the data, the data were regressed to a smooth curve, and the deviation of the measured values from the smooth curve were calculated. The following equation was used to fit the experimental data:

$$S = \sum_{n=0}^{\infty} a_n C^{n/2}, \quad (1)$$

where S is the solubility in weight percent salt, C is temperature in degrees Celsius, and a_n are the derived empirical constants listed in table 1. Of the 64 solubilities measured, only 2 show deviations greater than $2\mu_s$. The average deviation of all 64 determinations from their respective curves is ± 0.04 weight percent salt. The data appear to be internally consistent within the restrictions imposed by the experimental method.

NaCl (halite) and KCl (sylvite)

A comparison of the solubility data in table 1 with the available data in the literature shows that the data sets are essentially in agreement within their respective precisions. However, the deviation of our data from the literature data appears to be systematic. The previous data indicate solubilities greater than those we found. To check this anomaly, a tube was prepared with a bulk composition of 26.48 weight percent NaCl and equilibrated at temperatures greater than the equilibrium temperature indicated by the Earl of Berkeley (1904). Figure 3 illustrates the results. Despite equilibrating the salt solution plus crystals at temperatures as high as 6°C above the saturation temperatures of the Earl of Berkeley (1904) for as long as 24 h, the salt crystals would not completely dissolve until the solubility curve determined in this study was exceeded. Two reasons for this discrepancy might be the analytical method used by the Earl of Berkeley (1904) (weighing the solution, then evaporating to dryness and weighing the salt crystals, which undoubtedly contain fluid inclusions) or the presence of small skeletal crystals of NaCl or KCl remaining in suspension from the vigorous stirring used to overcome the density stratification. Although the temperature difference between the two curves is large, the compositional differences are quite small, less than 0.15 weight percent salt.

A recent study by Sunier and Baumbach (1976) on KCl solubility up to 86°C confirmed the results found in this study. The scatter of their data around a smooth curve is about ± 0.10 weight percent KCl. Their results have a scatter of ± 0.07 weight percent KCl about the smooth curve obtained by regressing our experimental results. Hence, both data sets appear to be compatible within their respective precisions.

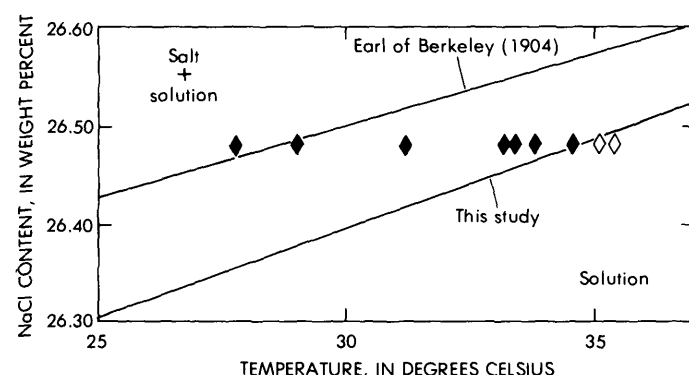


FIGURE 3.—Stability of NaCl crystals in a system with bulk composition of 26.48 weight percent NaCl. Solid diamonds represent crystals present; open diamonds represent crystals absent.

Na₂SO₄ (thenardite) and K₂SO₄

The comparison of the experimental data for the sulfates with the literature data (Linke, 1965) shows the same anomaly as the chlorides; that is, the literature data is systematically higher than the values obtained in this study by about 0.10 to 0.15 weight percent salt. Because much of the literature data has a precision of 0.1 to 0.2 weight percent and was determined either by the Earl of Berkeley (1904) or by others using a similar procedure, the result is not too surprising.

The sodium sulfate runs proved to be the most challenging as sodium sulfate undergoes a phase transition, $\text{Na}_2\text{SO}_4 \cdot 10\text{H}_2\text{O}$ (mirabilite) \rightleftharpoons Na_2SO_4 (thenardite), and thenardite exhibits retrograde solubility. Linke (1965) reports the transition point as $32.38^\circ \pm 0.10^\circ\text{C}$, which is in agreement with the transition temperature of $32.43 \pm 0.05^\circ\text{C}$ we determined. The retrograde solubility allowed us to approach reversibility most closely using the visual method. Runs were conducted both by cooling until the last crystal disappeared and by heating until the Na_2SO_4 would not dissolve. The saturation temperatures were generally the same within $\pm 0.1^\circ\text{C}$; however, the heating runs proved to be less precise than the cooling runs. Due to the difficulties encountered with such bracketing, most of the runs in table 1 represent cooling runs only for the retrograde solubility encountered above the transition.

CaCl₂

The system CaCl₂-H₂O proves to be a quite difficult one for determining phase relations due to the conflicting data and the numerous phases reported. For example, Linke (1965) reported α , β , and γ phases of

$\text{CaCl}_2 \cdot 4\text{H}_2\text{O}$ as all being stable and having solubilities of 51.5, 53.9, and 54.8 weight percent, respectively, at 35°C. Simple considerations by the phase rule indicate that the β and γ phases are metastable with respect to the α phase. Linke simply drew the best curve he could through the data and reported it accordingly. Not surprisingly, our data agrees with Linke's smoothed values only in the range 25° to 28°C; in fact, we used Linke's values for 25° and 27.5°C in the regression of our data for $\text{CaCl}_2 \cdot 6\text{H}_2\text{O}$ (table 1). At high temperatures, our data disagree by as much as 2 weight percent CaCl_2 . Long-term (24-h) static experiments similar to those done for NaCl (fig. 3) confirmed that the solubilities reported by Linke are indeed too high.

A probable explanation for the higher solubilities lies in the high viscosity of CaCl_2 solutions, which allows small crystals to remain suspended almost indefinitely. The studies summarized by Linke (1965) relied on sampling the fluid phase and analyzing it by evaporation to "dryness" or by an instrumental method. Because all these systems employed vigorous stirring to prevent density stratification, the high solubilities that were reported were undoubtedly due to suspended solids taken in the sampling procedure and were presumed to be quench crystals.

The transition temperatures have been reported as $30.1^\circ \pm 0.2^\circ\text{C}$ for $\text{CaCl}_2 \cdot 6\text{H}_2\text{O} \rightleftharpoons \text{CaCl}_2 \cdot 4\text{H}_2\text{O}$ and $45.1^\circ \pm 0.2^\circ\text{C}$ for $\text{CaCl}_2 \cdot 4\text{H}_2\text{O} \rightleftharpoons \text{CaCl}_2 \cdot 2\text{H}_2\text{O} + 2\text{H}_2\text{O}$ (Linke, 1965). These data from the "dry" system are in good agreement with the transition temperatures of $30.08^\circ \pm 0.05^\circ\text{C}$ and $45.13^\circ \pm 0.05^\circ\text{C}$ found in our study.

CONCLUSIONS

This study of the solubility of the five most common highly soluble salts in geothermal and hydrothermal systems has shown the reliability of the modified visual method for determining solubilities. The modified visual method has several advantages over other commonly used methods:

1. The system can be readily assembled and does not require sophisticated analytical systems.
2. The stirring overcomes density stratification and, at the same time, does not introduce suspended material which subsequently is analyzed as dissolved salt.
3. The method is moderately fast and avoids the

difficulties of obtaining a representative sample of the fluid for analysis.

4. The same tube can be run several times, thus increasing the precision of any measurement.
5. The larger sample size in comparison to the sealed-tube visual method (20 g compared to about 2 g) increases the precision with which the bulk composition is known.
6. The precision for the method is on the order of 0.02 to 0.19 weight percent salt compared with 0.1 to 1.0 weight percent with other methods.

The solubility data on NaCl , KCl , K_2SO_4 , Na_2SO_4 , and CaCl_2 from the literature have been shown to be systematically high with respect to the solubilities determined in our studies. Experiments such as those on NaCl (fig. 3) have shown that the previous literature data are, in fact, systematically in error. The systematic errors are probably related to analytical methods and (or) the presence of fine suspended salt crystals in the quench samples. It should be noted, however, that with the exception of the CaCl_2 data, the reported solubilities overlap the values reported here within the experimental precision of the data sets.

The values reported here appear to be the most reliable solubility data currently available for the five highly soluble salts studied and thus can be used in establishing the necessary data base for modeling the chemical behavior of saturated brines.

REFERENCES

- Earl of Berkeley, 1904, On some physical constants of saturated solutions: Royal Soc. London Philos. Trans., Ser. A, v. 203, p. 189-215.
- Linke, W. F., [1965], Solubilities of inorganic and metal organic compounds [4th ed.]: Am. Chem. Soc., 1914 p.
- Potter, R. W., II, Babcock, R. S., and Brown, D. L., 1975, Solubility relationships in the $\text{NaCl}-\text{KCl}-\text{H}_2\text{O}$ systems: EOS, Trans. Am. Geophys. Union, v. 56, p. 1075.
- 1977, A new method for determining the solubility of salts in aqueous solutions at elevated temperatures: U.S. Geol. Survey Jour. Research, v. 5, p. 389-397.
- Sunier, A. A., and Baumbach, J., 1976, The solubility of potassium chloride in ordinary and heavy water: Jour. Chem. Eng. Data, v. 21, p. 335-337.
- Wood, J. R., 1975, Thermodynamics of brine salt equilibria, pt. 1, The systems $\text{NaCl}-\text{KCl}-\text{MgCl}_2-\text{CaCl}_2-\text{H}_2\text{O}$ and $\text{NaCl}-\text{MgSO}_4-\text{H}_2\text{O}$ at 25° C: Geochim. et Cosmochim. Acta, v. 39, p. 1147-1163.
- 1976, Thermodynamics of brine-salt equilibria, pt. 2, The system $\text{NaCl}-\text{KCl}-\text{H}_2\text{O}$ from 0 to 200° C: Geochim. Cosmochim. Acta, v. 40, p. 1211-1220.

IRON-TITANIUM OXIDE MINERALS AND ASSOCIATED ALTERATION PHASES IN SOME URANIUM-BEARING SANDSTONES

By RICHARD L. REYNOLDS and MARTIN B. GOLDHABER,
Denver, Colo.

Abstract.—Detrital iron-titanium (Fe-Ti) oxide minerals of the ulvöspinel-magnetite (titanomagnetite) and ilmenite-hematite (titanoxyhematite) solid solution series are common in uranium-bearing sandstones. Alteration of Fe-Ti oxide minerals in oxidizing environments formed secondary products (primarily hematite) that are distinct from those produced under reducing conditions (iron disulfide minerals). Oxidation of sulfidized Fe-Ti oxide minerals, by the processes that formed uranium rolls, produced ferric oxide minerals (limonite) having textures that mimic those of the iron disulfides. Titanomagnetite and titanoxyhematite have been severely depleted in the ore-bearing zones of some uranium deposits. The alteration of detrital Fe-Ti oxide minerals near uranium ore deposits may produce characteristic signatures in the magnetization of the sandstone. Knowledge of the distribution and magnetic properties of these minerals can aid in interpreting data from total magnetic-field and magnetic-susceptibility surveys of uranium deposits.

Iron-titanium (Fe-Ti) oxide minerals may record important information on the geochemical environment of deposition of uranium in sandstone. Shawe (1976) noted the lack of detrital black opaque minerals in and near uranium ore in the Slick Rock district of western Colorado and concluded that epigenetic uranium-bearing solutions dissolved the black opaque minerals. A paucity of detrital Fe-Ti oxide minerals in the vicinity of uranium deposits is also well documented in the Morrison Formation of the Grants mineral belt, New Mexico (Adams and others, 1974; Squyres, 1970; Kendall, 1971). Adams and his co-workers concluded that the destruction of magnetite and ilmenite was probably the result of dissolution by oxygen-poor and organic-rich ground water and was related to the formation of the uranium deposits. Similar observations have been made by King and Austin (1966) in the Gas Hills district of Wyoming. However, complete or nearly complete destruction of black opaque minerals adjacent to or within uranium deposits is not universal. Files (1970) found detrital black opaque minerals throughout mineralized, oxi-

dized, and reduced sandstone in the Gas Hills, Crooks Gap, and Shirley Basin districts of Wyoming.

Recent application of total magnetic-field and magnetic-susceptibility techniques to uranium exploration (Smith and others, 1976; Scott and Daniels, 1976) further underscores the importance of the Fe-Ti oxide minerals in uranium-bearing rocks. Because many of the detrital Fe-Ti oxide minerals (magnetite and titanoxyhematite) and some of their alteration products (notably ferric oxide minerals) are magnetic, recognition of these phases and characterization of their magnetic properties are essential to the interpretation of data from these geophysical surveys.

In spite of the recent attention to black opaque minerals in uranium-bearing sandstone, there is presently no detailed description of the relationship between detrital Fe-Ti oxide minerals and their alteration phases and the genesis of roll-type uranium deposits and of the relationship between the minerals and geophysical data. Our paper briefly summarizes some optical properties that are useful for identifying Fe-Ti oxide and associated secondary minerals. In addition, the compositions and textures of secondary products of the Fe-Ti oxide minerals are described because of their usefulness in deciphering alteration histories of uranium deposits. Finally, we relate our observations of the magnetic Fe-Ti oxide minerals and associated alteration phases to possible variations in magnetic properties that may be characteristic of uranium-bearing sandstones. The observations presented here should be useful for modeling and interpreting geophysical data.

AREAS OF STUDY

Samples from five mineralized formations in three of the major uranium-producing districts of the western United States and from one formation, the Laramie, in an undeveloped area were examined for Fe-Ti

oxide minerals and their alteration products. The number of samples collected from each of the six formations and the distribution of sampling locations relative to the position of the uranium ore vary. Nevertheless, oxidized and reduced barren zones and ore-bearing zones are represented in the sample suites of each locality. The formations studied are listed below in order of increasing age.

1. The Oakville Sandstone (Miocene) of Live Oak County, southeast Texas (Eargle and others, 1975; and Eargle and Weeks, 1973; Dickinson, 1976);
2. The Catahoula Tuff (Oligocene-Miocene) of Webb County, southeast Texas (Eargle and others, 1975; and Eargle and Weeks, 1973);
3. The Whitsett Formation (Eocene) of Karnes County, southeast Texas (Dickinson, 1976; Eargle and others, 1975; Eargle, 1959; Eargle and Weeks, 1973);
4. The Wasatch Formation (Eocene) in the Powder River Basin, Johnson County, Wyo. (Mrak, 1968; Davis, 1969; Sharp and others, 1964);
5. The Laramie Formation (Late Cretaceous), Weld County, northern Colorado;
6. The Morrison Formation (Late Jurassic) in the vicinity of the Grants mineral belt, New Mexico (Society of Economic Geologists, 1963; Granger, 1968; Granger and others, 1961).

These rock units range from Late Jurassic to Miocene and represent varied depositional environments including fluvial, beach, and backbeach regimes. Although some of the units were derived from widely separated and geologically different source areas, these sandstones contained similar detrital and authigenic opaque phases. Sediments of the Wasatch Formation were primarily derived from the Precambrian crystalline complex of central Wyoming with some contribution from uplifted Paleozoic and Mesozoic sedimentary rocks adjacent to the uplifted blocks of Precambrian basement (Davis, 1969). Precambrian igneous and metamorphic rocks of the Front Range, Colo., were the primary source of sediments of the Laramie Formation (Goldstein, 1950), but some of the detritus of the Laramie was derived locally from older sedimentary rocks along the uplifted margins of the range (Moody, 1947). Similarly, much of the Morrison Formation in west-central New Mexico was derived primarily from Precambrian igneous and metamorphic highlands, but some sediment came from older sedimentary rocks adjacent to the San Juan Basin (Craig and others, 1955) and from volcanic sources (Waters and Granger, 1953). The Whitsett Formation, Cata-

houla Tuff, and Oakville Sandstone of the southeast Texas Coastal Plain consist in part of sediment derived from rocks of the uplands of central Texas, but they also contain pyroclastic material from volcanic source areas farther to the west (Plummer, 1933; Callender and Folk, 1958; and Seewald, 1966). The Catahoula Tuff, as its name suggests, locally contains abundant air-fall ash and volcanic conglomerate. Much of the detritus in these formations has gone through more than one episode of sedimentation. Recycling and winnowing, especially in the beach sand of the Whitsett, have no doubt increased the concentration of heavy minerals, particularly the Fe-Ti oxide minerals which constitute a substantial part of the heavy minerals in these sandstones.

IRON-TITANIUM OXIDE MINERALS AND THEIR ALTERATION PRODUCTS

It is convenient to illustrate the Fe-Ti oxide minerals on the ternary diagram for the system $\text{FeO}-\text{Fe}_2\text{O}_3-\text{TiO}_2$ (fig. 1). The common detrital Fe-Ti oxide minerals are represented by the minerals of two solid-solution series: (1) those of the cubic ulvöspinel-magnetite series ($\text{Fe}_2\text{TiO}_4-\text{Fe}_3\text{O}_4$, the titanomagnetites), and (2) those of the rhombohedral ilmenite-hematite series ($\text{FeTiO}_3-\text{Fe}_2\text{O}_3$, the titanohematites). The pseudobrookite phases may be present in the detrital Fe-Ti oxide suite where they generally occur as minor constituents within titanomagnetite and titanohematite grains as the result of high-temperature oxidation during initial cooling of igneous source rocks.

Two of the important secondary products formed by alteration of Fe-Ti oxide minerals are also shown on the ternary diagram on figure 1. These are hematite (Fe_2O_3) and anatase (TiO_2), both of which are useful in interpreting the diagenetic histories of uranium-bearing sandstone. Other secondary phases that cannot be represented on figure 1 but that are essential to this study are the secondary iron disulfide phases, pyrite and marcasite (FeS_2), which are intimately associated with Fe-Ti oxide minerals in reduced rock, and the complex uranium-bearing phases that have replaced titanomagnetite and titanohematite within ore in at least one of the deposits studied.

The Fe-Ti oxide minerals and their alteration phases are easily identified by viewing polished sections and polished grain mounts by reflected light under oil-immersion conditions. Optical properties of isotropy and color most useful in petrographic identification are listed adjacent to the mineral series shown on figure 1. Ramdohr (1969), Haggerty (1976), and Uytendbogaardt and Burke (1971) gave more detailed de-

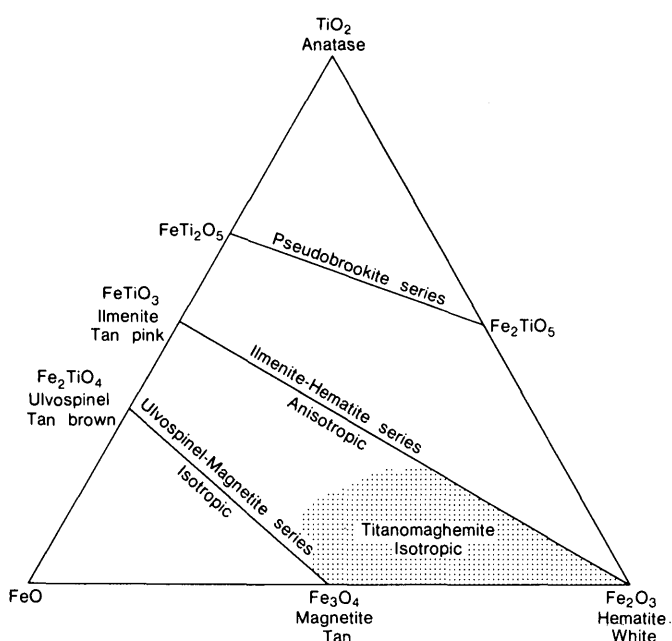


FIGURE 1.—The system FeO-Fe₂O₃-TiO₂ showing the solid-solution joins for the ulvöspinel-magnetite, ilmenite-hematite, and pseudobrookite series. Isotropy, anisotropy, and color are the optical properties seen in oil-immersion reflected-light microscopy. Pattern shows chemical composition of isotropic titanomaghemitite. Modified from Haggerty (1976).

scriptions of optical properties of the opaque phases discussed here.

The appearance of detrital Fe-Ti oxide minerals in sandstone depends not only upon the geochemical environment in the sediment but also upon conditions of high-temperature and subsequent low-temperature alteration within the source rocks. Although a variety of complex textures and coexisting phases can occur such as intergrowths of pleonastic spinel, ulvöspinel, pseudobrookite, sphene, and rutile with minerals of the titanomagnetite series and pleonastic spinel, rutile, hematite, sphene, and perovskite with minerals of the titanohematite series, we discuss only certain diagnostic textures and phases that are useful in interpreting the geochemical environments associated with uranium deposits.

Minerals of the ulvöspinel-magnetite solid-solution series are optically isotropic and range in color from tan brown (ulvöspinel) to tan or light brown (magnetite). Ilmenite lamellae along (111) planes are diagnostic features of many titanomagnetite grains, in which they occur as a trellis pattern that formed as the result of high-temperature (greater than 600°C) oxidation during initial cooling of host grains in the source area (fig. 2A).

Minerals of the ilmenite-hematite solid-solution series are anisotropic and range in color from tan or

pinkish brown for end-member ilmenite to white for hematite. The most common titanohematite grains observed in this study are those that are optically homogeneous (fig. 2B), having been either quenched at temperatures above the ilmenite-hematite miscibility gap (Lindsley, 1973) or crystallized from initial compositions on either side of the gap. Also present but less common are intergrowths of end-member ilmenite and hematite that formed by exsolution during initial cooling from elevated temperatures.

Hematite, an important secondary Fe-Ti oxide mineral, occurs as a white anisotropic phase formed by low-temperature oxidation of magnetite and ilmenite and commonly shows red internal reflections when it is present as a finely disseminated phase. Incipient oxidation of magnetite commonly results in the development of hematite along the (100) planes. With further oxidation, the magnetite may be entirely replaced by hematite, forming grains of martite. Ilmenite lamellae contained in titanomagnetite are also replaced by hematite under oxidizing conditions but commonly with retention of the characteristic texture along (111) planes. The relict texture is preserved even though much of the titanomagnetite grain may have been converted to hematite or dissolved (fig. 2C).

Maghemite and titanomaghemitite, other low-temperature oxidation products of magnetite and titanomagnetite, respectively, are optically isotropic, light gray or light bluish gray, and occur unevenly and without crystallographic control along the margins and along fractures in the host grains. We have observed maghemite in the oxidized zones of some uranium-bearing sandstones, but we cannot determine if the maghemite resulted from oxidation in the sedimentary environment or from oxidation in the source area. Nevertheless, unlike hematite, maghemite is uncommon in the oxidized sandstones we have studied and will not be discussed further.

Under sulfidic reducing conditions, pyrite and marcasite may replace or form rims around titanomagnetite and titanohematite grains (Reynolds, 1975; Adams and others, 1974; Carroll, 1960; Dimanche and Bartholomé, 1976; Ramdohr, 1969). Iron disulfide minerals generally replace titanomagnetite grains from the grain margin inward (fig. 3A). Minerals of the rhombohedral Fe-Ti oxide mineral series are less susceptible to sulfidization than is magnetite, as attested by relict ilmenite lamellae which are frequently observed within sulfidized titanomagnetite grains (fig. 3B) and by grains of titanohematite which have persisted in the rock under sulfidizing conditions which have destroyed most of the magnetite. Nevertheless, strongly reducing conditions are capable of converting

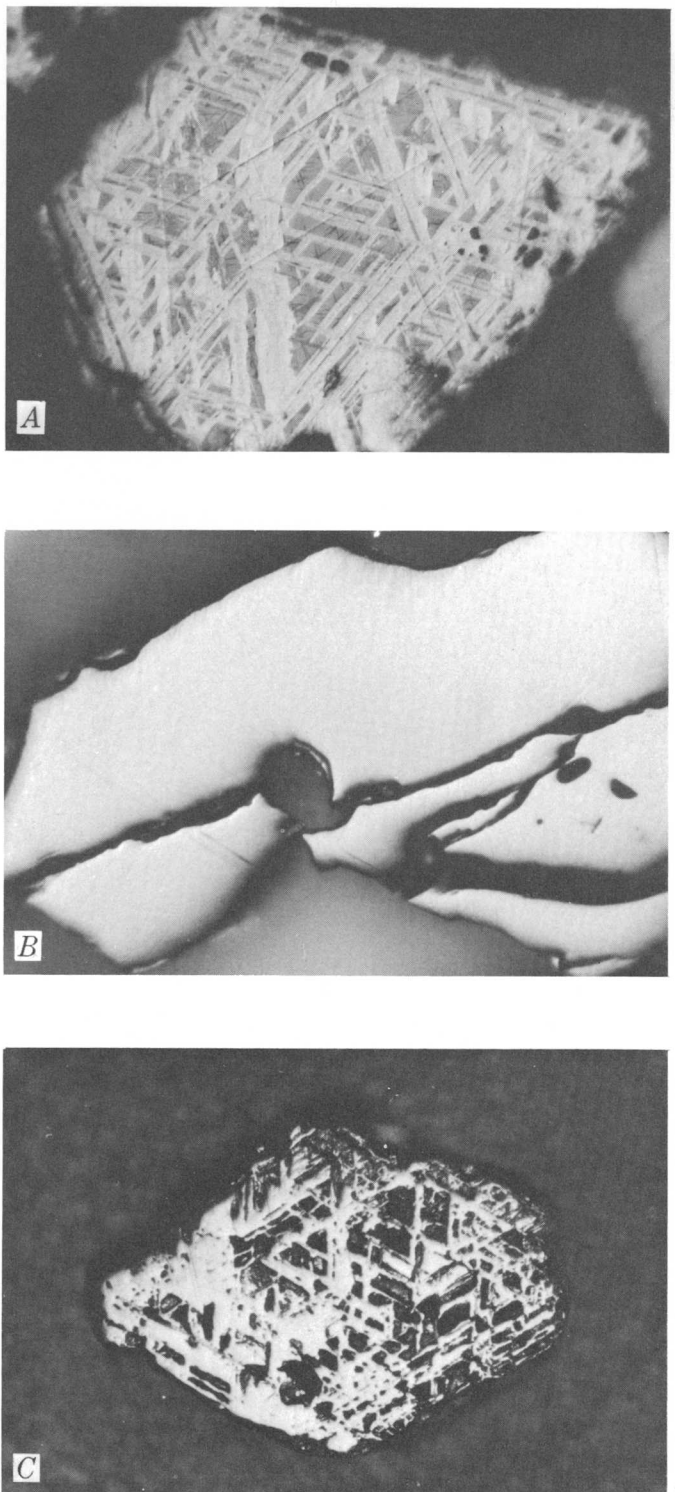


FIGURE 2.—Iron-titanium oxide minerals in oxidized sandstone.
A. Magnetite (dark gray) with ilmenite lamellae (light gray) along (111) planes. Hematite (white) has partly replaced both ilmenite and magnetite. Dark rods within magnetite are pleonastic spinel. Length of field, 158 μm (micrometers). B. Optically homogeneous mineral of the ilmenite-hematite solid-solution series. Length of field, 158 μm . C. Grain, formerly titanomagnetite, in which both the original

titanohematite to iron disulfide minerals on grain boundaries and especially along fractures within the grain (fig. 3C). In one of the deposits studied, that in the Catahoula Tuff, iron disulfide has commonly replaced titanomagnetite and titanohematite, but in other deposits (such as those of the Powder River Basin and northeast Colorado) the Fe-Ti oxide minerals are primarily rimmed by iron disulfide minerals without substantial replacement. Reasons for these disparities are presently unclear, but our current studies suggest that factors controlling the intensity of sulfidization, such as the availability of sulfur and perhaps the source of reductant, are responsible for the differences. Iron disulfide minerals also occur in uranium-bearing sandstone as discrete euhedral crystals, as interstitial cement of detrital grains, and, where carbonaceous matter is present, as replacements of and overgrowths on plant debris and as framboids.

Replacement of titanohematite and titanomagnetite by iron disulfide minerals requires retention of most of the iron in the sulfide phase coupled with expulsion of the titanium. In the Catahoula deposit, expelled titanium crystallized as rims of TiO_2 (anatase) on sulfidized titanohematite and to a lesser extent on sulfidized titanomagnetite. In polished section, TiO_2 is obvious as a fine-grained white nonopaque phase. It occurs, however, not only as a secondary phase in reduced rock but also as a secondary phase in oxidized rock where it formed by oxidation of detrital titanium-bearing oxide minerals.

Oxidation of iron disulfide minerals results in the development of ferric oxide and hydroxide minerals in a variety of colors and textures that we group together as limonite. Occurring as intermixed yellow, orange, red, and grayish-red phases, limonite is characterized commonly by textures that mimic those of the precursory iron disulfide minerals (fig. 4; Reynolds and Goldhaber, 1978).

Some very red internal reflections observed in limonite may in fact be from hematite, but we distinguish between the hematite in limonitic phases and the hematite that replaced Fe-Ti oxide minerals under oxidizing conditions because of their different associations and modes of generation.

Titanomagnetite and titanohematite also may have altered in a characteristic pattern in the ore-bearing zones of some roll-type deposits. Detrital Fe-Ti oxide

ilmenite lamellae along (111) planes and the host magnetite have been replaced by hematite with retention of the characteristic trellis texture. Dark areas within grain are voids resulting from the dissolution of magnetite. Length of field, 390 μm . Reflected-light oil-immersion microscopy.

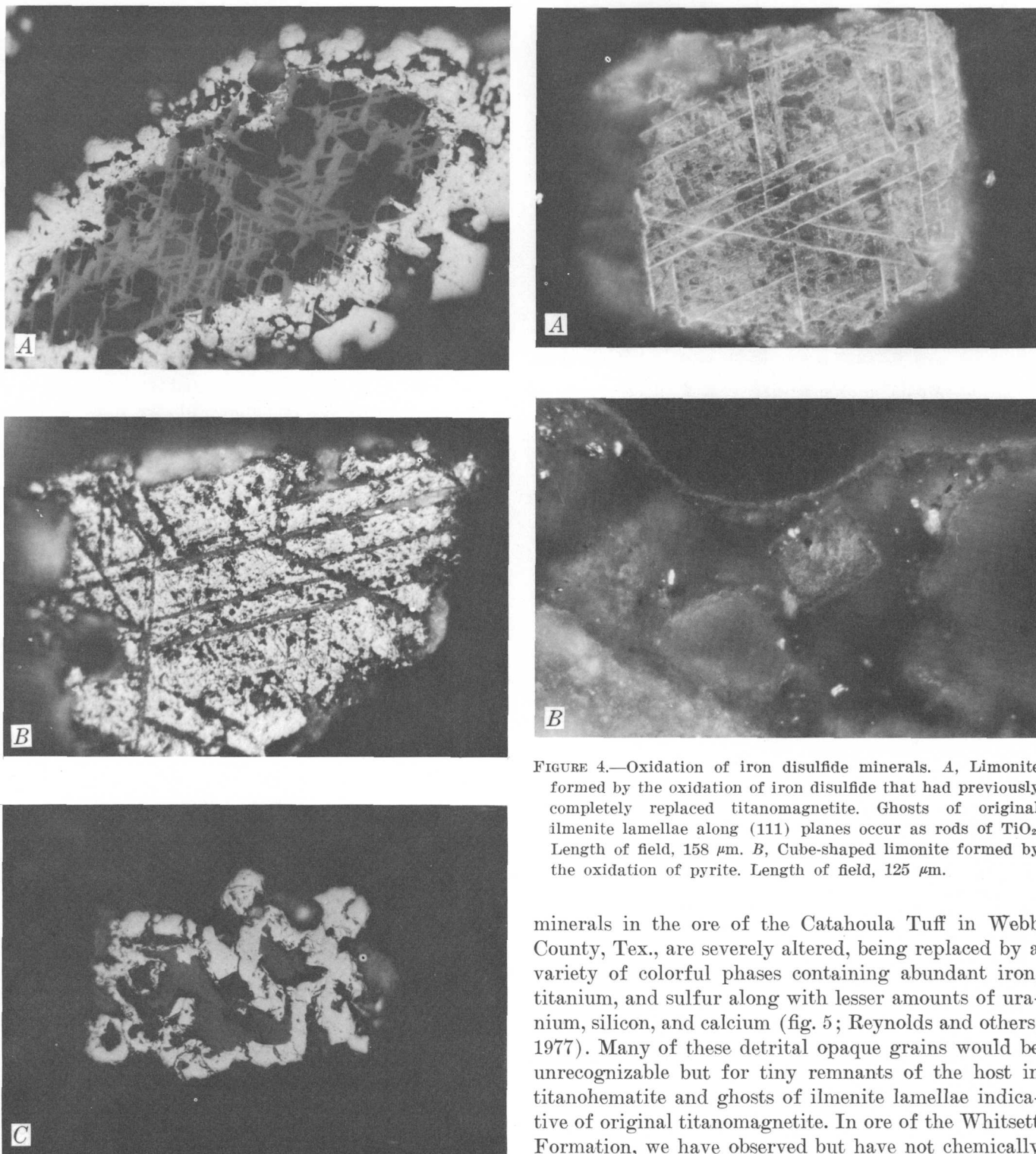


FIGURE 3.—Sulfidization of iron-titanium oxide minerals. *A*, Partial replacement of titanomagnetite grain by pyrite (white) along grain margins. Dark gray, magnetite; light gray, ilmenite lamellae along (111) planes. Black areas within grain are voids. Length of field, 158 μm . *B*, Replacement of titanomagnetite grain by pyrite; all host magnetite was replaced leaving relict ilmenite lamellae, some of which

FIGURE 4.—Oxidation of iron disulfide minerals. *A*, Limonite formed by the oxidation of iron disulfide that had previously completely replaced titanomagnetite. Ghosts of original ilmenite lamellae along (111) planes occur as rods of TiO_2 . Length of field, 158 μm . *B*, Cube-shaped limonite formed by the oxidation of pyrite. Length of field, 125 μm .

minerals in the ore of the Catahoula Tuff in Webb County, Tex., are severely altered, being replaced by a variety of colorful phases containing abundant iron, titanium, and sulfur along with lesser amounts of uranium, silicon, and calcium (fig. 5; Reynolds and others, 1977). Many of these detrital opaque grains would be unrecognizable but for tiny remnants of the host in titanohematite and ghosts of ilmenite lamellae indicative of original titanomagnetite. In ore of the Whitsett Formation, we have observed but have not chemically

have altered to TiO_2 , along (111) planes. Light-gray phase on grain margin is TiO_2 . Length of field, 158 μm . *C*, Replacement of titanohematite grain by pyrite (white) along grain margins. TiO_2 (light gray) occurs beyond pyrite rim. Length of field, 158 μm .

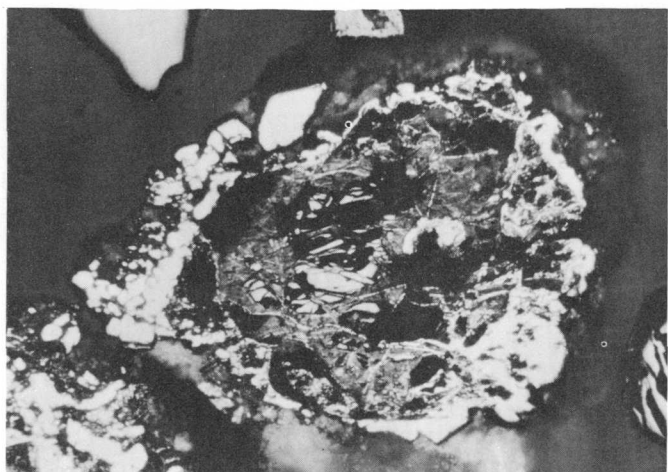


FIGURE 5.—Alteration of a detrital grain of titanohematite in uranium ore. Mottled light- and dark-gray phases contain abundant sulfur, iron, and titanium, and lesser amounts of uranium, calcium, and silicon. The light-gray phase in the grain interior is relict titanohematite. Pyrite and marcasite (white) occur on the grain margins where they formed by replacement and by overgrowth and occur within the grain where they formed by replacement and along fractures. Length of field, 390 μm .

analyzed phases that appear to be petrographically similar to the grains from the Catahoula in Webb County. In addition, some grains of titanomagnetite in ore of the Morrison and Whitsett Formations have been completely destroyed, leaving merely a fragile network of TiO_2 lamellae in the trellis pattern characteristic of ilmenite.

DISCUSSION

Alteration products of the detrital Fe-Ti oxide minerals are sensitive indicators of the geochemical environments associated with the development of uranium deposits because the compositions of the secondary phases directly reflect the chemical conditions under which they formed. In reducing environments, titanomagnetite and titanohematite grains have been completely or partly replaced by iron disulfide minerals (pyrite or marcasite or both) if sulfur was sufficiently abundant. Later oxidation of the reduced rock, by oxygenated ground water responsible for the mobilization and transport of uranium, transformed the iron disulfide minerals to limonite that has characteristic textures that mimic those of the precursor sulfide minerals. However, titanomagnetite grains in sandstone that was never sulfidized have been replaced by ferric oxide minerals (primarily hematite) which differ greatly in optical properties and texture from the ferric oxide minerals (limonite) formed by oxidation

of iron disulfide minerals in proximity to uranium deposits.

Studies of the detrital Fe-Ti oxide minerals provide information useful for the interpretation of measurements from total magnetic-field and magnetic-susceptibility surveys of uranium deposits. In the past, data from these surveys have been modeled in terms of the magnetite content of the host rock (Ellis and others, 1968; Dodd and Eschliman, 1971; Scott and Daniels, 1976; Smith and others, 1976). Thermomagnetic, X-ray diffraction, and petrographic analyses, however, indicate that magnetic titanohematite is present and is commonly more abundant than titanomagnetite in each of the formations studied (Reynolds, 1977). Magnetic titanohematite, then, is an important contributor to the permanent magnetization of these rocks.

Recognition of the secondary phases that form by the alteration of the detrital Fe-Ti oxide minerals is also essential to the interpretation of data from magnetic-field and magnetic-susceptibility studies. Both oxidation and reduction can result in the partial to total destruction of detrital magnetic minerals. Under oxidizing conditions, magnetite commonly is replaced by hematite which, although magnetic, carries a much weaker moment than magnetite of the same volume. In certain reducing environments, magnetite and titanohematite may be replaced by nonmagnetic iron disulfide minerals. In addition, magnetic Fe-Ti oxide minerals have been dissolved or replaced by nonmagnetic uraniferous phases in some mineralized zones. We have also seen petrographic evidence of the dissolution of the detrital Fe-Ti oxide minerals in both oxidized and reduced sandstone. These alterations obviously result in a net decrease in the total magnetic moment of a rock.

Later oxidation of iron disulfide minerals, however, generates authigenic ferric oxide minerals, some of which are magnetic, which are commonly seen within the oxidized tongue of roll-type deposits and which are also associated with the redistribution of uranium in some tabular deposits. Ferric oxide minerals also can form by oxidation of paramagnetic iron-bearing silicates such as biotite, hornblende, pyroxene, and olivine, which are metastable in oxidizing environments (Walker, 1967). Alterations such as these may impart a magnetization to rocks in the oxidized tongue which is higher than the magnetization of rocks in the adjacent mineralized zone and in reduced rock ahead of the roll front.

Factors controlling the distribution and abundance of the Fe-Ti oxide minerals and their alteration phases in sandstone and the consequent effects on the magnetization of the rock are many and complex and will

vary not only between different deposits but also within the same deposit. Such factors include alteration in the source area, paleosedimentary environment, early diagenetic alterations, the sources and strengths of reductants and oxidants, processes related to mineralization, and permeability of host rocks as controlled by lithic type and later alterations. For these reasons, it cannot be expected that all uranium deposits will show identical magnetic properties. Nevertheless, some generalizations can be made in light of recent geophysical data gathered in and above uranium deposits.

Total magnetic-field and magnetic-susceptibility surveys are among the promising geophysical techniques being developed for exploration of uranium deposits. Total magnetic field surveys have thus far identified two types of anomalies associated with uranium deposits (Smith and others, 1976). One type of anomaly occurs over a deposit in the Laramie Formation in northern Colorado; the other type occurs over the Oakville Sandstone in south Texas. We have not sampled either of these deposits in the surveyed area. A survey of the deposit in northern Colorado revealed a pronounced negative anomaly of 15–20 nT (nanoteslas) directly above a roll front. The anomaly might arise from a number of factors such as response from strata other than the host rocks or, as suggested by Smith and others (1976), development of a chemical remanent magnetization (CRM) within the ore. We have seen, however, no evidence of the generation of secondary magnetic phases that could impart such a CRM in any samples of ore. The anomaly may also result from relatively greater depletion of magnetic Fe-Ti oxide minerals within the one zone than on either side of the roll.

A magnetic profile across the south Texas deposit shows a difference of 4 nT from high magnetization in rocks behind the roll front to lower magnetization in rocks in front of the roll. Magnetic-susceptibility measurements of core samples from the deposit also indicate the presence of an anomaly that ranges from 38×10^{-5} (in SI) 1000 m behind the roll to about 21×10^{-5} in the vicinity of the roll and in front of it (Scott and Daniels, 1976). Detailed mineralogical data is not available for this deposit, but it seems likely that relatively greater depletion of magnetic Fe-Ti oxide minerals in the ore and reduced rock ahead of the roll front might be fully or partly responsible for the anomaly.

Adler (1973) has proposed that paleomagnetic study of uranium-bearing sandstone might be useful as an exploration guide for uranium. This idea is based on the premise that CRM, carried by secondary magnetic

phases developed by ore-forming processes, records a remanent magnetization that either by virtual geomagnetic pole position or by polarity can be related to the timing of the formation of the deposit. The general process of chemical remagnetization is not fully understood and is surely very complex for the geochemical systems that control concentration of uranium. Later acquisition of CRM by processes unrelated to ore formation may further complicate paleomagnetic studies. Nonetheless, petrographic and rock magnetic studies of the Fe-Ti oxide minerals and their alteration phases must complement paleomagnetic studies to enable understanding of the source of the remanent magnetization and meaningful interpretation of the paleomagnetic data.

CONCLUSION

The examples presented in this paper do not cover the range of possible alterations of the complex geochemical systems that control the concentration of uranium in sandstone. We have not studied, for example, sandstones that have undergone later reduction or multiple episodes of reduction and oxidation, but we believe that studies outlined here would help to elucidate such complicated histories.

REFERENCES CITED

- Adams, S. S., Curtis, H. S., and Hafen, P. L., 1974, Alteration of detrital magnetite-ilmenite in continental sandstones of the Morrison Formation, New Mexico, in *Formation of uranium ore deposits; sedimentary basins and sandstones-type deposits*: Internat. Atomic Energy Agency Proc. Ser., no. STI/PUB/374, p. 219–253.
- Adler, H. H., 1973, Exploration for uranium in sandstones; geochemical, remanent magnetic, and sulfur-isotope applications, in *Uranium exploration methods*: Internat. Atomic Energy Agency Panel Proc. Ser., p. 155–169.
- Callender, D. L. and Folk, R. L., 1958, Idiomorphic zircon, key to volcanism in the lower Tertiary sands of central Texas: Am. Jour. Sci., v. 256, no. 4, p. 257–269.
- Carroll, Dorothy, 1960, Ilmenite alteration under reducing conditions in unconsolidated sediments: Econ. Geology, v. 55, p. 618–619.
- Craig, L. C., and others, 1955, Stratigraphy of the Morrison and related formations, Colorado Plateau region, a preliminary report: U.S. Geol. Survey Bull. 1009-E, p. 125–168.
- Davis, J. F., 1969, Uranium deposits of the Powder River Basin: Wyoming Univ. Contr. Geology, v. 8, no. 2, pt. 1, p. 131–141.
- Dickinson, K. A., 1976, Sedimentary depositional environments of uranium and petroleum host rocks of the Jackson Group, South Texas: U.S. Geol. Survey Jour. Research, v. 4, no. 5, p. 615–629.
- Dimanche, F., and Bartholomé, P., 1976, The alteration of ilmenite in sediments: Minerals Sci. and Eng., v. 8, no. 3, p. 187–201.

- Dodd, P. H., and Eschliman, D. H., 1971, Borehole logging techniques for uranium exploration and evaluation, in S. H. U. Bowie and others, eds., Uranium prospecting handbook: Proc. NATO-sponsored Advanced Study Institute: London, Inst. Mining Metallurgy, p. 244-276.
- Eargle, D. H., 1959, Sedimentation and structure, Jackson Group, south-central Texas: Gulf Coast Assoc. Geol. Soc. Trans., v. 9, p. 31-39.
- Eargle, D. H., Dickinson, K. A., and Davis, B. O., 1975, South Texas uranium deposits: Am. Assoc. Petroleum Geologists Bull., v. 59, no. 5, p. 766-779.
- Eargle, D. H., and Weeks, A. M. D., 1973, Geologic relations among uranium deposits, south Texas, Coastal Plain region, U.S.A., in G. C. Amstutz, and A. J. Bernard, eds., Ores in sediments: Internat. Union Geol. Sci., Ser. A., no. 3, New York: Springer-Verlag, p. 101-113.
- Ellis, J. R., Austin, S. R., and Drouillard, R. F., 1968, Magnetic susceptibility and geochemical relationships as uranium prospecting guides: U.S. Atomic Energy Comm. AEC-RI D-4, 21 p.
- Files, F. G., 1970, Geology and alteration associated with Wyoming uranium deposits: Univ. Calif., Berkeley, Ph. D. thesis, 113 p.
- Granger, H. C., 1968, Localization and control of uranium deposits in the southern San Juan Basin mineral belt, New Mexico—an hypothesis, in Geological Survey Research 1968: U.S. Geol. Survey Prof. Paper 600-B, p. B60-B70.
- Granger, H. C., Santos, E. S., Dean, B. G., and Moore, F. B., 1961, Sandstone-type uranium deposits at Ambrosia Lake, New Mexico—an interim report: Econ. Geology, v. 56, no. 7, p. 1179-1210.
- Goldstein, August, Jr., 1950, Mineralogy of some Cretaceous sandstones from the Colorado Front Range: Jour. Sed. Petrology, v. 20, no. 2, p. 85-97.
- Haggerty, S. E., 1976, Opaque mineral oxides in terrestrial igneous rocks, in D. Rumble, III, ed., Oxide minerals: Mineralog. Soc. America Short Course Notes, v. 3, p. 1-96.
- Kendall, E. W., 1971, Trend orebodies of the Section 27 mines, Ambrosia Lake uranium district, New Mexico: Univ. Calif., Berkeley, Ph. D. thesis, 167 p.
- King, J. W., and Austin, S. R., 1966, Some characteristics of roll-type uranium deposits at Gas Hills, Wyoming: Mining Eng., v. 18, no. 5, p. 73-80.
- Lindsley, D. H., 1973, Delimitation of the hematite-ilmenite miscibility gap: Geol. Soc. American Bull., v. 84, no. 2, p. 657-662.
- Moody, J. D., 1947, A study of the Laramie Formation in the Golden [Colorado] area: Compass, v. 24, no. 3, p. 147-156.
- Mrak, V. A., 1968, Uranium deposits in the Eocene sandstones of the Powder River Basin, Wyoming, in Ore deposits of the United States, 1933-1967 v. 1 (The Graton-Sales Volume): New York, Am. Inst. Mining, Metall., and Petroleum Engineers, p. 838-848.
- Plummer, F. B., 1933, Cenozoic systems in Texas, in E. H. Sellards, W. S. Adkins, and F. B. Plummer, Geology of Texas: Texas Univ. Bull. 3232, p. 519-818.
- Ramdohr, Paul, 1969, The ore minerals and their intergrowths [3d ed.]: Oxford, Pergamon Press, 1174 p.
- Reynolds, R. L., 1975, Alteration of iron-titanium oxide minerals associated with uranium deposits in sandstone, in L. C. Craig, R. A. Brooks, and P. C. Patton, eds., Abstracts of the 1975 Uranium and Thorium Research and Resources Conference: U.S. Geol. Survey Open-File Rept. 75-595, p. 38-39.
- , 1977, Magnetic titanohematite minerals in uranium-bearing sandstones: U.S. Geol. Survey Open-File Rept. 77-355, 21 p.
- Reynolds, R. L., and Goldhaber, M. B., 1978, Recognition of oxidized sulfide minerals as an exploration guide for uranium: U.S. Geol. Survey Jour. Research, v. 6, no. 4, p. 483-488.
- Reynolds, R. L., Goldhaber, M. B., and Grauch, R. I., 1977, Uranium associated with iron-titanium oxide and their alteration products in a south Texas roll-type deposit, in J. A. Campbell, ed., Short papers of the U.S. Geological Survey Uranium-Thorium Symposium, 1977: U.S. Geol. Survey Circ. 753, p. 37-39.
- Seewald, C. R., 1966, Sedimentology of the Whitsett Formation (upper Eocene), south-central Texas: Texas Univ. M.S. thesis, 196 p.
- Scott, J. H., and Daniels, J. J., 1976, Non-radiometric borehole geophysical detection of geochemical halos surrounding sedimentary uranium deposits: U.S. Geol. Survey Open-File Rept. 76-228, 16 p.
- Sharp, W. N., McKay, E. J., McKeown, F. A., and White, A. M., 1964, Geology and uranium deposits of the Pumpkin Buttes area of the Powder River Basin, Wyoming: U.S. Geol. Survey Bull. 1107-H, p. 541-638.
- Shawe, D. R., 1976, Sedimentary rock alteration in the Slick Rock District, San Miguel and Dolores Counties, Colorado: U.S. Geol. Survey Prof. Paper 576-D, p. D1-D51.
- Smith, B. D., Cady, J. W., Campbell, D. L., Daniels, J. J., and Flanigan, V. J., 1976, A case for "other" geophysical methods in exploration for uranium deposits, in Exploration for uranium ore deposits: Internat. Atomic Energy Agency, Vienna, 1976, p. 337-351.
- Society of Economic Geologists, 1963, Geology and technology of the Grants uranium region: New Mexico Bur. Mines and Mineral Resources Mem. 15, 277 p.
- Squyres, J. B., 1970, Origin and depositional environment of uranium deposits of the Grants region, New Mexico: Stanford Univ. Ph. D. thesis, 228 p.
- Uyttenbogaardt, J. W. H., and Burke, E. A. J., 1971, Tables for microscopic identification of ore minerals [2d ed.]: Amsterdam, Elsevier Publishing Co., 430 p.
- Walker, T. R., 1967, Formation of red beds in modern and ancient deserts: Geol. Soc. America Bull., v. 78, no. 3, p. 353-368.
- Waters, A. C., and Granger, H. C., 1953, Volcanic debris in uraniferous sandstones, and its possible bearing on the origin and precipitation of uranium [Colorado Plateau]: U.S. Geol. Survey Circ. 224, 26 p.

SIGNIFICANCE OF AGE RELATIONS ABOVE AND BELOW UPPER JURASSIC OPHIOLITE IN THE GEYSERS-CLEAR LAKE REGION, CALIFORNIA

By R. J. McLAUGHLIN and E. A. PESSAGNO, Jr.¹

Menlo Park, Calif., Dallas, Tex.

Abstract.—In The Geysers-Clear Lake area of northern California, a fragmented Upper Jurassic ophiolite overlain depositionally by the Great Valley sequence is juxtaposed over deformed and metamorphosed rocks of the Franciscan assemblage along the Coast Range thrust. The basal strata of the Great Valley sequence consist of thick breccias of mafic clasts, identical in composition to the upper part of the ophiolite. These breccias and their contact relations suggest that more than 1 km of the upper part of the ophiolite was locally eroded in early Tithonian time. On the basis of their radiolarian faunas, cherts in the Franciscan assemblage below the ophiolite range in age from Late Jurassic (early Tithonian) to Late Cretaceous (early Cenomanian). Of particular significance is an individual chert body (= The Geysers chert) of this age range. The early Cenomanian radiolarians, except for two occurrences associated with pelagic limestone, are significantly younger than those previously reported from the Franciscan assemblage. The existence of a sequence of Late Jurassic to Late Cretaceous radiolarian chert places critical constraints on subduction models for emplacement of the Franciscan assemblage beneath the Coast Range ophiolite and Great Valley sequence in The Geysers-Clear Lake area. From early Tithonian to post-early Cenomanian time, the Franciscan assemblage received pelagic sedimentation far from any site of subduction. By other data, blueschist metamorphism of subducted Franciscan strata also occurred during this time. The radiolarian data from The Geysers area permit a correlation with Upper Cretaceous pelagic limestones in the Laytonville area northwest of The Geysers and also imply that the Great Valley sequence was never depositionally in contact with the Franciscan assemblage.

ing on the age of some Franciscan rocks and the Great Valley sequence of the northern California Coast Ranges. These data clarify the relation of Franciscan rocks to the overlying Upper Jurassic ophiolite at the base of the Great Valley sequence and have critical implications for plate tectonic models.

Acknowledgments.—Numerous scientists of the U.S. Geological Survey have provided support to this project. We should like to acknowledge D. L. Jones for collaboration of paleontologic data and molluscan fossil identifications; W. V. Sliter for his work on Late Cretaceous foraminifers; J. M. Donnelly and F. E. Goff for their collaboration of geologic mapping in the vicinity of Harbin Springs; H. N. Ohlin for his help in drafting, extraction of radiolarians from cherts, and assistance in the field; and D. H. Sorg for assistance in field mapping. W. R. Evitt of Stanford University, is gratefully acknowledged for his pollen study of several carbonate concretions. The work was in part supported by grants to E. A. Pessagno from the National Science Foundation (GA-35094 and DES-72-01528-A01). Finally, we thank C. A. Hopson, of the University of California at Santa Barbara, for his helpful insights into the ophiolite sequences at Harbin Springs and Geyser Peak.

REGIONAL RELATIONS

A laboratory technique developed by Pessagno and Newport (1972) has made it possible to rapidly extract radiolarian assemblages from cherty pelagic sedimentary rocks for paleontologic dating. This extraction technique has been particularly useful in dating pelagic sediments above ophiolite sequences. In this report, we present new biostratigraphic data, based largely on radiolarian cherts dated by Pessagno, bear-

The Franciscan assemblage (Bailey and others, 1964), designated the "Franciscan Complex" by Berkland and others (1972), is composed of highly deformed and, in places, chaotically mixed sedimentary and igneous rocks. Present plate tectonic models imply that these rocks were deposited west of or over an east-dipping subduction zone along the western American continental margin in late Mesozoic time. Some workers (Bailey and others, 1964; Dickinson,

¹University of Texas at Dallas.

1970) interpret the Great Valley sequence to have been deposited in an arc-trench gap, located to the east and upslope from the Franciscan trench. However, others (Blake and Jones, 1974) suggest that the trench was separated by an island arc from the basin in which sediments of the Great Valley sequence were deposited. Evidence for the existence of this hypothetical island arc has been controversial.

The complex depositional framework of the Franciscan assemblage is poorly understood. Most Franciscan strata are graywacke turbidites representing marine deposition on channelized parts of deep-sea fans or in associated submarine canyons. Pelagic limestones and cherts are present in small, but significant, amounts. These pelagic sedimentary rocks were deposited as siliceous and calcareous ooze on the tops and flanks of submarine volcanic highs or on distal abyssal plains in oceanic areas far from the influence of terrigenous sediment. Basaltic volcanic rocks of oceanic affinity are associated with the pelagic and terrigenous sedimentary rocks.

During late Mesozoic and early Tertiary time, Franciscan strata were deformed and metamorphosed along an east-dipping subduction zone formed at the continental margin (Blake and others, 1967; Ernst, 1970; Blake and Jones, 1974). During this eastward underthrusting, the Franciscan strata were concurrently overridden by oceanic crust depositionally overlain by strata of the Great Valley sequence. The more deeply subducted Franciscan rocks were metamorphosed to blueschist mineral assemblages and locally to greenschist and amphibolite assemblages (Platt, 1975). Rocks subducted to shallower depths were metamorphosed to pumpellyite, prehnite-pumpellyite, and laumontite assemblages (Blake and others, 1974; Blake and Jones, 1974). At the present time, Franciscan rocks are separated from the less deformed Great Valley sequence by serpentized ultramafic and related mafic rocks of the late Mesozoic ophiolitic ocean crust upon which Great Valley strata were originally deposited. The underthrusted lower contact between the ophiolite and Franciscan assemblage was named the "Coast Range thrust" by Bailey, Blake, and Jones (1970).

OPHIOLITE AND GREAT VALLEY SEQUENCE OF THE GEYSERS-CLEAR LAKE AREA

The regional distribution of the ophiolite that underlies the Great Valley sequence in the northern Coast Ranges is shown on figure 1. Its distribution within The Geysers-Clear Lake region, where it is highly deformed as the result of early Tertiary to late Quaternary folding, thrusting, and strike-slip faulting, is

shown in more detail on the geologic map (fig. 2) and on the cross sections (fig. 3) of the area. In parts of the area, this deformation has made recognition of the sole of the Coast Range thrust extremely difficult.

As a result of deformation of the ophiolite sheet in the upper plate of the Coast Range thrust, serpentinite crops out in numerous narrow, discontinuous linear belts entirely bounded by Franciscan rocks.

Most of these linear belts of serpentinite can either be traced into the ophiolite sheet or along shear zones that cut major masses of the ophiolite. These relations strongly suggest that most of the serpentinite bodies in this area were derived from the ophiolite sheet at the base of the Great Valley sequence by local down faulting of the ultramafic lower part of the ophiolite into underlying Franciscan rocks. Exceptions are a few serpentinite bodies having serpentine mineral assemblages of antigorite, talc, and actinolite that have higher temperature-pressure stability fields than the lizardite and chrysotile assemblages characterizing serpentinites in the ophiolite. Such higher temperature-pressure serpentinite mineral assemblages may characterize ultramafic rocks underthrust with the Franciscan assemblage beneath the Great Valley sequence. Downdropping of the ophiolite into underlying Franciscan rocks possibly resulted from folding together with lateral and vertical adjustment of subducted Franciscan slabs beneath the overlying ophiolite during the Cenozoic (fig. 3). Subsequent removal of the upper part of the ophiolite would then result in the linear pattern of serpentinite shown on the geologic map of The Geysers area (fig. 2).

Thick sections of mafic igneous rocks overlie the serpentized ultramafic part of the Coast Range ophiolite at the following three localities in The Geysers area: Harbin Springs, Mount St. Helena, and Geyser Peak. At each locality, the ophiolite sections are overlain by strata of the Great Valley sequence (fig. 2). The chemistry and petrology of the ophiolite sections at Harbin Springs and Mount St. Helena were previously studied by Bezore (1969); the section at Geyser Peak has not previously been described in detail. The main ophiolite sections at all three localities are schematically summarized by figure 4; for comparison, a composite of these sections is shown with a standard section of modern oceanic crust, as suggested by Ludwig, Nafe, and Drake (1970), on figure 4B.

The ophiolites of Harbin Springs and Mount St. Helena are nearly equivalent, although some difference in thickness of gabbro units is evident (fig. 4A). The Geyser Peak section differs significantly from the others in that it contains only a thin unit of ultramafic rock, a small amount of uralitized gabbro, and a thick unit

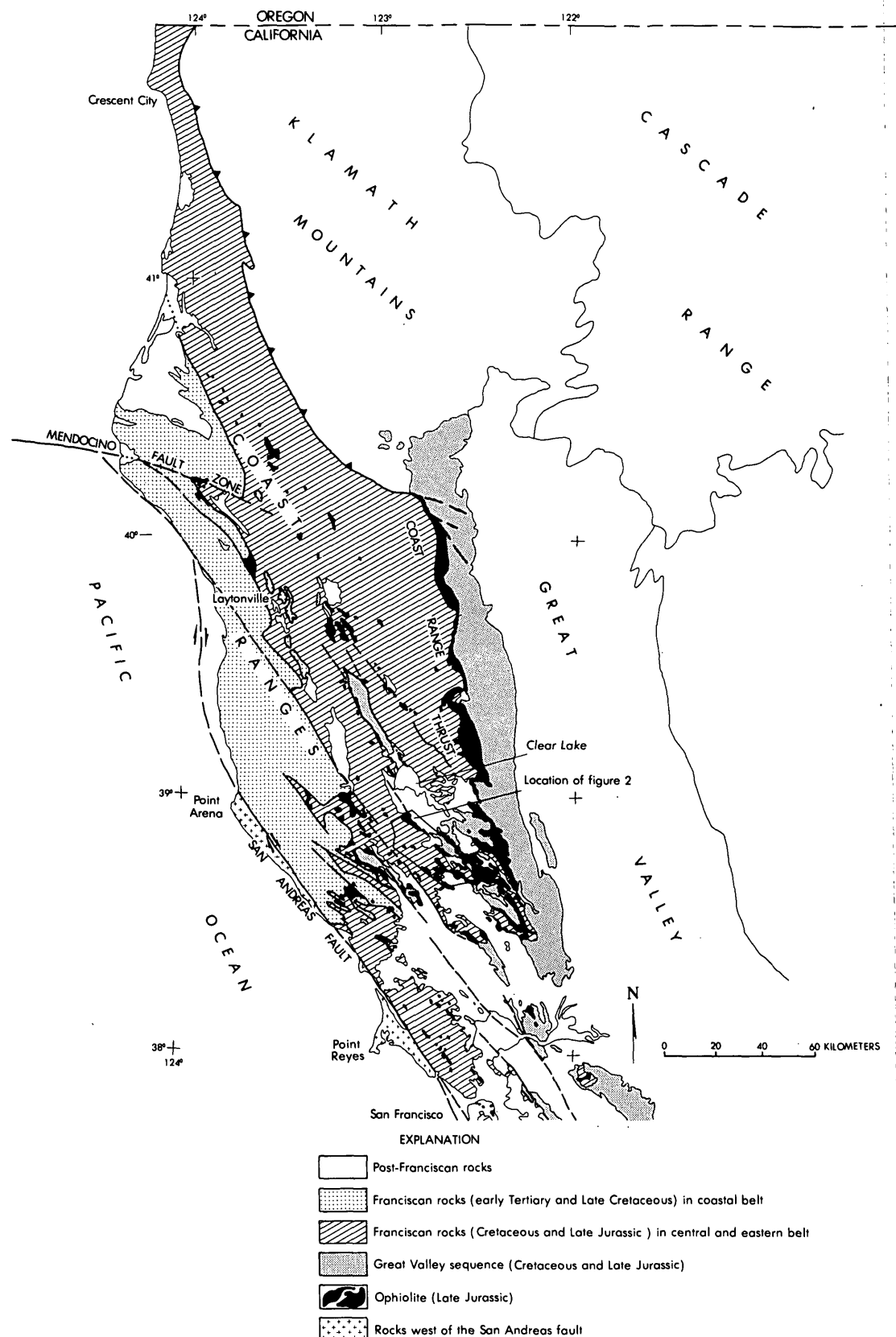


FIGURE 1.—Location of The Geyser-Clear Lake region in the northern California Coast Ranges, showing distribution of ophiolite at the base of the Great Valley sequence.

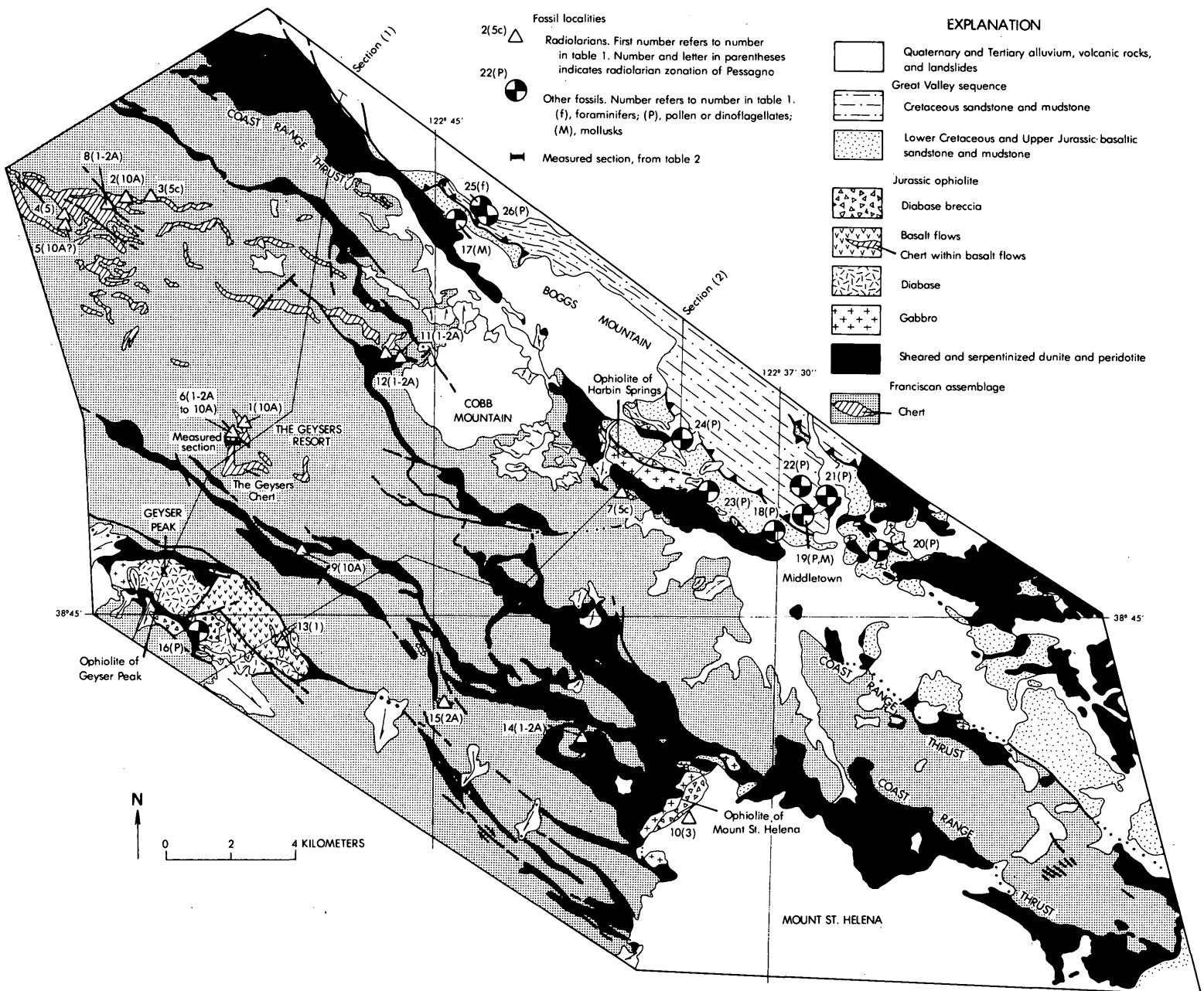


FIGURE 2.—Generalized geologic map of The Geysers area showing distribution of ophiolite and fossil localities.

of composite diabase sills overlain by basalt pillows and pillow breccia not present at the other two ophiolite localities.

Of particular significance is the presence at the top of the ophiolite at all three localities, and at a number of other localities in the Coast Ranges as far north as Paskenta, of a distinctive breccia composed largely of angular fragments of diabase, locally abundant glassy basalt, and, rarely, chert. The close association of the breccia locally with basaltic sandstone at the base of the Great Valley sequence, together with its persistence at the top of the ophiolite, resting locally upon dif-

ferent units, strongly suggests that this breccia is a sedimentary deposit (perhaps a talus accumulation) eroded from the top of the ophiolite. The comparative sections for Harbin Springs, Mount St. Helena, and Geyser Peak (fig. 4) suggest that at least the upper 1 km of ophiolite was eroded locally. Wagner (1975), in studying a similar breccia unit in the Pope Valley area about 20 km southeast of Middletown, came to similar conclusions as to its origin.

Differential erosion cannot account for all differences between the ophiolite section at Geyser Peak and those at Mount St. Helena and Harbin Springs. Cer-

RADIOOLARIAN ZONATION
FROM PESSAGNO (1977)

SERIES	STAGE	RADIOOLARIAN ZONATION			
		Zone	Subzone	Number	
Cretaceous	Maestrichtian	<i>Orbiculiforma renillaformis</i>			
	Campanian	<i>Patulibracchium dickinsoni</i>			
		<i>Crucella espartoensis</i>	<i>Phaseliforma carinata</i>	14C	
			<i>Patulibracchium lawsoni</i>	14B	
			<i>Protoxyphotracus perplexus</i>	14A	
	Santonian	<i>Alievium gallowayi</i>			
	Coniacian	<i>Alievium praegallowayi</i>	<i>Orbiculiforma vacaensis</i>	12B	
			<i>Archaeospongoprnum triplum</i>	12A	
	Turonian	<i>Alievium superbum</i>	<i>Archaeospongoprnum venadoensis</i>	11B	
			<i>Halesium sexangulum</i>	11A	
	Cenomanian	<i>Rotiforma hessi</i>	<i>Quinquecapsularia spinosa</i>	10B	
			<i>Cassideus riedeli</i>	10A	
		<i>Archaeospongoprnum tehamaensis</i>			
Lower Cretaceous	Albian	U	<i>Petasiforma foremanae</i>		
		L	<i>Kozurium zingulai</i>		
	Aptian	U	<i>Parvingula</i>	6	
		L			
	Barremian		<i>Thanarla conica</i>		
	Hauterivian		<i>Obesacapsula</i>	5	
	Valanginian	U			
		M			
	Berrriasian	L			
Upper Jurassic	Upper and Middle Tithonian		<i>Parvingula altissima</i>		
	Lower Tithonian		<i>Trilonche ordinaria</i> — <i>Parvingula hsui</i>		
	Lower Tithonian	<i>Emiluvia hopsoni</i>	<i>Mirifusus baileyi</i>	2B	
			<i>Mirifusus guadalupensis</i>	2A	
	Upper Kimmeridgian	<i>Parvingula</i> s.s.— <i>Emiluvia hopsoni</i>		1	
		<i>Eucrytidium(?) ptyctum</i> — <i>Parvingula</i> s.s.		0	

FIGURE 2.—Continued

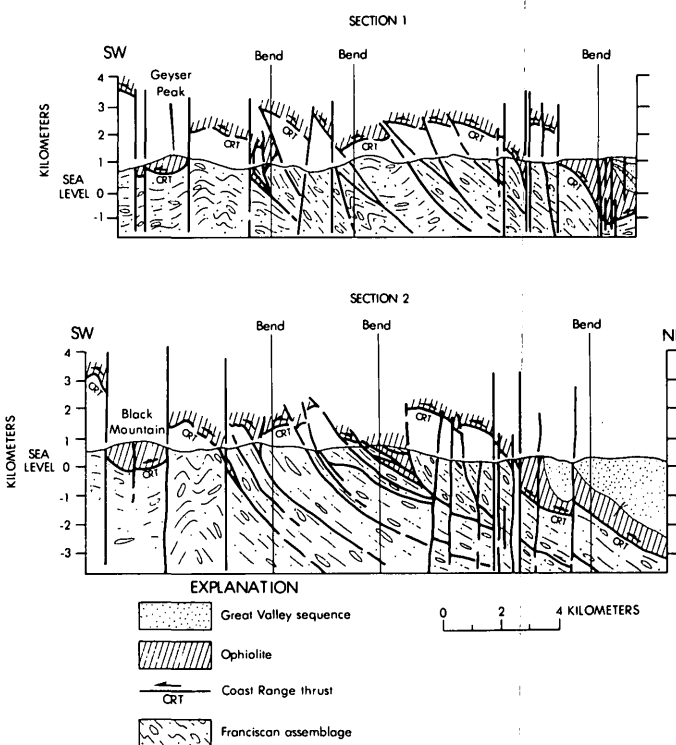


FIGURE 3.—Cross sections through The Geysers area, showing Cenozoic deformation of the Coast Range thrust of Bailey, Blake, and Jones (1970). Section lines are as indicated on fig. 2.

tainly much of the ultramafic section was cut out by faulting, and differences in thicknesses of gabbroic and basaltic rocks may be partly or wholly accounted for by faulting. Saleeby (1975) described an ophiolite in the western Sierra Nevada foothills of California that he interpreted to have been deformed by tectonic transport and progressive serpentinization. Serpentinization was thought to increase the mobility of the ultramafic lower part of the ophiolite, which then intruded and fragmented the overlying less mobile basaltic and gabbroic rocks, thereby distending the ophiolite section. A similar process may partly explain differences in composition and thickness of ophiolite sections in the northern Coast Ranges.

The Coast Range ophiolite has been dated in the northern Coast Ranges by potassium-argon methods (Lanphere, 1971) and to the south at Point Sal, Calif., by the uranium-lead method (Hopson and others, 1975). The potassium-argon dates on amphiboles associated with gabbro and peridotite and the uranium-lead dates on zircons in gabbroic parts of the ophiolite both indicate an age range of 150 to 160 million years.

Within the area of this study at Geyser Peak (fig. 2, loc. 11; table 1), a thin, discontinuous tuffaceous chert zone is present within basalt flows in the upper part of the ophiolite (fig. 4A). Well-preserved radiolarians

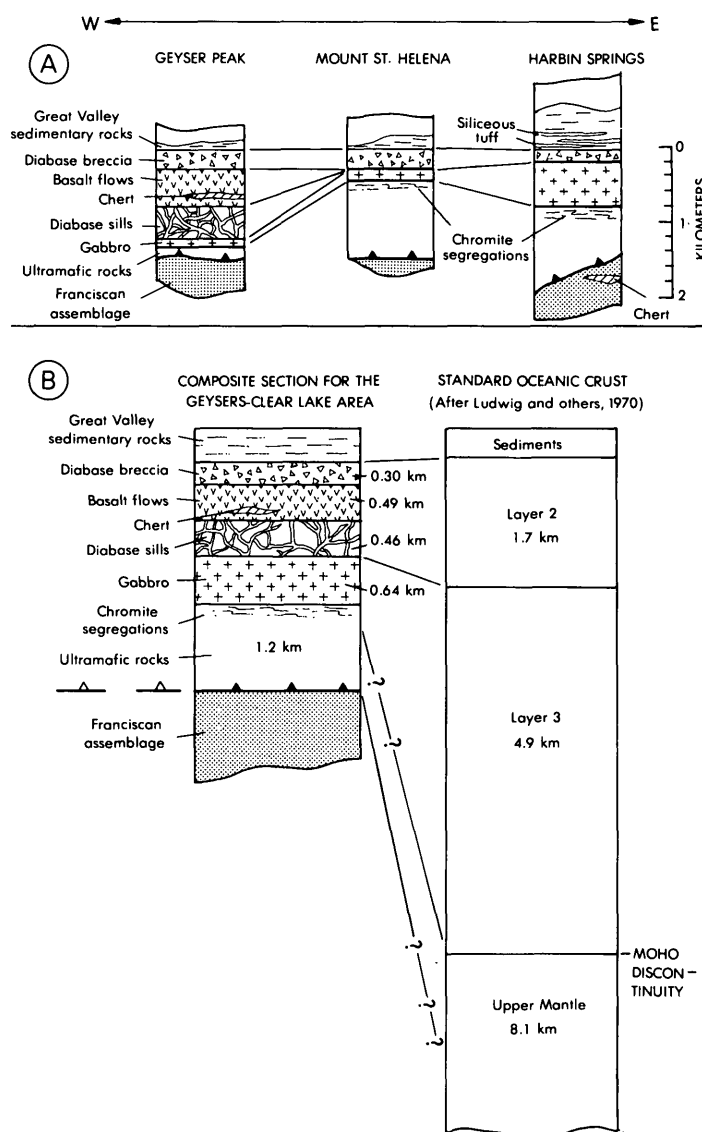


FIGURE 4.—Major ophiolite sections in The Geysers area compared with a standard section of oceanic crust. A, Ophiolite sections at Geyser Peak, Mount St. Helena, and Harbin Springs (localities shown on fig. 2). B, Composite of ophiolite sections on figure 4A compared with a standard section of oceanic crust. Modified from Ludwig, Nafe, and Drake (1970).

present in the thickest part of this chert are of late Kimmeridgian or early Tithonian age (Zone 1 of Pessagno, 1977). (The data of Van Hinte (1976, p. 493) and Pessagno (1977) indicate that the upper Kimmeridgian should now be included in the lower Tithonian. The Tithonian as defined in this fashion would be equivalent to the Russian Volgian.) There are no reliable absolute ages for the Kimmeridgian and Tithonian Stages of the Jurassic (see, for instance, Van Hinte, 1976; Van Eysinga, 1975). From the available data, we can say only that the middle and

upper parts of the Coast Range ophiolite (excluding structurally lower sheared ultramafic rocks) formed some time between 160 m.y. ago and early Tithonian time.

Strata of the Great Valley sequence depositionally above the ophiolite contain *Buchia piocchii* (Swe and Dickinson, 1970; fig. 2, loc. 17, and table 2) and are, therefore, assignable, in part, to the middle and upper Tithonian (Zone 4 of Pessagno, 1977). At Mount St. Helena, radiolarians (fig. 2, loc. 10) in calcareous mudstone approximately 76 m stratigraphically above the diabase breccia are of early Tithonian age (Zone 3 of Pessagno, 1977). The age of the breccia at the top of the ophiolite must therefore be early Tithonian (Zones 1-3).

These age relations indicate that, briefly during the late Kimmeridgian or early Tithonian, pelagic sediments and volcanic tephra were deposited between extrusions of submarine basalt, perhaps along the crest of a submarine ridge, to form tuffaceous radiolarian chert. Somewhat later in early Tithonian time, the ophiolite underwent submarine erosion that locally removed as much as 1 km of the upper part of the section. The material now present as diabase and basalt breccia may represent talus or rubble accumulations around eroded submarine highs. The presence of this coarse ophiolite detritus at the base of the Great Valley sequence implies the existence of a major western source for Great Valley sediment during Late Jurassic time.

FRANCISCAN ROCKS STRUCTURALLY BELOW OPHIOLITE

Subducted Franciscan rocks structurally below the Great Valley sequence and Coast Range thrust in this area consist of a series of northeast- to southeast-dipping slabs of graywacke, basaltic volcanic rock, and chert separated by units of melange and (or) sheared serpentinite (McLaughlin and Stanley, 1976; McLaughlin, 1974, 1975). These rocks are largely unfossiliferous, except for abundant radiolarians in cherts. The age of the radiolarian assemblage occurring in the various chert bodies varies considerably (fig. 2, table 1). Most localities contain radiolarians assignable to the late Kimmeridgian or early Tithonian (subzone 1-2A). At some localities, including one where a prominent chert lens lies structurally below the ophiolite of Harbin Springs (loc. 7), the radiolarians are of Early Cretaceous (late Valanginian, subzone 5C) age. At several localities, Late Cretaceous (early Cenomanian, subzone 10A) radiolarian faunas are present. These early Cenomanian faunas were earlier considered to be Early Cretaceous (Hauterivian) by McLaughlin

TABLE 1.—List of Radiolaria localities

Map No. on figure 2	Formation	Location ¹	Age
1	Franciscan assemblage.	457.5 m E, 366 m S, NW cor. sec. 23 T. 11 N., R. 9 W.	Late Cretaceous (early Cenomanian, subzone 10A).
2	— do —	793 m S, 762.5 m W, NE cor. sec. 28 T. 12 N., R. 9 W.	Do.
3	— do —	732 m S, 152.5 m W, NE cor. sec. 28 T. 12 N., R. 9 W.	Early Cretaceous (late Valanginian, subzone 5C).
4	— do —	533.8 m N, 152.5 m W, SE cor. sec. 30 T. 12 N., R. 9 W.	Early Cretaceous (Berriasian and Valanginian, zone 5).
5	— do —	518.5 m N, 152.5 m W, SE cor. sec. 30 T. 12 N., R. 9 W.	Questionably Late Cretaceous (early Cenomanian, subzone 10A?).
6	— do —	610 m S, 137.3 m E, NW cor. sec. 13 T. 11 n., R. 9 W.	Late Jurassic (late Kimmeridgian and early Tithonian, subzone 1-2A) to Late Cretaceous (early Cenomanian subzone 10A).
7	— do —	274.5 m E, 213.5 m S, NW cor. sec. 30 T. 11 N., R. 9 W.	Early Cretaceous (late Valanginian, subzone 5C).
8	— do —	579.5 m S, 152.5 m W, NE cor. sec. 29 T. 12 N., R. 9 W.	Late Jurassic (late Kimmeridgian and early Tithonian, subzone 1-2A).
9	— do —	289.8 m S, 640.5 m E, NW cor. sec. 31 T. 11 N., R. 8 W.	Late Cretaceous (early Cenomanian, subzone 10A).
10	Great Valley sequence.	701.5 m N, 793 m W, SE cor. sec. 20 T. 10 N., R. 7 W.	Late Jurassic (early Tithonian, zone 3).
11	Franciscan assemblage.	579.5 m N, 690.5 m E, SW cor. sec. 8 T. 11 N., R. 8 W.	Late Jurassic (late Kimmeridgian and early Tithonian, subzone 1-2A).
12	— do —	579.5 m N, 503.3 m E, SW cor. sec. 8 T. 11 N., R. 8 W.	Do.
13	Ophiolite of Geyser Peak.	732 m S, 457.5 m W, NE cor. sec. 1 T. 10 N., R. 9 W.	Late Jurassic (late Kimmeridgian or early Tithonian, zone 1).
14	Franciscan assemblage.	762.5 m E, 579.5 m S, NW cor. sec. 13 T. 10 N., R. 8 W.	Late Jurassic (late Kimmeridgian and early Tithonian, subzone 1-2A).
15	— do —	671 m N, 335.5 m W, SE cor. sec. 9 T. 10 N., R. 8 W.	Late Jurassic (late Kimmeridgian and early Tithonian, subzone 2A).

¹ Location data originally given in feet and miles, are converted to metric units in accordance with the system adopted by the U.S. Geological Survey.

(1976) and McLaughlin and Stanley (1976); samples from a detailed measured section near The Geysers Resort now indicate a Late Cretaceous (Cenomanian) age. An early Cenomanian fauna was extracted from a chert clast enclosed in locally conglomeratic graywacke (loc. 9), indicating that these cherty graywacke units are early Cenomanian or younger in age and that

detritus in these graywackes was probably, in part, locally derived from older Franciscan cherts.

The Geysers chert

The most completely studied Franciscan chert in the area (loc. 6) forms a lens, 67.4 m thick, that crops out in a roadcut 1.1 km northwest of The Geysers Resort

TABLE 2.—List of other fossil localities

Map No. on figure 2	Formation	Location ¹	Fossils	Age	Identified by	Reference
16	Great Valley sequence.	1373 m W, 1190 m N, SE cor. sec. 2 T. 10 N., R. 9 W.	Dinoflagellate fragments.	Early Cretaceous?	W.R. Evitt	Written commun., 1973.
17	-- do --	915 m N, 640.5 m E, SE cor. sec. 28 T. 12 N., R. 8 W.	Mollusks (<i>Bucania piochii</i>).	Late Jurassic (middle Tithonian).	D.L. Jones	Oral commun., 1976.
18	-- do --	0.3 km slightly west of N from Harbin Springs-Big Canyon road junction	Dinoflagellates	Early Cretaceous or Late Jurassic.	W.R. Evitt	Swe, 1968.
19	-- do --	1.01 km N from Harbin Springs-Big Canyon road junction	Pollen, mollusks	Late Cretaceous	W.R. Evitt A.M. Keen	Do.
20	-- do --	2.7 km N of junction, Hwy 53 and Hwy 29, along Hwy 53	Dinoflagellates	Late Jurassic	W.R. Evitt	Do.
21	-- do --	0.4 km upstream on Harbin Creek from junction of Harbin and Putah Creeks, 3.2 km N of Middletown	Pollen	Early Cretaceous (Aptian?).	-- do --	Do.
22	-- do --	2.1 km N of Harbin Springs-Big Canyon road junction	Pollen, dinoflagellates.	Late Cretaceous	-- do --	Do.
23	-- do --	0.16 km SW from NE cor. sec. 29 in Creek, T. 11 N., R. 7 W.	Dinoflagellates	Early Cretaceous (Berriasian and Valanginian).	-- do --	Do.
24	-- do --	0.16 km E from SW cor. sec. 17 T. 11 N., R. 7 W.	Pollen, dinoflagellates.	Early Cretaceous or Upper Jurassic.	-- do --	Do.
25	-- do --	0.08 km E, 1.05 km N, SW cor. sec. 27, T. 11 N., R. 8 W. on Harrington Flat Road	Foraminifers	Late Cretaceous (Campanian).	W. Sliter	Oral commun., 1976.
26	-- do --	0.16 km E, 0.68 km S, NW cor. sec. 27, T. 12 N., R. 8 W.	Pollen, dinoflagellates.	Late Cretaceous	W.R. Evitt	Swe, 1968.

¹ Location data originally given in feet and miles, are converted to metric units in accordance with the system adopted by the U.S. Geological Survey.

and is traceable for more than 2 km along its strike. The chert, herein informally designated "The Geysers chert," depositionally overlies pillow basalt and is overlain by hydrothermally bleached and sheared graywacke. A Late Jurassic to Late Cretaceous age is assigned to this chert on the basis of the radiolarians in samples collected in 1974 by Pessagno and McLaughlin and subsequent resamplings in 1975 and 1976. A measured section of The Geysers chert is presented in table 3.

Two major zones of recrystallization in The Geysers chert that yielded no dateable radiolarians are subject to interpretation. A lower zone of recrystallization at 40.4–51.1 m separates the lower Tithonian from the upper Valanginian part of the chert in the measured section (table 3) and might conceivably represent in-place recrystallization of the missing upper Tithonian, Berriasian, and lower Valanginian. It is also possible

that part of the Lower Cretaceous section is cut out along a bedding-plane fault within the recrystallized zone because there is no evidence of erosion or reworking of the chert across this Tithonian to Valanginian break.

An upper zone of recrystallization between 63.9 and 65.9 m from the base separates the upper Valanginian from the lower Cenomanian part of the chert (table 3). This zone may represent a condensation of the missing Hauterivian, Aptian, and Albian Stages of the Lower Cretaceous. The presence in the overlying Cenomanian beds of numerous reworked Valanginian radiolarians, however, suggests the presence of an upper Valanginian to lower Cenomanian unconformity.

The Mesozoic absolute time scale is reliably correlated with the chronostratigraphic scale only in the Upper Cretaceous. Through radiometric dating of bentonites occurring in strata bearing ammonites, it

TABLE 3.—*Measured section of The Geyser chert near The Geysers Resort, Sonoma County, Calif.*
 [Section measured by R. J. McLaughlin and H. N. Ohlin, September 1976.]

Measured interval (in meters)	Series	Stage	Radiolarian subzone	Lithology
Top of section 65.9 - 67.4±	Upper Cretaceous	Lower Cenomanian	10A	Contact with graywacke. White to gray, impure porcelaneous chert with reworked Valanginian radiolarians intersheared with hydrothermally bleached graywacke.
63.9 - 65.9	-----	Indeterminate (Unconformity?)	-----	Zone of recrystallization. Green to white chert, extensively recrystallized, partly covered by slope wash and faulted in region of fold hinge.
51.1 - 63.9	Lower Cretaceous	Upper Valanginian	5C	Blue-green, gray, and black chert, massive to bedded, with sporadic gray to gray-green porcelaneous shale partings to 96 mm thick. Displays sporadic differential recrystallization.
40.4 - 51.1	-----	Indeterminate	-----	Zone of recrystallization. Light-green to white chert, extensively recrystallized, and devoid of shale partings.
32.8 - 40.4	-----	-----	-----	Predominantly green-blue to white chert, in beds to 96 mm thick; blue-green shale partings to 36 mm thick.
20.7 - 32.8	Upper Jurassic	Lower Tithonian to upper Kimmeridgian.	1-2A	Predominantly green-blue to white chert with red mottling. Chert in beds to 96 mm thick; red shale partings to 24 mm thick.
0 - 20.7	-----	-----	-----	Red to blue-green chert, grading upward from red chert at base to mottled red and green chert; chert in beds as thick as 84 mm, with red shale partings to 24 mm thick.
Base of chert	-----	-----	-----	Contact with locally pillowved basaltic volcanic rocks.

has been possible to relate many Upper Cretaceous stages to the absolute time scale (Lanphere and Jones, 1977). Unfortunately, an integration of chronologic, chronostratigraphic, and biostratigraphic data is lacking for most of the Lower Cretaceous and Jurassic; only the following horizons can be accurately dated (from Lanphere and Jones, 1977) :

1. Base of Cenomanian (Upper Cretaceous)—96 m.y. (five radiometric dates),
2. Base of the Hauterivian—134 m.y. (four radiometric dates),
3. Upper part of the Valanginian— 137 ± 5 m.y. (one radiometric date), and
4. The Jurassic-Cretaceous boundary is estimated, on a consensus of meager existing data, to be 138 ± 3 m.y.

These data suggest that the upper 16.3 m of The Geysers chert containing late Valanginian and early Cenomanian radiolarians, represents approximately 41 m.y. (see table 3). The implied hiatus in pelagic sedimentation between late Valanginian and early Cenomanian time appears to be 38 m.y. A substantial

amount of time is probably represented in the underlying 40.4 m of upper Kimmeridgian or lower Tithonian chert, but the durations of Jurassic stages are so poorly defined at present that speculations on this part of the time scale may be highly inaccurate. A crude estimate of pelagic sediment accumulation rates for the 12.8 m of upper Valanginian chert in this section can be made by assuming from these data that the upper Valanginian part of the chert represents the interval 137–134 m.y. ago (base of the Hauterivian Stage), a total of about 3 m.y. The rate of at least 12.8 m in 3 m.y. is equivalent to a minimum pelagic sediment accumulation rate of the order of 0.43 centimeter per 1000 years, disregarding the probable effects of post-depositional compaction and dewatering of the sediment.

From drilling in the modern oceans, rates of pelagic sedimentation have been determined for red clays and oozes composed of radiolarians, diatoms, and globigerinids. The rates range from 0.0 to 9.0 cm/1000 yr (Dietrich, 1963; Heath, 1974; Hays, 1971; Hays and Opdyke, 1967; Hamilton, 1967; von Huene and Kulm, 1971; Scholl and Creager, 1973; and Berger, 1974); the most common rates are 0.2–0.4 cm/1000 yr. The es-

timated minimum sedimentation rate of 0.43 cm/1000 yr for the Valanginian part of The Geysers chert is consistent with these observed modern pelagic sedimentation rates.

Other pelagic Franciscan rocks

Franciscan rocks of early Cenomanian age are present at other places in the Coast Ranges, notably in melanges to the north and west of The Geysers-Clear Lake area. Discontinuous pods of pink to gray limestone cropping out in a melange north of Laytonville contain Cenomanian to Turonian and possibly Coniacian planktonic foraminifers (Gucwa, 1975; Wachs and Hein, 1975; Bailey and others, 1964). Another limestone of similar age, associated with locally pillowed basaltic flows and diabase, extends from an area west of Montara Mountain on the San Francisco peninsula southward to the vicinity of San Juan Bautista.

These limestone occurrences probably indicate areas of midocean carbonate deposition above the carbonate compensation depth and may thereby delineate the former presence of midocean topographic rises during Cenomanian and Turonian times. Rocks of Late Cretaceous and early Tertiary age in the Franciscan coastal belt (Evitt and Pierce, 1975) are in tectonic contact with older Franciscan rocks west of Laytonville.

CONSTRAINTS ON SUBDUCTION MODELS

The large time interval spanned by the 67.4 m-thick chert unit near The Geysers Resort places constraints on timing of subduction of Franciscan rocks in this area critical to the validity of currently disputed models of Franciscan subduction. It is clear from the biostratigraphic and structural data that the youngest Franciscan rocks beneath the Coast Range thrust in The Geysers area are of Late Cretaceous age and are, therefore, much younger than either the structurally overlying Coast Range ophiolite or the basal strata of the Great Valley sequence. These Late Cretaceous Franciscan rocks include, along with the dated cherts, sandstones metamorphosed to pumpellyite grade and locally to lawsonite grade (McLaughlin, 1975; McLaughlin and Stanley, 1976). Northeast of, and also within, The Geysers-Clear Lake area are metacherts, which are too highly metamorphosed to be dated paleontologically, associated with intact terranes of lawsonite and jadeite-grade metasandstone and metavolcanic rocks. These jadeite and lawsonite-bearing Franciscan rocks are thought to have undergone high-pressure metamorphism to blueschist in a subduction zone prior to Late Cretaceous time (Suppe and Armstrong, 1972; Lanphere and others, 1975; McLaughlin,

1975). For The Geysers area to have received pelagic sedimentation during the same time interval that active underthrusting and blueschist metamorphism occurred deep in an east-dipping subduction zone requires The Geysers to be situated far to the west-northwest or south-southwest of the subduction site. Alternatively, The Geysers area at that time may have been part of the upper plate of the Coast Range thrust, and the site of underthrusting might have been to the west-northwest or south-southwest. This reconstruction would require that subduction jump east of the The Geysers-Clear Lake area during post-early Cenomanian time.

Franciscan pelagic strata, including cherts and limestones, in the Coast Ranges are more than 95 percent by volume late Kimmeridgian to early Tithonian (sub-zone 1-2A) in age; the total volume of pelagic sediment in the Franciscan assemblage is proportionately very small. Early Cenomanian chert of the Franciscan assemblage, where examined in The Geysers-Clear Lake area, is associated with, or deposited at the top of, early Tithonian and late Valanginian cherts. Nowhere does the Cenomanian chert rest directly on basalt. If pelagic Franciscan strata were deposited on basaltic ocean crust that formed from sea-floor spreading throughout Late Jurassic to Late Cretaceous time, then a representative record of pelagic strata deposited directly upon basalt and spanning Late Jurassic to Late Cretaceous time would be expected. The chert data, however, suggest that east-directed sea-floor spreading was in fact extremely slow or inactive between late Valanginian and early Cenomanian time, a conclusion that is contradictory to previous studies indicating appreciable blueschist metamorphism and, by implication, subduction of other Franciscan strata during this interval (Suppe and Armstrong, 1972; Lanphere and others, 1975).

The notable absence of pelagic strata of post-Valanginian age except for the rare Upper Cretaceous limestones and cherts that are mostly in contact with older pelagic strata strongly suggests that if appreciable sea-floor spreading did occur during middle Cretaceous time, then such spreading was independent of the crust upon which Franciscan pelagic strata were deposited. Clearly, a model of Late Jurassic to Late Cretaceous west-stepping subduction is too simplistic to explain the time-space distribution of pelagic strata in the Franciscan assemblage.

Jones, Silberling, and Hillhouse (1978) have recently cast some doubt on tectonic models assuming that late Mesozoic sediments deposited along the western North American continental margin were subducted directly eastward. These workers present pale-

ontologic and paleomagnetic data indicating that a large allochthonous terrane of Triassic volcanic and sedimentary rocks, traced from Vancouver Island, British Columbia, to south-central Alaska, called Wrangellia, formed at low equatorial paleolatitudes. They suggest displacement of Wrangellia nearly 30° northward, implying large right-lateral motion and (or) oblique underthrusting between Wrangellia and the North American craton. By this model, suturing of Wrangellia to the craton would have occurred in eastern Oregon during Late Jurassic time (Jones and others, 1978). No paleomagnetic evidence for large-scale right-lateral motion between the upper plate Great Valley sequence and the lower plate Franciscan assemblage exists, but the possibility of such motion cannot be discounted in light of the data presented.

The relations shown indicate that Franciscan rocks in The Geysers-Clear Lake area could at no time have been in depositional contact with strata of the structurally overlying Great Valley sequence as suggested by Maxwell (1974). It is apparent that basal strata of the Great Valley sequence are significantly older than the youngest Franciscan rocks below the Coast Range ophiolite and that the Franciscan rocks were probably separated from Great Valley strata by many tens to hundreds of kilometers at the time of deposition.

CONCLUSIONS

We have demonstrated the age and structural relations of rock units above, below, and within the ophiolite sheet that regionally overlies the Franciscan assemblage in the northern California Coast Ranges. From these relations, the following conclusions are drawn:

The middle and upper part of the Coast Range ophiolite in The Geysers-Clear Lake region formed prior to and during early Tithonian time. The ophiolite underwent submarine erosion later in early Tithonian time, when as much as 1 km of the upper part of the ophiolite was locally stripped off. This erosion contributed coarse mafic debris to basal strata of the Great Valley sequence.

Radiolarian chert ages and structural relations in The Geysers-Clear Lake area clearly demonstrate that the Franciscan assemblage is younger than the structurally overlying Coast Range ophiolite and, in part, younger than basal strata of the Great Valley sequence that depositionally overlies the ophiolite. This relation necessitates a plate tectonic model for emplacement of the Franciscan beneath the Coast Range ophiolite. The available data do not support deposition of the Great Valley sequence on Franciscan rocks

in the Clear Lake region as suggested by Maxwell (1974). In fact, a model requiring large-scale original horizontal separation between pelagic sediments of the Franciscan assemblage and the Great Valley sequence seems mandatory. Pelagic sediments represented by The Geysers chert could not have been situated on a subducting oceanic plate near any active subduction zone during deposition because at least 41 m.y. elapsed before these sediments were thrust beneath ophiolite and the Great Valley sequence in post-early Cenomanian time. The chert data suggest that The Geysers area may have been part of the upper plate of the Coast Range thrust until post-early Cenomanian time.

The discovery of discrete chert units representing Late Jurassic to Late Cretaceous pelagic sedimentation in the Franciscan assemblage allows a correlation with coeval planktonic carbonate sedimentation in Franciscan terranes to the north and west of The Geysers-Clear Lake region. This correlation suggests the existence during Cenomanian time of significant submarine relief. Carbonate sedimentation occurred on submarine highs above the carbonate compensation depth. Pelagic deposition in The Geysers area occurred in deeper water below the carbonate compensation depth, perhaps along the flanks of or on top of, less elevated rises or on an abyssal plain.

REFERENCES CITED

- Bailey, E. H., Blake, M. C. Jr., and Jones, D. L., 1970, On-land Mesozoic oceanic crust in California Coast Ranges, in Geological Survey research, 1970: U.S. Geol. Survey Prof. Paper 700-C, p. C70-C81.
- Bailey, E. H., Irwin, W. P., and Jones, D. L., 1964, Franciscan and related rocks and their significance in the geology of western California: California Div. Mines and Geology, Bull. 183, 177 p.
- Berger, W. H., 1974, Deep sea sedimentation, in Burk, C. A., and Drake, C. L., eds., The geology of continental margins; New York, Springer-Verlag, p. 213-241.
- Berkland, J. O., Raymond, L. A., Cramer, J. C., Moores, E. M., and O'Day, M., 1972, What is Franciscan?: Am. Assoc. Petroleum Geologists Bull., v. 56, p. 2295-2302.
- Bezore, S. P., 1969, The Mount St. Helena ultramafic complex of the northern California Coast Ranges: Geol. Soc. of America Abs. with Programs, v. 1, no. 3, p. 5.
- Blake, M. C., Jr., and Irwin, W. P., and Coleman, R. G., 1967, Upsidedown metamorphic zonation, blueschist facies, along a regional thrust in California and Oregon, in Geological Survey research, 1967: U.S. Geol. Survey Prof. Paper 575-C, p. C1-C9.
- Blake, M. C., Jr., and Jones, D. L., 1974, Origin of Franciscan melanges in northern California: Soc. Econ. Paleontologists and Mineralogists, Spec. Pub. 19, p. 345-357.
- Blake, M. C., Jr., Jones, D. L., and Landis, C. A., 1974, Active continental margins; contrasts between California and New Zealand, in Burk, C. A., and Drake, C. L., eds., The geology of continental margins: New York, Springer Verlag, p. 853-872.

- Dickinson, W. R., 1970, Clastic sedimentary sequence deposited in shelf, slope, and trough settings between magmatic arcs and associated trenches: *Pacific Geology*, v. 3, p. 15-30.
- Dietrich, G., 1963, General oceanography, an introduction: New York, John Wiley & Sons, p. 19-24.
- Ernst, W. G., 1970, Tectonic contact between the Franciscan melange and the Great Valley sequence-crustal expression of a Late Mesozoic Benioff zone: *Jour. Geophys. Research*, v. 75, p. 886-902.
- Evitt, W. R., and Pierce, S. T., 1975, Early Tertiary ages from the coastal belt of the Franciscan Complex, northern California: *Geology*, v. 3, p. 433-437.
- Gucwa, P. R., 1975, Middle to Late Cretaceous sedimentary melange, Franciscan complex, northern California: *Geology*, v. 3, p. 105-108.
- Hamilton, E. L., 1967, Marine geology of abyssal plains in the Gulf of Alaska: *Jour. Geophys. Research*, v. 72, p. 4208-4210.
- Hays, J. D., 1971, Faunal extinctions and reversals of the earth's magnetic field: *Geol. Soc. America Bull.*, v. 82, p. 2433-2447.
- Hays, J. D., and Opdyke, N. D., 1967, Antarctic radiolaria, magnetic reversals, and climatic change: *Science*, v. 158, p. 1003-1004.
- Heath, G. R., 1974, Dissolved silica and deep sea sediments, in Hay, W. W., ed., *Geologic history of the oceans*: Soc. Econ. Paleontologists and Mineralogists, Spec. Pub. 20, p. 88.
- Hopson, C. A., Mattinson, J. M., and Pessagno, E. A., Jr., 1975, Record of Late Jurassic sea-floor spreading, California Coast Ranges: *Geol. Soc. America Abs. with Programs*, v. 7, no. 3, p. 326.
- Jones, D. L., Silberling, N. J., and Hillhouse, John, 1978, Wrangellia—A displaced continental block in northwestern North America: *Canadian Jour. Earth Sci.* (In press.)
- Lanphere, M. A., 1971, Age of the Mesozoic oceanic crust in the California Coast Ranges: *Geol. Soc. America Bull.*, v. 82, p. 3209-3212.
- Lanphere, M. A., Blake, M. C., Jr., and Irwin, W. P., 1975, Early Cretaceous metamorphic age of the South Fork Mountain Schist in the northern Coast Ranges of California: *Geol. Soc. America Abs. with Programs*, v. 7, no. 3, p. 340.
- Lanphere, M. A., and Jones, D. L., 1978, Cretaceous time scale from North America: *Am. Assoc. Petroleum Geologists*. (In press.)
- Ludwig, W. J., Nafe, J. E., and Drake, C. L., 1970, Seismic refraction, in Maxwell, A. E., ed., *The sea*: New York, Interscience, v. 4, pt. 1, p. 53-84.
- Maxwell, J. C., 1974, Anatomy of an orogen: *Geol. Soc. America Bull.*, v. 85, p. 1195-1204.
- McLaughlin, R. J., 1974, Preliminary geologic map of The Geysers steam field and vicinity, Sonoma County, California: U.S. Geol. Survey Open-File Rept. 74-238.
- , 1975, Structure of Franciscan rocks in the central Mayacamas Mountains, Sonoma and Lake Counties, California: *Geol. Soc. America Abs. with Programs*, v. 7, no. 3, p. 345.
- , 1976, Significance of age relationships above and below Upper Jurassic ophiolite in The Geyser-Clear Lake region, California: *Geol. Soc. America Abs. with Programs*, v. 8, no. 3, p. 394.
- McLaughlin, R. J., and Stanley, W. D., 1976, Pre-Tertiary geology and structural control of geothermal resources, The Geysers steam field, California: United Nations symposium on development and use of geothermal resources, 2d Proc., San Francisco, v. 1, p. 475-485.
- Pessagno, E. A., Jr., and Newport, R. L., 1972, A technique for extracting radiolaria from radiolarian cherts: *Micro-paleontology*, v. 18, no. 2, p. 231-234.
- , 1977, Lower Cretaceous radiolarian biostratigraphy of the Great Valley sequence and Franciscan complex, California Coast Ranges: Cushman Found. for Foraminiferal Research, Spec. Pub. 15, 87 p.
- Platt, J. P., 1975, Metamorphic and deformational processes in the Franciscan complex, California—Some insights from the Catalina schist terrane: *Geol. Soc. America Bull.*, v. 86, p. 1337-1347.
- Saleeby, Jason, 1975, Breaking and mixing of Permian oceanic lithosphere-southwestern Sierra Nevada foothills, California: *Geol. Soc. America Abs. with Programs*, v. 7, no. 7, p. 1256.
- Scholl, D. W., and Creager, J. S., 1973, Geologic synthesis of Leg 19: Reports Deep Sea Drilling Project, v. 19, p. 900-902.
- Suppe, John, and Armstrong, R. L., 1972, Potassium-argon dating of Franciscan metamorphic rocks: *Am. Jour. Sci.*, v. 272, p. 217-233.
- Swe, Win, 1968, Stratigraphy and structure of Late Mesozoic rocks south and southeast of Clear Lake, California: Stanford Univ., Ph.D. thesis, 76 p.
- Swe, Win, and Dickinson, W. R., 1970, Sedimentation and thrusting of Late Mesozoic rocks in the Coast Ranges near Clear Lake, California: *Geol. Soc. American Bull.*, v. 81, p. 165-188.
- Van Eysinga, F. W. B., 1975, Geological time table (3d ed.): Elsevier Pub. Co.
- Van Hinte, J. E., 1976 A Jurassic time scale: *Am. Assoc. Petroleum Geologists Bull.*, v. 60, p. 489-497.
- Von Huene, Roland, and Kulm, L. V., 1971, Tectonic summary of Leg 18: Initial Reports Deep Sea Drilling Project, v. 18, p. 966-969.
- Wachs, D., and Hein, J. R., 1975, Franciscan limestones and their environments of deposition: *Geology*, v. 3, p. 29-33.
- Wagner, D. L., 1975, Mesozoic geology of the Walter Springs area, Napa County, California: San Jose State Univ., San Jose, Calif., M.S. thesis, 68 p.

AGE AND COMPOSITION OF IGNEOUS ROCKS, EDNA MOUNTAIN QUADRANGLE, HUMBOLDT COUNTY, NEVADA

By RALPH L. ERICKSON, MILES L. SILBERMAN, and S. P. MARSH,
Denver, Colo.; Menlo Park, Calif.; Denver, Colo.

Abstract.—Six pulses of igneous activity ranging in age from Jurassic to Pliocene have been identified in the Edna Mountain quadrangle, Humboldt County, Nev. Porphyritic syenite and quartz monzonite of Jurassic age (146–164 million years) at Buffalo Mountain are highly potassic through a wide range in SiO₂ content from olivine-bearing syenite to quartz-rich monzonite, and their composition contrasts sharply with plutons elsewhere in north-central Nevada. Granodiorite and quartz monzonite plutons of Cretaceous age (88–106 m.y.) are chemically and mineralogically similar to other calc-alkaline plutons in north-central Nevada.

Four episodes of Tertiary volcanism include rhyolite ash-flow tuffs and slightly younger andesitic basalt flows and tuffs of Oligocene age, rhyolite vitrophyre of late Miocene age, and olivine basalt flows of Pliocene age. Their age and mineralogical and chemical compositions are similar to other Tertiary volcanic rocks in north-central Nevada.

Six pulses of igneous activity were identified during the course of geological and geochemical studies of the Edna Mountain 15-minute quadrangle, Humboldt County, Nev. (Erickson and Marsh, 1974a, b; Marsh and Erickson, 1977, 1978). All of these pulses fit well into the timetable established for igneous activity elsewhere in north-central Nevada (McKee and Silberman, 1970; Silberman and McKee, 1971). Granitic rocks were emplaced during two pulses: Jurassic (146–164 million years) at Buffalo Mountain and Cretaceous (88–106 m.y.) at Edna Mountain and the northeast end of Buffalo Mountain (fig. 1, table 1). Tertiary volcanic rocks were deposited in four pulses (fig. 1, table 1). Rhyolite ash-flow tuffs in the Goldrun Creek 7½-minute quadrangle are the oldest dated volcanic rocks in the study area (24.2–25.9 m.y.). Andesitic basalt and tuffs in the Golconda 7½-minute quadrangle are only slightly younger (23–24 m.y.) than the rhyolite ash-flow tuffs, but they are unrelated compositionally and have a different source. After an apparent hiatus in igneous activity marked by highland erosion and deposition of thick alluvial fans of boulder gravel, a thin blanket of rhyolite vitrophyre of late Miocene age (approximately 14.5 m.y.) was

deposited in the southwestern part of the Goldrun Creek quadrangle. Only thin remnants and large isolated float blocks of rhyolite vitrophyre have been preserved on the top of the actively eroding gravel fans of Tertiary age. The youngest recognized igneous activity was the extrusion of olivine basalt flows about 5 m.y. ago.

Sedimentary rocks in the area range in age from Cambrian to Permian and include near-shore, transitional, and deep-basin clastic rocks telescoped by thrust faults related to at least four different orogenic episodes. The orogenic episodes predate the igneous activity described here. Sedimentary rocks and interbedded greenstones were thermally metamorphosed by at least the last stage of igneous intrusion, and K-Ar ages from minerals separated from samples of hornfels, schist, and whole-rock greenstone samples probably reflect the ages of emplacement of the last major stage of igneous intrusion during the Late Cretaceous.

PLUTONIC COMPLEX OF BUFFALO MOUNTAIN

The plutonic complex of Buffalo Mountain is a composite stock of Late Jurassic age composed of a late quartz monzonite core partly surrounded by an

TABLE 1.—Summary of ages of igneous rocks, Edna Mountain quadrangle, Humboldt County, Nev.

Rock type	Age, in millions of years
Olivine basalt flows-----	5
Rhyolite vitrophyre-----	14.3- 14.6
Andesitic basalt flows and tuffs-----	22.8- 23.8
Rhyolite ash-flow tuffs-----	24.2- 25.9
Quartz monzonite stock and associated dikes, north end of Buffalo Mountain-----	88
Metamorphism of Preble and Pumpernickel Formations-----	86 - 105
Granodiorite plutons and associated dikes and sills at Edna Mountain-----	102 - ¹ 106
Main plutonic complex of Buffalo Mountain	
Quartz monzonite phase-----	146 - 154
Porphyritic syenite phase-----	153 - 164

¹Represents ages of unaltered or unweathered samples only. See later discussion.

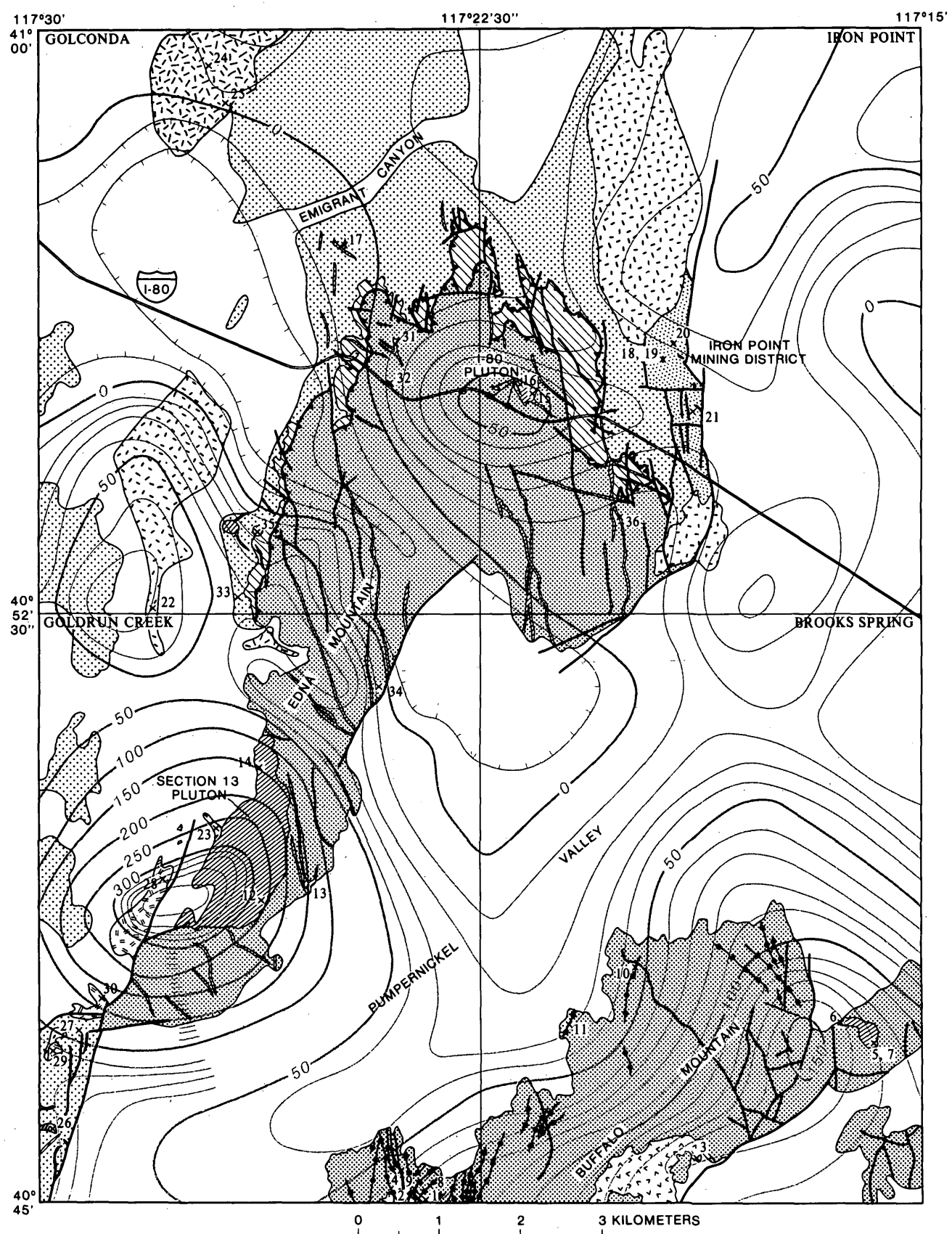


FIGURE 1.—Generalized geologic and aeromagnetic map showing chemically analyzed and age-dated igneous rocks, Edna Mountain 15-minute quadrangle, Humboldt County, Nev.

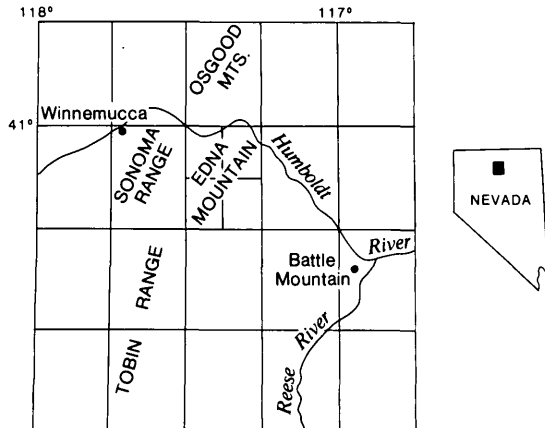
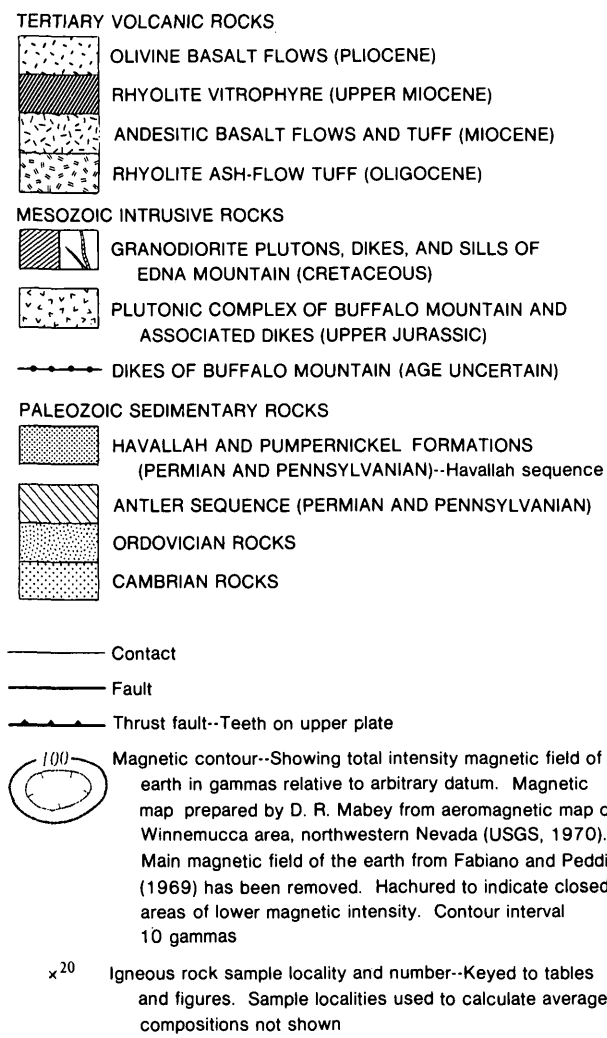


FIGURE 1.—Continued.

early porphyritic syenite and cut by a northwest-trending felsite dike swarm. The complex crops out over an area of about 80 km², but only two small lobes of the northern part of the complex extend into the southeast part of the Edna Mountain quadrangle (fig. 1).

The petrology and structure of the pluton has been mapped and studied in detail by Neff (1969), who reported that the surface area of the complex is approximately 75 percent quartz monzonite and 25 percent porphyritic syenite. His maps showed both gradational and sharp contacts between these two rocks types. Neff's average mode of 10 samples of porphyritic syenite and 14 samples of quartz monzonite (table 2)

TABLE 2.—Average mode, in percent, for 10 samples of porphyritic syenite and 14 samples of quartz monzonite, plutonic complex of Buffalo Mountain
[Calculated from analyses given in Neff, 1969]

Porphyritic syenite		Quartz monzonite	
Mineral	Mode	Mineral	Mode
Perthite	50.7	K-feldspar	34.6
Plagioclase	25.0	Plagioclase	33.6
Quartz	1.0	Quartz	20.4
Augite	9.0	Biotite	8.9
Hypersthene	1.4	Hornblende	1.4
Hornblende	1.8	Magnetite	
Biotite	5.7	Apatite	
Olivine	1.0	Sphene	
Magnetite	3.2		
Apatite-sphene	1.2		

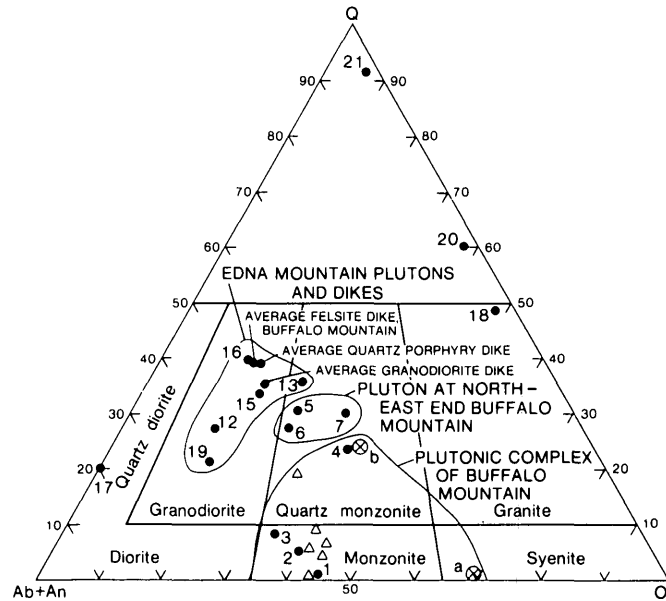


FIGURE 2.—Ternary plots of normative minerals in intrusive igneous rocks, Edna Mountain 15-minute quadrangle, Nevada, and modal plot of Neff's (1969) average syenite (a) and average quartz monzonite (b). Dots are samples collected and analyzed for this study; triangles are from unpublished chemical analyses contributed by Silberman. Sample numbers are keyed to figures and tables.

AGE AND COMPOSITION OF IGNEOUS ROCKS, NEVADA

TABLE 3.—Chemical and spectrographic analysis and CIPW norms, Buffalo Mountain area

Sample locality Number	Plutonic complex of Buffalo Mountain								Northeast end, Buffalo Mountain							
	Porphyritic syenite				Quartz monzonite				Quartz monzonite				Felsite porphyry dikes			
	1	2	Average ¹	Range ¹	3	4	Average ¹	Range ¹	5	6	7	8	9	10	11	
Chemical analyses (in percent) [Paul Elmore, analyst except sample number 3, Lowell Artis analyst]																
SiO ₂	54.8	58.8	58.0	54.8 - 60.0	58.0	69.9	63.5	58.0 - 69.9	69.1	66.6	68.0	70.3	67.7	69.5	72.2	
Al ₂ O ₃	17.9	19.1	17.8	16.9 - 19.1	16.8	15.0	16.2	15.0 - 17.1	16.7	16.1	15.9	15.6	16.4	15.0	14.6	
Fe ₂ O ₃	2.3	1.6	1.7	0.85 - 2.3	2.2	.00	1.2	.00	1.0	.59	1.8	.11	.88	.80	1.3	
FeO	4.1	3.0	3.6	3.0 - 4.1	3.5	1.6	2.6	1.6 - 4.1	.16	.56	.36	1.9	1.2	1.3	.36	
MgO	2.6	1.2	2.1	1.2 - 2.9	2.7	.37	1.6	.37 - 2.7	.43	1.3	.85	1.2	1.2	1.2	.40	
CaO	5.2	4.1	4.4	3.4 - 5.2	6.5	1.6	3.8	1.6 - 6.5	2.9	5.6	1.8	1.2	3.5	3.1	1.8	
Na ₂ O	3.1	3.7	3.5	3.1 - 3.7	3.4	3.4	3.5	3.4 - 3.8	3.2	2.9	2.8	3.8	3.8	4.3	3.5	
K ₂ O	5.7	5.8	5.9	5.5 - 6.3	4.4	6.0	5.2	4.4 - 6.0	4.0	3.9	5.1	2.3	2.1	2.0	3.1	
H ₂ O ⁺	.71	.64	.28	.00 - .71	.86	.49	.60	.06 - 1.0	1.1	.65	1.2	1.7	1.5	1.7	1.4	
H ₂ O ⁻	.14	.15	.42	0.14 - 0.76	.06	.09	.26	.06 - .84	.62	.55	.54	.26	.15	.13	.18	
TiO ₂	1.2	1.1	1.0	.86 - 1.2	.59	.31	.66	.31 - 1.0	.45	.56	.30	.30	.28	.20	.04	
P ₂ O ₅	1.1	.51	.64	.51 - 1.1	1.1	.08	.46	.08 - 1.1	.20	.32	.34	.09	.12	.05	.12	
MnO	.12	.10	.09	.08 - .12	.06	.06	.06	.05 - .08	.04	.00	.00	.07	.08	.01	.03	
CO ₂	.05	.03	.06	.03 - .11	.04	.08	.05	.03 - .08	.02	.30	.03	.57	.37	1.2	.61	
SUM	99	100			100	100			100	100	99	99	99	100	100	
Spectrographic analyses (parts per million) [R. E. Mays, analyst, except sample numbers 6, 7, 10, 11, Janet D. Fletcher, analyst. N = Not detected at value shown]																
B	220	220	70	10- 150	210	2100	40	N - 100	2N 10	3N 10	326	250	250	339	351	
Be	3,000	2,000	2,000	1,500-3,000	2,000	1,000	2,000	1,000-3,000	1,000	1,800	1,420	700	500	1,620	1,160	
Co	2	7	6	2- 10	5	10	6	5- 10	2	2	2	1	1	2	3	
Cr	15	7	15	7- 20	20	N 5	10	N - 20	N 5	2	7	N 5	N 5	4	2	
Cu	50	7	25	7- 50	65	7	25	7- 65	3	6	6	20	10	23	6	
La	150	100	90	15- 150	90	1	35	1- 90	300	58	680	20	1	2	12	
Mo	N (2)	N (2)	3	N - 100	75	N 50	40	N - 100	N 50	24	24	N 50	N 50	---	29	
Nb	N (10)	(20)	20	N - 30	7	20	15	7- 20	N 7	3	3	N 10	N 10	1	2	
Ni	15	3	15	7- 30	20	N 3	10	N - 20	N 3	3	3	20	5	10	2	
Pb	30	50	40	30- 50	30	50	35	30- 50	50	15	7	13	15	15	27	
Sc	10	10	15	10- 20	30	N 5	12	N - 30	5	8	4	5	5	4	3	
Sr	700	700	1,150	700-1,500	1,250	200	1,000	200-1,500	300	740	620	150	200	420	280	
V	150	50	100	50- 150	200	15	100	15- 200	50	67	74	20	15	34	17	
Y	15	15	25	15- 30	40	10	20	10- 40	10	14	11	N 10	N 10	8	15	
Zr	100	100	250	100- 500	700	150	270	100- 700	100	100	200	100	100	150	180	
CIPW norms [Leaders indicate no data]																
Quartz	1.3	4.6	----	----	6.3	22.3	----	----	28.3	23.5	28.0	36.1	29.3	31.4	37.7	
Orthoclase	33.9	34.5	----	----	26.1	35.6	----	----	23.9	22.8	30.0	13.3	12.2	11.7	18.4	
Albite	26.2	31.4	----	----	28.8	28.8	----	----	27.2	24.6	23.6	32.0	32.0	36.2	29.3	
Anorthite	17.8	17.0	----	----	17.5	7.2	----	----	13.6	19.5	7.2	1.4	14.5	7.8	4.2	
Corundum	----	0.4	----	----	0.2	----	2.	----	3.2	6.0	2.6	3.0	4.0	3.0	4.0	
Diopside	1.1	----	----	----	6.6	----	----	----	3.7	----	----	----	----	----	----	
Hypersthene	9.7	5.6	----	----	7.0	3.3	----	----	1.1	1.6	2.1	5.8	4.1	4.2	1.0	
Ilmenite	2.1	2.1	----	----	1.2	0.6	----	----	2	3	0.6	0.6	1.2	1.2	1.2	
Magnetite	3.2	2.3	----	----	3.2	----	----	----	.3	.7	.2	1.4	----	3	3	
Apatite	2.7	1.3	----	----	2.7	0.3	----	----	1.	.6	1.6	0.3	0.3	----	.5	
Calcite	----	----	----	----	----	----	----	----	.7	----	1.3	0.8	2.7	1.4	1.4	

¹Includes 4 unpublished analyses of porphyritic syenite and 2 unpublished analyses of quartz monzonite from the main part of the pluton south of the study. Location, description, and K-Ar ages of most of these rocks are reported by Silberman and McKee (1971).

²Results are to be identified with geometric brackets whose boundaries are 1.2, 0.83, 0.56, 0.38, 0.26, 0.18, 0.12, ..., but are reported arbitrarily as midpoints of these brackets, 1, 0.7, 0.5, 0.3, 0.2, 0.15, 0.1, ... Precision of a reported value is approximately plus or minus one bracket at 68 percent or two brackets at 95 percent confidence level.

³Concentration ranges of elements determined by computerized spectrographic analyses; standard deviation is plus 50 percent and minus 33 percent.

Sample locality	Field number	Description
1	GC-519	Dark-gray, coarse-grained olivine-bearing porphyritic syenite. Late-forming perthite laths, as much as 5 cm long and about 50 percent of the rock, poikilitically include all other minerals. Oligoclase-andesine (about 25 percent) and a small amount of myrmekite are the other felsic minerals. Mafic minerals (about 20 percent) include pink-tinted augite, deep-red-brown biotite, and minor olivine. Magnetite and apatite are abundant (about 5 percent) accessory minerals.
2	GC-517	Gray, coarse-grained olivine-free porphyritic syenite. Perthite laths as much as 4 cm long comprise about 60 percent of the rock. Compared to GC-519 (above) biotite is lighter colored, augite gives way to hornblende and total mafic content is less and myrmekite is more abundant.
3	BS-740	Salt-and-pepper, medium-grained, granitic-textured biotite quartz monzonite. Anhedral perthite patches poikilitically include all other minerals. Small oligoclase-andesine laths, and myrmekite are the other felsic minerals. Biotite, partly altered to chlorite is the most abundant mafic mineral; hornblende and augite are minor. Magnetite, apatite, and sphene are accessory minerals. This rock, chemically and mineralogically, is clearly related genetically to the porphyritic syenite and probably represents a gradational phase between syenite and quartz monzonite. Note that the K-Ar age is older than the much more silicic quartz monzonite below.
4	GS-521	Biotite hornblende quartz monzonite from a dike that cuts porphyritic syenite. Although much more silicic than sample BS-740, this rock too is clearly related genetically to the syenite and less silicic quartz monzonite. Perthite and myrmekite are common to all rock types; the principal changes are from olivine-augite-biotite in syenite to biotite-hornblende and higher free quartz content in quartz monzonite.
5	BS-742	Biotite quartz monzonite porphyry. Subhedral zoned andesine laths, biotite, and rounded, embayed, euhedral quartz phenocrysts in a fine-grained mosaic-textured groundmass of orthoclase and quartz. Sphene and apatite are accessory minerals.
6	BS-134	Augite quartz monzonite porphyry. Description same as sample BS-742 above except that augite is the chief mafic mineral rather than biotite or hornblende.
7	BS-741B	Altered biotite quartz monzonite porphyry. Plagioclase phenocrysts are intensely sericitized and biotite is completely altered to sericitic, chlorite, and iron oxides. Groundmass is fine-grained mosaic of orthoclase and quartz as sample BS-742 above.
8	GC-519A	Altered rhyodacite porphyry dike. In thin section the rock is intensely argillized; plagioclase phenocrysts altered to kaolinite and sericitic; biotite phenocrysts altered to chlorite, sericitic, and calcite; and rare quartz eyes; all in a fine-grained groundmass of alkali feldspar and quartz.
9	GC-517B	Dacite porphyry dike. Consists of milky-white altered plagioclase and altered mafic phenocrysts in a greenish-gray aphanitic groundmass of alkalic feldspar, quartz, and pale-green to white shreds of muscovite. The mafic phenocrysts consist of a mixture of clinzoisite, epidote, and calcite replacing original(?) pyroxene.
10	BS-442	Rhyodacite porphyry dike. Zoned, subhedral plagioclase phenocrysts in a fine-grained groundmass of quartz and feldspar. Mafic relics are rare and almost totally replaced by chlorite and calcite.
11	BS-484	Quartz porphyry dike. Small quartz phenocrysts in a groundmass of kaolinized feldspar. Tiny biotite shreds are mostly altered to chlorite and magnetite.

plot in the syenite and quartz monzonite fields, respectively, of the quartz-orthoclase-plagioclase diagram (fig. 2). However, the composition of individual rock samples ranges from dark, coarse-grained, olivine-bearing syenite to pyroxene-rich syenite to hornblende monzonite to quartz monzonite. Perthite, biotite, and small amounts of myrmekite are common to all rock types. Thin sections, stained slabs, chemical analyses (table 3), and a ternary plot of normative minerals (fig. 2) all show the genetic relationship of these rock types and clearly indicate that they belong to a different association than typical plutons in north-central Nevada. CIPW norms of porphyritic syenite plot in the monzonite field rather than in the syenite field (fig. 2), because all normative albite is included in plagioclase (Ab + An) rather than portioned between modal plagioclase and modal perthite.

Porphyritic syenite in the Edna Mountain quadrangle is dark gray to gray, is coarse grained, and commonly weathers to dark-brown, rounded, spalled outcrops on ridge tops and coarse grus on slopes (Marsh and Erickson, 1978). Gray perthite in laths as much as 5 cm long and 1.5 cm wide poikilitically includes all other minerals and is the most abundant mineral in the rock. Subhedral plagioclase (oligoclase-andesine) and small amounts of myrmekite are the other light-colored minerals. Apatite, magnetite, and sphene are accessory minerals. Mafic minerals locally make up as much as 30 percent of the rock and include biotite, titaniferous augite, hornblende, and olivine. The mafic-rich rocks are best described as shonkinite.

Quartz monzonite in the Edna Mountain quadrangle is gray to light gray, is medium grained, and contains quartz, perthite, oligoclase-andesine, myrmekite, biotite, hornblende, and a few residual augite grains mantled with hornblende. Apatite, sphene, and magnetite are accessory minerals. Quartz often contains abundant dark needles and rods tentatively identified as tourmaline. Mafic minerals locally make up almost 50 percent of the rock, and quartz content is very low so that the rock is really a monzonite.

Chemical and spectrographic analyses and CIPW norms of rocks from the plutonic complex of Buffalo Mountain (table 3) and the silica variation diagrams (fig. 3) show the high potassic character (4.3–6.4 percent K₂O) and high total alkali metal oxide content (7.8–10 percent K₂O + Na₂O) of these rocks through a wide range in SiO₂ content (54.8–69.0 percent) from olivine-bearing syenite to quartz-rich monzonite. Despite high total alkali contents, the rocks are not nepheline normative, and their K, Na, Ca, Fe, Mg, and Al variation diagrams are not typical of the alkalic rock series (Nockolds and Allen, 1954). The Buffalo

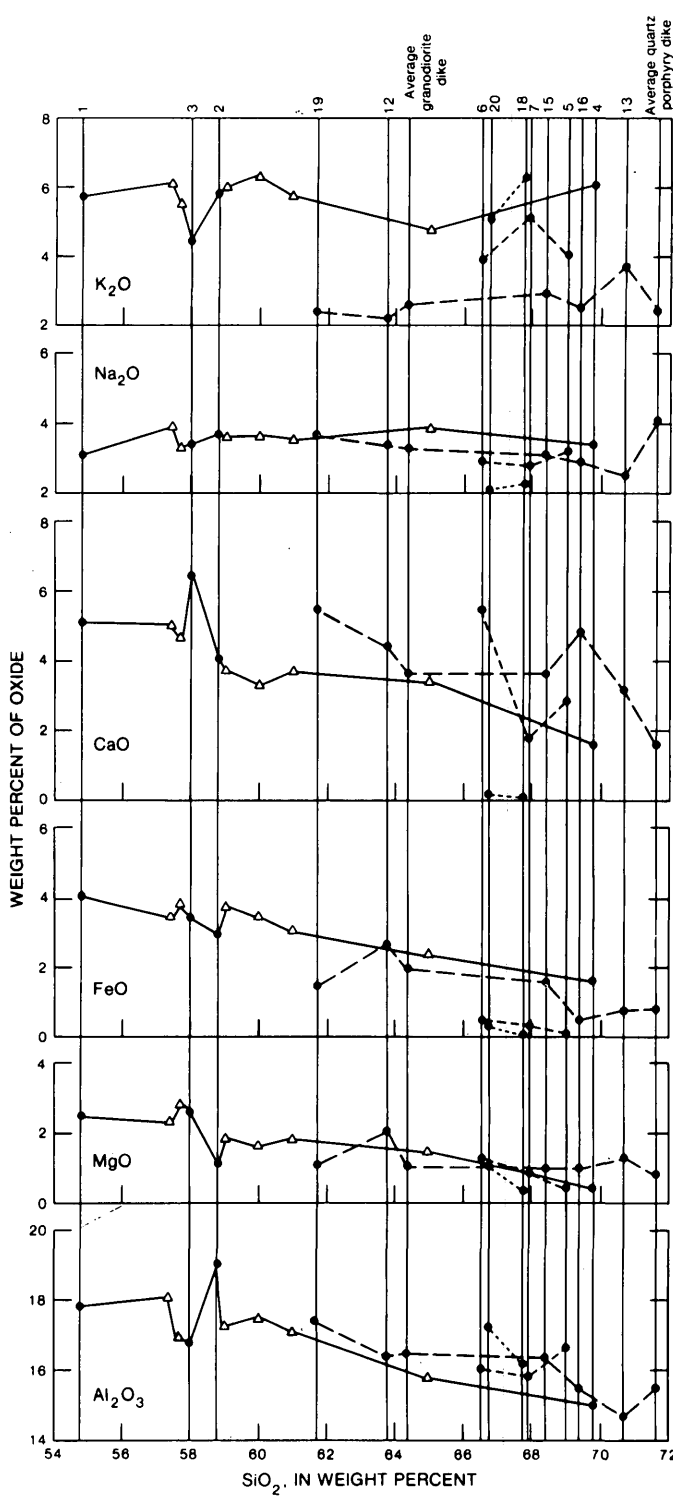


FIGURE 3.—Silica-variation diagrams of intrusive igneous rocks of the plutonic complex of Buffalo Mountain (solid lines), Edna Mountain granodiorite plutons and dikes (long-dashed lines), quartz monzonite pluton at northeast end of Buffalo Mountain (short-dashed lines), and two altered granitic-textured rocks from the Iron Point mining district (dotted lines). Dots are samples collected and analyzed for this study; triangles are unpublished chemical analyses contributed by Silberman. Sample numbers are keyed to figures and tables.

Mountain rocks are not calc-alkaline either, and their composition contrasts sharply with the mostly calc-alkaline granodiorite plutons at Edna Mountain, at the northeast end of Buffalo Mountain, and at other localities in north-central Nevada.

Because of the unique chemical and mineralogical composition of the Buffalo Mountain pluton, samples of the syenite and quartz-monzonite phases were analyzed for their K, Rb, and Sr contents by X-ray fluorescence and for their U and Th contents by instrumental neutron activation analysis. The results of these analyses, when compared to similar data for other granitic plutons from north-central Nevada (38 samples, M. L. Silberman, B. P. Fabbi, and Richard Shimek, unpub. data, 1975), show the strong enrichment of some of these elements in the Buffalo Mountain pluton particularly in the syenite phase (table 4). The dacite dikes that intrude the plutonic complex have approximately the same contents of K, Rb, Sr, U, and Th as do the other normal plutonic rocks in the region.

The histograms for these five elements (fig. 5) show that syenite and quartz monzonite of the Buffalo Mountain pluton are strongly enriched in K, Rb, and Sr compared to typical granodiorite at Edna Mountain, quartz monzonite at the northeast end of Buffalo Mountain, and the dacite dikes and other plutons in north-central Nevada. Thorium and particularly uranium have ranges of concentrations that overlap those of the other north-central Nevada plutons, although, for both elements, the highest regional values occur at Buffalo Mountain. Silica-variation diagrams for the elements K, Rb, and Sr are plotted for Buffalo Mountain rocks (fig. 4), along with the range of composition for other plutons in the region, and for the Sierra

Nevada batholith where these data are available from similar methods of analysis. For both K and Rb, the granitic rocks from north-central Nevada and the Sierra Nevada show a positive correlation with SiO₂ content. At Buffalo Mountain, both these elements are strongly enriched relative to their concentrations in the other plutons, but these two elements show no clear-cut variations with SiO₂ content. The slightly younger quartz monzonite at Buffalo Mountain has higher SiO₂ contents than does the syenite but has about the same content of K and Rb. Sr is negatively correlated with SiO₂ in Buffalo Mountain rocks as well as in other granitic rocks of north-central Nevada.

Figure 4 also shows variation diagrams for K:Rb, K:Sr, Rb:Sr, and U:Th for analyses of rocks from Buffalo Mountain, the other plutons in the region, and the Sierra Nevada where analyses are available. K and Rb tend to correlate negatively with Sr in cogenetic granitic rocks because late crystallizing phases such as K-feldspar and biotite tend to be enriched in K and Rb whereas early formed plagioclase tends to be enriched in Sr. Plutons in both the Sierra Nevada and north-central Nevada follow this trend. At Buffalo Mountain, Rb follows the trend, but the Rb content is much higher in the Buffalo Mountain rocks than in the others. Potassium shows no variation with Sr content. K:Rb tends to be lower and Rb:Sr tends to be higher in the Buffalo Mountain rocks than in the other granitic rocks in north-central Nevada (fig. 5, table 4). The syenite appears to show strong enrichment in Rb relative to K and follows the pegmatitic-hydrothermal trend of strong Rb enrichment (Shaw, 1968), whereas the north-central Nevada plutons and the Sierra Nevada batholith appear to follow the more usual "main trend" defined by Shaw (1968), which has an average K:Rb of about 230.

TABLE 4.—Average content and ratios of some elements in rocks from the plutonic complex of Buffalo Mountain and other north-central Nevada plutons
[ppm, parts per million]

	K, in percent	Rb, in ppm	Sr, in ppm	U, in ppm	Th, in ppm	K/Sr ⁴	K/Rb ⁴	Rb/Sr ⁴	Th/U ⁴
Quartz monzonite	4.24 ^{+0.72} _{-.36}	255 ^{+ 114} _{-.57}	657 ^{+ 233} _{-.116}	6.1 ^{+ 3.0} _{-.1.5}	23.3 ^{+ 19.0} _{-.9.5}	64.5	166	0.39	3.82
Porphyritic syenite-----	5.02 ^{+.17} _{-.07}	283 ^{+ 63} _{-.26}	955 ^{+ 186} _{-.76}	6.6 ^{+ 3.5} _{-.1.4}	26.4 ^{+ 16.7} _{-.6.8}	52.6	177	.30	4.00
Dacite dikes-----	1.91 ^{+.11} _{-.08}	126 ^{+ 11} _{-.8}	328 ^{+ 53} _{-.37}	3.1 ^{+.6} _{-.4}	10.2 ^{+.3.5} _{-.2.5}	58.2	151	.38	3.29
Other Nevada plutons ¹ -----	2.89 ^{+.70} _{-.11}	121 ^{+ 47} _{-.8}	526 ^{+ 203} _{-.33}	3.1 ^{+ 1.7} _{-.3}	13.2 ^{+.9.1} _{-.1.5}	54.9	239	.23	4.22

¹M. L. Silberman, B. P. Fabbi, and Richard Shimek, unpub. data, 1975.

²Standard deviation.

³Standard error.

⁴Ratios calculated from average contents.

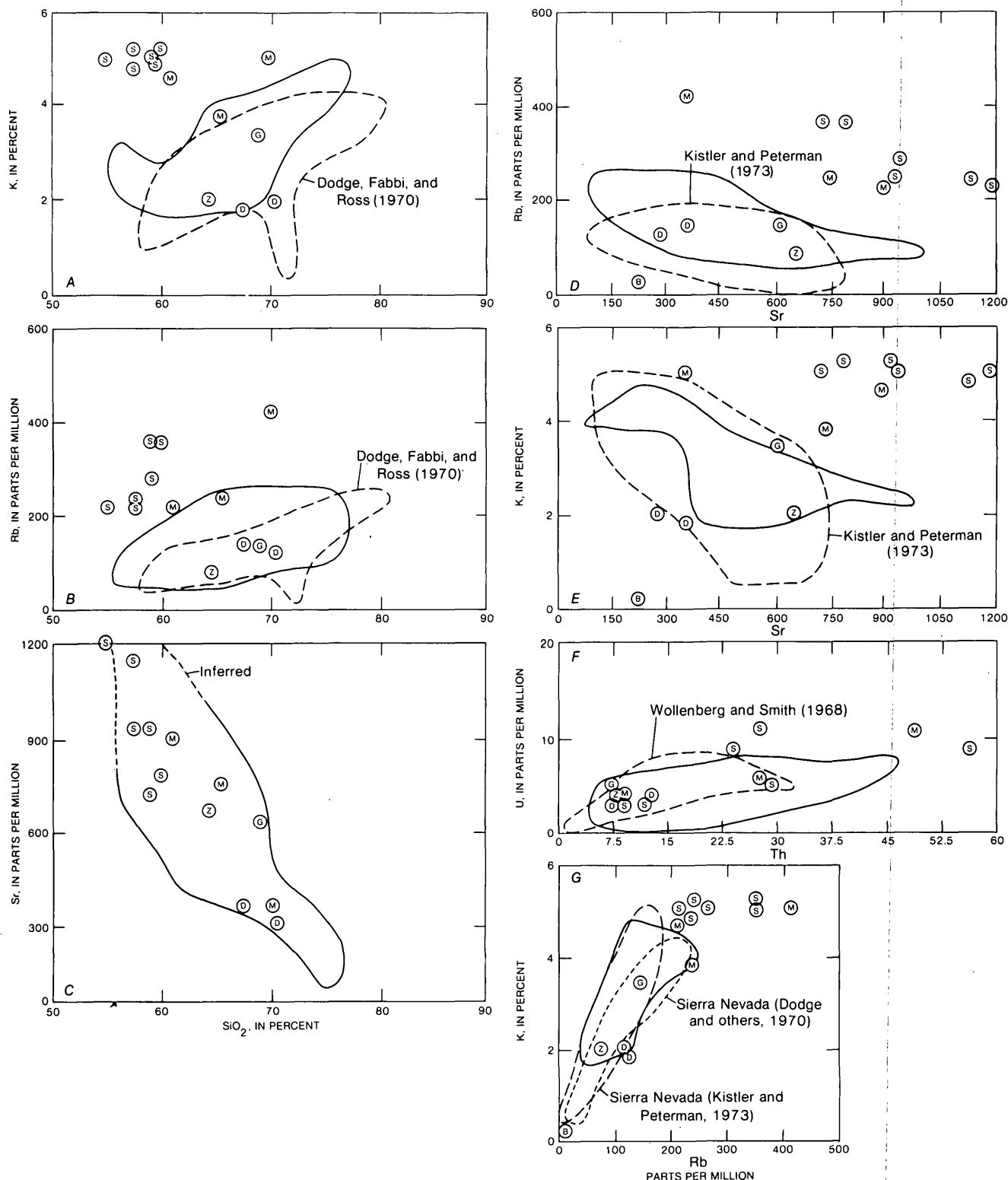


FIGURE 4.—Silica-variation diagrams (A-C) on left and element-variation diagrams (D-G) on right. Rocks are from the plutonic complex of Buffalo Mountain (S, syenite; M, quartz monzonite; D, dacite dikes), from quartz monzonite (G) at the north end of Buffalo Mountain, and from granodiorite (Z) at Edna Mountain. The diagrams also show variation of values of plutons in north-central Nevada (solid line) and in the Sierra Nevada (dashed line).

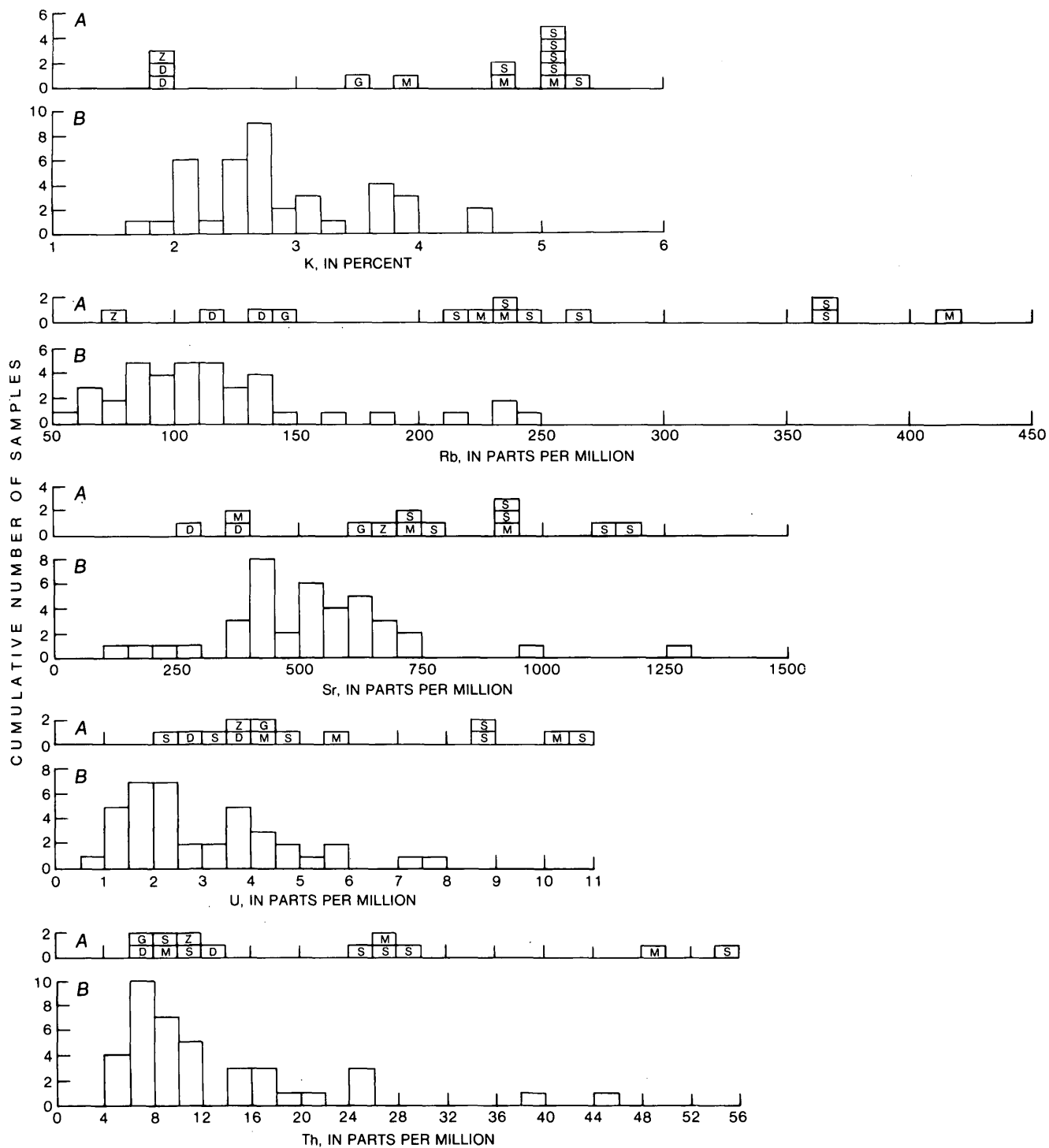


FIGURE 5.—Distribution of K, Rb, Sr, U, and Th (A) in the plutonic complex of Buffalo Mountain (S, syenite; M, quartz monzonite; D, dacite dikes), in granodiorite (Z) at Edna Mountain, and in quartz monzonite (G) at the northeast end of Buffalo Mountain, compared to other plutons (not labeled) in north-central Nevada (B).

The negative correlations of Sr with SiO_2 and Rb with Sr in rocks of Buffalo Mountain appear to show the normal calc-alkaline variations in these elements, and the relationship could be explained by fractionation of basic plagioclase from a single parent magma

because Sr tends to be concentrated in plagioclase relative to the melt. Plagioclase fractionation would also enrich the melt in SiO_2 ; however, the lack of any apparent variation of K with Rb and both K and Rb with SiO_2 suggests to us that the different Buffalo

Mountain rock types are not related by any simple scheme of fractional crystallization. Biotite is modally more concentrated in the younger quartz monzonite (table 2), which should cause a lower K:Rb in the quartz monzonite because biotite tends to be enriched in Rb relative to other mineral phases (Shaw, 1968). However, the K:Rb does not vary appreciably between these units.

We suggest that a better explanation for the geochemistry of the Buffalo Mountain rocks is differing degrees of partial melting of a similar source material, which itself may be enriched in the elements Sr, Rb, and K.

Both U and Th contents show considerable range, and there is some irregular enrichment of U relative to Th in the porphyritic syenite of the Buffalo Mountain pluton, but the range is not much different from that found in other granitic rocks in the region or in rocks from the Sierra Nevada (fig. 5).

Major-element, minor-element, and modal analyses all point to a unique composition for the quartz monzonite and syenite phases of the plutonic complex of Buffalo Mountain compared to other plutons in north-central Nevada. Similar chemical compositions have been found only in three small plutons of similar age in the Sonoma Range, 10–20 km west of Buffalo Mountain (M. L. Silberman, B. P. Fabbri, and Richard Shimek, unpub. data, 1975). The mineralogical and chemical compositions of the complex indicate that it was generated by processes unlike those that were involved in evolution of the more typical calc-alkaline quartz monzonites and granodiorites elsewhere in north-central Nevada or in the Sierra Nevada. Strontium isotope studies in progress will hopefully clarify the origin of the Buffalo Mountain pluton, but, tentatively, we suggest derivation of the rocks by varying amounts of partial melting of mantle-derived, mafic material of tholeiitic affinity. Melting of crustal rocks, which were enriched in the elements reported above, is also a possible derivation.

Age

The age of the plutonic complex of Buffalo Mountain is well documented as Late Jurassic ranging from 146–164 m.y. old. Four new K-Ar ages on biotite and hornblende (table 5) support four ages, including two concordant biotite and hornblende ages, reported earlier by Silberman and McKee (1971). Geologic mapping of the entire complex by Neff (1969), together with our mapping and petrographic and major-element geochemical studies in the north part of the complex, suggests that coarse-grained syenite prophyry

and quartz monzonite are related magma types, but our studies of the trace-element analyses indicate that these magmas may not be related by simple fractional crystallization. The K-Ar age dates show a progression from early emplacement of syenite through later emplacement of monzonite and quartz monzonite in gradational contact with syenite to latest quartz-rich monzonite dikes that sharply cut the syenite (table 5).

Unfortunately, the age of the felsite porphyry dike swarm that cuts porphyritic syenite (Marsh and Erickson, 1978) (fig. 1) is unknown. These fine-grained porphyritic rocks are altered to clay minerals, sericite, and chlorite; only residual outlines of plagioclase and biotite phenocrysts remain. No suitable material for K-Ar age determination was obtained from any of our samples of these dike rocks. Although it is reasonable to assign intrusion of the felsite porphyry dike swarm to the age of the plutonic complex of Buffalo Mountain, the CIPW norms of the dike rocks plot in the quartz-rich granodiorite field (fig. 2), and they are very similar chemically and petrographically to the fine-grained porphyritic dike rocks that are associated with the granodiorite plutons at Edna Mountain and the small quartz monzonite stock at the northeast end of Buffalo Mountain, all of which are of Late Cretaceous age. Chemical and petrographic affinity thus strongly suggests a Cretaceous age for the dike swarm, but lack of any isotopic ages on these rocks precludes determining their correct age.

QUARTZ MONZONITE, NORTHEAST END, BUFFALO MOUNTAIN

A small quartz monzonite stock, less than 0.125 km² of exposed area, crops out at the northeast end of Buffalo Mountain where it intrudes quartzite and limestone of the Havallah Formation of Middle Pennsylvanian and Early Permian age (fig. 1). Parts of the stock are thinly mantled by gravel and alluvium of Quaternary age not shown on figure 1 (Marsh and Erickson, 1977). The stock is composed of light-gray, medium-grained to porphyritic quartz monzonite and granodiorite that is commonly altered by addition of silica and potash. The rock characteristically has subhedral zoned andesine, biotite, and subhedral quartz phenocrysts that constitute as much as 50 percent of the rock in a fine-grained granular groundmass of quartz and orthoclase with accessory sphene, apatite, and magnetite. Hornblende and augite locally comprise part or all of the mafic suite of minerals. The zoned plagioclase phenocrysts and absence of perthite and myrmekite distinguish these rocks from the older plutonic complex of Buffalo Mountain of Late Jurassic age to the south. Several prospect pits and trenches

TABLE 5.—*K-Ar ages of igneous rocks, Edna Mountain quadrangle, Nevada*

Sample locality Number	Field Number	Quadrangle	Rock type	Mineral in percent	K_2O	$Ar^{40}(\text{RAD})$ moles/gm	$Ar^{40}(\text{RAD})$ Ar^{40} total	Age (m.y.)	Remarks
Volcanic rocks									
22	G294	Golconda----	Olivine basalt-----	Whole rock---- 0.367	2.728×10^{-12} 2.47 $\times 10^{-12}$ 2.702 $\times 10^{-10}$	0.16 .19 .17	4.98 ± 0.15		
27	GC492	Goldrun Creek	Rhyolite vitrophyre-	Biotite----- 8.64	1.824×10^{-10}	.70	14.6 ± 0.4		
26	GC15	---do-----	Sanidine----- 8.83	1.825×10^{-10}	.80	14.3 ± 0.4			
24	G1004	Golconda-----	Basaltic andesite--	Biotite----- 8.57	1.811×10^{-10}	.73	14.6 ± 0.4		
25	G1003	---do-----	Andesite tuff-----	Whole rock---- 3.31	1.094×10^{-10}	.82	22.8 ± 0.7		
28	GC331	Goldrun Creek	Rhyolite ash-flow tuff-----	Hornblende----- .742	$.2554 \times 10^{-10}$.52	23.8 ± 0.7		
30	GC501	---do-----	Sanidine----- 6.36	2.229×10^{-10}	.62	24.2 ± 0.7			
29	GC479	---do-----	Sanidine----- 4.40	1.611×10^{-10}	.51	25.2 ± 0.8			
				Sanidine----- 6.60	2.481×10^{-10}	.54	25.9 ± 0.8		
Granitic plutons and dikes, Edna Mountains									
12	GC213	Goldrun Creek	Granodiorite-----	Biotite----- 9.16	14.46×10^{-10}	0.92	106 ± 3		
				Hornblende----- .535	$.8405 \times 10^{-10}$.88	106 ± 3		
14	GC412	---do-----	Syenite-----	Clinopyroxene----- .397	$.598 \times 10^{-10}$.71	102 ± 3		
35	G41	Golconda-----	Altered granodiorite	Muscovite----- 10.30	15.87×10^{-10}	.98	104 ± 3		
15	IP24	Iron Point---	Altered granodiorite	Biotite----- (Chloritized). 3.82	5.727×10^{-10}	.95	101 ± 3	Minimum age.	
32	G(GC10)	Golconda-----	Altered granodiorite dike.	Biotite----- 5.39	5.733×10^{-10}	.75	72.5 ± 2.2		
31	GT27A	---do-----	---do-----	Hornblende----- .350	$.9303 \times 10^{-10}$.70	176 ± 5		
Altered rocks, Iron Point									
19	IP New	Iron Point--- Cut.	Altered granodiorite	Biotite----- 3.06 (Chloritized).	1.911×10^{-10}	0.35	42.9 ± 1.3	Minimum age.	
18	Silver Coin	---do-----	Altered granodiorite	Sericite----- 3.63	3.924×10^{-10}	.21	73.6 ± 2.9		
18	Silver Coin	---do-----	Silver-bearing siliceous jarosite.	Jarosite----- 7.99	1.798×10^{-10}	.11	15.1 ± 0.5		
					1.688×10^{-10}	.10			
Pumpernickel and Preble Formations									
33	G52	Golconda-----	Schist of Preble----- Formation.	Muscovite----- 8.59	13.30×10^{-10}	0.92	105 ± 3	Metamorphic age reset from Cretaceous plutonism.	
36	GC-9	Iron Point---	Hornfels of-----	Hornblende----- .680	$.9549 \times 10^{-10}$.87	92.7 ± 2.8	Recrystallized adjacent to granodiorite dike.	
34	GC212A	Goldrun Creek	Greenstone of-----	Whole rock---- 1.268	1.612×10^{-10}	.88	86.2 ± 2.6	Recrystallized age.	
Plutonic complex of Buffalo Mountain									
7	BS742	Brooks Spring	Quartz monzonite-----	Biotite----- 8.69	11.27×10^{-10}	0.87	88.0 ± 2.6		
4	GC521	Goldrun Creek	Quartz monzonite----- dike.	Hornblende----- 1.562	3.418×10^{-10}	.92	146 ± 6		
3	BS740	Brooks Spring	Quartz monzonite-----	Biotite----- 8.98	20.40×10^{-10}	.93	151 ± 6		
2	GC517A	Goldrun Creek	Porphyritic syenite-----	Biotite----- 5.94	13.65×10^{-10}	.94	153 ± 6		
1	GC519	---do-----	Porphyritic syenite-----	Biotite----- 8.79	20.51×10^{-10}	.93	155 ± 6		
	MB27	Smelser Pass	Quartz monzonite-----	Biotite----- 9.16	21.20×10^{-10}	.92	154 ± 5	These ages revised from Silberman & McKee, 1971 due to change in K decay constants and abundance figures.	
MB-1	Cherry Creek	Quartz monzonite-----	Biotite----- 9.08	18.13×10^{-10}	.89	149 ± 4			
MB-4	Smelser Pass	Porphyritic syenite-----	Biotite----- 7.80	1.737×10^{-10}	.74	148 ± 4			
MB-3	---do-----	Medium-grained----- syenite.	Biotite----- 9.05	18.57×10^{-10}	.67	157 ± 5			
				21.97×10^{-10}	.95	161 ± 5			
				Hornblende----- .641	1.582×10^{-10}	.78	164 ± 5		

ANALYTICAL TECHNIQUES AND PROCEDURES USED IN K-AR AGE DETERMINATIONS

Mineral separates were prepared from crushed and ground samples after petrographic examination by standard heavy-liquid, magnetic, and inclined vibrating table techniques. Whole-rock samples of basalt were prepared by crushing and grinding the specimens to approximately 1- to 2-mm size fraction. Purified mineral concentrates and whole-rock samples were split with a Jones micro-splitter into separate aliquots for K and Ar analyses. For whole-rock samples, the K splits were pulverized in an alundum mortar to less than 0.1 mm size.

Potassium was analyzed by flame photometer, using a lithium metaborate fusion technique, the lithium serving as an internal standard (Ingamells, 1970). Lois Schlocker and Wayne Mountjoy were the analysts.

Argon was extracted from whole-rock samples or purified mineral concentrates in a pyrex-high-vacuum system using external RF induction heating. During fusion, a calibrated spike of purified Ar^{38} was introduced. Reactive gases were removed by an artificial molecular sieve, and by copper-copper oxide and titanium furnaces. Mass analyses of the purified argon were made with a Neir-type 60° sector, 15.2-cm-radius mass spectrometer, operated in the static mode. The technique is described in detail by Dalrymple and Lanphere (1969).

The + figures represent analytical uncertainty only, and are a combination of uncertainty in the potassium and argon analyses, and are estimated at one standard deviation. For most samples, this is on the order of 3 to 4%. For samples with large amounts of atmospheric argon, the argon analyses were made in duplicate or triplicate, and the uncertainty in age is reported as the standard deviation of the mean age calculated from the analyses.

Constants used in age calculation are:

$$\lambda_B = 4.963 \times 10^{-10} \text{ yr}^{-1}$$

$$\lambda_E = 0.572 \times 10^{-10} \text{ yr}^{-1}$$

$$\lambda_F = 8.78 \times 10^{-13} \text{ yr}^{-1}$$

$$40K/40Ar (\text{total}) = 1.167 \times 10^{-4} \text{ (mole/mole)}$$

Analyst was M. L. Silberman.

have been dug on shows of secondary green copper minerals, iron oxides, and disseminated sparse pyrite and chalcopyrite in quartz veins and shear zones that cut the quartz monzonite.

Chemical and spectrographic analyses and CIPW norms of three samples of quartz monzonite (sample locs. 5-7, table 3) show a narrow range in SiO_2 content (66.6-69.1 percent), very low FeO content (less than 1 percent), and K_2O greater than Na_2O . Examination of thin sections and stained slabs suggests that some K_2O has been added by hydrothermal alteration, chiefly as sericite, and the rocks may have been granodiorite originally (Na_2O greater than K_2O). The spectrographic analyses indicate that a small amount of copper also was added to these rocks (table 3). The high CaO in the samples from locality 6 (fig. 3, table 3) is contained in modal augite and is somewhat atypical for these rocks. The silica variation diagram (fig. 3) clearly shows that rocks from this pluton do not fit the differentiation trends for any of the major oxides from rocks of the plutonic complex of Buffalo Mountain to the south. Further, the ternary diagram (fig. 2) shows that the composition of this stock is distinctly different from all other plutons in the Edna Mountain quadrangle.

Age

Only one sample of the quartz monzonite (BS742) contained adequately fresh magmatic biotite for K-Ar age determination (table 5). The age of 88.0 ± 2.6 m.y. suggests that the quartz monzonite was emplaced in the Late Cretaceous. The dated biotite is not secondary hydrothermal biotite such as is frequently found in K-silicate altered zones of porphyry copper deposits. In general, porphyry copper mineralization occurs within the cooling history of associated granitic stocks (Damon and Mauger, 1966) and magmatic biotites from these rocks usually give ages that approximate the time of emplacement, even in K-silicate altered rocks (Theodore and others, 1973). Thus, the indicated K-Ar age is probably a good approximation of the time of emplacement, alteration, and mineralization of the stock.

INTRUSIVE IGNEOUS ROCKS, EDNA MOUNTAIN

Granodiorite stocks, dikes, and sills of mostly Late Cretaceous age are common throughout the length of Edna Mountain. The largest pluton is a north-trending elongate body exposed over about 3.5 km^2 in the Goldrun Creek $7\frac{1}{2}$ -minute quadrangle (Marsh and Erickson, 1978; fig. 1). Smaller, poorly exposed granodiorite plutons occur in the Golconda and Iron Point $7\frac{1}{2}$ -minute quadrangles (Erickson and Marsh, 1974

a, b). The numerous dikes and sills strike northwest, are commonly altered, have great textural and color variation, are chemically similar, and plot in the granodiorite field (fig. 2). The aeromagnetic map of the area (fig. 1) reflects the known plutons and suggests that intrusive igneous masses may be widespread beneath a relatively shallow cover.

The largest pluton is chiefly light-gray medium- to coarse-grained biotite-hornblende granodiorite. Graphic granite, coarse-grained pyroxene-hornblende sphene-rich syenite, and a few aplitic dikes are minor phases that are best exposed on the northwest flank of the pluton (Marsh and Erickson, 1978; fig. 1). The main granodiorite mass consists of subhedral to euhedral, zoned andesine laths as long as 5 mm (about 50 percent), late anhedral orthoclase (15 percent), and small amounts of myrmekite. Sphene, apatite, and magnetite are accessory minerals. Locally, chalcopyrite and molybdenite occur in narrow quartz veins near and along the southern contact of the granodiorite with Paleozoic sedimentary and volcanic rock units.

A small granodiorite pluton just east of the main pluton (sample loc. 13, fig. 1) has been altered by the addition of quartz, sericite, and sparse amounts of copper minerals and molybdenite (Marsh and Erickson, 1975).

The poorly-exposed and altered granodiorite pluton along and north of U.S. Interstate Highway 80 (fig. 1) is light-gray, is medium-grained to porphyritic, and is commonly altered by addition of silica. The freshest rock found contains andesine, biotite, quartz, and hornblende phenocrysts (about 50 percent of the rock) in a mosaic-textured groundmass of quartz, plagioclase, and orthoclase. Sphene and apatite are accessory minerals.

The dikes and sills of Edna Mountain have been mapped as quartz porphyry and quartz diorite (Erickson and Marsh, 1974a, b; Marsh and Erickson, 1977, 1978), and are part of the granodiorite complex of Edna Mountain. Quartz porphyry dikes and sills are light brown to cream colored, are dense to fine grained, and are almost everywhere intensely kaolinized, but sparse euhedral quartz and relics of small plagioclase and biotite phenocrysts are present. The dikes and sills mapped as quartz diorite are mostly granodiorite in composition. They are grayish green, are medium grained to porphyritic, and are composed of milky white sericitized plagioclase; quartz; biotite; and hornblende altered to chlorite, magnetite, and calcite; and small amounts of orthoclase. Only one mafic-rich quartz diorite dike was found in the area of this study (Erickson and Marsh, 1974a; sample loc. 17, fig. 1).

TABLE 6.—*Chemical and spectrographic analyses and CIPW norms of intrusive igneous rocks, Edna Mountain area*

Section 13 pluton Goldrun Creek quadrangle			I-80 pluton Iron Point quadrangle		Granodiorite dikes		Quartz porphyry dikes		Quartz diorite dike ¹											
Sample locality Number	Granodiorite (principal phase)	Altered granodiorite (minor phase)	Syenite	Granodiorite	Altered granodiorite	Average (6)	Average (3)		Altered granitic textured rocks, Iron Point mining district		12	13	14	15	16	17	18	19	20	21
Chemical analyses (in percent) [Paul Elmore, analyst, for sample numbers 13, 14, 17, 18, 20, and 21; Lowell Artis, analyst for sample numbers 12, 15, 16, 19]																				
SiO ₂	63.8	70.8	60.2	68.5	69.5	64.4	71.7	46.9	67.8	61.7	66.8	80.2								
Al ₂ O ₃	16.4	14.7	17.2	16.1	15.5	16.5	15.7	12.6	16.2	17.5	17.3	12.8								
Fe ₂ O ₃	2.4	1.0	.75	1.1	.43	1.5	.93	1.5	3.2	2.2	2.0	.80								
FeO	2.7	.76	.96	1.6	.52	2.0	.78	6.4	.12	1.5	.36	.04								
MgO	2.1	1.3	2.3	.96	.86	1.4	.79	11.1	.56	1.1	.11	.07								
CaO	4.5	3.2	6.9	3.7	4.9	3.7	1.6	8.0	.09	5.6	.21	.10								
Na ₂ O	3.4	2.5	4.0	3.1	2.9	3.3	4.1	2.0	.26	3.7	.12	.13								
K ₂ O	2.2	3.7	5.8	2.9	2.3	2.6	2.4	.13	6.3	2.4	5.0	.77								
H ₂ O ⁺	.98	1.0	.45	1.1	.96	1.9	1.3	5.4	2.5	1.5	4.3	4.2								
H ₂ O ⁻	.12	.15	.12	.19	.24	.36	.38	.78	.15	.72	.35	.10								
TiO ₂	.77	.51	.80	.41	.38	.51	.22	.81	.86	.37	.62	.47								
P ₂ O ₅	.43	.23	.36	.27	.24	.27	.11	.33	.26	.47	.24	.15								
MnO	.01	.02	.05	.10	.05	.07	.09	.15	.00	.05	.02	.00								
CO ₂	.01	.01	.15	.01	1.0	1.3	.17	3.7	.01	.17	.50	.01								
SUM	100	100	100	100	100	99														
Spectrographic analyses (parts per million) [Joseph L. Harris, analyst ¹ except sample number 19, Janet D. Fletcher, analyst ² , N = not detected at value shown]																				
B	N 10	N 10	N 10	N 10	N 10	N 10	15	N 10	200	11	30	30								
Ba	1,000	10,000	2,000	1,000	1,500	1,500	2,000	5,000	10,000	820	10,000	500								
Be	1.5	1	3	2	3	2	1.5	N 1	2	2	1	1								
Co	7	10	N 5	N 5	5	N 5	30	N 5	N 5	N 5	N 5	N 5								
Cr	30	20	50	7	7	7	15	1,000	30	7	15	70								
Cu	3	100	5	20	20	15	10	20	15	39	50	70								
La	100	50	70	50	N	50	N 50	N 50	N 50	25	N 50	N 50								
Mo	5	10	N	3	20	N 3	N 3	N 3	N 3	2	N 3	10								
Nb	20	20	20	3	5	10	3	N 3	20	4	10	20								
Ni	15	N 5	7	N 5	N 5	N 5	N 5	150	N 5	4	N 5	N 5								
Pb	N 5	10	N 5	10	7	5	7	N 5	20	14	30	10								
Sc	10	10	15	7	7	10	5	20	7	11	20	5								
Sr	1,000	1,000	1,500	1,000	700	1,000	500	1,000	200	890	500	200								
V	70	70	100	50	50	50	15	150	200	130	200	200								
Y	30	20	30	15	10	20	10	30	20	22	15	10								
Zr	200	150	200	150	150	150	100	50	150	270	150	70								
CIPW Norms [Leaders indicate no data]																				
Quartz	23	34	3.6	30	35	28.8	34.8	8	36.4	18.4	45.7	76.3								
Orthoclase	13	22	34.5	17	13.3	15.5	14.5	.6	37	145	29.5	5								
Albite	29	21	34	26	24.6	28.1	34	17	2.1	314	1	1								
Anorthite	20	15	11.7	17	17.2	9.3	6.3	15	-----	23.3										
Corundum	1	1.1	-----	2	1.9	4.6	4	4	9	-----	11.2	11.5								
Diopside	-----	-----	2.3	-----	-----	-----	-----	-----	-----	-----	-----	-----								
Hypersthene	8	3.2	-----	4	2.1	5.4	2.3	37	1.4	40	2.7	.2								
Wollastonite	-----	-----	1.2	-----	-----	-----	-----	-----	-----	-----	-----	-----								
Ilmenite	1.5	9	1.5	1	.8	0.9	.4	1.5	.9(rutile)	.7	.8	.5(rutile)								
Magnetite	3.5	1.4	.8	1.5	70	1.6	1.5	2.1	-----	3.25	2.1	.8								
Hematite	-----	-----	-----	-----	-----	-----	-----	-----	-----	3.2	-----	2.1								
Apatite	1	.3	1	1	.3	0.5	.3	.7	.7	134	.3	.3								
Calcite	-----	-----	.3	-----	2.3	2.7	-----	-----	-----	.4	-----	-----								

¹Results are to be identified with geometric brackets whose boundaries are 1.2, 0.83, 0.56, 0.38, 0.26, 0.18, 0.12, ..., but are reported arbitrarily as midpoints of these brackets 1, 0.7, 0.5, 0.3, 0.2, 0.15, 0.1, Precision of a reported value is approximately plus or minus one bracket at 68 percent or two brackets at 95 percent confidence.

ent or two brackets at 95 percent confidence.

<u>Sample locality</u>	<u>Field number</u>	<u>Description</u>
12	GC-213	Granodiorite. Hypautomorphic granular texture composed of oligoclase-andesine as subhedral laths as much as 5 mm long, and as euhedral zoned crystals (about 50 percent); late-forming, interstitial, and anhedral orthoclase (about 15 percent), rounded anhedral quartz (about 15 percent), and biotite and hornblende partially replaced by chlorite (about 20 percent). A small amount of myrmekite and accessory sphene, apatite, and magnetite are the other minerals.
13	GS-393	Altered biotite granodiorite. Original rock very similar to the sample from locality 12 except that K-feldspar has been added, hornblende destroyed, and biotite altered by hydrothermal solutions.
14	GC-412	Syenite. Minor phase of main pluton. Composed of sericitized plagioclase laths (about 25 percent), pale-green diopside-augite and hornblende (about 30 percent), late-interstitial orthoclase (about 40 percent) and small amounts of quartz, sphene, and apatite.
15	IP-24	Granodiorite porphyry. Composed of andesine (An_{35}), biotite and euhedral quartz phenocrysts (about 50 percent) in a groundmass (about 50 percent) of quartz and orthoclase. Biotite is dark-brown, partly altered to chlorite, and occasionally contains small ravaged pyroxene reliefs. Hornblende is present, but much less abundant than biotite. Sphene and apatite are accessory.
16	IP-22	Altered granodiorite porphyry. Very similar to sample 15 above except that mafic minerals have been altered almost completely to chlorite and calcite, quartz phenocrysts are embayed, and narrow quartz veinlets have been introduced.
17	G-914	Diorite. (See text, p. .)
18	Silver Coin	Altered biotite granodiorite. Equigranular texture and composed of intensely sericitized and kaolinized zoned plagioclase, quartz, orthoclase, and biotite completely altered to chlorite, sericite, and leucoxene. Small amounts of epidote occur as anhedral granular masses, euhedral crystals, and tiny veinlets. Secondary quartz also occurs in veinlets.
19	IP New Cut	Petrographic description not available because rock is chiefly grus.
20	IP-427	Petrographic description not available. Called altered granodiorite in the field.
21	IP-99	Light-gray quartz-fllooded rock (about 60 percent) with chalky-white, completely kaolinized feldspar phenocrysts (about 40 percent). A few shreds of sericite, iron oxide, and rare zircon are the only other minerals noted.

Brown hornblende and patches of chlorite, calcite, and magnetite after pyroxene (?) compose more than 50 percent of the diorite. Intensely altered plagioclase (about 40 percent), minor quartz, and accessory sphene make up the remainder of the diorite.

Chemical and spectrographic analyses and CIPW norms of unaltered plutons, dikes, and sills of Edna Mountain (table 6) show the characteristic $\text{Na}_2\text{O} > \text{K}_2\text{O}$ and moderate SiO_2 content of rocks of granodiorite composition. The chemical analysis of the sample from the largest pluton (sample loc. 12, table 6) is most typical of the bulk of Edna Mountain intrusive rock, as determined from the study of thin sections and stained slabs. Altered granodiorite shows addition of silica, depletion of iron and magnesium, and, in one case (sample loc. 13, table 6), some addition of potassium, barium, and copper. The average chemical analysis of six granodiorite dikes is very similar to the chemical analysis of the largest pluton; the average chemical analyses of quartz porphyry dikes show the expected high silica and low iron oxides, magnesia, and lime content. CIPW norms of all rocks, however, plot in the granodiorite field and show little variation in normative orthoclase content (fig. 2). The silica variation diagram (fig. 3) shows the distinctively different chemical composition of these rocks from the plutonic complex of Buffalo Mountain.

Age

Potassium-argon ages listed in table 5 show that most of the granitic rocks at Edna Mountain are of Cretaceous age. Concordant K-Ar ages of biotite and hornblende from the largest pluton (sample loc. 12, fig. 1; table 5) of 103 m.y. (on both minerals) establish this as the age of crystallization of this granitic body. An altered satellite stock to the west (sample loc. 34, fig. 1; table 5) gave a muscovite age of 104 ± 3 m.y., and clinoamphibole from a small syenitic phase of the larger pluton gave an age of 102 ± 3 m.y.

A small altered stock just north of Interstate 80 (sample loc. 15, fig. 1; table 5) yielded an age of 101 m.y. from strongly chloritized biotite. This should be considered a minimum age.

Two age determinations were made from minerals separated from quartz diorite dikes, just north of Interstate 80. A sample of chloritized biotite separated from strongly weathered granodiorite (sample loc. 32, fig. 1; table 5) gave an age of 72.5 ± 2.2 m.y., which should be considered a minimum age. Hornblende separated from another dike (sample loc. 31, fig. 1; table 5) yielded an age of 176 ± 5 m.y. This is the oldest date reported from any granitic rock in north-

central Nevada (Silberman and McKee, 1971; Carlson and others, 1975) and suggests that some of these dikes may be older than Cretaceous. The other age dates (table 5), however, suggest that most of the intrusive granitic rocks at Edna Mountain were emplaced in the Late Cretaceous, about 100 m.y. ago. The age dates in table 5 also indicate that some range in ages of emplacement of the dikes occurred.

IRON POINT MINING DISTRICT

Small irregular masses, dikes, and sills of altered granitic-textured rocks intrude an isolated fault-bounded block of Ordovician rock at the northeast end of Edna Mountain known as the Iron Point mining district (Erickson and Marsh, 1974b; fig. 1).

This complex structural block was affected by at least three episodes of hydrothermal alteration and mineralization. Igneous intrusive masses are altered to clay minerals or flooded by silica, and anomalous amounts of metals of diverse suites occur in the same rocks (Erickson and Marsh, 1971, 1972; Marsh and Erickson, 1975). We suspect that the intrusive rocks were originally granodiorite.

Chemical and spectrographic analyses and norms of four samples of these altered granitic-textured rocks are given in table 6. One sample collected from a newly opened cut immediately south of the Silver Coin mine (sample loc. 19, fig. 1; table 6), although disaggregated to a grus, contained fairly fresh biotite and feldspar. The chemical analysis and CIPW norm (table 6) and the ternary plot (fig. 2) show this rock to be typical granodiorite, very similar to the main granodiorite plutons of Edna Mountain. Two of the other rocks analyzed (sample locs. 18 and 20, fig. 1; table 6) show strong addition of SiO_2 , K_2O , and Ba and depletion of FeO , MgO , CaO , and Na_2O , and they plot very close to the quartz-orthoclase join on the ternary diagram (fig. 2). The intense silica flooding of the fourth analyzed rock (sample loc. 21, fig. 1; table 6) drastically reduces the content of the other major oxides. The high normative corundum in the three most altered rocks (sample locs. 18, 20, 21, fig. 1; table 6) is contained modally in kaolinite formed from alteration of feldspar.

Age

The intense hydrothermal alteration seen in the few exposures of intrusive igneous rocks in the Iron Point mining district has made it difficult to obtain minerals suitable for K-Ar determination of the age of original crystallization. Three different minerals from the Silver Coin mine area gave three widely discordant

K-Ar ages (sample locs. 18 and 19, fig. 1; table 5). Muscovite, from altered biotite granodiorite at the Silver Coin mine (sample loc. 18, fig. 4; table 5), gave an age of 74 ± 3 m.y. Jarosite coating fracture surfaces on the same rock gave 15 ± 0.5 m.y. The jarosite age falls within a prominent pulse of hydrothermal activity and mineralization in central Nevada (Silberman and McKee, 1974; Silberman and others, 1976). The argon retention characteristics of jarosite have not yet been investigated in detail, although Gustavson and Hunt (1975) reported anomalously young ages from supergene jarosite, which are discordant with those of supergene alunite in the same rocks from El Salvador, Chile. A chloritized biotite (sample loc. 19, fig. 1; table 5) from the disaggregated grus south of the Silver Coin mine gave an age of 43 ± 1 m.y. Probably all of these ages represent minimum figures, but we suggest that two alteration events occurred, a Late Cretaceous one producing the sericite and the other, probably of Tertiary age, resulting in additional alteration and deposition of jarosite on the fracture surfaces.

A fission-track age of 87 ± 10 m.y. on zircon from a sample of silicified, granitic-textured rock (sample loc. 21, fig. 1) was reported by C. W. Naeser (written commun., 1975). Naeser reported that uranium in most of the zircons was strongly zoned and that only four crystals could be dated. He further stated that a fission-track age on zircon should be considered as a minimum age. Ashley and Silberman (1976) demonstrated, however, that zircon fission-track ages did not seem to be affected by hydrothermal alteration. They reported that at Goldfield, Nev., zircon fission-track ages appeared to give reliable crystallization ages for both volcanic and granitic rocks when K-Ar ages from those rocks were totally or partially reset or could not be run at all for lack of unaltered phases. The Late Cretaceous age of the zircon does approach the range in age of the granodiorite plutons at Edna Mountain and indeed fits into one of the main episodes of plutonism ($87\text{--}105$ m.y.) in north-central Nevada defined by Silberman and McKee (1971).

METAMORPHIC ROCKS

We attempted to determine metamorphic recrystallization ages of three lithologically different samples of the Middle and Upper Cambrian Preble and Lower Pennsylvanian to Lower Permian Pumpernickel Formations (sample locs. 33, 34, 36, figs. 1; table 5). A muscovite separate from a schist bed in the Preble Formation (sample loc. 33, fig. 1; table 5) gave an age of 105 ± 3 m.y. The nearest intrusive rocks to this locality are the granodiorite dikes that crop out about

0.5 km to the east, but the granodiorite of Edna Mountain, or its apophyses, also occurs nearby (sample locs. 14 and 35, fig. 1). The age of metamorphism of the schist is the same, within analytical uncertainty, as the ages of several of the Edna Mountain rocks (table 5).

A sample of hornfels from the Pumpernickel Formation collected near quartz porphyry and granodiorite dikes (sample loc. 36, fig. 1; table 5) gave a hornblende age of approximately 93 ± 3 m.y. This age is slightly younger than the $101\text{--}106$ m.y. major plutonic pulse recorded at Edna Mountain but does fall within the $97\text{--}105$ m.y. intrusive episode demonstrated in north-central Nevada by Silberman and McKee (1971). It is, of course, possible that these dikes were emplaced over a range in age, as indeed our age dates do suggest (table 5).

A sample of basalt of the Pumpernickel Formation, altered to greenstone, with heavy replacement of mafic phenocrysts and plagioclase by chlorite gave an age of 86 ± 3 m.y. (sample loc. 34, fig. 1; table 5). This basalt date represents a minimum metamorphic age because the major phases containing K, principally the plagioclase, were so badly altered. More confidence is placed in the 93 and 105 m.y. ages of the first two metamorphosed samples. However, the metamorphic ages of the Pumpernickel and Preble Formations suggest that thermal events did affect the area for a longer period of time than is indicated by the tight grouping of K-Ar ages for the Edna Mountain pluton and its satellite bodies.

VOLCANIC ROCKS

Four episodes of Tertiary volcanism (rhyolite ash-flow tuff, andesitic basalt flows and tuff, rhyolite vitrophyre, and olivine basalt flows) have been identified in the Edna Mountain area. Oligocene rhyolite ash-flow tuffs in the Goldrun Creek quadrangle (Marsh and Erickson, 1978; fig. 1) are the oldest dated volcanic rocks. They are pale yellowish gray to pinkish gray and are composed of sanidine phenocrysts with dark elongate schiller-like inclusions, occasional rounded and embayed quartz phenocrysts, flattened and aligned pumice fragments, and lithic fragments in a dirty, devitrified-glass matrix. X-ray diffraction analysis of the glass shows that it has been altered to alkali feldspar and tridymite. Zeolite minerals were not detected. Curved and forked microlites and finely disseminated red-brown iron oxide are common in the matrix.

Chemical and spectrographic analyses and CIPW norms of rhyolite ash-flow tuff (table 7) show charac-

TABLE 7.—*Chemical and spectrographic analyses and CIPW norms of volcanic rocks, Edna Mountain quadrangle*

	Olivine basalt	Andesite flow	Andesite tuff	Rhyolite vitrophyre	Rhyolite ash-flow tuff				
Sample locality Number---	22	23	24	25	26	27	28	29	30
Field Number-----	G-294	GC-216	G-1004	G-1003	GC-15	GC-492	GC-331	GC-479	GC-501
Chemical analyses (in percent)									
[Lowell Artis, analyst except sample numbers 25, 26, Paul Elmore, analyst]									
SiO ₂	49.4	49.4	60.9	57.6	70.9	69.9	73.1	73.1	70.0
Al ₂ O ₃	17.3	17.3	16.1	19.2	14.0	14.6	13.2	13.0	13.2
Fe ₂ O ₃	3.2	4.1	2.3	5.4	1.0	0.60	.97	2.1	2.5
FeO	6.6	5.7	3.2	.52	1.5	1.6	.12	.12	.08
MgO	7.4	7.0	3.0	.58	.42	.40	.31	.12	.36
CaO	11.0	11.3	5.1	5.3	1.3	1.7	1.2	.50	2.7
Na ₂ O	2.1	2.4	2.9	4.5	3.0	3.0	3.9	3.9	3.8
K ₂ O	.32	.35	2.7	1.2	4.8	4.7	4.8	4.9	4.8
H ₂ O ⁺	.56	.75	1.9	2.7	2.3	2.1	1.0	.96	.96
H ₂ O ⁻	.17	.45	.85	2.0	.15	.68	.44	.34	.54
TiO ₂	1.2	1.2	.83	.68	.42	.38	.19	.18	.27
P ₂ O ₅	.20	.23	.37	.28	.17	.28	.05	.07	.05
MnO	.00	.00	.16	.07	.04	.00	.00	.00	.01
Co ₂	.01	.04	.04	.01	.01	.02	.54	.01	1.1
SUM	100	100	100	100	100	100	100	99	100
Spectrographic analyses (parts per million)									
[Joseph L. Harris, analyst ¹ for samples 22 through 26, Janet D. Fletcher ² , analyst for samples 27 through 30, N = not detected at value shown]									
B	N 10	N 10	N 10	N 10	30	17	33	36	26
Ba	100	150	1,500	1,000	1,000	1,150	220	310	720
Be	1	N 1	1	1	3	3	3	4	3
Co	30	30	10	N 5	N 5	2	1	N 1	1
Cr	300	300	200	5	5	5	3	3	3
Cu	70	50	20	7	1.5	3	7	10	28
La	N 50	N 50	50	N 50	N 50	42	45	59	58
Mo	3	3	N 3	N 3	3	1	N 1	1	2
Nb	N 3	N 3	N 3	N 3	20	6	26	28	20
Ni	100	100	50	N 5	N 5	1	5	3	8
Pb	N 5	5	5	N 5	20	37	16	25	30
Sc	30	50	10	10	7	4	3	5	8
Sr	300	500	1,000	1,500	300	230	53	37	89
V	200	200	50	70	20	20	10	70	22
Y	20	20	20	20	50	24	28	42	34
Zr	100	100	200	70	150	100	410	560	460
CIPW norms									
[Leaders indicate no data]									
Quartz	2.	1.6	17	15	31.6	30.5	30.8	31.	26.7
Orthoclase	1.7	2.2	16	7	28.7	28	28.5	29.3	28.4
Albite	17.8	20.4	24.6	38	25.	25.6	33.2	33.3	32.2
Anorthite	37	35.3	22.8	24.7	5.6	6.5	2.2	2.	4.8
Corundum	--	--	--	1.3	1.8	2.2	.8	.6	--
Diopside	13.4	16.	--	--	--	--	--	--	.6
Hypersthene	19.6	15.	10.4	1.4	2.3	2.8	.8	.3	.6
Magnetite	4.6	6.	3.2	--	1.4	.9	--	--	--
Ilmenite	2.3	2.3	1.5	1.4	.8	.7	.3	.3	.2
Apatite	.3	.3	1.	.7	.3	.7	.1	.2	.1
Hematite	--	--	--	5.4	--	--	1.	2.1	2.5
Calcite	--	--	--	--	--	--	1.2	--	2.5

¹Results are to be identified with geometric brackets whose boundaries are 1.2, 0.83, 0.56, 0.38, 0.26, 0.18, 0.12, ..., but are reported arbitrarily as midpoints of these brackets, 1, 0.7, 0.5, 0.3, 0.2, 0.15, 0.1 ... Precision of a reported value is approximately plus or minus one bracket at 68 percent or two brackets at 95 percent confidence.

²Concentration ranges of elements determined by computerized spectrographic analyses; standard deviation is plus 50 percent and minus 33 percent.

teristically high SiO_2 contents, K_2O contents are greater than Na_2O contents, and the felsic normative minerals total more than 90 percent of the rock.

A second episode of volcanism consists of dark-weathering, ledge-forming andesite and andesitic basalt flows of Miocene age about 60 m thick, underlain by andesite and latite tuff that in turn lies unconformably on folded Osgood Mountain Quartzite of Early Cambrian(?) age in the northwest part of Golconda quadrangle (Erickson and Marsh, 1974a; fig. 1). The flows are very scoriaceous at the base and weather to thin plates above the scoria. In thin section, the rock consists of euhedral orthopyroxene (enstatite) phenocrysts (about 5 percent of the rock) in a dense flow-textured groundmass of tiny plagioclase fibers and brown glass. The underlying tuff is pale-yellowish-gray, brownish-gray, and cream-colored lithic andesite and latite tuff containing thin, discontinuous conglomerate stringers. This tuff contains subhedral and euhedral andesine, biotite, hornblende, magnetite, and rock granules and pebbles.

Chemical and spectrographic analyses and CIPW norms of a sample of one flow selected for whole-rock age dating (loc. sample 24, fig. 1; table 7) show this rock to be of andesitic composition. The silica content is a little high for andesite (near dacite) and is reflected in rather high normative quartz. Much of the K_2O and SiO_2 contents are contained in the brown glass of the groundmass. Modal orthopyroxene and the high Cr, Ni, and Co contents attest to the mafic character of the rock.

Chemical analysis of the andesite tuff shows the expected low SiO_2 content, but the low FeO and MgO content is surprising. Perhaps the ash has been leached by the surface waters that deposited conglomerate stringers in the tuff sequence. Contamination from included lithic fragments also serves to mask the true chemical composition of the tuff.

Rhyolite vitrophyre of Miocene age is the third recognized episode of volcanic activity in the area. Only thin isolated patches and large float blocks on gravel-covered ridges in the southwest part of the Goldrun Creek quadrangle have been preserved; the total original areal extent of the vitrophyre is not known. The rock is gray to pink and composed of rounded and embayed quartz crystals, sanidine, sodic andesine, and biotite in a glass matrix with abundant microlites. Zircon is an accessory mineral. Phenocrysts are so abundant locally that the rock appears coarse textured and spalls easily to form grus.

Chemical and spectrographic analyses and CIPW norms of vitrophyre (table 7) reflect the characteristic rhyolite composition—high SiO_2 ; low FeO , MgO ,

and CaO ; $\text{K}_2\text{O} > \text{Na}_2\text{O}$; high normative quartz and orthoclase; and low normative anorthite.

Olivine basalt flows of Pliocene age, the most recent volcanic episode recognized in the area, have been found in the Golconda, Iron Point, and Goldrun Creek quadrangles (Erickson and Marsh, 1974 a, b; Marsh and Erickson, 1978; fig. 1). The flows are dark gray, vesicular, dense, and composed of labradorite laths (60–70 percent) surrounded by optically continuous masses of augite (20–30 percent). Olivine phenocrysts (5–10 percent) and magnetite and ilmenite (up to 5 percent) make up the rest of the rock.

Chemical and spectrographic analyses and CIPW norms show very low SiO_2 ; high FeO , MgO , and CaO ; very low Na_2O and K_2O ; high Co, Cr, Ni, and Sc; high normative anorthite; and high normative femic mineral contents typical of olivine basalts (table 7). The rock has very low K_2O content for basaltic rocks in the Great Basin, which tend to be subalkaline to alkali olivine basalt in character (Leeman and Rogers, 1970; M. L. Silberman and C. D. Noble, unpub. data, 1976).

Age

The four episodes of Tertiary volcanism recognized in the Edna Mountain quadrangle fit well in the two major Tertiary volcanic pulses in central Nevada described by Silberman and McKee (1974). They reported that the principal period of igneous activity occurred between 38 and 20 m.y. ago with a change from dominantly andesite volcanism in the older rocks to dominantly rhyolite and quartz-latite ash flows in the younger rocks. The rhyolite ash-flow tuffs in the Goldrun Creek quadrangle (sample locs. 28–30) range from 24.2–25.9 m.y. old as determined from K-Ar dates on sanidine from three different sample localities (table 5). The andesitic basalt flows and andesite tuff in the Golconda quadrangle also belong to this major period of activity, but they are unrelated as to source and composition to the rhyolite ash-flow tuffs. A K-Ar whole-rock age of 22.8 m.y. on one sample (loc. 25, fig. 1) of flow rock and a hornblende age of 23.8 m.y. (sample loc. 25, fig. 1) from underlying andesite tuff were obtained in this study (table 5).

The second distinctive period of volcanic activity reported by Silberman and McKee (1974) occurred 16–10 m.y. ago, was dominantly basalt flows and associated rhyolite flows and flow dome complexes, and was of much smaller volume than the earlier activity. The rhyolite vitrophyre in the Goldrun Creek quadrangle belongs to this period of activity. Concordant ages from biotite-sanidine (14.6 ± 0.4 and 14.3 ± 0.4

m.y., sample loc. 26, fig. 1) and from biotite (14.6 ± 0.4 m.y., sample loc. 27, fig. 2) give a good confidence to these age dates (table 5). Although the vitrophyre occurs only in small thin isolated patches and large float blocks, it probably extended over a much larger area in Miocene time. The age of 5 m.y. reported on the olivine basalt flow from the Goldrun Creek quadrangle (sample loc. 22, table 5) places this rock unit within a limited group of young basalts erupted in the central and west Great Basin during the last 6 m.y. In the region near Edna Mountain, a few of these younger basalts were erupted as cinder cones and associated flows, usually in the vicinity of hot springs. Most of them occur farther west in the Carson Sink and Walker Lane regions in west-central and southwest Nevada (Silberman and others, 1976; Stewart and Carlson, 1976).

REFERENCES CITED

- Ashley, R. P., and Silberman, M. L., 1976, Direct dating of mineralization at Goldfield, Nevada, by K-Ar and fission-track methods: *Econ. Geology*, v. 71, no. 5, p. 904-924.
- Carlson, J. E., Laird, D. W., Peterson, J. A., Schilling, J. H., Silberman, M. L., and Stewart, J. H., 1975, Preliminary map showing distribution and isotopic ages of Mesozoic and Cenozoic intrusive rocks in Nevada: U.S. Geol. Survey Open-File Rept. 75-499, scale 1:1 000 000.
- Dalrymple, G. B., and Lanphere, M. A., 1969, Potassium-argon dating—Principles, techniques and applications to geochronology: San Francisco, W. H. Freeman and Co., 258 p.
- Damon, P. E., and Mauger, R. L., 1966, Epeirogeny-orogeny viewed from the Basin and Range province: *Soc. Mining Engineers Trans.*, v. 235, p. 99-112.
- Dodge, F. C. W., Fabbi, B. P., and Ross, D. C., 1970, Potassium and rubidium in granitic rocks of central California, in *Geological Survey research 1970*, chap. D: U.S. Geol. Survey Prof. Paper 700-D, p. D108-D115.
- Erickson, R. L., and Marsh, S. P., 1971 [1972], Geochemical, aeromagnetic, and generalized geologic maps showing distribution and abundance of mercury, arsenic, antimony, tungsten, gold, copper, lead, and silver, Golconda and Iron Point quadrangles, Humboldt County, Nevada: U.S. Geol. Survey Misc. Field Studies Maps MF-312, 313, 314, 315 scale 1:24 000.
- , 1972, Geochemical, aeromagnetic, and generalized geologic maps showing distribution and abundance of molybdenum and zinc, Golconda and Iron Point quadrangles, Humboldt County, Nevada: U.S. Geol. Survey Misc. Field Studies Map MF-345, scale 1:24 000.
- , 1974a, Geologic map of the Golconda quadrangle, Humboldt County, Nevada: U.S. Geol. Survey Geol. Quad. Map GQ-1174, scale 1:24 000.
- , 1974b [1975], Geologic map of the Iron Point quadrangle, Humboldt County, Nevada: U.S. Geol. Survey Geol. Quad. Map GQ-1175, scale 1:24 000.
- Fabiano, E. G., and Peddie, N. W., 1969, Grid values of total magnetic intensity IGRF-1965: ESSA Tech. Rept. C & GS 38.
- Gustavson, L. B., and Hunt, J. P., 1975, The porphyry copper deposit at El Salvador, Chile: *Econ. Geology*, v. 70, no. 5, p. 857-912.
- Ingamells, C. O., 1970, Lithium metaborate flux in silicate analysis: *Anal. Chim. Acta*, v. 52, no. 2, p. 323-334.
- Kistler, R. W., and Peterman, Z. E., 1973, Variations in Sr, Rb, K, Na, and initial $\text{Sr}^{87}/\text{Sr}^{86}$ in Mesozoic granitic rocks and intruded wallrocks in central California: *Geol. Soc. America Bull.*, v. 84, no. 11, p. 3489-3512.
- Leeman, W. P., and Rogers, J. J. W., 1970, Late Cenozoic alkali-olivine basalts of the Basin and Range province, U.S.A.: *Contr. Mineralogy and Petrology*, v. 25, no. 1, p. 1-24.
- Marsh, S. P., and Erickson, R. L., 1975, Integrated geologic and geochemical studies, Edna Mountain, Nevada, in Elliott, I. L., and Fletcher, W. K., eds., *Geochemical Exploration 1974*: New York, Elsevier Sci. Pub. Co., p. 239-250.
- , 1977, Geologic map of the Brooks Spring quadrangle, Humboldt County, Nevada: U.S. Geol. Survey Geol. Quad. Map GQ-1366.
- , 1978, Geologic map of the Goldrun Creek quadrangle, Humboldt County, Nevada: U.S. Geol. Survey Geol. Quad. Map GQ-1407.
- McKee, E. H., and Silberman, M. L., 1970, Geochronology of Tertiary igneous rocks in central Nevada: *Geol. Soc. America Bull.*, v. 81, no. 8, p. 2317-2327.
- Neff, T. R., 1969, Petrology and structure of the Buffalo Mountain Pluton, Humboldt County, Nevada: Stanford Univ., Ph.D. thesis, 120 p.
- Nockolds, S. R., and Allen, R., 1954, The geochemistry of some igneous rock series—pt. 2: *Geochim. et Cosmochim. Acta*, v. 5, no. 6, p. 245-285.
- Shaw, D. M., 1968, A review of K-Rb fractionation trends by covariance analysis: *Geochim. et Cosmochim. Acta*, v. 32, p. 573-601.
- Silberman, M. L., and McKee, E. H., 1971, K-Ar ages of granitic plutons in north-central Nevada: *Isochron/West*, no. 1, p. 15-32.
- , 1974, Ages of Tertiary volcanic rocks and hydrothermal precious-metal deposits in central and western Nevada: *Nevada Bur. Mines and Geology Rept.* 19, p. 67-72.
- Silberman, M. L., Stewart, J. H., and McKee, E. H., 1976, Igneous activity, tectonics, and hydrothermal precious-metal mineralization in the Great Basin during Cenozoic time: *Am. Inst. Mining, Metall. Engineers Trans.*, v. 260, p. 258-263.
- Stewart, J. H., and Carlson, J. E., 1976 Cenozoic rocks of Nevada—four maps and brief description of distribution, lithology, age, and centers of volcanism: *Nevada Bur. Mines Map* 52, 4 sheets, scale 1:1 000 000.
- Theodore, T. G., Silberman, M. L., and Blake, D. W., 1973, Geochemistry and potassium-argon ages of plutonic rocks in the Battle Mountain mining district, Lander County, Nevada: U.S. Geol. Survey Prof. Paper 798-A, p. A1-A24.
- U.S. Geological Survey, 1970, Aeromagnetic map of the Winnemucca area, northwestern Nevada: U.S. Geological Survey open-file rept., scale 1:62 500.
- Wollenberg, H. A., and Smith, A. R., 1968, Radiogeologic studies in the central part of the Sierra Nevada batholith, California: *Jour. Geophys. Research*, v. 73, no. 4, p. 1481-1495.

PRESSURE GRADIENTS AND BOILING AS MECHANISMS FOR LOCALIZING ORE IN PORPHYRY SYSTEMS

By CHARLES G. CUNNINGHAM, Denver, Colo.

Abstract.—Fluid inclusions in ore zones of porphyry systems indicate that extensive boiling of hydrothermal fluids accompanies deposition of ore and gangue minerals. The boiling commonly accompanied a change from a lithostatic to a hydrostatic environment during evolution of an epizonal stock. Pressure gradients near the margin of the stock can determine whether ore or only a diffuse zone of mineralization is formed. A sharp drop in pressure in an epizonal environment is more likely to cause extensive boiling than a comparable change in a deeper environment, as the slope of the boiling curve steepens with an increase in pressure. The drop in pressure causes the hydrothermal fluids to boil and creates a crackle (stockwork) breccia, which hosts the veinlets of gangue quartz and ore minerals. The boiling selectively partitions CO_2 , H_2S , and HCl into the vapor phase, changing the pH, composition, ionic strength, and thus the solubility product of metal complexes in the remaining liquid and causing the ore and gangue to come out of solution. Fluid inclusions trapped from boiling solutions can exhibit several forms, depending on the physical and chemical conditions of the hydrothermal fluid from which they were trapped. In one case, inclusions when heated can homogenize to either liquid or vapor at the same temperature, which is the true boiling temperature. In another case, homogenization of various inclusions can occur through a range of temperatures. The latter case results from the trapping of mixture of liquid and vapor. Variations in salinity can result from boiling of the hydrothermal fluid, or intermittent incorporation of high-salinity fluids from the magma, or trapping of fluids of varying densities at pressure-temperature conditions above the critical point of the fluid. In places, paleo-pressure-temperature transition zones can be recognized by fluid-inclusion homogenization temperatures and phase relationships and by the presence of anhydrite daughter minerals. Boiling of a hydrothermal fluid in the porphyry environment affects light stable isotopes. Hydrogen is preferentially fractionated into the vapor phase from water boiling below 223° C; above this temperature deuterium is selectively enriched in the vapor phase. In certain environments boiling creates a vapor-dominated system in which the condensate is swept away by meteoric waters and the H/D in the residual fluids is progressively increased through time.

Fluid inclusions, containing samples of the hydrothermal fluid trapped under the physical and chemical conditions that prevailed at the time of ore deposition, are common in porphyry ore deposits. Roedder (1971) was among the first to point out that the phase relationships observed within fluid inclusions formed

in the porphyry environment indicate that the ore was deposited from solutions that had periodically boiled. Nash (1976), in a careful study of 37 porphyry copper deposits, demonstrated that coexisting high-salinity, halite-bearing fluid inclusions and vapor-rich inclusions may be effective guides in exploring for porphyry copper deposits.

The hydrothermal fluid phase associated with the evolution of an epizonal intrusion is subject to certain physicochemical constraints which indicate that drops in pressure sufficient to cause boiling should be common. Decreases in pressure can result from emplacement into shallow levels of the crust, but sudden pressure changes occur when an environment goes from lithostatic to hydrostatic conditions during crystallization. Fluid inclusions in porphyry ore deposits indicate that pervasive boiling commonly takes place during ore deposition. A hydrothermal fluid will often boil in response to a change in pressure, and the physical and chemical changes that occur during boiling are likely to cause quartz and sulfides to be deposited. Changes in the fugacity of oxygen and sulfur from interaction with wallrocks and from dilution of the ore fluid by meteoric water can have a significant effect on ore deposition, especially in the latter stages when, as indicated by stable-isotope studies, extensive circulation of meteoric water takes place.

Deposition of ore and gangue in the porphyry environment is dynamic and complex, and fluid inclusions give us unique insight into the physicochemical changes at many instances during the process. Integrated evidence from several disciplines emphasizes the role of pressure gradients and boiling in the process of ore deposition in porphyry systems and gives insight into the physicochemical changes that result from boiling.

Acknowledgments.—I deeply appreciate the discussions and perceptive comments on this manuscript by Robert J. Kamilli, Donald E. White, Robert O. Rye, Thomas A. Steven, and Edwin Roedder.

SUBVOLCANIC SETTING OF PORPHYRY INTRUSIVES

The model of a porphyry-type ore body in an epizonal intrusion (fig. 1) used in this report is a general composite that draws on concepts developed by many people (Lowell and Guilbert, 1970; White and others,

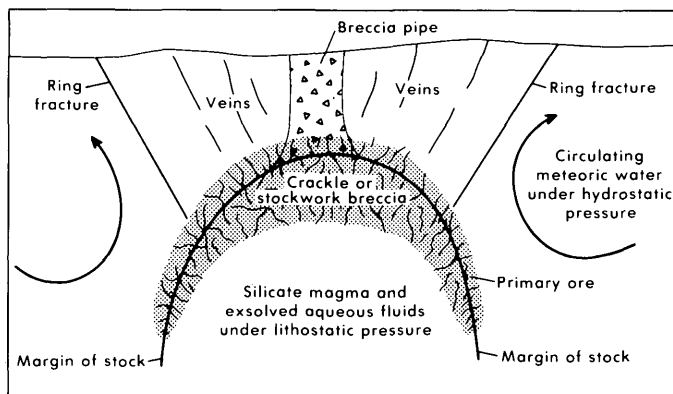


FIGURE 1.—Composite model of an epizonal porphyry intrusive. Circulating meteoric water on the borders and top of the system is under hydrostatic pressure, but pressures on fluids in interior parts of the intrusion are lithostatic.

1971; Phillips, 1973; Sillitoe, 1973; Hall and others, 1974; Taylor, 1974; and others). Stocks with associated porphyry copper- and molybdenum-bearing ore bodies commonly were emplaced within 3 km of the surface and in places within 1.5 km (Fournier, 1969). Some cut the lower part of genetically related volcanic piles. The magma generally started out undersaturated in volatiles (Burnham, 1967). During intrusion, volatiles tended to accumulate near the top of the advancing magma column (Lipman and others, 1966) and in places achieved saturation. If the system vented, quenched textures developed within the stock, breccia pipes developed in the overlying rocks, and welded tuffs were typically formed at the surface.

Light stable isotopes (Sheppard and Taylor, 1974; Taylor, 1974; Rye, 1966; Hall and others, 1974) indicate that magmatic waters are often involved in the initial stages of ore deposition in the porphyry environment. In the surrounding rocks, however, heat from the epizonal stock sets up convective cells of meteoric water to form geothermal systems. Some of the hot water may surface as hot springs. As the whole system cools, the elevated isotherms collapse inward, causing an influx of meteoric water into the porphyry environment.

Detailed three-dimensional studies of porphyry systems, as epitomized by the Bingham, Utah, deposit (fig. 2) (James, 1971), have shown that primary

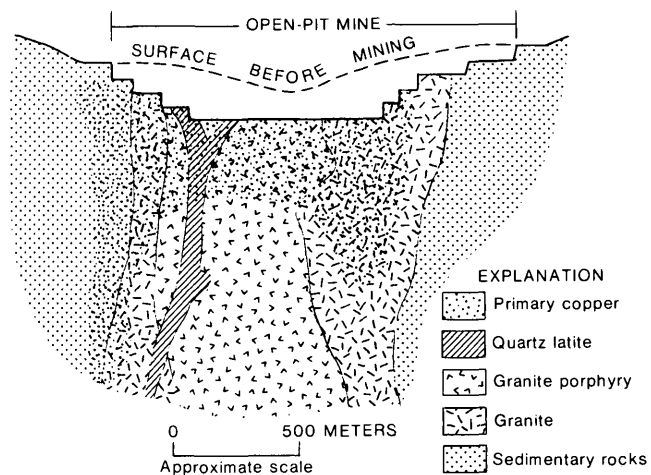


FIGURE 2.—Diagrammatic interpretation of the distribution of primary copper in the Bingham, Utah, porphyry copper deposit (modified from James, 1971, p. 44).

copper and molybdenum ore bodies are commonly draped over the top of the related stocks. The mineralized material is in crackle breccia formed near the margins of the intrusions; the cores of the stocks are commonly barren. Studies at Climax, Colo. (Wallace and others, 1968), have shown that, in some porphyry deposits, several ore bodies with similar cross sections occur in a stacked arrangement, one upon another.

Moore and Nash (1974) found that at Bingham (fig. 3) the biotitic (potassium-silicate) altered rocks and high-salinity fluid inclusions have the same areal distribution as the copper ore zone. Nash (1976) has examined 36 other porphyry copper deposits and found that most evolved through a stage characterized by

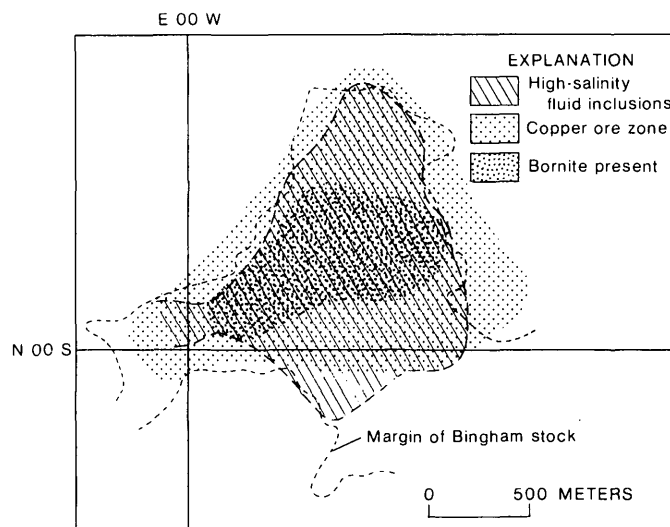


FIGURE 3.—Generalized map of Bingham, Utah, porphyry copper deposit showing the spatial relationships of the stock, the copper ore zone, and highly saline fluid inclusions (modified from Moore and Nash, 1974).

high-salinity hydrothermal fluids that boiled. Such boiling can occur at many places in the porphyry environment where the right combinations of temperature, composition, and pressure of the fluid are achieved. The distribution of ore as an inverted cuplike form near the margin of its host intrusion probably reflects the geometry of the zone of steepest pressure gradients where boiling was most likely. The juxtaposed high-salinity fluid inclusions and vapor-rich fluid inclusions, which indicate boiling fluids, are generally found closely associated with the ore and evidently formed at the same time as the ore.

PRESSURE GRADIENTS

Where pressure gradients exist, they will affect the physical-chemical conditions of hydrothermal fluids and can cause deposition of ore in porphyry systems. Fournier (1969) noted that, at shallow depths in highly faulted regions, sudden pressure drops from lithostatic to hydrostatic conditions are likely, resulting in rapid, even explosive loss of volatiles from the magma. If a granitic magma is intruded to a shallow level in the crust, heat loss to the wallrocks would be expected to produce a crystallized shell, containing the liquid interior of the stock. The pressure on the shell would be lithostatic and approximately equal to the weight of the overlying rock. Therefore, the pressure on the confined silicate magma would also be lithostatic and the pressure on any exsolved aqueous fluid within the magma would also initially be lithostatic. During the course of crystallization of anhydrous minerals, it is possible to generate fluid pressures even greater than lithostatic; this may be a major mechanism for explosive volcanic eruptions (Morey, 1922). At the same time, the pressure on meteoric water circulating in the wallrocks adjacent to a cooling intrusion would be hydrostatic. A pressure gradient from approximately lithostatic to hydrostatic conditions should then exist near the edge of the stock. In this transition zone, the pressure gradient is the steepest, hydrothermal fluids escaping from the magma commonly boil, crackle breccia forms, and ore and gangue minerals are deposited. If the pressure gradient is steep, a localized ore deposit can form; whereas, if the pressure gradient is gradual, boiling may be more dispersed and less violent, and the resulting mineralized rock may be more diffuse and of lower grade.

Hydrothermal fluids associated with a granitic stock emplaced at a shallow depth are more likely to boil in response to changes in pressure than are those emplaced at a greater depth. Figure 4 (modified from Haas, 1971, 1976; Sourirajan and Kennedy, 1962)

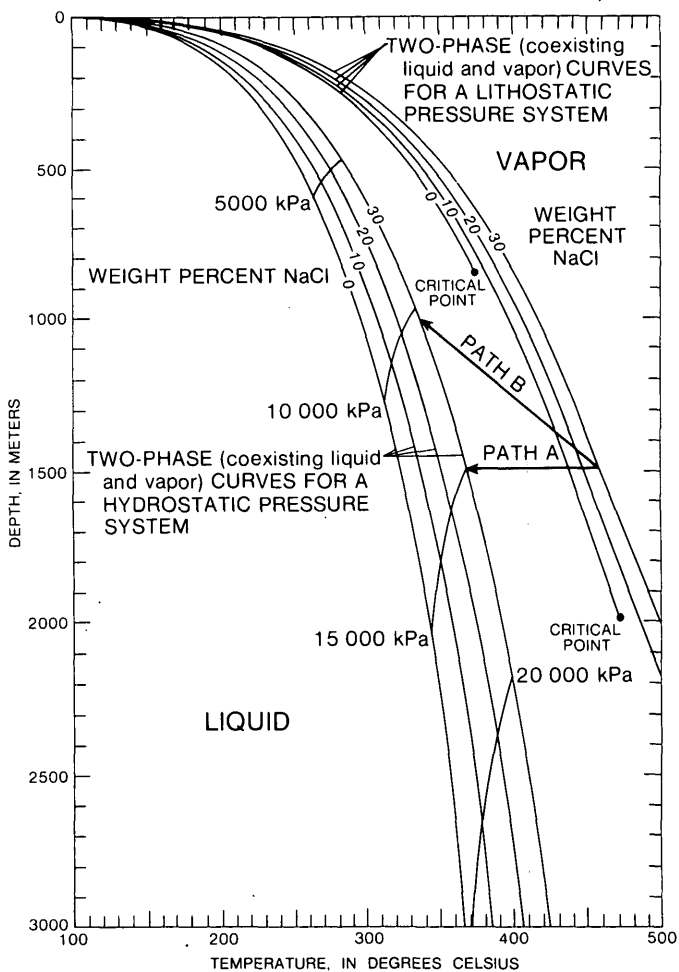


FIGURE 4.—Temperature-pressure-depth diagram of the two-phase boundaries in the $\text{H}_2\text{O}-\text{NaCl}$ system (modified from Haas, 1971, 1976; Sourirajan and Kennedy, 1962). Arrows show pressure and temperature paths for fluids crossing the transition zone. See text for discussion.

shows the position of two-phase (boiling) curves for various salinities of hydrothermal fluids as a function of depth and temperature. In all cases, the slope of the two-phase curve steepens markedly with depth. Therefore, an isothermal change in pressure, represented on such a graph, would be more likely to intercept the two-phase curve at shallow depth; this means a change of pressure at shallow depth is much more likely to cause a nonboiling liquid to start boiling. The slope flattens markedly at the shallower depths commonly associated with the epizonal environment; this is probably a major reason why boiling is so common in epizonal porphyry systems, especially near their tops.

A crackle breccia can form from hydrofracturing of the rock by boiling hydrothermal fluids (Phillips, 1973). A typical crackle breccia is formed around the perimeter of an epizonal stock and is most extensively

developed at the top. The fracturing greatly increases the permeability of the rock and allows a convective system to be set up which, especially in the latter stages of the stock's history, permits entry of meteoric waters. The fractures in the crackle breccia often contain quartz deposited with sulfides, which together form a stockwork breccia. The quartz usually contains fluid inclusions whose phase relationships indicate that the hydrothermal fluid was boiling when the quartz was deposited. The fracturing of the host rock results in a drop in pressure which can cause the fluids to boil and the quartz and sulfides to precipitate.

Various triggering mechanisms can cause rapid release of pressure, consequent boiling of fluids, formation of crackle breccia, and deposition of ore minerals. The sudden failure of the pressure seal can result from the progressive crystallization of anhydrous minerals. A similar effect can result from (1) the upward passage of a magma from a tight host rock to a broken host rock (for example, passing from tight shale to broken sandstone, encountering a thrust fault, or going from sedimentary basement rocks into volcanic rocks), (2) tumescence of overlying rocks above an advancing magma column and resulting fracturing, or (3) intrusion with progressive crystallization into a tectonically active area accompanied by sudden fracturing.

FLUID INCLUSIONS IN THE ORE ZONE

Fluid inclusions in the ore zone of porphyry intrusions range from hydrous saline melts containing more than 60 weight percent dissolved salts in solution and high-density steam (Roedder, 1971) to virtually fresh water and low-density steam. The variations in salinity commonly observed in fluid inclusions in the ore zone can result from juxtaposed primary and secondary inclusions, "necking down" of inclusions (Roedder, 1972), entrapment of fluids with various densities from a progressively boiling system, intermittent incorporation of high-salinity fluids given off by the magma, or entrapment of fluids of various densities at fluctuating pressure-temperature conditions above the critical point of the fluid. The multicomponent brines entrapped in fluid inclusions may precipitate several daughter minerals on cooling (fig. 5), and these may be identified by thermal or optical techniques or by the scanning-electron microscopy techniques (fig. 6) recently developed by Metzger and others (1977). Vapor-rich fluid inclusions (fig. 7) representing trapped steam (Roedder, 1967) commonly coexist with inclusions containing high- or low-salinity fluids representing the boiling solutions (Nash, 1976). The vapor-rich inclusions are

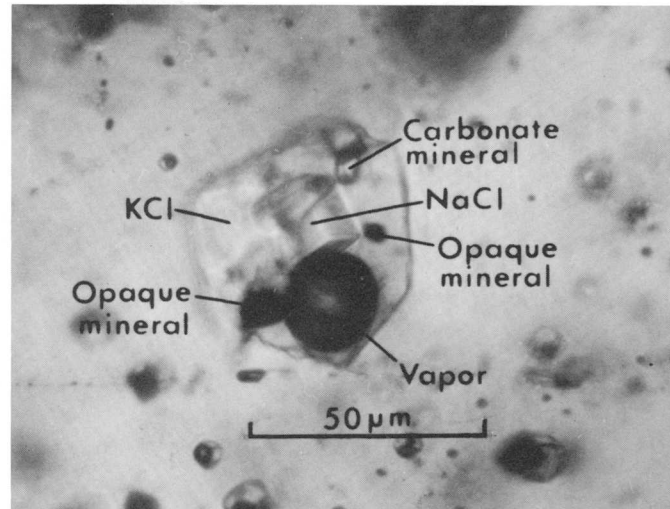


FIGURE 5.—Fluid inclusion in quartz containing daughter minerals of NaCl and KCl, a carbonate, and two opaque minerals.

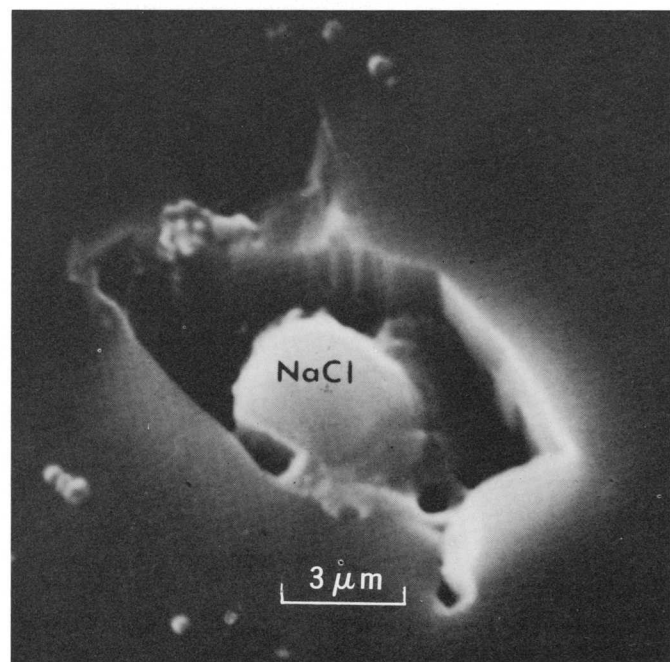


FIGURE 6.—Scanning-electron microscope view of an opened fluid inclusion in vein quartz from a porphyry copper deposit. A daughter crystal of NaCl coated with salts deposited from the evaporated inclusion fluid rests in the opened cavity.

common in early quartz in porphyry systems and less common in later vein deposits.

ORE DEPOSITION AS A RESULT OF BOILING

The deposition of ore from a boiling hydrothermal fluid can result from any of several physical and chem-

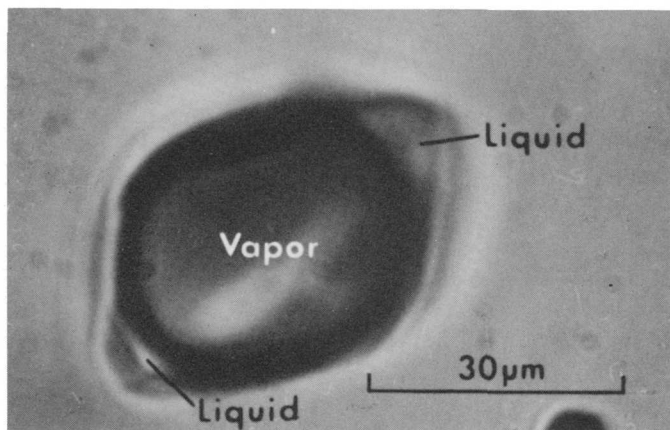


FIGURE 7.—Vapor-rich fluid inclusion representing trapped steam in vein quartz from a porphyry copper deposit.

ical changes that take place in a fluid, some of which may actually increase metal solubility. In the pressure and temperature range for which experimental data are available, the most immediate and direct control on the deposition of ore is boiling itself. The vapor that forms can hold only a limited quantity of metals, principally the metals that travel as fluoride complexes. Metal sulfide and metal chloride complexes can be broken by the loss of volatile anions and the metals then become precipitated. If H_2S is present, it is partitioned into the vapor phase, decreasing the solubility of sulfides and thus causing the precipitation of ore minerals under some circumstances. Appreciable quantities of HCl may also be present in a high-temperature, low-pressure vapor phase (Fournier, 1972), resulting in further breakdown of chloride complexes and deposition of ore minerals. If CO_2 is present, it is selectively partitioned into the vapor phase, and the resulting decrease in solubility of some carbonates breaks carbonate complexes in which some elements may be transported. Boiling results in changes in the pH, oxygen fugacity, composition, and ionic strength of the hydrothermal fluid, which change the solubility product of metal complexes.

A drop in pressure and the resultant boiling (or increased rate of boiling) would also decrease the fluids' temperature. Reodder (1971) recognized that the ore at Bingham was not deposited by a simple drop in temperature. Barton and Toulmin (1961) considered several mechanisms for cooling hydrothermal fluids and cited adiabatic expansion (including boiling) of the hydrothermal fluid as a process that could significantly affect the thermal balance during ore deposition. They point out that if the pressure on a fluid is reduced below its vapor pressure, the fluid will boil and cooling will result. The case of reversible boiling may be significant in some vein systems but a sudden pres-

sure drop with the liquid flashing to steam is more likely in a porphyry system. Such flashing can result in marked cooling, especially at temperatures above about $350^\circ C$ (Barton and Toulmin, 1961). If a pressure transition from lithostatic to hydrostatic takes place at a given depth, such as 1500 m (fig. 4), the boiling point suddenly decreases by about $100^\circ C$, and a fluid that was on the high pressure curve, and was probably boiling slowly as it rose, must then boil extensively. In addition, the heat stored in the rock through this $100^\circ C$ interval is then made available for extensive additional boiling, which would leave the residual fluid much more saline than it would be after normal adiabatic boiling. The higher salinities might make the Cu-Cl complexes more stable, but lower temperatures and the higher pH's caused by loss of CO_2 and H_2S to vapor might more than offset salinity changes.

Figure 4 illustrates two possible paths for the change in pressure and temperature of a hydrothermal fluid as it crosses the pressure gradient at the boundary of an epizonal stock. In both cases, the starting hydrothermal fluid has an assumed composition of 30 weight percent NaCl and is confined within a crystallizing stock at a depth of 1500 m. The fluid is confined by a lithostatic pressure of about 39 000 kPa and has a temperature of $460^\circ C$. If the shell is fractured or the fluid allowed suddenly to enter a fracture, pressure will drop (path A) to hydrostatic conditions (15 000 kPa). This will cause immediate, extensive boiling of the fluid. After boiling and conduction of the heat, the temperature will drop to a stable point at $360^\circ C$ resulting in deposition of ore and gangue. Evaporation of the fluid will also cause deposition of the ore and gangue if the solubility limits are exceeded. In the alternative situation (path B), the pressure is released gradually. Path B shows the pressure-temperature path a fluid will follow going from lithostatic to hydrostatic pressure over a 500-m interval. Actual conditions probably would fluctuate back and forth from crackle breccia events (which decrease pressure) to self-sealing events (which permit pressures to build up again, boiling points to increase, and some heat being stored in the rock to be available for extra boiling when next brecciated). This case of isoenthalpic boiling would increase the salinity and cause the ore to be dispersed throughout the 500-m zone. If salinity did not change, the resultant hydrothermal fluid would be at a pressure of about 10 500 kPa and temperature of $335^\circ C$.

If the change in pressure and temperature for a given composition of fluid and amount of recharge is such that a large quantity of liquid is converted to steam, a vapor-dominated regime can form (White

and others, 1971). This would be most likely to happen near the top of the stock where confining pressure is least. Cathles (1977) has shown by modeling systematic changes in permeability, level of intrusion, and volume of a stock that a self-supported, vapor-dominated steam zone is commonly (but briefly) formed. This zone would be bounded above by condensed water and below by a zone of boiling if the hydrothermal solutions are saline.

FLUID INCLUSION EVIDENCE OF BOILING

Fluid inclusions trapped from boiling solutions can exhibit several forms, depending on the physical and chemical conditions of the hydrothermal fluid involved. Two different cases seem to prevail, as noted by Roedder (1967), Kelly and Turneaure (1970), and Kamilli and Ohmoto (1977). In both cases, all fluid inclusions in a sample group are known or assumed on reasonable grounds to have been trapped at the same time.

In the first case, all inclusions in the group, on heating, homogenize to either liquid or vapor at the

same temperature. This is generally the case observed in the Bolivian tin and tungsten deposits by Kelly and Turneaure (1970). Roedder (1967) has suggested that the vapor-rich inclusions are a result of vapor bubbles sticking to the side of a growing crystal and eventually being enveloped and the liquid-rich inclusions area are a result of trapping homogeneous liquid. Experimental work on growing crystals (Wilcox and Kuo, 1973) has confirmed that vapor bubbles may either be trapped as discrete bubbles, as chains of bubbles, as tubes, or they may float away. Inclusions of this first type formed under conditions of gentle boiling and slow crystal growth, which are reversible adiabatic processes. Such conditions are most commonly observed in vein systems and probably result from fluids rising along a hydrostatic boiling curve accompanied continuously or episodically by boiling. In this case, the boiling is not as intense or as localized as that taking place in a porphyry environment.

The behavior of fluid inclusions in the first case can be modeled using the system $H_2O-NaCl$ (fig. 8).

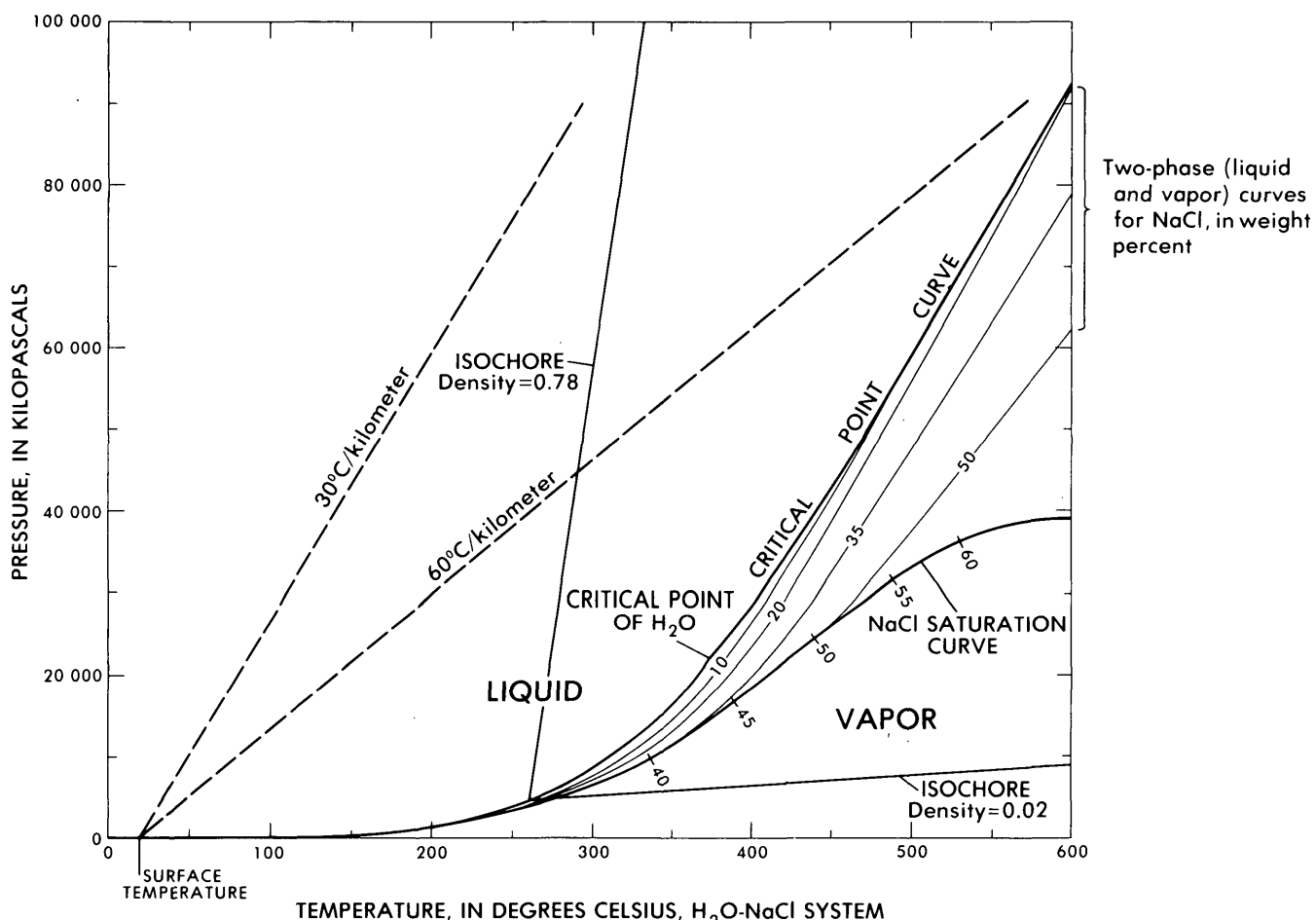


FIGURE 8.—Pressure-temperature section of the $H_2O-NaCl$ system showing the saturation curve, two-phase boundaries, and critical-point curve. Isochores for fluid inclusions homogenizing to liquid and vapor are shown. Normal and high geothermal gradients plotted for scale.

Upon heating, the temperature and internal pressure of both the liquid-rich and vapor-rich inclusions proceed along the two-phase boundary curve; pressure increases slightly as temperature increases. Both types of inclusions homogenize at the same temperature and, with further heating, their pressure and temperature values leave the two-phase boundary curve and proceed along positive-sloping isochores (fig. 8) appropriate for the respective densities of the inclusions. Barring possible complications such as the presence of noncondensable gases, the temperature of homogenization is the actual temperature of boiling. The total pressure on the fluid can be easily determined because the total pressure at any given temperature equals the vapor pressure for the boiling fluid at that temperature. A good approximation of the conversion of pressure to depth can be made using the data of figure 4 for appropriate lithostatic or hydrostatic models.

In the second case, fluid inclusions trapped at the same time are more likely to homogenize to liquid or vapor at different temperatures when heated. In ordinary thin sections this can be seen in the different ratios of liquid to vapor within the inclusions. Obviously, one would have to recognize and discard the inclusions which had undergone necking down (Roedder, 1967) or were secondary in origin. This trapping of different ratios of vapor to liquid has been interpreted by Ermakov (1950), Roedder (1967), Nash (1976), and others as resulting from deposition from a boiling fluid. When both liquid and vapor were trapped in the same inclusion, they had to coexist, which means the temperature and pressure conditions were on the two-phase boundary and by definition the fluid was boiling. This second case is commonly observed in the ore zone of porphyry systems and results from rapid boiling of the fluid. This origin has been confirmed by experimental work by Robertson (1968), who grew sodium nitrate crystals from boiling and nonboiling solutions and measured the homogenization temperatures of the fluid inclusions. Roedder (1967) and Robertson (1968) have pointed out that the minimum homogenization temperature results from inclusions that trapped only a single phase and therefore is the true temperature of boiling. Furthermore, if the temperature and composition of a boiling solution is known, then the total pressure is known because it equals the vapor pressure (fig. 8). The maximum temperature that would be measured would be on inclusions that fortuitously trapped just the right proportions of vapor and liquid to homogenize at the critical temperature for their particular composition.

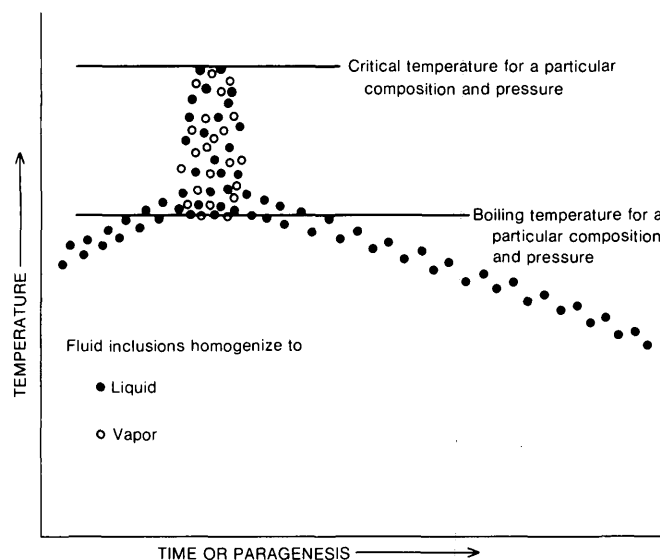


FIGURE 9.—Diagrammatic homogenization temperatures of fluid inclusions in a vein system shown as a function of time or paragenesis.

VEIN SYSTEMS

Boiling of a hydrothermal fluid can be an important mechanism for depositing ore in any epithermal vein system and it need not be related spatially to known intrusives. Figure 9 shows the idealized variations in homogenization temperatures of fluid inclusions as a function of paragenesis or time. It is similar to diagrams developed by Kelly and Turneaure (1970), Slack (1976), and Kamilli and Ohmoto (1977). If the homogenization temperatures of fluid inclusions are measured for most stages of ore deposition, the inclusions generally homogenize to a liquid, indicating that the host was deposited from a homogeneous, non-boiling fluid. Sometimes, during the formation of a deposit, the pressure and temperature conditions are such that boiling occurs. This is reflected in the variations in phase proportions within fluid inclusions for a particular stage in the ore, and often in the texture and composition of the ore. Kamilli and Ohmoto (1977) found that minerals containing the most Au and Ag and exhibiting finest grained textures coincide with a zone in which the inclusions had been trapped from boiling solutions. The location of the boiling, and thus of the best ore, is controlled by several factors. Periodic reopening of a vein structure by tectonic adjustments can momentarily drop the pressure and cause boiling. Depending upon the distribution of pressure and temperature within the vein, boiling could be either restricted to a horizon or could occur throughout the vein, thus localizing ore in a certain band in a paragenetic sequence. The effect of

elevation on pressure control (Kamilli and Ohmoto, 1977) of the boiling zone can also be critical in the hydrostatic environment of a vein system.

PALEOHYDROLOGIC PATTERNS

Figure 8 presents a convenient format for displaying the time-temperature evolution of fluid inclusions during either the formation of an ore deposit or during a heating stage run. Normal and high geothermal gradients are plotted for perspective. Dissolved salts lower the vapor pressure and increase the critical temperature and (generally) the pressure of a solution. A fluid inclusion containing an NaCl daughter mineral and vapor bubble at room temperature would be represented by a point on the saturation curve. As the inclusion was heated, its temperature and pressure would plot progressively higher along the saturation curve until the point at which the daughter mineral dissolved. With further heating, the fluid would be represented by points along a two-phase curve for its composition. When the vapor bubble disappears, the plot for this fluid would leave the two-phase curve and proceed along its isochore. The data from heating and freezing stage runs, in combination with other compositional data on the fluid, allow calculation of the densities of hydrothermal fluids. Knowledge of the distribution of fluid densities is a major factor in the reconstruction of the paleohydrologic circulation patterns.

In addition to using fluid-inclusion filling temperatures and phase relationships, we may be able to recognize paleo-pressure-temperature transition zones by examining daughter mineral compositions in fluid inclusions. Figure 10 shows the solubility of CaSO_4 in $\text{NaCl}-\text{H}_2\text{O}$ solutions as a function of pressure and temperature (Blount and Dickson, 1969). Anhydrite has been identified in daughter minerals (Rosasco and Roedder, 1976) in the porphyry environment. The mineral is unusual in that it has both prograde and retrograde solubilities as a function of pressure, temperature, and other salts in solution. In the environment of porphyry systems, where pressure and temperature decrease, anhydrite can be deposited. With a further drop in pressure and temperature, the anhydrite may be dissolved and the only record of its existence may be its presence in fluid inclusions. The distribution of anhydrite-bearing fluid inclusions in a porphyry system thus could give additional evidence to help in reconstructing the pressure and temperature regime at the time of ore deposition.

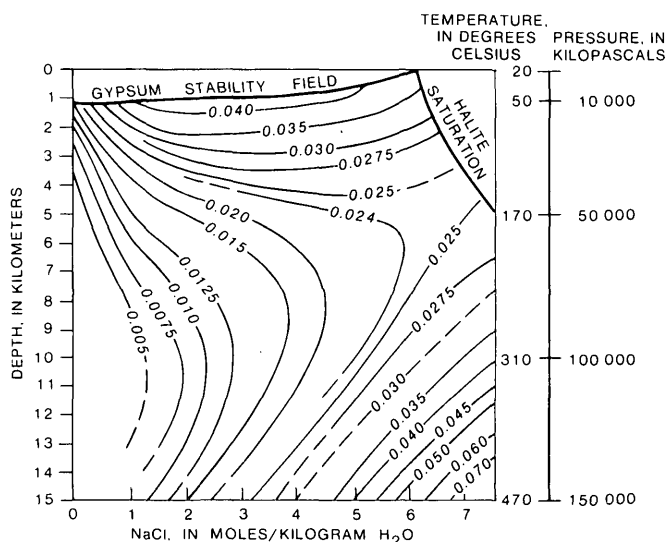


FIGURE 10.—Constant composition curves representing anhydrite solubility in $\text{NaCl}-\text{H}_2\text{O}$ solutions under hydrostatic pressures in a geothermal gradient of $30^\circ\text{C}/\text{km}$. Anhydrite solubilities are in moles CaSO_4/kg of H_2O (modified from Blount and Dickson, 1969, p. 242).

BOILING AND LIGHT STABLE ISOTOPES

The role of data on the light stable isotopes in understanding the process of ore-forming mechanism in the porphyry environment has been investigated by Rye (1966), Sheppard and others (1969, 1971), White (1968, 1974), Hall and others (1974), and Taylor (1974). Sheppard and others (1969) were the first to document by hydrogen and oxygen isotopes the massive influx of meteoric water late in the evolution of porphyry systems. White and others (1971) have shown that if the heat supply is high enough and if recharge through a low-permeability border zone is low enough, a vapor-dominated hydrothermal system can be developed. The systematics of H/D and $^{18}\text{O}/^{16}\text{O}$ isotopic fractionation between coexisting liquid and vapor H_2O is known up to 350°C (Friedman and O'Neil, 1977), but the effects of pressure and dissolved solutes are not as well documented. Oxygen-16 is fractionated preferentially into the vapor phase in H_2O (liq)/ H_2O (vapor) equilibria at least up to 350°C (Friedman and O'Neil, 1977). H/D fractionation is quite different, as Bottinga and Craig (1968) have shown that with pure water hydrogen is fractionated into the vapor phase below 223°C , but above this temperature deuterium is selectively enriched in the vapor phase. At the Salton Sea geothermal field (White, 1968), reservoir temperatures are near 350°C , and the steam is enriched in deuterium but depleted in oxygen-16 relative to the concentrated brine. Although vapor-dominated systems are probably rare in the porphyry environment and restricted to early

stages, the implications are that, if boiling occurs and a vapor-dominated system is generated, the condensate may be swept away by the meteoric waters and residual fluids would show a progressive increase in the H/D with time. This may account for some of the apparent progression to meteoric waters noted in the late stages of the formation of some porphyry deposits.

The shallow depths of emplacement of epizonal stocks, the high temperatures of hydrothermal fluids (on the order of 350°–400°C) in porphyry ore deposits, the formation of crackle breccias, and the obvious presence of boiling fluids as seen in fluid inclusions in the ore zone suggest that pressure gradients exert a major control on the localization of porphyry deposits. When used in conjunction with careful petrologic, paragenetic, alteration-mineral-assemblage, and stable-isotope studies, fluid inclusions can be an important guide for exploration and evaluation of ore zones in porphyry deposits.

REFERENCES CITED

- Barton, P. B., and Toulmin, Priestley, 3d, 1961, Some mechanisms for cooling hydrothermal fluids: U.S. Geol. Survey Prof. Paper 424-D, p. D348–D352.
- Blount, C. W., and Dickson, F. W., 1969, The solubility of anhydrite (CaSO_4) in $\text{NaCl}-\text{H}_2\text{O}$ from 100 to 450°C and 1 to 100 bars: *Geochim. et Cosmochim. Acta*, v. 33, p. 227–245.
- Bottinga, Y., and Craig, H., 1968, High-temperature liquid-vapor fractionation factors for $\text{H}_2\text{O}-\text{HDO}-\text{H}_2\text{O}^{18}$: EOS (Am. Geophys. Union Trans.), v. 49, p. 356.
- Burnham, C. W., 1967, Hydrothermal fluids at the magmatic stage, Chap. 2 of Barnes, H. L., ed., *Geochemistry of hydrothermal ore deposits*: New York, Holt, Rinehart, and Winston, p. 34–76.
- Cathles, L. M., 1977, An analysis of the cooling of intrusives by ground-water convection which includes boiling: *Econ. Geology*, v. 72, no. 5, p. 804–826.
- Ermakov, N. P., 1950, *Issledovaniya mineraloobrazuyushchikh rastvorov*: Kharkov, U.S.S.R., State Univ. of Kharkov Press, 460 p. [Translated into English as *Studies of mineral-forming solutions*, in Yermakov, N. P., and others, 1965, *Research on the nature of mineral-forming solutions with special reference to data from fluid inclusions*: Oxford, Pergamon Press, Internat. Ser. Mon. Earth Sci., v. 22, p. 1–348.]
- Fournier, R. O., 1969, Depths of intrusion and conditions of hydrothermal alteration in porphyry copper deposits [abs]: *Geol. Soc. America Spec. Paper* 121, p. 101.
- , 1972, The importance of depth of crystallization on the character of magmatic fluids: Internat. Geol. Cong., 24th, Montreal 1972, Proc., sec. 10, p. 214.
- Friedman, Irving, and O'Neil, J. R., 1977, Compilation of stable isotope fractionation factors of geochemical interest in *Data of geochemistry*: U.S. Geol. Survey Prof. Paper 440-KK, 12 p.
- Haas, J. L., Jr., 1971, The effect of salinity on the maximum thermal gradient of a hydrothermal system at hydrostatic pressure: *Econ. Geology*, v. 66, no. 6, p. 940–946.
- , 1976, Thermodynamic properties of the coexisting phases and thermodynamic properties of the NaCl component in boiling NaCl solutions: U.S. Geol. Survey Bull. 1421-B, 71 p.
- Hall, W. E., Friedman, Irving, and Nash, J. T., 1974, Fluid inclusion and light stable isotope study of the Climax molybdenum deposits, Colorado: *Econ. Geology*, v. 69, no. 6, p. 884–901.
- James, A. H., 1971, Hypothetical diagrams of several porphyry copper deposits: *Econ. Geolgy*, v. 66, no. 1, p. 48–47.
- Kamilli, R. J., and Ohmoto, Hiroshi, 1977, P ragenesis, zoning, fluid inclusion and isotopic studies of the Finlandia vein, Colqui district, central Peru: *Econ. Geology*, v. 72, no. 6, p. 950–982.
- Kelly, W. C., and Turneaure, F. S., 1970, Mineralogy, paragenesis and geothermometry of the tin and tungsten deposits of the eastern Andes, Bolivia: *Econ. Geology*, v. 65, no. 6, p. 609–680.
- Lipman, P. W., Christiansen, R. L., and O'Connor, J. T., 1966, A compositionally zoned ash-flow sheet in southern Nevada: U.S. Geol. Survey Prof. Paper 524-F, 47 p.
- Lowell, J. D., and Guilbert, J. M., 1970, Lateral and vertical alteration-mineralization zoning in porphyry ore deposits: *Econ. Geology*, v. 65, no. 4, p. 373–408.
- Metzger, F. W., Kelly, W. C., Nesbitt, B. E., and Essene, E. J., 1977, Scanning electron microscopy of daughter minerals in fluid inclusions: *Econ. Geology*, v. 72, no. 2, p. 141–152.
- Moore, W. J., and Nash, J. T., 1974, Alteration and fluid inclusion studies of the porphyry copper ore body at Bingham, Utah: *Econ. Geology*, v. 69, no. 5, p. 631–645.
- Morey, G. W., 1922, The development of pressure in magmas as a result of crystallization: *Washington Acad. Sci. Jour.*, v. 12, p. 219–230.
- Nash, J. T., 1976, Fluid-inclusion petrology—Data from porphyry copper deposits and applications to exploration: U.S. Geol. Survey Prof. Paper 907-D, 16 p.
- Phillips, W. J., 1973, Mechanical effects of retrograde boiling and its probable importance in the formation of some porphyry ore deposits: *Inst. Mining and Metallurgy Trans., sec. B*, no. 801, p. B90–B98.
- Robertson, J. M., 1968, Crystal growth from boiling solutions: an experimental study: Ann Arbor, Michigan Univ., M.S. thesis, 53 p.
- Roedder, Edwin, 1967, Fluid inclusions as samples of ore fluids, Chap. 12 of Barnes, H. L., ed., *Geochemistry of hydrothermal ore deposits*: New York, Holt, Rinehart, and Winston, p. 515–574.
- , 1971, Fluid inclusion studies on the porphyry type ore deposits at Bingham, Utah, Butte, Montana, and Climax, Colorado: *Econ. Geology*, v. 66, no. 1, p. 98–120.
- , 1972, Composition of fluid inclusions, in *Data of geochemistry* U.S. Geol. Survey Prof. Paper 440-JJ, 164 p.
- Rosasco, G. J., and Roedder, Edwin, 1976, Application of a new laser-excited raman spectrometer to nondestructive analysis of sulfate in individual phases in fluid inclusions in mineral: *Geol. Soc. America Abs. with Programs*, v. 8, no. 6, p. 1075.
- Rye, R. O., 1966, The carbon, hydrogen, and oxygen isotopic composition of the hydrothermal fluids responsible for the lead-zinc deposits at Providencia, Zacatecas, Mexico: *Econ. Geology*, v. 61, p. 1399–1427.

- Sheppard, S. M. F., Nielsen, R. L., and Taylor, H. P., Jr., 1969, Oxygen and hydrogen isotope ratios of clay minerals from porphyry copper deposits: *Econ. Geology*, v. 64, p. 755-777.
- , 1971, Hydrogen and oxygen isotope ratios in minerals from porphyry copper deposits: *Econ. Geology*, v. 66, no. 4, p. 515-542.
- Sheppard, S. M. F., and Taylor, H. P., Jr., 1974, Hydrogen and oxygen isotope evidence for the origins of water in the Boulder batholith and the Butte ore deposits, Montana: *Econ. Geology*, v. 69, no. 6, p. 926-946.
- Sillitoe, R. H., 1973, The tops and bottoms of porphyry copper deposits: *Econ. Geology*, v. 68, no. 6, p. 799-815.
- Slack, J. F., 1976, Hypogene zoning and multistage vein mineralization in the Lake City area, western San Juan Mountains, Colorado: Stanford, Calif., Stanford Univ., Ph. D. thesis, 327 p.
- Sourirajan, S., and Kennedy, G. C., 1962, The system H_2O - $NaCl$ at elevated temperatures and pressures: *Am. Jour. Sci.*, v. 260, p. 115-141.
- Taylor, H. P., Jr., 1974, The application of oxygen and hydrogen isotope studies to problems of hydrothermal alteration and ore deposition: *Econ. Geology*, v. 69, no. 6, p. 843-883.
- Wallace, S. R., Muncaster, N. K., Jonson, D. C., Mackenzie, W. B., Bookstrom, A. A., and Surface, V. E., 1968, Multiple intrusion and mineralization at Climax, Colorado in Ore deposits of the United States, 1933-1967 (the Graton-Sales Volume): New York, The American Institute of Mining, Metallurgical, and Petroleum Engineers, Inc., v. 1, p. 605-640.
- White, D. E., 1968, Environments of generation of some base-metal ore deposits: *Econ. Geology*, v. 63, no. 4, p. 301-335.
- , 1974, Diverse origins of hydrothermal ore fluids: *Econ. Geology*, v. 69, no. 6, p. 954-973.
- White, D. E., Muffler, L. J. P., and Truesdell, A. H., 1971, Vapor-dominated hydrothermal systems compared with hot-water systems: *Econ. Geology*, v. 66, p. 75-97.
- Wilcox, W. R., and Kuo, V. H. S., 1973, Gas bubble nucleation during recrystallization: *Jour. Crystal Growth*, v. 19, p. 221-228.

PHOSPHORUS IN HYDROTHERMAL WATERS OF YELLOWSTONE NATIONAL PARK, WYOMING

By ROBERT E. STAUFFER¹ and JOHN M. THOMPSON,
Madison, Wisc.; Menlo Park, Calif.

Abstract.—Ninety-seven hot-spring and geyser samples (field acidified to $\text{pH} < 1.4$ with HCl or HNO_3) from Yellowstone National Park, Wyo., were analyzed for $\text{PO}_4\text{-P}$ using reduced molybdenum-blue and the selective arsenate reducing agent, metabisulfite-thiosulfate. The $\text{PO}_4\text{-P}$ concentrations ranged from below detection limit (~ 1 -73 micrograms per liter). Twenty-five springs had $\text{PO}_4\text{-P}$ concentrations exceeding 6.8 $\mu\text{g/L}$; seven spring samples exceeded 20 $\mu\text{g/L}$. Elevated $\text{PO}_4\text{-P}$ contents were invariably associated with mixed springs, as evidenced by diluted chloride concentrations and, commonly, subboiling temperatures, low pH's, and elevated calcium concentrations. Alkaline high-chloride (> 400 milligrams per liter) hydrothermal waters from Upper and Norris Geyser Basins had $\text{PO}_4\text{-P}$ concentrations below 2 $\mu\text{g/L}$ and represent the low end of the range of $\text{PO}_4\text{-P}$ contents in natural waters.

The chemistry of trace elements in geothermal waters has attracted research interest because of the unique geochemical and ecological features of these waters and as part of the environmental impact assessment of their commercial exploitation. Previous estimates of phosphoric acid (H_3PO_4) in geothermal waters of the United States have been positively biased by the high concentrations of arsenic characteristic of these waters. The biased $\text{PO}_4\text{-P}$ data (phosphorus as phosphoric acid) include the extensive ecological studies of hot springs and their receiving surface waters in Yellowstone National Park, Wyo. (Brock, 1967; Brock and others, 1971; Boylen and Brock, 1973; Zeikus and Brock, 1972), and the published and unpublished $\text{PO}_4\text{-P}$ data obtained previous to this work by the U. S. Geological Survey in extensive chemical surveys of hot springs in the Western United States (for example, Willey and others, 1974). Axtmann (1974) noted that New Zealand researchers have identified $\text{PO}_4\text{-P}$ contents of Wairekei drillhole waters as being typically very low (≈ 2 micrograms per liter), which has been corroborated by W. A. J. Mahon (oral commun., 1975). The analytical method used by the New Zealanders was not described. How-

ever, if the sulfide-bearing drillhole waters are acidified prior to oxidation of the dissolved sulfide by air, then the arsenic is preserved in the reduced (As^{3+}) state, which does not chemically interfere in the determination of $\text{PO}_4\text{-P}$.

A logical first step in the construction of a realistic chemical model for $\text{PO}_4\text{-P}$ in geothermal waters involves recognition of the incidence patterns for $\text{PO}_4\text{-P}$ in that class of natural waters. Alternatively, a theoretical solubility model can be conceived on the basis of chemical thermodynamics. Under fortunate circumstances, the theoretical model may be adequate. In complex situations, the recognition of incidence patterns provides clues to the judicious selection of a prototype model, and, at later stages, analysis of model residuals guides the evolutionary development from the prototype model to the proper model. Excellent examples of model development involving geothermal waters are provided by the silica and Na-K-Ca geothermometry models (Fournier and Rowe, 1966; Fournier and Truesdell, 1973). In this paper, we focus on the incidence patterns of $\text{PO}_4\text{-P}$ in a diverse set of geothermal waters in Yellowstone Park, Wyo.

Acknowledgments:—We are especially indebted to A. H. Truesdell, E. A. Jenne, J. W. Ball, and J. N. Burchard for assistance in collecting hot-spring samples. The assistance of the National Park Service staff in Yellowstone Park also was essential to the success of the project.

EXPERIMENTAL DATA

Sample sources

Samples from 96 hot springs analyzed for $\text{PO}_4\text{-P}$ and reported here were obtained during 1973-75 from Yellowstone National Park, Wyo. The samples were acidified in the field to a $\text{pH} < 1.4$, using either HNO_3 or HCl. Unacidified samples lead to low $\text{PO}_4\text{-P}$ results (R. E. Stauffer, unpub. data, 1977). The field pro-

¹ Water Chemistry Laboratory, University of Wisconsin.

cedure of filtering (through 0.45- or 0.1- μm pore-size membrane filters) and then acidifying the hot samples probably safeguards adequately against biological uptake of PO_4-P during sample storage. Carter (1976) has shown that low pH (<1.5) prevents subsequent biological activity in natural water samples. Furthermore, the natural bacterial flora of the alkaline hot springs is specifically adapted to alkaline environments. The usual objection to preservation by acid is that labile organic phosphorus compounds can be hydrolyzed during storage, thus leading to positive biases in the estimated PO_4-P levels. Hydrolysis is unlikely to be important for the thermal waters studied because of the very short time during which the waters were cool enough for biological activity. The special procedures required for sampling boiling hot springs have been described elsewhere (Ball and others, 1975; Rowe and others, 1973).

The sample domain represents 96 individual springs mostly from West Thumb (23 samples), Upper (23 samples), Midway (8 samples), Lower (21 samples), and Norris (7 samples) Geyser Basins; Potts Hot Springs Basin (2 samples); Mammoth Hot Springs (3 samples); and Lone Star (2 samples) (fig. 1). Interchange Spring, in the Upper Geyser Basin, was sampled and analyzed twice. The Upper Geyser Basin samples include waters from Geyser Hill, Cascade Group, Black Sand Basin, Biscuit Basin, Mystic Falls, and Hillside. The Lower Geyser Basin samples include waters from the White Creek, Black Warrior Lake, Sentinel Meadow, Imperial, River, and Nez Perce groups. Three samples from Gibbon Geyser Basin and Terrace Spring represent the geographic area between Norris and Madison Junction (fig. 1). Five samples are from the Yellowstone Canyon area, including Calcite Spring and two adjacent warm springs with low chloride contents and two from Washburn Hot Springs, perched on the slopes of Mount Washburn (fig. 1). The samples include both acidic and alkaline waters and a broad range in chloride concentrations and spring temperatures.

The two Washburn Hot Springs samples are geochemically unique in the set studied. The Washburn Hot Springs samples are low-chloride, ammonium sulfate waters ($\text{NH}_4^+ = 210$ and 270 milligrams per liter; Thompson and others, 1975) probably derived from condensed vapors. In the other waters NH_4^+ is not an important part of the cation-anion balance. Except for several waters from Norris Geyser Basin, all the samples were initially buffered by bicarbonate ion. No pure "acid sulfate"-type water (White and others, 1971) is represented. The acidic waters of Norris are interpreted as being mixtures of acid-sulfate-type

water of surficial origin and high-chloride deep Norris water.

Analytical procedures

Phosphate (PO_4-P) was analyzed by the ascorbic acid reduction-molybdenum-blue method after a preliminary As^{5+} reduction step (to As^{3+}) using thiosulfate-metabisulfite (R. E. Stauffer, unpub. data, 1977). Standard additions of As^{5+} in large quantities were used to prove quantitative reduction of the interfering As^{5+} ion by the thiosulfate. Phosphorus as measured by this technique is frequently called orthophosphate; more properly it is also called soluble reactive phosphorus (Strickland and Parsons, 1968) because some especially labile organic phosphate molecules can hydrolyze to phosphoric acid under the test conditions. The chemical conditions and color-development time (phospho-antimonyl-molybdate complex) were adjusted to minimize the potential silica interference in these very high SiO_2 waters (R. E. Stauffer, unpub. data, 1977). Nevertheless, spectral studies on both samples and silica standards indicated that "apparent" PO_4-P concentrations below 1 $\mu\text{g}/\text{L}$ may represent a silica response residual. Because of the relatively uniform SiO_2 contents of the hydrothermal waters studied and the polymerization of SiO_2 at concentrations above approximately 115 mg/L at 25°C, the positive silica bias in the PO_4-P data is probably uniformly in range 0–1 $\mu\text{g}/\text{L}$. This residual error is tolerable, insofar as the lowest PO_4-P concentrations found (<1 $\mu\text{g}/\text{L}$) cannot be distinguished from 0. R. E. Stauffer (unpub. data, 1977) showed that there was no significant difference between PO_4-P and total phosphorus for the clear hot-spring waters.

RESULTS AND DISCUSSION

Geochemical patterns

Table 1 lists the general physical and chemical characteristics of the waters sampled, analyzed for PO_4-P , and discussed in the text.

The frequency distribution for PO_4-P (fig. 2) reveals that 9 samples had undetectable levels of PO_4-P (<1 $\mu\text{g}/\text{L}$) and that most samples (65) contained less than 5 $\mu\text{g}/\text{L}$. Twenty-three samples contained 5–12 $\mu\text{g}/\text{L}$, and nine remaining samples had concentrations as high as 73 $\mu\text{g}/\text{L}$.

A basic familiarity with the main geochemical classification of geothermal waters is vital to the interpretation of the PO_4-P patterns. The chloride concentration provides critical information on the mode of enthalpy transport (high chloride being associated with a water-dominated system), which is responsible

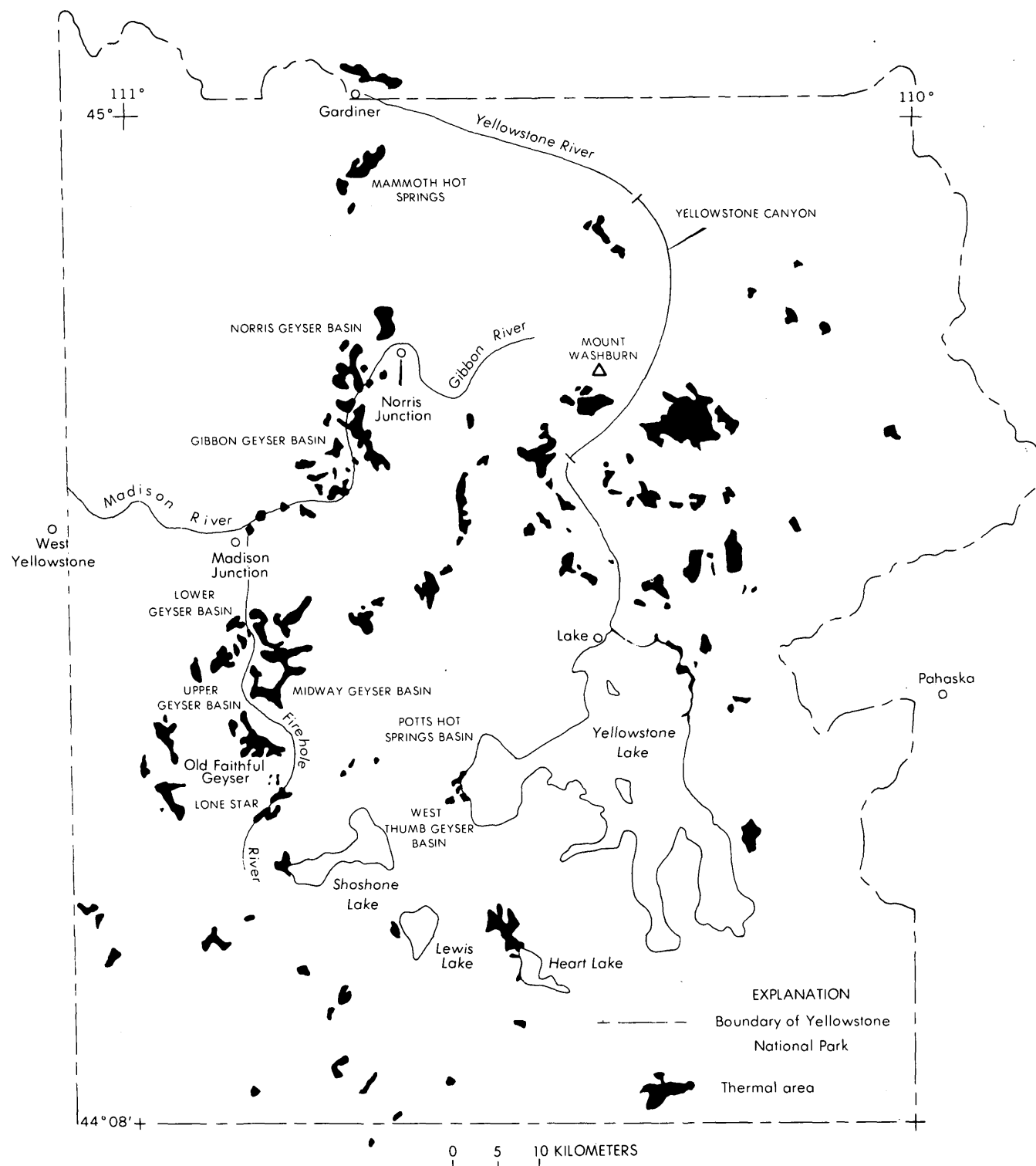


FIGURE 1.—Location of thermal areas where samples were taken from hot springs, Yellowstone National Park.

for a spring's thermal character. The diagnostic value of chloride has been established through a long sequence of geochemical and geophysical investigations (Ellis and Wilson, 1955; White and others, 1971;

Fournier and others, 1974; Fournier and Truesdell, 1974; Fournier and others, 1976).

The PO₄-P concentration is <1 µg/L, or below the analytical detection limit, for the three samples rep-

TABLE 1.—PO₄-P and other chemical parameters for representative hydrothermal waters, Yellowstone National Park[ΣCO₃ reported has HCO₃ in mg/L; pH_f is field pH; ..., not determined]

Name	Sample No.	T°C	pH _f	Ca	Cl	ΣCO ₃ ← (mg/L)	SO ₄	F	PO ₄ -P →(μg/L)	
									—	—
Lone Star area:										
L. Pool S. of Footbridge - - - - -	YJ-75-37	67	7.5	6.90	392	183	21	18.5	0.7	
Spring near Lone Star - - - - -	YJ-75-42	93	8.0	1.52	416	191	27	16.0	.7	
Upper Geyser Basin:										
Geyser Hill:										
Old Faithful run-off - - - - -	YJ-75-57	93	9.5	.73	480	213	23	31.0	.7	
Unnamed seep near Old Faithful - -	YS-74-122	89.5	8.2	1.23	365	160	29	24.0	1.2	
Ear Spring - - - - -	YT-73-71	95	9.0	.6	403	174	22	26.0	2.2	
Other springs:										
Tortoise Shell - - - - -	YS-74-123	93.5	8.4	.74	389	399	31	30.0	1.7	
Unnamed spring across from Sawmill-	YS-74-124	89.5	8.6	1.80	382	377	24	30.0	1.7	
Witches Cauldron - - - - -	YS-74-125	91	7.9	.41	377	422	14	30.8	4.0	
Unnamed spring - - - - -	YS-74-126	87	7.1	1.11	272	240	21	25.0	11.0	
Spring group NNW of Interchange -	YJ-74-130	82	7.2	.49	353	532	17	30.0	4.0	
Unnamed Spg Sprite Pool (Cascade Gp)-	YJ-74-35	48	6.7	1.78	<10	52	27	9.0	10.4	
Black Sand:										
Spouter Geyser - - - - -	YS-74-127	85	8.2	1.31	317	618	17	29.0	1.7	
Large spr. across from Cliff Geyser	YS-74-129	88.5	8.3	.88	314	582	18	27.6	6.4	
Interchange Spring - - - - -	YS-74-128	73.5	7.4	.77	242	268	18	16.8	21.9	
Interchange Spring - - - - -	YJ-74-17	74	8.6	.27	226	366	18	16.5	11.8	
Unnamed cold spring - - - - -	YJ-74-16	14	7.1	1.64	<10	33	4	3.5	6.3	
Unnamed spring (Mystic Falls) - - -	YJ-75-1	90	8.0	7.85	62	229	13	11.5	3.8	
Unnamed spring (Mystic Falls) - - -	YJ-75-2	92	7.9	7.87	59	256	14	11.5	3.3	
Unnamed spring base of Hillside - -	YJ-75-3	68	7.3	6.60	44	256	13	10.5	3.0	
Unnamed spring Hillside (N) - - - -	YJ-75-4	84.5	7.2	7.40	68	234	15	11.5	4.5	
Unnamed spring Hillside (N) - - - -	YJ-75-5	85	7.1	7.45	66	256	16	10.8	4.2	
Unnamed spring Hillside (S) - - - -	YJ-75-6	81	7.7	7.35	69	237	16	11.5	4.9	
Unnamed spring Hillside (S) - - - -	YJ-75-7	81	7.3	7.40	69	236	22	11.7	4.9	
Unnamed spring Hillside (S) - - - -	YJ-75-8	86	7.3	7.30	68	249	15	11.5	4.5	
Sapphire Geyser Crater (Biscuit Basin)	YT-73-62	93	9.5	--	297	--	--	--	--	3.3
Midway Geyser Basin:										
Excelsior Geyser Crater - - - - -	YT-73-76	--	--	--	266	--	--	--	.4	
Unnamed spring Flood Group - - - -	YJ-74-36	88	8.4	.48	226	434	18	19.5	8.0	
Unnamed spring Flood Group - - - -	YJ-74-38	80	7.5	.40	206	333	14	16.2	20.5	
Unnamed spring Rabbit Group - - - -	YJ-74-42	72	6.9	.80	216	331	13	18.8	8.2	
Unnamed spring Rabbit Group - - - -	YJ-74-43	42	7.0	.30	261	358	18	23.8	10.0	
Unnamed spring headwaters area - -	YJ-75-18	91.5	9.5	.35	291	383	20	25.0	4.1	
Unnamed spring Rabbit group - - - -	YJ-75-20	85.5	9.3	.65	248	332	24	22.0	5.5	
Unnamed spring Rabbit Group - - - -	YJ-75-21	41	8.6	.8	303	344	17	27.0	.7	
Lower Geyser Basin:										
White Creek:										
Source "B" - - - - -	YJ-75-44	73	5.0	14.2	19	117	23	6.8	9.6	
Eastern end of thermal activity - -	YJ-75-45	71	5.9	11.8	34	136	23	8.3	4.8	
White Creek - - - - -	YJ-75-47	74	6.5	13.4	50	146	24	8.7	4.5	
Spring near confluence A & B - -	YJ-75-48	61	4.8	14.5	18	122	20	6.8	4.5	
Unnamed spring W. of confluence - -	YJ-75-49	93	7.1	5.2	143	271	18	13.7	4.8	
Octopus Spring - - - - -	YS-74-112	85	7.8	.54	262	340	19	22.0	2.0	
White Creek - - - - -	YS-74-119	51	8.0	11.2	70	166	20	10.1	1.7	

resenting the highest chloride waters in the park south (Old Faithful runoff, Cl=480 mg/L) and north (Norris, Cl>700 mg/L) of Madison Junction (Fournier and others, 1976). Near-surface dilution by meteoric water was minimal in these three samples. Furthermore, the higher Cl:ΣCO₃ imply that interaction with wallrock was minimal during the rapid vertical ascent of these waters from intermediate fluid reservoirs at temperatures exceeding 210°C (Fournier and others, 1976).

If the class of high-chloride waters is broadened to include all alkaline waters with Cl≥350 mg/L in the Upper Geyser Basin and Cl≥300 mg/L for other hot-spring basins investigated, then 26 samples are identified. Among these samples, only four have PO₄-P concentrations ≥3 μg/L and only one has a concentration ≥5 μg/L (table 2). The high value (14.2 μg/L) is from a nondischarging spring in West Thumb Geyser Basin; the absence of discharge is probably sufficient grounds to exclude it from the incidence

TABLE 1.—PO₄-P and other chemical parameters for representative hydrothermal waters, Yellowstone National Park
—Continued

Name	Sample No.	T°C	pH _f	Ca	Cl	ΣCO_3	SO_4	F	PO ₄ -P
					← (mg/L) →				($\mu\text{g/L}$)
Lower Geyser Basin (continued):									
Black Warrior Lake:									
Steady Geyser	YT-74-69	93	6.8	15.1	46	165	27	10.0	1.5
Unnamed Spr near Steady Geyser	YJ-74-55	93.5	8.4	11.0	32	176	29	9.7	1.4
Unnamed Spr near Steady Geyser	YJ-74-56	73	8.4	10.7	38	188	44	9.0	1.4
Zomar	YJ-74-57	74	8.3	12.8	61	178	24	10.0	3.4
Young Hopeful	YJ-75-9	94.5	8.1	11.0	50	163	21	21.7	1.0
Near Young Hopeful	YJ-75-10	93.5	8.0	10.7	49	172	25	10.0	1.0
River Group:									
Azure	YJ-75-58	86	8.6	1.2	318	188	52	29.8	1.8
Azure satellite	YJ-75-59	89	7.5	2.1	310	184	50	28.6	1.1
Ojo Caliente	YJ-75-60	95.5	7.8	.75	318	241	26	30.0	1.0
Gentian (Fountain Flats)	YJ-73-68	--	--	300	--	--	--	--	.7
Spray Geyser (Imperial Group)	YJ-75-46	89	8.9	.99	184	383	19	19.0	2.7
Steep Cone (Sentinel Meadow)	YJ-75-48	96	8.3	.23	255	312	16	29.0	2.4
Queen's Laundry (Sentinel Meadow)	YJ-75-50	90	8.2	.41	226	338	22	26.5	.7
Snort (Nez Perce Group)	YJ-75-11	95	9.3	1.5	331	186	21	31.0	1.0
Gibbon Geyser Basin:									
Terrace	YJ-73-16	59	6.7	21.8	65	778	13	6.8	10.2
Unnamed spring S. of Beryl	YJ-73-15	32	6.2	10.5	8.5	197	20	6.3	10.2
Unnamed Spr in Artist's Paint Pots	YJ-74-24	93	8.5	1.56	448	94	157	12.3	2.8
Norris Geyser Basin:									
Fenner Drillhole spring	YJ-75-27	93	6.8	3.22	664	10.4	34	6.0	5.8
Realgar Springs	YJ-75-30	88.5	3.7	4.80	493	0	112	11.5	1.7
Pork Chop Spring	YJ-75-34	70	7.3	5.32	712	38.5	26	6.3	.3
Echinus Geyser	YJ-75-35	85	3.6	4.0	103	0	273	10.5	2.7
Emerald Spring	YJ-75-36	89	3.5	2.0	460	0	110	4.4	18.2
Base of Porcelain Terrace Spring	YT-73-74	--	--	--	704	--	--	--	.7
Little Whirligig Geyser	YT-73-61	--	--	--	587	--	--	--	8.0
Mammoth Hot Springs:									
New Highland Terrace	YT-73-65	~73	~6.6	~350.0	166	~850	~570	~2.5	4.0
New Highland Terrace	YS-74-146	~73	~6.6	~350.0	171	~850	~570	~2.5	6.9
New Highland Terrace	YS-74-149	~73	~6.6	~350.0	~166	~850	~570	~2.5	5.2
Yellowstone Canyon:									
Calcite Spring	YS-74-144	90	7.7	28.0	242	261	203	4.25	2.3
Unnamed spring near Calcite	YS-74-141	40	6.9	232.0	127	800	279	2.45	57.0
Unnamed spring near Calcite	YS-74-143	14	7.5	62.0	35	207	86	1.56	57.0
Upper Washburn	YJ-73-4	91	8.1	2.0	7	107	900	.1	9.8
Lower Washburn	YJ-73-5	89	7.9	2.5	22	140	712	1.8	7.6
West Thumb Geyser Basin:									
Unnamed spring	YJ-74-64	76	7.3	.62	290	580	55	22.5	7.1
Twin Geyser	YJ-74-65	95	8.2	.48	287	623	44	20.0	4.4
Roadside Steamer	YJ-74-65	92	8.3	.44	292	636	46	20.0	4.0
Big Cone	YJ-74-67	82	6.2	.84	237	337	51	15.0	11.6
Lakeside Spring	YJ-74-68	85	8.4	.52	301	550	46	20.0	1.8
Blue Bell Spring	YJ-74-69	79	7.2	.64	304	549	61	21.0	2.2
Ephedra Spring	YJ-74-70	83	7.3	.48	301	608	49	16.5	2.2
Overhanging Geyser	YJ-74-71	71	8.5	.28	181	447	36	10.5	2.2
Occasional Geyser	YJ-74-72	91	6.9	1.12	201	385	36	10.0	44.4

matrix. The three samples with $4 < \text{PO}_4\text{-P} < 5 \mu\text{g/L}$ represent springs with low Cl: ΣCO_3 , which indicate CO₂ reaction with silicic volcanic rocks during fluid migration (Fournier and Truesdell, 1970).

The correlatives of high PO₄-P concentration are also of interest. With the two exceptions of samples YJ-74-81 and YJ-74-84 from nondischarging springs in West Thumb Geyser Basin (tables 1 and 3), all of the 25 springs with PO₄-P concentrations above 6.5

$\mu\text{g/L}$ have chloride concentrations that apparently indicate mixing (table 3). Sample YJ-74-84 from Lake-shore Geyser also has an anomalously high magnesium concentration (0.6 mg/L), which is interpreted as contamination. Interchange Spring (YS-74-128, YJ-74-17) is a prime example of mixed spring with relatively high PO₄-P levels (tables 1 and 3); the low chloride levels identify the near-surface dilution of the high-chloride parent water by cold meteoric water. The two

TABLE 1.— $\text{PO}_4\text{-P}$ and other chemical parameters for representative hydrothermal waters, Yellowstone National Park
—Continued

Name	Sample No.	$T^\circ\text{C}$	pH_f	Ca	C1	ΣCO_3 (mg/L)	SO_4	F	$\text{PO}_4\text{-P}$ ($\mu\text{g/L}$)
West Thumb Geyser Basin (continued):									
Unnamed spring	YJ-74-73	73	7.5	0.54	291	502	52	16.0	3.3
Unnamed spring	YJ-74-74	91	6.8	.46	155	435	30	7.8	72.5
King Geyser	YJ-74-75	88	7.9	.80	261	531	42	12.0	43.2
Unnamed Spring	YJ-74-76	77	8.3	.44	291	589	44	15.5	2.9
Unnamed Spring	YJ-74-77	--	7.1	.60	308	544	55	16.0	4.4
Unnamed Spring	YJ-74-78	79	7.0	.48	285	572	69	15.0	2.5
Unnamed Spring	YJ-74-79	86	7.2	.78	287	511	78	15.0	2.2
Lone Pine Geyser	YJ-74-80	95	8.9	.64	270	517	45	13.5	5.1
Unnamed Spring	YJ-74-81	89	8.9	.46	318	615	49	14.5	14.2
"Jug spring"	YJ-74-82	77	7.0	.32	286	535	52	15.0	3.6
"Man Trap spring"	YJ-74-83	67	8.8	.40	301	432	54	15.5	2.5
Lakeshore Geyser	YJ-74-84	90	6.8	2.0	296	531	55	14.5	8.0
Unnamed spring	YJ-74-85	61	6.9	.84	251	465	89	11.5	2.2
Unnamed spring	YJ-74-86	76	7.2	.46	303	564	53	14.5	2.9
Potts Hot Springs Basin:									
Unnamed spring	YJ-75-54	91	8.8	.28	315	579	38	35.0	1.0
Unnamed spring	YJ-75-56	68	5.9	.70	48	44	56	5.5	5.5

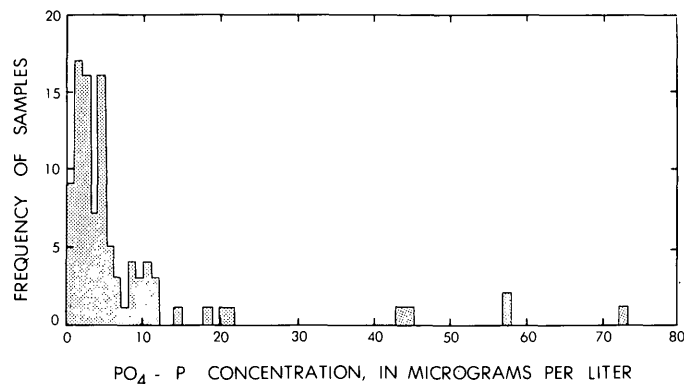


FIGURE 2.—Frequency distribution for $\text{PO}_4\text{-P}$ among 97 sampled geothermal waters, Yellowstone National Park.

Interchange Spring samples have the highest $\text{PO}_4\text{-P}$ concentrations among the 23 samples tested from Upper Geyser Basin.

The measured temperatures (T_s) of most of the high-phosphorous spring samples ($\text{PO}_4\text{-P} \geq 6.5 \mu\text{g/L}$) were well below boiling ($\approx 93^\circ\text{C}$ on the Yellowstone Plateau); hence, the springs are classified as warm rather than hot. Because chloride is the prime enthalpy tracer in hot-water-dominated systems, the low chloride levels and spring temperatures are related (Fournier and others, 1976; Fournier and Truesdell, 1974).

The diluted Norris waters are special cases of acidic boiling hot springs with relatively high chloride and $\text{PO}_4\text{-P}$ concentrations. Samples from Little Whirligig (YT-73-61) and Emerald Spring (YJ-75-36) are the only Norris waters in the high-phosphorous category (top 25 percent). The anomalously high $\text{PO}_4\text{-P}$ con-

TABLE 2.—Orthophosphate incidence matrix for high-chloride hot springs

[Criteria for inclusion in the high-chloride category are $\text{Cl} > 700 \text{ mg/L}$ (Norris), $\text{Cl} > 350 \text{ mg/L}$ (Upper-Lone Star), and $\text{Cl} > 300 \text{ mg/L}$ (other basins).]

Thermal basin	Micrograms per liter						Total
	0 < 1	1 < 2	2 < 3	3 < 4	4 < 5	> 5	
Upper - Lone Star	3	3	1	0	2	0	9
Midway	1	0	0	0	0	0	1
Lower -	1	4	0	0	0	0	5
West Thumb - Potts	0	2	4	0	1	1	8
Norris	2	0	0	0	0	0	2
Artist's Paint Pots	0	0	1	0	0	0	1
Summation	7	9	6	0	3	1	26
Percentage	27	35	23	0	12	4	100

tents of these waters (table 3) are probably the result of sulfuric acid attack on country rock in the near-surface environment, a process which has been well identified for aluminum, iron, and magnesium in such waters (White and others, 1971). Two other Norris samples also have $\text{PO}_4\text{-P}$ concentrations above $2 \mu\text{g/L}$, in contrast to the undetectable ($< 1 \mu\text{g/L}$) concentrations in the samples from Pork Chop (YJ-75-34) and the base of Porcelain Terrace (YT-74-73) (table 1). One of the Norris springs with an intermediate $\text{PO}_4\text{-P}$ level ($5.8 \mu\text{g/L}$) is the Fenner Drillhole spring (YJ-75-27; $\text{Cl} = 664 \text{ mg/L}$) (table 1). In spite of its relatively high chloride and SiO_2 concentrations, the spring is acidic (Thompson and others, 1975). The other Norris sample with an intermediate $\text{PO}_4\text{-P}$ level ($2.7 \mu\text{g/L}$) is Echinus Spring (table 1). Both of these springs are probably being diluted with meteoric water containing sulfuric acid of surficial origin.

Ignoring for now the special cases of the acidic mixed Norris waters, all the bicarbonate-buffered

TABLE 3.—*Spring samples identified with the upper 25 percent of PO₄-P concentrations*

Name	Sample No.	T°C	pH	Cl (mg/L)	Cl: Σ CO ₃ (molar) ³	PO ₄ -P (μg/L)
West Thumb Geyser Basin:						
Unnamed spring along "Panhandle"	YJ-74-74	91	6.8	155	0.61	72.5
Occasional Geyser	YJ-74-72	91	6.9	201	.90	44.4
King Geyser	YJ-74-75	88	7.9	261	.85	43.2
Unnamed geyser near road	YJ-74-81	89	8.9	318	.89	14.2
Big Cone	YJ-74-67	82	6.4	237	1.21	11.6
Unnamed spring in marsh	YJ-74-64	76	7.3	290	.86	9.1
Lakeshore Geyser	YJ-74-84	90	6.8	296	.96	8.0
Upper Geyser Basin:						
Interchange Spring	YS-74-128	73.5	7.4	242	1.55	21.9
Interchange Spring	YJ-74-17	74	8.6	226	1.06	11.8
Unnamed spring	YS-74-126	87	7.1	272	1.95	11.0
Unnamed near Sprite Pool	YJ-74-35	48	6.7	<10	.33	10.4
Midway-Lower Geyser Basin:						
Spring from gravel deposit below road	YJ-74-38	80	7.5	206	1.06	20.5
Unnamed Rabbit Group	YJ-74-43	42	7.0	261	1.25	10.0
Source of "B" White Creek	YJ-74-44	73	5.0	19	.28	9.6
Unnamed Rabbit Group	YJ-74-42	72	6.9	216	1.12	8.2
Unnamed Flood Group	YJ-74-36	88	8.4	226	.90	8.0
Madison Junction:						
Terrace Spring	YJ-73-16	59	6.7	65	.14	10.2
Gibbon Geyser Basin:						
One mile S. of Beryl E. side road	YJ-74-15	32	6.2	8.2	.07	10.2
Norris Geyser Basin:						
Emerald Spring	YJ-75-36	89	3.5	460	0.0*	18.2
Little Whirligig	YT-73-61	93	3.1	587	0.0*	8.0
Mammoth Hot Springs:						
New Highland Spring	YS-74-146	~75	~7.2	171	.368	6.9
Yellowstone Canyon area:						
Near Calcite Spring	YS-74-141	40	6.9	127	.27	57.0
Near Calcite Spring	YS-74-143	14	7.5	25	.21	57.0
Upper Washburn	YJ-73-4	91	8.1	7	.11	9.8
Lower Washburn	YJ-73-5	87	7.9	2.2	.03	7.6

*Acidified samples - ratio not defined.

springs with high PO₄-P levels (6.5 μg/L) have relatively low Cl: Σ CO₃, in addition to low chloride levels (table 3). The maximum Cl: Σ CO₃ is 1.55 for Interchange Spring. West Thumb Geyser Basin is well represented in the high PO₄-P category. This basin has characteristically low Cl: Σ CO₃. In contrast to the typically low Cl: Σ CO₃ in table 3, the Cl: Σ CO₃ for Old Faithful Geyser is ≈4.0 and the ratios for the highest chloride waters exceed 40 at Norris.

An important feature common to many of the springs listed in table 3 is low pH. Among the 25 springs listed, only 4 had field pH's above 8.0. Field pH's exceeding 8 and even 9 are the rule rather than

the exception for hot-spring waters in Upper Geyser Basin. The high incidence of low pH values among the high-phosphorous class (table 3) is related to the mixed origin of the waters. When cooling occurs by mixing with cold meteoric water rather than by adiabatic cooling, loss of dissolved CO₂ can be prevented. During adiabatic cooling, the pH rises because of CO₂ losses accompanying the flashing of steam.

The following two statements are consistent with the PO₄-P incidence in representative Yellowstone geothermal waters: (1) If an alkaline hot-spring sample is high in chloride, then, it has a PO₄-P con-

centration at or near the analytical detection limit of 1 $\mu\text{g}/\text{L}$, and (2) if a sample is significantly enriched in $\text{PO}_4\text{-P}$ (above 6.5 $\mu\text{g}/\text{L}$), then the spring is in the mixed class. However, a sample with a low to intermediate chloride level need not have a high $\text{PO}_4\text{-P}$ content, as illustrated by the springs in the Black Warrior Lake area in Lower Geyser Basin (table 1). Steady Geyser and the springs near it are prime examples of relatively low chloride concentrations associated with $\text{PO}_4\text{-P}$ concentrations under 2 $\mu\text{g}/\text{L}$. Zomar ($T_s = 74^\circ\text{C}$) has the highest $\text{PO}_4\text{-P}$ level (3.4 $\mu\text{g}/\text{L}$).

The $\text{PO}_4\text{-P}$ concentration in the Hillside Spring and Mystic Falls areas (Upper Geyser Basin) range from 3.0 to 4.9 $\mu\text{g}/\text{L}$, higher than the very low levels characteristic of the high chloride springs, but much lower than the high erratic values that have been identified with many of the mixed springs (table 1). Hillside Springs have temperatures below boiling.

The relatively low $\text{PO}_4\text{-P}$ concentrations of the Hillside Springs, Mystic Falls, and Black Warrior Lake areas are of considerable interest, particularly since Fournier, White, and Truesdell (1976) identified Hillside Springs and Black Warrior Lake as having anomalously high SiO_2 (hence, enthalpy) for their chloride concentrations. The Black Warrior Lake area is unique in Yellowstone Park in that boiling springs of very high discharge have chloride concentrations as low as 46 mg/L. The $\text{PO}_4\text{-P}$ concentrations of these boiling Black Warrior Lake springs are not statistically distinguishable from those of Geyser Hill.

The Hillside Springs and Mystic Falls springs belong to a class of Yellowstone thermal waters with intermediate $\text{PO}_4\text{-P}$ levels (2–6.5 $\mu\text{g}/\text{L}$). Only three out of the nine springs in Upper Geyser Basin and Lone Star with $\text{Cl} > 350 \text{ mg/L}$ belong in the intermediate class (table 2). None of the high-chloride representatives from Norris or Lower Geyser Basins is in the intermediate class. By contrast, the samples from West Thumb Geyser and Potts Hot Springs Basins (table 2) fall mainly in the intermediate $\text{PO}_4\text{-P}$ range; only two out of eight concentrations are below 2 $\mu\text{g}/\text{L}$, and none is below 1 $\mu\text{g}/\text{L}$. Closer examination of the three Upper Geyser Basin samples with $\text{Cl} > 350 \text{ mg/L}$ and $\text{PO}_4\text{-P}$ of 2 $\mu\text{g}/\text{L}$ reveals that they have low $\text{Cl}:\Sigma\text{CO}_3$ compared to Geyser Hill. Ear Spring is an exception; its $\text{PO}_4\text{-P}$ level (2.2 $\mu\text{g}/\text{L}$) is close to the 2 $\mu\text{g}/\text{L}$ partitioning level. The West Thumb samples have notably low $\text{Cl}:\Sigma\text{CO}_3$. In the Lower Geyser Basin, high chloride levels are associated with relatively high $\text{Cl}:\Sigma\text{CO}_3$. The Hillside Springs have low $\text{Cl}:\Sigma\text{CO}_3$, in keeping with the

downward trend in the ratio northwest from Geyser Hill toward Biscuit Basin.

The relatively high and erratic $\text{PO}_4\text{-P}$ levels associated with mixed springs are not likely to have resulted from simple dilution of high-chloride parent water by cold meteoric water. The meteoric waters, even after passage through the upper soil horizons on the forested Yellowstone Plateau, are not likely to have $\text{PO}_4\text{-P}$ concentrations above 5–10 $\mu\text{g}/\text{L}$. This assertion is derived from the three following geochemical considerations: (1) the $\text{PO}_4\text{-P}$ content of rainfall is typically very low in remote forested regions such as the Yellowstone Plateau, (2) the $\text{PO}_4\text{-P}$ concentration of cold spring waters in forested regions of the temperate zone are typically low (<10 $\mu\text{g}/\text{L}$), and (3) the $\text{PO}_4\text{-P}$ analyses of the Firehole-Madison River system (fig. 1) during the September base flow period 1974 (R. E. Stauffer, E. A. Jenne, and J. W. Ball, unpub. data, 1977) fell in the concentration range of 2–8 $\mu\text{g}/\text{L}$. The Firehole River is approximately 85-percent cold spring water during the extended period of base flow (Fournier and others, 1976); the remaining 15 percent of the flow is from the hot springs, a component that has been shown to have very low $\text{PO}_4\text{-P}$ contents.

SUMMARY

The correlatives of $\text{PO}_4\text{-P}$ levels in Yellowstone geothermal waters are now apparent; high levels are associated with low chloride, low $\text{Cl}:\Sigma\text{CO}_3$, commonly subboiling temperatures, and low pH's. Very low $\text{PO}_4\text{-P}$ concentrations are associated with the alkaline, high-enthalpy, undiluted, high-chloride waters surging up from depth.

The reported $\text{PO}_4\text{-P}$ concentrations for Yellowstone geothermal waters are typically three orders of magnitude lower than previously reported estimates. If we accept the minimum estimate of $\text{PO}_4\text{-P}$ concentration for the high-chloride Norris waters (0.3 $\mu\text{g}/\text{L}$) as being most representative of the high-enthalpy, high-chloride parent water, then an arsenic-phosphorus atomic ratio of ≈ 4000 results for the most concentrated Norris waters. The arsenic-phosphorus ratio is remarkable; it suggests solubility controls on phosphorus in these natural waters. In contrast to other natural waters with extremely low $\text{PO}_4\text{-P}$ (oligotrophic lake and ocean waters), the geysering high-chloride waters of Yellowstone National Park are strongly superheated and biologically sterile only seconds to minutes before they erupt at the ground surface. Hence, the low $\text{PO}_4\text{-P}$ contents of these waters are independent of biological uptake.

REFERENCES CITED

- Axtmann, R. C., 1974, An environmental study of the Wairakei power plant: New Zealand Dept. Sci. and Indus. Research P.E.L. Rept. 445, 18 p.
- Ball, J. W., Jenne, E. A., and Burchard, J. M., 1975, Sampling and preservation techniques for waters in geysers and hot springs *with a section on gas samples by A. H. Truesdell*: Workshop on Sampling Geothermal Effluents, 1st, Las Vegas, 1975, Proc., p. 218-234.
- Boyle, C. W., and Brock, T. D., 1973, Effects of thermal additions from the Yellowstone geyser basins on the benthic algae of the Firehole River: *Ecology*, v. 54, p. 1282-1291.
- Brock, T. D., 1967, Relationship between standing crop and primary productivity along a hot spring thermal gradient: *Ecology*, v. 48, p. 566-571.
- Brock, T. D., Brock, M. L., Bott, T. L., and Edwards, M. R., 1971, Microbial life at 90°C—The sulfur bacteria of Boulder Spring: *Jour. Bacteriology*, v. 107, p. 303-314.
- Carter, J. J., 1976, The preservation of southern Lake Michigan water [abs.]: Am. Chem. Soc., Great Lakes Regional Mtg., June 17-19, Evanston, Ill., p. 5.
- Ellis, A. J., and Wilson, S. H., 1955, The heat from the Wairakei-Taupo thermal region calculated from the chloride output: *New Zealand Jour. Sci. and Technology*, v. B36, p. 622-631.
- Fournier, R. O., Truesdell, A. H., 1970, Chemical indicators of subsurface temperature applied to hot spring waters of Yellowstone National Park, Wyoming, USA, in *Proceedings of the United Nations symposium on the development and utilization of geothermal resources*, Pisa 1970: *Geothermics Spec. Issue* v. 2, pt. 1, p. 529-535.
- 1973, An empirical Na-K-Ca geothermometer for natural waters: *Geochim. et Cosmochim. Acta*, v. 37, p. 1255-1275.
- 1974, Geochemical indicators of subsurface temperature, pt. 2, Estimation of temperature and fraction of hot water mixed with cold water: *U.S. Geol. Survey Jour. Research*, v. 2, no. 3, p. 263-269.
- Fournier, R. O., White, D. E., and Truesdell, A. H., 1974, Geochemical indicators of subsurface temperature, pt. 1, Basic assumptions: *U.S. Geol. Survey Jour. Research*, v. 2, no. 3, p. 259-262.
- 1976, Convective heat flow in Yellowstone National Park: United Nations symposium on Development and Use of Geothermal Resources, 2d, San Francisco 1975, Proc., p. 731-739.
- Fournier, R. O., and Rowe, J. J., 1966, Estimation of underground temperatures from the silica content of water from hot springs and wet-steam wells: *Am. Jour. Sci.*, v. 264, p. 685-697.
- Rowe, J. J., Fournier, R. O., and Morey, G. W., 1973, Chemical analysis of thermal waters in Yellowstone National Park, Wyoming, 1960-1965: *U.S. Geol. Survey Bull.* 1303, 31 p.
- Strickland, J. R. D. and Parsons, T. R., 1968, A practical handbook of seawater analysis: *Fisheries Research Board of Canada Ottawa*, Bull. 167, 311 p.
- Thompson, J. M., Presser, T. S., Barnes, R. B., and Bird, D. E., 1975, Chemical analysis of the waters of Yellowstone National Park, Wyoming, from 1965-1973: *U.S. Geol. Survey Open-File Rept.* 75-25, 59 p.
- White, D. E., Muffler, L. J. P., and Truesdell, A. H., 1971, Vapor-dominated hydrothermal systems compared with hot-water systems: *Econ. Geol.*, v. 66, p. 75-97.
- Willey, L. M., O'Neill, J. R., and Rapp, J. B., 1974, Chemistry of thermal waters in Long Valley, Mono County, California: *U.S. Geol. Survey open-file Rept.* 19 p.
- Zeikus, J. G., and Brock, T. D., 1972, Effects of thermal additions from the Yellowstone Geyser basins on the bacteriology of the Firehole River: *Ecology*, v. 53, p. 283-290.

CONDUCTIVE HEAT FLOWS IN RESEARCH DRILL HOLES IN THERMAL AREAS OF YELLOWSTONE NATIONAL PARK, WYOMING

By DONALD E. WHITE, Menlo Park, Calif.

Abstract.—In convection systems with boiling springs, geysers, fumaroles, and other thermal features, the modes of heat flow become increasingly complex as a single liquid phase at depth rises into the near-surface environment where heat flows by convection of liquid and vapor and by conduction in high thermal gradients. This paper is mainly concerned with the changing patterns of conductive heat flow as related to channels of subsurface convective flow and to horizontal distance from spring vents. The primary data consist of temperatures measured in 13 cored drill holes as drilling progressed. Some temperatures plot convincingly on straight-line segments that suggest conductive gradients in rocks of nearly constant thermal conductivity. Temperature gradients and the conductive component of total heat flow nearly always decrease drastically downward; the gradient and heat flow of the lowest depth interval recognized in each hole is commonly only about 10 percent of the highest interval; the changes in gradient at interval boundaries are commonly interpreted as channels of near-boiling water or of cooler meteoric water. Temperature reversals are probably related to inflowing cooler water rather than to transient effects from recent changes. Some temperatures plot on curved segments that probably indicate dispersed convective upflow and boiling of water in ground penetrated by the drill hole. Other similar curved segments are too low in temperature for local boiling and are probably on the margins of hot upflow zones, reflecting conductive cooling of flowing water. The conifers of Yellowstone National Park (mainly lodgepole pine) seem to have normal growth characteristics where near-surface conductive heat flow is below about 200 heat-flow units ($1 \text{ HFU} = 10^{-6} \text{ cal/cm}^2 \cdot \text{s} = 41.8 \text{ mW/m}^2$). Most areas of abnormal "stunted" trees (low ratio of height to base diameter, and low density of spacing) are characterized by conductive heat flows of about 250 to 350 HFU. The critical factor affecting growth is probably the seasonal maximum soil temperature at the root depths preferred by each form, rather than the heat flow as such. Heat flows up to 300 HFU are greatly dominated near the surface by conduction and are little affected by convection within the measured intervals. With increasing total heat flow above 300 HFU, the convection component, as indicated by snowfall calorimetry, becomes increasingly important. Snowfall calorimetry and tree growth as related to heat flow are calibrated by the heat-flow data considered here. Both snowfall calorimetry and tree growth patterns can be extrapolated rapidly, although without high precision, to thermal areas that lack subsurface data.

Thirteen research holes were core drilled in the principal thermal areas of Yellowstone National Park in 1967-68 (White and others, 1975; fig. 1). Depths of the holes ranged from 73 meters to 831.6 m. Bottom-hole temperatures were measured as drilling progressed, with most temperatures (fig. 2) obtained about 16 hours after drilling to a new depth. These temperatures are likely to be within 1° to 2°C of original ground temperature, as shown by additional temperature measurements obtained after longer intervals of recovery. This rapid temperature recovery is due to the fact that heating at the hole bottom occurs from below as well as from the sides. Errors of more than 1° or 2°C occurred where the drilled bottom was

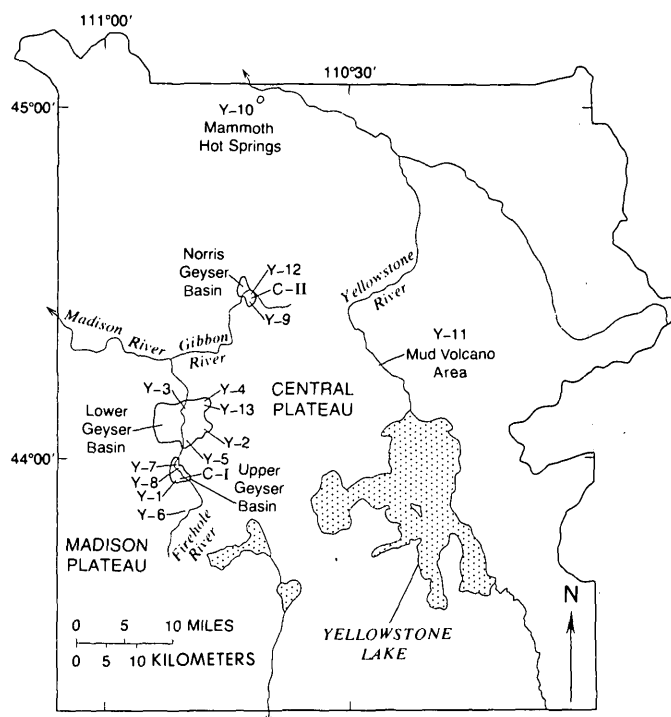


FIGURE 1.—Index map of Yellowstone National Park, Wyo., showing major geothermal areas and sites of research drill holes.

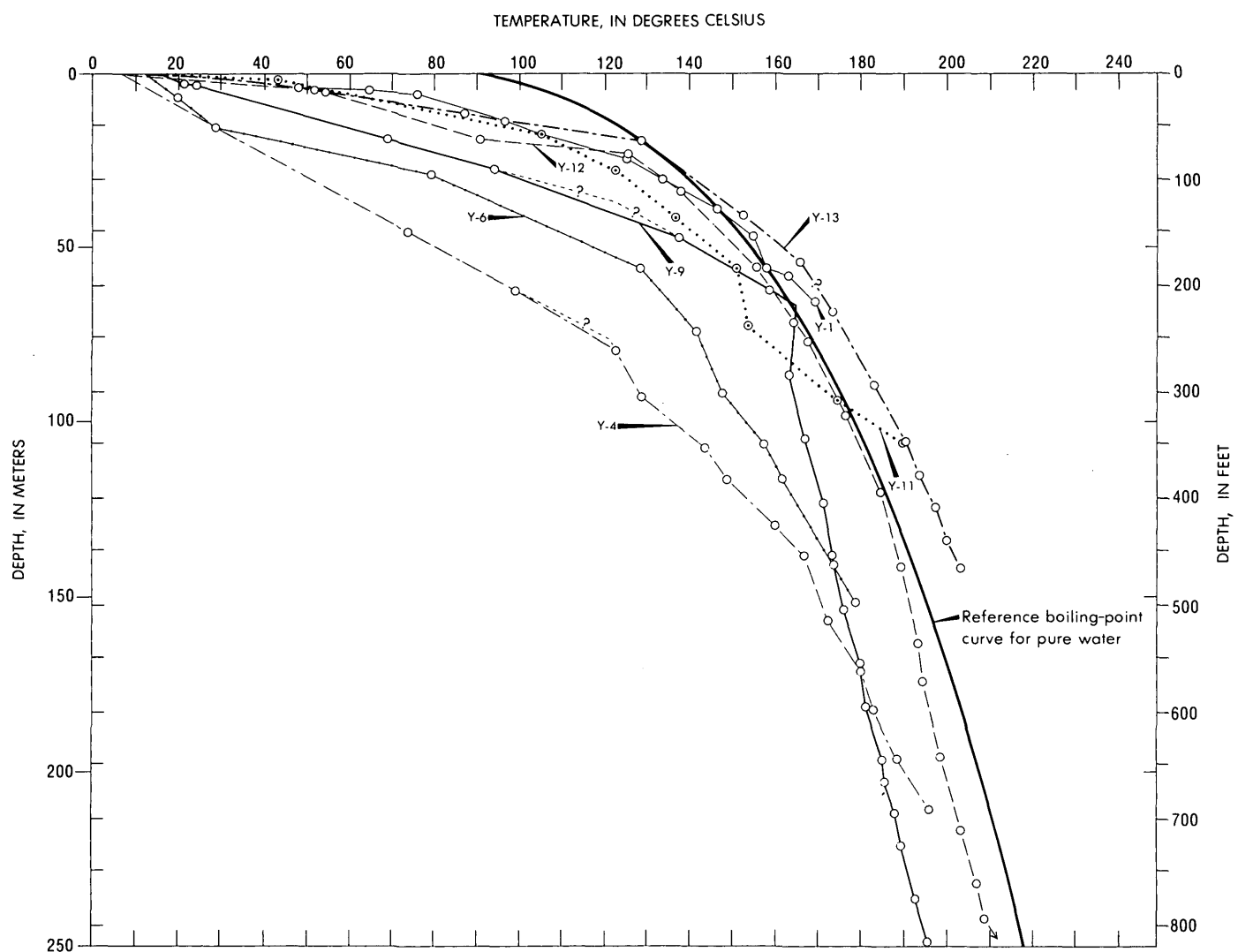


FIGURE 2.—Representative temperature profiles constructed from bottom-hole measurements made as drilling progressed.

within a zone of significant loss of drilling water, which cooled the immediate environment, thus requiring longer times for thermal equilibration. In the dynamic environment of a convection system, after the usual 16-h measurement, temperatures may continue to increase a little or may even decrease, either because of boiling and resultant loss of heat from the wallrock or because of downward flow of water from a cooler zone into an initially hotter zone (White and others, 1975). The "steady-state" temperatures measured long after completion of a hole, however, may differ greatly from original ground temperatures. Thus, the temperature data obtained from these research holes in Yellowstone Park, although not perfect, are probably the best that have yet been obtained from the shallow parts of high-temperature convection systems.

At depth where pressures are high enough to prevent boiling, convective flow of heat in liquid water is the dominant transfer mechanism. Chemical relations in the water permit total convective heat flow to be measured in favorable areas (Fournier and others, 1976). In areas of boiling springs, the modes of heat flow become increasingly complex as the ground surface is approached from below (Benseman, 1959). The conspicuous features at the surface are hot springs, geysers, vigorous noisy fumaroles, and mud pots (a type of fumarole where gases escape through fine-grained alteration products). Of these features, only the hot springs are relatively amenable to measurement of rates of discharge and heat flow. Boiling springs obviously discharge steam, but the rate of flow of steam is not precisely measurable. Geysers are

even more difficult to assess because of their large variations in rates of flow and proportions of vapor and liquid with time.

Much heat also escapes from hot spring areas in less conspicuous ways. Snowfall calorimetry (White, 1969) and temperature-depth measurements in drill holes show that even at considerable distances from conspicuous discharge vents (White and others, 1975), much heat escapes because temperature gradients and conducted heat flow are much higher than in "normal" areas. In addition, much convected heat in warm and hot gases escapes directly from many areas in Yellowstone. Where rates of flow are significant at the surface but the vapor is dispersed through porous soil, no live trees exist, and shrubs, grass, and even moss and lichen may be absent. In cold weather, condensation of water vapor may be observed just above the ground (White, 1969, fig. 1). In such places, native sulfur is commonly deposited in the shallow soil and around tiny vents in the porous ground; the soil moisture is strongly acid, with pH of 1 or less. A convex-upward temperature-depth profile is also characteristic of relatively high vapor convection (White and others, 1971, fig. 5), being related to condensation of water vapor and selective concentration of gases other than H_2O . H_2S , where present, oxidizes at least in part, thus accounting for the low pH, sulfuric acid, and native sulfur.

Snowfall calorimetry and shallow auger holes also reveal that, away from a relatively conspicuous hot center (as in White, 1969, fig. 1, and White and others, 1971, fig. 4), temperatures and heat flow decline. Low forms of vegetation first appear, then grasses, shrubs, and finally trees (where trees normally grow). The tree line¹ probably marks an outward rapid decline in convected heat flow. Some convection probably occurs even within the bordering forest, but not enough to kill trees by excessive soil acidity and heat. The data from auger holes suggest that where temperatures are at or near boiling at the water table, convective heat flow in vapor is the major mode of heat transfer. Very near the surface, where temperature gradients are steep enough to permit most of the water vapor to condense and drain downward, the other gases are selectively enriched in the remaining vapor (White and others, 1971, p. 86-88) as the heat from condensation of steam is conducted to the surface. Farther from hot centers, convective heat losses in vapor from the water table decrease abruptly as temperatures become

too low for vapor bubbles to form (a little below boiling for pure water, depending on content of other gases). Where temperatures at the water table are still lower, convection of water is essential in maintaining the temperatures, but heat flow between the water table and the ground surface is dominantly by conduction.

Evaporation of water vapor from the surfaces of hot pools is usually an inconspicuous mode of heat transfer except when atmospheric temperatures are low enough for the evaporated vapor to recondense as fog.

Of these complex near-surface modes of heat flow, only the conductive component of total heat flow is considered here in detail; it is calculated directly from existing data on temperature gradients and from laboratory-determined thermal conductivities of typical specimens of drill core. These data permit improved calibrations of total heat flow by snowfall calorimetry (White, 1969). Several of the assumptions and generalizations involve rather large uncertainties that can be assessed through comparison of calorimetric data with the conductive heat flows provided in this study. These data also yield approximate calibrations of major differences in growth patterns of conifers in terms of heat flow.

Acknowledgments.—I wish to acknowledge L. J. P. Muffler, R. O. Fournier, and A. H. Truesdell, who shared responsibility with me for obtaining temperature and pressure data and drill core from the holes as drilling progressed, thus providing the data and samples essential for this paper. Review of an early version by Manuel Nathenson helped greatly in distinguishing between dispersed upflow around a drill hole from channeled upflow at some distance from the hole but with subhorizontal communications.

DATA

Most of the primary data on temperatures measured in Yellowstone drill holes are included in tables and graphs in White and others (1975), along with discussions of reliability, limitations, and significance. Some temperatures, measured as drilling progressed, plot convincingly on straight-line segments that suggest conductive gradients in rocks of nearly constant thermal conductivity (table 1). The data from Y-4 drill hole are an especially convincing example (table 2; fig. 1; White and others, 1975, p. 38-41). Most other holes have segments that are probably nearly constant in gradient but lack sufficient data points to be completely convincing. Utilizing all available data, including changes in fluid pressure with depth, the 13 drill holes are divided in table 2 into intervals of relatively constant gradient.

¹The tree line is defined as the approximate line that can be drawn between ground characterized by trees and ground without trees. The boundary is generally a zone 5 to 30 m wide rather than a specific line, with trees typically decreasing in height and vigor of growth. On the border of an expanding hot area, mature trees are dead or dying; in a contracting area, young trees with shallow root systems are encroaching on ground that formerly was too warm.

TABLE 1.—*Thermal conductivities (K), densities, and porosities of cores from research drill holes, Yellowstone National Park, Wyo.*
 [Conductivities measured by R. J. Munroe, U.S. Geological Survey, in 10^{-3} cal/cm·s·°C ($= 4.184 \times 10^{-1}$ W/m·K)]

Hole	Depth (meters)	Density (dry)	K (dry)	Porosity (percent)	K (saturated)	Description
Y-1	16.0	1.70	2.01	17	2.71	Altered, cemented obsidian-rich sand.
Y-3	14.4	1.70	3.19	27	4.64	Altered cemented sand.
Y-4	41.6	2.17	4.10	6.8	5.10	Nez Perce Creek flow; rhyolite lava; considered representative of the thick, dense, monotonous Nez Perce Creek lava flow.
Y-5	26.4	1.95	3.30	21	4.69	Lava Creek tuff, altered.
Y-7	18.2	1.34	1.40	32	2.46	Altered, cemented obsidian-rich sand.
Y-8	91.7	1.42	1.98	37	3.49	Pumiceous tuff of Biscuit Basin rhyolite flow.
Y-9	2.1	2.13	3.49	12.3	4.65	Upper member of Lava Creek ash-flow tuff, altered.
	11.9a	2.14	3.42	12.2	5.33	Same, relatively fresh.
	11.9b	2.08	3.18	12.9	5.07	Same as (a) but altered next to fracture.
	25.9	2.24	4.45	4.9	4.92	Near base of upper member Lava Creek tuff.
	155.4	2.34	4.97	5.1	5.77	Near drilled center of lower member Lava Creek tuff.
Y-10	17.1	2.36	5.59	5.7	6.62	Travertine of Mammoth Terrace.
Y-11	23.0	1.60	2.40	24.7	3.62	Near local top of upper member Lava Creek tuff, altered.
Y-12	8.7	1.80	3.73	22.1	4.90	Near local top of upper member Lava Creek ash-flow tuff.
	25.6	2.10	4.73	13.0	6.19	Near base of same member.
Y-13	.3	1.32	1.53	21	2.23	Opaline sinter.
	16.6	2.20	5.47	6.9	5.48	Thoroughly altered and cemented gravel.
	43.3	2.30	6.94	6.2	7.99	Nez Perce Creek rhyolite, devitrified, dense.

Thermal conductivities of selected samples of drill core (table 1) were measured, both dry and water-saturated, by Robert J. Munroe of the U.S. Geological Survey, using the divided-bar technique (Sass and others, 1971). Utilizing these measured values as well as others on hydrothermally altered samples from Steamboat Springs, Nev. (White, 1968, p. C93–C94), the estimated average thermal conductivity of each interval is shown in table 2, thus permitting calculation of conductive heat flow for the interval. The water-saturated conductivity values are used for all intervals except for the upper interval of each hole, which includes the unsaturated zone above the water table; Y-11, which penetrates a vapor-dominated system (White and others, 1975), is also an exception.

The data for the upper interval of each hole are unreliable because the interval is generally short, the average temperature at ground level is not known,

temperatures measured in the zone had seldom reached equilibrium, and actual thermal conductivities of the near-surface materials, involving their degree of water saturation, are especially uncertain.

INTERPRETATIONS

Channels of fluid flow

Most of the depth intervals in table 2 are separated from each other by distinct changes in temperature gradient and by changes in fluid pressure as the hole was deepened into the underlying interval (White and others, 1975). Especially where no change in thermal conductivity is indicated (or change in degree of water saturation, as at the water table), the changes in gradient are interpreted as intersections of channels of fluid flow. Most of these interpretations are also supported by corresponding changes in fluid pressure

TABLE 2.—Thermal gradients and conductivities (K) and conductive heat flows in research drill holes, Yellowstone National Park, Wyo.

Drill hole	Interval limits ¹		Gradient ² ($^{\circ}\text{C}/\text{m}$)	K ³	Heat flow (HFU) ⁴	Remarks
	Depth m	Temp. ($^{\circ}\text{C}$)				
Y-1	0	~6				
	6.0	19.8	76.2	~11.7	~2	~230
	24.3	79.6	125.9	2.7	2.7	73
	46.6	152.8	155.0	1.3	~2.7	~35
	65.4	214.6	170.0	.84	~2.7	~23
Y-2	0	~6				
	5.2	16.9	81.8	~14.6	~2	~290
	41.0	134.4	134.4	1.5	~3.5	~53
	66.7	218.9	160.9	1.03	~5	~52
	157.4	516.5	203.1	.47	~5	~24
Y-3	0	~6				
	5.2	17.1	54	~9.2	~2	~184
	~27.4	~83.5	~140	3.9	3.2	125
	~42.4	136.0	~140	~0	~2.7	~0
	80.7	264.7	172.2	.84	~5	~42
	150.8	494.7	196.0	.34	~5	~17
Y-4	0	~6				
	15.1	49.7	29	~1.5	~4.8	~72
	~76.0	~232.0	~121	1.5	5.1	76
	137.5	451.2	166.8	.74	~5.1	~38
	210.5	689.1	195.8	.39	~5.1	~20
Y-5	0	~6				
	4.0	13.0	38	~8.0	~2.4	~192
	20.2	66.3	116.8	4.9	~3.5	~172
	31.5	103.3	147.3	2.7	4.7	127
	75.7	248.2	169.5	.5	~5	~25
	164.0	537.6	164.2	-.06	~5	-3
Y-6	0	~6				
	15.5	51.3	33.9	~1.8	~2.5	~45
	28.8	94.5	79.6	3.4	~4	~136
	55.6	182.5	128.8	1.8	~5	~90
	152.2	499.4	179.8	.53	~5	~27
Y-7	0	~6				
	2.4	8.0	34	~11.7	~1.7	~200
	18.9	62.0	86.0	3.2	2.5	80
	73.0	239.6	141.8	1.03	~3.5	~36
Y-8	0	~6				
	1.9	6.4	72	~34.7	~1.9	~660
	49.7	162.9	153.1	1.7	~2.7	~46
	~79.6	~261.0	169.6	.55	~3.1	~17
	151	496.0	165.5	-.06	3.5	~2
Y-9	0	~6				
	3.0	10.0	24.5	~6.1	~2.7	~166
	~36.6	~120.0	~124	~3.0	5.2	154
	~65.5	~220.0	~165	~1.4	~5.5	~77
	86.0	282.1	163.3	~-.08	~5.5	~4
	247.8	812.8	195.7	.2	5.8	11.6
Y-10	0	~6				
	6.2	20.5	57	~8.2	~4	~330
	14.3	47.7	71.3	~1.7	~6.6	~117
	46.7	153.8	73.1	~.06	6.6	3.7
	100.1	331.3	73.0	~0	~4.5	~0
Y-11	0	~14				
	~2.3	~7.0	~88	~32	~1.7	~550
	57	186.8	151.9	~1.17	3.6	~42
	105.7	346.8	191.4	~.81	~4	~32
Y-12	0	~6				
	5.2	17.2	54.2	~9.3	~3.5	~325
	22.6	74.3	125.7	~4.1	~5.5	~225
	76.3	250.3	167.6	~.78	~5.5	~43
	331.6	1087.8	237.5	~.27	~6	~16
Y-13	0	~6				
	4.8	15.7	52	~9.6	~3	~290
	18.8	61.6	128.9	~5.5	5.5	302
	53.9	177.0	166.1	1.06	~7	~74
	105.6	346.3	190.9	.48	~6	~29
	141.4	464.0	198.4	.21	~6	~13

¹Temperature at ground level (except for Y-11) assumed to be $\sim 6^{\circ}\text{C}$ (from Y-4, projected to surface). Interval limits partly selected from physical evidence for aquifers and partly from changes in temperature gradient not explained by changes in conductivity. Refer to White and others (1975) for detailed data of individual holes.

²Conductive thermal gradients are customarily stated in $^{\circ}\text{C}/\text{km}$, which is not appropriate at the small scale of changes in a convection system. In order to emphasize the local significance of thermal gradients in such systems, $^{\circ}\text{C}/\text{m}$ is preferred.

³Thermal conductivity, in $10^{-3}\text{cal/cm}\cdot\text{s}\cdot^{\circ}\text{C}$; ~ indicates estimate from table 1 and White's (1968) table 41. All conductivities below water table assume water saturation; above water table, nearly dry.

⁴Heat-flow units, $10^{-6}\text{cal/cm}^2\cdot\text{s}$ (41.8 mW/m^2). Most reliable near-surface conductive heat flow indicated by underlining.

and also by physical evidence of fracturing and mineral deposition in the drill core. Some of them occurred near the end of the day's drilling and are closely controlled by physical measurements. Other changes in gradient occur between two series of measurements, and the assumed channels and their depths are interpreted from changes in gradient and fluid pressure, as well as from characteristics of the drill core (queried parts of Y-4 and Y-9, fig. 2).

The model of near-surface fluid flow that best explains the temperature relations in most drill holes assumes that primary upflow supplying the local hot springs and geysers is in restricted, probably steeply dipping faults or fractures in ground at some distance from the drill hole. A few feeding fractures may be cut by each hole, but in general the upflow is not dispersed through porous ground penetrated by the hole.

Several of the curves shown on figure 2 could be explained from temperature alone, either by dispersed upflow or by subhorizontal leakage from steep channels in adjacent ground. Critical supplementary data that bear on the flow regime consist of: (1) Pressure changes with increasing depth. Y-4 (fig. 2) could have been interpreted as an example of dispersed upflow, especially below -50 m; however, water levels are sensitive indicators of pressure gradients but showed no significant change until high water overpressure was suddenly encountered below -200 m. The temperature curve of Y-6 seems to be an even better example of dispersed upflow except that two zones with little or no water overpressure are overlain and underlain by relative uniform overpressure (White and others, 1975, p. 25-28). Thus, a consistent vertical pressure gradient is lacking. (2) Hydrothermal minerals in originally obsidian-rich lava flows and volcaniclastic sediments commonly alternate with depth between assemblages that require pore water high in dissolved silica and other assemblages that require relatively lower silica. The drill core of Y-1 (Honda and Muffler, 1970) demonstrates alternations between clinoptilolite-cristobalite (a metastable, relatively soluble form of silica) and analcime-quartz (the stable and least soluble form of silica). Thoroughly dispersed upflow is incompatible with such alternations, which favor, instead, subhorizontal flow from primary channels in adjacent ground. Other drill holes characterized by similar alternations in mineralogy include Y-2, Y-8, and Y-13, but detailed data are not yet published.

Possible examples of dispersed upflow within ground penetrated by drill holes are provided by Y-10 and Y-11. The first hole is in a low-temperature system (about 75°C) in sedimentary rocks. The upflow is so

large and is dispersed through so much ground that significant conductive cooling can occur only on the borders and near the surface (White and others, 1975). Y-11 (fig. 2) penetrates the border of a vapor-dominated system where dispersed steam and other gases flow upward and water from condensing steam percolates downward (White and others, 1971).

General decrease in gradient downward

Nearly all thermal gradients and conducted heat flows decrease with depth. A few changes in gradient relate to changes in thermal conductivity with little change in heat flow; a few intervals involve temperature reversals (White and others, 1975; Y-9, fig. 2) or show no significant differences in temperature.

The temperature reversals are probably due to inflow of cooler water into the hot, less dense, water of the system.² The minor reversal of temperature in Y-9 near -86 m is the clearest example; other possible reversals may be related to cooler aquifers that could not be positively confirmed, as in Y-2 near -150 m and Y-13 near -60 m (see complete data of White and others, 1975, partly ignored in table 2 and fig. 2). The reversals in temperature in the lower parts of Y-5 and Y-8 are presumably due to deep underflow of cooler water rather than to transient effects.

The constant-gradient segment of Y-3 from -27 to -42 m (table 2) is likely to be caused by thorough convective mixing in a rather thick permeable aquifer; the nearly constant temperature in the lower part of Y-10, as previously mentioned, is probably related to a high rate of upflow of low-temperature water (about 73°C), with negligible loss of heat at depth by conduction and with no separation of vapor at depths below about -50 m.

The data of table 2 demonstrate the strong tendency for conductive heat flows to decrease drastically with depth, generally to values that are less than 10 percent of near-surface values. The decreases in conducted heat flow with depth must be offset by higher convective flow. Stated in another way, convective transport of heat is strongly dominant at depth but the role of conduction increases upward, where thermal gradients are higher.

Temperatures directly influenced by boiling

Some of the depth intervals of table 2 and figure 2 are not purely conductive, but instead are influenced

²In general, temperature reversals in the Yellowstone drill holes and at Steamboat Springs, Nev., are interpreted as nearly steady-state effects from entry of cooler water into a hot system. A contrasting interpretation (Bodvarsson, 1973) assumes transient effects in young hot channels of flow with a significant horizontal component; no moving colder water at depth is required. Examples of reversals related to cooler fluids of contrasting water composition were identified by White (1968) in several wells at Steamboat Springs,

by boiling. Boiling is suspected wherever temperatures (corrected for water table and overpressure relationships) plot close to the reference boiling-point curve. Such plots (fig. 2; White and others, 1975) indicate that the pressures in some holes (Y-4, Y-6, and Y-7) are much too high to permit boiling at the existing temperatures. Y-10 of Mammoth is too cool for true boiling to occur, but the vapor pressure of CO₂ is so high that CO₂-rich vapor forms at depths at least as great as 50 m (White and others, 1975, p. 65). Waters of the geyser basins are much lower in gas content than Mammoth, but gases are abundant enough for vapor bubbles to form at temperatures several degrees below the reference boiling curve for pure water. Boiling (or cooling related to formation of vapor) is assumed to be absent in the parts of the geyser basin holes where pressure-corrected temperatures are at least 4°C below this reference curve. The temperature profile of Y-12 drill hole between -60 and -120 m and a deep segment below -300 m (fig. 2; White and others, 1975, p. 56) is affected by boiling in rocks penetrated by the hole. Another clear example of boiling in penetrated rocks is provided by Y-13 drill hole at depths below -30 m (fig. 2), where temperatures corrected for overpressure plot precisely on the reference boiling curve within the precision of the measurements (White and others, 1975, p. 42-45).

The plotted temperatures of Y-6 and perhaps Y-4 of figure 2 and Y-7 (White and others, 1975) are roughly parallel to, but below, the reference boiling curve. Temperatures are clearly too low at existing pressures for boiling to be occurring in or near these drill holes. White and others (1975) suggested that boiling does influence temperatures in the principal zones of upflow at some horizontal distance away from these three holes. Leakage from the main channels, with lateral flow and conductive heat loss, probably accounts for the temperatures that plot crudely parallel to but below the reference boiling curve.

Self-sealing

Processes generally known as self-sealing have been important in localizing the convective flow of fluids in major channels or aquifers and inhibiting flow in minor channels by deposition of hydrothermal minerals in open spaces. The evidence is especially conclusive for Y-7 and Y-8 drill holes (Keith and others, 1978), which are only 130 m apart. Drill core from the upper 53 m of both holes consists of obsidian-bearing silt, sand, and gravel that were initially so porous that large pressure differences could not have been maintained between the two holes. However, Y-8 has an

important zone of boiling, and pressures almost throughout its depth are considerably above hydrostatic. In contrast, boiling does not occur in Y-7, and no pressures exceed hydrostatic (calculated to ground level). The failure to transmit the high pressures of Y-8 to Y-7 through intervening sediment of original high permeability must be due to a low-permeability barrier that has formed between the two holes. The chemical and mineralogical nature of the changes are described in detail by Keith and others (1978).

The immediate walls of upflow channels also decrease greatly in permeability with time because of self-sealing. Most holes drilled near active springs and geysers had initial near-surface water levels that were considerably below those of nearby flowing vents (Y-1, -3 m; Y-2, -4 m; Y-8, -1 m; Y-10, -3 m; Y-12, -3 m; and Y-13; -2.0 m). In all these, the near-surface pressure gradients from vents to drill holes are high, and the permeabilities of near-surface core recovered from the drill holes are also high. These vents could not be discharging at the surface if their immediate channel walls were equally permeable. The obvious explanation is that water seeping into the walls of fractures, faults, and irregular channels has precipitated hydrothermal minerals on surfaces and in pore spaces. Veinlets and breccia zones in drill core generally contain opal near the surface and other silica minerals and zeolites at greater depth. Deposition of these minerals has drastically decreased the permeabilities of the immediate walls. Boiling in response to upward decrease in pressure is probably prevalent in all major upflow channels except in parts of large-diameter geyser tubes, where free convection tends to decrease temperatures below boiling in the lower parts of each convection cell. Steam loss by boiling results in selective concentration of silica and other constituents and thereby an increase in the degree of supersaturation in the water seeping into the channel walls. Diagrammatic representations of these processes are shown in figures 13 and 25 of White and others (1975). With time and decreasing permeability, the rate of leakage declines. Even the principal channels of upflow are eventually filled with hydrothermal minerals, so that the whole systems of upflow decrease in discharge and eventually cease until or unless new channels are formed, either by tectonic and volcanic forces, or by development of sufficient fluid overpressure to exceed the local strength of the rocks (hydraulic fracturing; Grindley and Browne, 1976). These processes are probably involved in triggering some hydrothermal explosions (Muffler and others, 1971) and are clearly involved in the formation of some new spring vents and geyser tubes (Marler and White, 1975).

Decreasing importance of conductive cooling with depth

Considerations of boiling in rising fluids and the continuous decrease in temperature gradient with depth along the reference boiling curve (fig. 2) ensure that conductive heat flow must decrease with depth in the convecting parts of high-temperature geothermal systems; at still greater depths, below the convecting fluids, high conductive gradients are probably required to supply the heat to initially cold meteoric water, but deep conduction is not considered here. The data of table 2 present convincing evidence that conductive heat flows do generally decrease with depth. In 10 of the 13 holes, conductive heat flow in the highest segment is at least 10 times the conductive flow of the lowest segment. Only two holes exceed 30 HFU in their lowest segments, and seven have conductive heat flows of less than 20 HFU. All these systems are at least 10 000 years old—old enough for heat flows to have reached approximate steady states (although a true steady state is probably never reached, for reasons considered in previous sections). In view of these considerations, we must conclude that the relative importance of convective heat flow increases downward to offset the conductive decrease. Of the two modes of convective flow, liquid water and vapor, transport in vapor also generally decreases downward. Neither of these conclusions is surprising and, indeed, both are intuitively to be expected.

Tree growth as related to heat flow

The near-surface conductive heat flows of table 2 that are considered most reliable are arranged in table 3 according to their environments with respect to nearby conifers (lodgepole pines for all holes except Y-10). Our Yellowstone studies agree with earlier New Zealand studies (Dawson, 1964) in showing close general relations between plant associations and heat flow. Relations that can be recognized on aerial photographs are especially useful in rapid recognition of hot, warm, and cold ground and in making semiquantitative estimates of total heat flow near the surface.

In and near the thermal basins of Yellowstone Park, areas of normal vegetation are characterized by conductive heat flows that range up to about 200 HFU and probably average about 100 HFU. Other areas of high topography that are more remote from obvious hydrothermal activity no doubt generally have lower heat flows, probably near or below the caldera average of about 40 HFU for convective flow (Fournier and others, 1975) or 20 HFU for the part of the caldera that underlies Yellowstone Lake (Morgan and others, 1977).

TABLE 3.—Near-surface conductive heat flows in research drill holes as related to nearby conifers in Yellowstone National Park, Wyo.

[Data in heat-flow units (1 HFU = 10^{-6} cal/cm 2 ·s = 41.8 mW/m 2)]

No normal trees nearby	In or near stunted trees	In or near normal trees
¹ Y-8 660	¹ Y-1 230	Y-3 184
² Y-11 550	Y-2 290	³ Y-4 <u>76</u>
	Y-10 330	³ Y-5 <u>172</u>
	Y-12 325	Y-6 45
	³ Y-13 <u>302</u>	Y-7 200
		³ Y-9 <u>154</u>

¹Absence or stunting of trees may be in part due to recent discharge of sinter-depositing water near the site.

²Convective heat flow also clearly involved; nearly on line of smallest trees with indicated total heat flow by snow-fall calorimetry near 900 HFU (White and others, 1971, p. 85).

³Most reliable values; conductive heat flow strongly dominant near the surface, indicated by nearly equal calculated flows in the upper two intervals in each hole (see table 2).

Five drill holes were sited in or near conifers that did not have the normal density of spacing, height, or ratio of height to base diameter (table 3). No specific measurements were used in defining the stunted trees of this intermediate group, but visual qualitative criteria were used. Their heat flows range from 230 to 330 HFU, but the upper limit is not well established and may be as high as 500 HFU. The average heat flow of this category is probably close to 300 HFU. Y-1 was included because the nearest tree did not have normal growth; the hole was located midway up the flank of a sinter cone that was an active geyser vent in the recent past (Marler, 1973, Whistle Geyser), thus emphasizing the effect of spring and geyser discharge on the growth of vegetation. Abundant dead and dying trees in areas of active discharge are clear evidence that other factors than conductive heat flow alone must be considered.

For comparison with these Yellowstone data, Dawson (1964) concluded that the characteristic heat flow for small (stunted) pines (*Pinus radiata*, or Monterey pine) in New Zealand is 100 HFU (converted from cal/m 2 ·s). The actual upper limit of tolerance is probably not set by heat flow as such but by the seasonal maximum soil temperature at the root depths preferred by each form of vegetation. The discrepancy of a factor of 3 between New Zealand and Yellowstone data may be related to differences in precision of calibration, not discussed by Dawson (1964) or others who have followed his system. If largely explained by

precision, the average Yellowstone value of about 300 HFU for stunted pines is almost certainly the more reliable. However, because of the possible critical role of maximum seasonal temperature at the root zone, both values may be essentially correct, with the higher Yellowstone value being related to lower summer temperatures, relative abundance of summer rain, and systematic differences in thermal conductivities of near-surface materials of the two areas. The warmer climate and abundance of porous volcanic ash of low thermal conductivity in New Zealand would result in higher temperatures at any specific heat flow and root-zone depth.

Data are not sufficient to characterize soil temperatures and heat flows that are too high for conifers to grow, but the limited data of table 3 suggest that the upper limit may be near 500 HFU. However, all barren areas must be evaluated with caution; many are devoid of conifers because of water saturation at depths so shallow that the required root zone is submerged, as in meadows and marshes, rather than because of thermal limitations. Thus, low, flat, barren areas should normally be considered nonthermal unless other evidence such as adequate drainage and associated thermal features clearly favor thermal influences.

The criteria developed here for calibrating vegetation in terms of heat flow are useful in helping to establish the approximate total heat flow of Norris Geyser Basin, where significant parts have heat flows that are too high for lodgepole pines to grow and other parts permit only stunted growth.

SUMMARY

At considerable depth in hydrothermal convection systems, most heat is convected upward in liquid water and in vapor; probably a relatively small proportion of the heat of most systems is lost directly by thermal conduction from deep fluid reservoirs. If upward flow of fluids is rapid enough for extensive boiling to occur as depths and pressures decrease, the proportion of heat convected in vapor increases upward.

Near the surface the total heat-flow budget becomes extremely complicated. Much heat is discharged directly from vents as hot water and vapor, and flow rates must be measured either directly or indirectly. Heat is also dispersed through warm porous ground, especially where vapor separates from an underlying hot water table and flows upward, being condensed entirely or in part near the surface where flow rates are low enough for conduction to become dominant (White and others, 1971, p. 84-88).

The walls of the principal channels of upflowing water tend to become self-sealed from deposition of silica minerals and zeolites in pore spaces. The Yellowstone drill hole data indicate that water levels are commonly several meters higher in spring and geyser vents than in surrounding porous ground, thus providing high pressure gradients that permit some thermal water to escape into surrounding ground.

The drill-hole data also demonstrate that near-surface conductive losses through ground close to thermal features commonly range from 100 HFU to more than 500 HFU, and that this shallow conductive flow is largely controlled by depth to the first near-boiling channel, as well as by the thermal conductivities of rocks between the surface and the channel. At greater depths, each hole generally intersects other near-boiling channels. The configuration of the reference boiling curve requires that conductive heat flows generally decrease with increasing depth. The shallowest conductive interval in most of the Yellowstone holes is characterized by heat flows of 100 to over 300 HFU and is commonly about ten times higher than the conductive flow in the deepest conductive interval recognized in each hole.

The data considered here have proved to be useful in calibrating total near-surface heat flows as measured by snow-fall calorimetry (White, 1969), and they also permit recognition of differences in the response of conifers to heat flow. Both of these rather imprecise methods for measuring local variations in heat flow in turn permit our findings from a few individual drill holes to be extrapolated over large areas that lack subsurface data. Areas that are too warm for conifers to grow are likely to have conductive heat flows of more than 500 HFU; areas with thermally stunted trees generally have heat flows of 200 to 400 HFU; and areas of normal conifers are likely to have heat flows of less than 200 HFU.

REFERENCES CITED

- Benseman, R. F., 1959, Subsurface discharge from thermal springs: *Jour. Geophys. Research*, v. 64, p. 1063-1065.
Bodvarsson, Gunner, 1973, Temperature inversions in geothermal systems: *Geoexploration*, v. 11, p. 141-149.
Dawson, G. B., 1964, The nature and assessment of heat flow from hydrothermal areas: *New Zealand Jour. Geology and Geophysics*, v. 7, p. 155-171.
Fournier, R. O., White, D. E., and Truesdell, A. H., 1976, Convective heat flow in Yellowstone National Park: United Nations Symposium on Development and Use of Geothermal Resources, 2d, San Francisco 1975, Proc., v. 1, p. 731-740.
Grindley, George, and Browne, P. R. L., 1976, Structural and hydrologic factors controlling the permeabilities of some hot-water geothermal fields: *United Nations Symposium*

- on Development and Use of Geothermal Resources, 2d, San Francisco 1975, Proc., v. 1, p. 377-386.
- Honda, S., and Muffler, L. J. P., 1970, Hydrothermal alteration in core from research drill hole Y-1, Upper Geyser Basin, Yellowstone National Park, Wyo.: Am. Mineralogist, v. 55, p. 1714-1737.
- Keith, T. E. C., White, D. E., and Beeson, M. H., 1978, Hydrothermal alteration and self-sealing in Y-7 and Y-8 drill holes in northern part of Upper Geyser Basin, Yellowstone National Park, Wyo.: U.S. Geol. Survey Professional Paper 1054-A, 26 p.
- Marler, G. D., 1973, Inventory of thermal features of the Firehole River Geyser Basins and other selected areas of Yellowstone National Park: Natl. Tech. Inf. Service, PB-221 289, 648 p. (revised 1976).
- Marler, G. D., and White, D. E., 1975, Seismic Geyser and its bearing on the origin and evolution of geysers and hot springs of Yellowstone National Park: Geol. Soc. America Bull., v. 86, p. 749-759.
- Morgan, Paul, Blackwell, D. D., Spafford, R. E., and Smith, R. B., 1977, Heat flow measurements in Yellowstone Lake and the thermal structure of the Yellowstone Caldera: Jour. Geophys. Research, v. 82, p. 3719-3732.
- Muffler, L. J. P., White, D. E., and Truesdell, A. H., 1971, Hydrothermal explosion craters in Yellowstone National Park: Geol. Soc. America Bull., v. 82, p. 723-740.
- White, D. E., 1968, Hydrology, activity, and heat flow of the Steamboat Springs thermal system, Washoe County, Nevada: U.S. Geol. Survey Prof. Paper 458-C, 109 p.
- , 1969, Rapid heat-flow surveying of geothermal areas, utilizing snowfalls as calorimeters: Jour. Geophys. Research, v. 74, p. 5191-5201.
- White, D. E., Fournier, R. O., Muffler, L. P., and Truesdell, A. H., 1975, Physical results of research drilling in thermal areas of Yellowstone National Park, Wyoming: U.S. Geol. Survey Prof. Paper 892, 70 p.
- White, D. E., Muffler, L. J. P., and Truesdell, A. H., 1971, Vapor-dominated hydrothermal systems compared with hot-water systems: Econ. Geology, v. 66, p. 75-97.

UPPER DEVONIAN RADIOLARIANS SEPARATED FROM CHERT OF THE FORD LAKE SHALE, ALASKA

By BRIAN K. HOLDSWORTH,¹ D. L. JONES, and CAROL ALLISON,²
Keele, England; Menlo Park, Calif.; Fairbanks, Alaska

Abstract.—Leaching of black bedded chert from the Ford Lake Shale, Kandik Basin, Alaska, with dilute hydrofluoric acid resulted in the complete separation of moderately well preserved radiolarians. Preliminary study of an assemblage obtained from the lower half of the formation revealed six to eight forms apparently identical to specimens previously known from the Tournaisian of southern France and northwestern Turkey, including four genera not previously described from North America. Sparse, poorly preserved conodonts in the same sample are of Late Devonian age. We conclude that certain radiolarian species, hitherto known only from the early Carboniferous, span the Devonian-Carboniferous boundary. The radiolarian assemblage of the Ford Lake Shale sample contrasts markedly with Late Devonian assemblages known from the Canol Shale of northern Canada and the Huron Member of the Ohio Shale; the Ford Lake Shale fauna may reflect greater oceanic influences than these other localities, which lie farther inland from the Devonian continental margin.

The most informative modern studies of Paleozoic Radiolaria have been based upon well-preserved assemblages found in carbonate and phosphate rocks, not on material occurring in chert. Radiolaria can be readily separated from the former rocks and studied in three dimensions, which allows for much more detailed description and comparison than is possible from thin sections of chert. Since Deflandre's pioneer work on separated early Carboniferous radiolarians of Cabrières, Montagne Noire, France (Deflandre, 1952), separated Radiolaria in excellent preservation have been described from the Early Ordovician (Fortey and Holdsworth, 1972) Late Ordovician (Nazarov, 1975; Dunham and Murphy, 1977), Silurian (Holdsworth, 1977), Middle-Late Devonian (Nazarov, 1975; Foreman, 1963), early Carboniferous (Holdsworth, 1973; Ormiston and Lane, 1976), and Namurian (Holdsworth, 1966, 1969). Late Permian examples are known (A. R. Ormiston, written commun., 1977) but not yet described.

A limited amount of information has thus built up regarding the detailed structure of radiolarian skeletons at certain well-dated horizons and regarding the probable environment-controlled contrasts that exist between assemblages of broadly similar age. The majority of Paleozoic Radiolaria, however, are found in chertified sedimentary rocks. It is in the dating and environmental interpretation of cherts that Radiolaria will prove to be most valuable. Some useful information on the radiolarian-content of cherts can be obtained from thin sections, the study of which can be supplemented by the use of alkali-etched (Schwartz, 1924) and varnished (Stürmer, 1966) slabs. But comparison of relatively poorly preserved chert radiolarians with type material from carbonates and phosphorites is most reliably achieved with specimens completely separated from the chert matrix.

Separation of radiolarians from Mesozoic cherts has proved feasible (see, for example, Pessagno and Newport, 1972), but few previous attempts have been made to extract them from Paleozoic cherts. One of us (D. L. Jones) has experimented with extraction processes on a variety of North American Paleozoic cherts. In a great number of cases, complete separation of radiolarians has been achieved. In this report, we describe the first Paleozoic assemblage of post-Silurian age that we obtained by using the HF leaching methods; many other samples are now being studied and will be reported on later.

The assemblage described herein was discovered by Carol Allison in thin sections of a chert from the Ford Lake Shale, Kandik Basin, Alaska. Though preservation is not perfect and useful specimens are sparse, this assemblage is of special interest in that it contains eight forms that can be identified with fair confidence as known European morphotypes. It also throws new light upon the stratigraphic range of certain forms; for example, two Ford Lake pylentonemid

¹ Keele University.
² University of Alaska.

genera were previously unknown below the lower Carboniferous.

LOCALITY AND STRATIGRAPHY OF RADIOLARIAN SAMPLE

The radiolarian-bearing sample (A-854—Univ. of Alaska) comes from lower beds of the Ford Lake Shale that crop out on the north bank of the Yukon River 15 km by river north of Eagle in east-central Alaska (see fig. 1). The lower part of the formation is incompletely exposed in a thin band extending about 3.5 km along the river (Foster, 1976). As described by Brabb (1969, p. I2-I7), the Ford Lake Shale comprises about 600 m of grayish-black siliceous shale and laminated grayish-black chert. Yellow sulfate minerals are locally abundant on weathered surfaces, and phosphatic and carbonate concretions occur sporadically. The Ford Lake Shale overlies the Nation River Formation of Devonian age and is overlain by the Calico Bluff Formation of Mississippian age.

The fossils discussed herein were collected³ about 2 km west of Shade Creek in the lower part of the Ford Lake Shale where 65 m of black, dominantly fissile shale with some thin argillaceous chert, a few carbonate concretions, and very rare thin carbonate beds is overlain by about 56 m of black, dominantly cherty pyritic shale with numerous, closely spaced beds of relatively pure chert. The lower beds commonly display powdery yellowish sulfurous coatings on exposed surfaces, whereas the upper, truly cherty beds tend to weather reddish orange. The radiolarian assemblage occurs in a pure chert 18 m above the base of the reddish-weathering cherts. Abundant radiolarians occur in samples from a nearby cherty bed, and they are present, though less well preserved and abundant, in samples from the lower fissile shales. The fissile shales also contain poorly preserved small filaments, presumably algal, as well as occasional fragments of chitinophosphatic material. As much as 64 m of shale may be present between these fissile shales and the top of the Nation River Formation, but they are poorly exposed and were not sampled during this study.

A Late Devonian to Late Mississippian age was assigned by Brabb (1969) to the Ford Lake Shale on the basis of its apparently conformable relation with the underlying Nation River Formation and clearly conformable relation with the overlying Calico Bluff Formation. Brachiopods and wood of Late Devonian

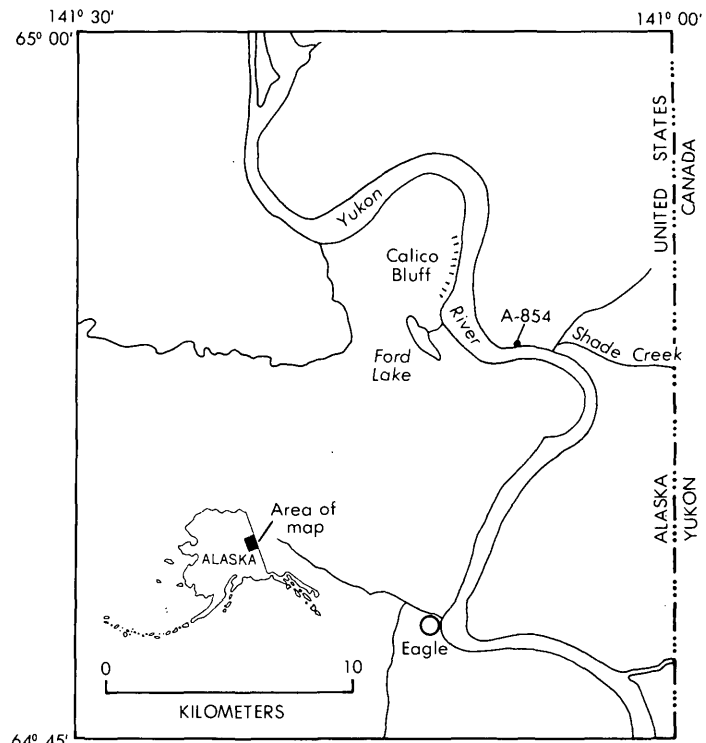


FIGURE 1.—Kandik Basin and location of University of Alaska Museum Locality A-854.

or Early Mississippian age were reported by Brabb (1969) from the lower part of the type Ford Lake Shale just east of the radiolarian locality, and corals, brachiopods, gastropods, bryozoa, and foraminifers are now known from the upper part of the type Ford Lake Shale (E. E. Brabb, written commun., 1976). Calamarian and other plant fragments from exposures of the Ford Lake north of the type section are not sufficiently complete to provide more definitive age information (Brabb, 1969).

COLLECTING AND PROCESSING PALEOZOIC CHERTS

Our methods of collecting and processing Paleozoic cherts in HF are essentially the same as those used for Mesozoic cherts by Pessagno and Newport (1972) and Pessagno (1977). Careful field examination of fresh rock surfaces is necessary to select radiolarian-bearing samples. Good-quality hand lenses of 10 to 20 power are desirable, as is strong sunlight or artificial light. Wetting the rock surface aids in detecting the radiolarians, which appear under the lens as minute glassy round blebs scattered throughout the matrix. Under optimum conditions, spines and other skeletal features can be detected.

Careful sample selection is particularly important in areas where the chert has been strongly deformed,

³ University of Alaska Museum Locality A-854: North bank of Yukon River, approximately 18 m stratigraphically above lowest appearance of cherty beds overlying black shale. NW $\frac{1}{4}$, NE $\frac{1}{4}$ sec. 25, T. 1 N., R. 32 E., Fairbanks Meridian, Eagle D-1 quadrangle. Lat 64° 53.3' N., long 141° 8.4' W.

sheared, and recrystallized. This is because successful preparation of the fossils depends on a difference in the degree of crystallinity between the radiolarian test and the matrix (Murata and Norman, 1976). If the matrix is strongly recrystallized, this difference disappears and selective leaching is impossible. Careful searching is needed to find the samples that have the least amount of specular reflection thus indicating a low degree of recrystallization of the matrix, and that contain radiolarians which still exhibit sharp boundaries with the matrix. In some instances, only one or two thin layers within a large outcrop of chert may yield useful fossils; the remainder may be too recrystallized to allow separation of the fossils from the matrix.

The color of the chert seems to have little influence on the quality or richness of enclosed radiolarian faunas, with the exception that milky, translucent cherts appear to have been altered and their faunas largely destroyed. Likewise, secondary cherts derived from silica replacement of limestone obviously should be avoided as they contain no original fossil material. Field recognition of radiolarians is difficult in black carbonaceous cherts similar to some Ford Lake samples.

Processing involves digestion of the sample for 24 hr in HF (50–52 percent) diluted to 1 part acid to 9 parts water, as recommended by Pessagno and Newport (1972). Weaker concentrations (up to 1 part acid to 20 parts water) and longer runs were also used but with no appreciable difference in quality of preservation of the tests. The original Ford Lake sample measured about $30 \times 15 \times 15$ mm. It was run repeatedly in the acid 20 or more times, the resulting residue being sieved and dried after each run. Little of the original sample remains. Techniques for further cleaning samples involve boiling the residue in concentrated HCl and H_2O_2 (Pessagno, 1977) but were not deemed necessary for Ford Lake materials. Standard micropaleontological techniques were utilized to examine the dried residues.

This HF technique is very simple to use and is relatively safe, providing that caution is used in handling both the concentrated and dilute HF. An adequate fume hood is required. After the initial success with the Ford Lake sample, we have collected and processed hundreds of samples of Paleozoic chert with equal success. We have determined that cherts as old as Ordovician can be dated by following the procedures outlined above. This new biostratigraphic tool has opened the door to dating many rock sequences that hitherto could not be dated directly and for which ages were either guessed at or established on the basis

of association with fossiliferous rocks. Many of these assumed ages have not been substantiated when the chert itself has been independently dated (Irwin and others, 1977).

The digestion of pre-Jurassic chert in HF has also resulted in the discovery of abundant conodonts in some cherts prepared for radiolarians. Such fortunate associations have added a greater precision to the dating method and have allowed a more rapid calibration of the radiolarian biostratigraphic succession.

NATURE OF RESIDUE AND PRESERVATION

The dry radiolarian-bearing residue contains abundant pyrite. Identifications of 1000 grains in randomly chosen microscope fields showed a composition very roughly 71.0-percent pyrite crystal-aggregates; 14.0-percent radiolarians with no shell structure preserved; and 11.0-percent siliceous aggregates, presumably derived from the chert matrix. Minor components are less than 2.0-percent sponge megascleres, less than 1.0-percent silicified dolomite rhombs, and traces of recrystallized conodonts and of sponge microscleres. Also present is a considerable amount of siliceous dust, impracticable to include in grain counts, so that the total silica content is higher than the figures cited. Radiolarians with the shell structure preserved constitute less than 2.0 percent, and specimens with the shell completely preserved and unbroken make up only about 0.2 percent of the whole residue.

Most forms that have survived with the lattice structure more or less intact are relatively robust species with single spherical shells. Solution of their internal structures hinders identification (see section on "Paleontology-of-sample A-854").

Many originally spheroidal tests are strongly deformed but still retain well-preserved lattice shell details. The crushed nature of subspherical to ellipsoidal specimens is revealed in asymmetry of the ellipse and lack of symmetry between the ellipsoidal shell and spines (see fig. 2 *p, q, t, u, w*). Such features are less easily detected in thin section and there is little doubt that some earlier records of "ellipsoidal" and "discoidal" taxa from Paleozoic cherts are based upon distorted spheroids. Davis (1947) recognized very highly crushed specimens in late Paleozoic Turkish cherts but probably underestimated the extent of distortion in the assemblage.

AGE AND PALEOENVIRONMENT OF SAMPLE A-854

A preliminary account of the more distinctive Radiolaria present in this sample is given in the section, "Paleontology of sample A-854." The most significant

forms encountered are the apparent palaeoactinomids *Triaenosphaera sicarius* Deflandre s.s., *T. sicarius* s.l., and "*Cenosphaera*" cf. "*C.*" *cabrierensis* Deflandre together with the pylentonemids ?*Pylentonema* sp. cf. *P. antiqua* Deflandre s.s., *P. antiqua* s.l., *Cyrtisphaeractenium mendax* Deflandre, *C. aff. C. mendax*, and *Archocyrtium* species nova.

As described in detail below, all but one of these forms are known from phosphatic nodules associated with bedded cherts of the Baltalimani Formation, Istanbul region (Kaya, 1973; Holdsworth, 1973). These cherts are conformably overlain by Forminifera-containing limestones belonging to Zone 9 (Mamet, 1973) of highest Tournaisian age (Sando and others, 1969). Limestone underlying the Baltalimani Formation contains early Famennian trilobites and possibly early Carboniferous goniatites (Kaya, 1973). There seems little doubt that the Baltalimani radiolarian assemblage is of post-Devonian, Tournaisian, age. The species "*C.*" *cabrierensis*, *T. sicarius*, *P. antiqua*, and *C. mendax* were all first described by Deflandre from phosphatic nodules associated with bedded cherts of the Cabrières region, Montagne Noire, southern France, and many other species are common to both the Cabrières and Baltalimani nodules (Holdsworth, 1973). Though Deflandre in many papers referred to the Cabrières cherts as "Viséan," Peterlongo (1971) stated that they are late Tournaisian and lie disconformably on beds of Famennian age.

Though total stratigraphic ranges are unknown for any of the species above and many Cabrières and Baltalimani species are absent from the Ford Lake sample, nevertheless, the very close similarity between Ford Lake and Baltalimani morphotypes suggests that the assemblages are close in age. The only reservation regarding an early Carboniferous age for A-854 arises from the total absence of *Albaillella* Deflandre, a genus widely distributed in Carboniferous rocks and not known to occur in pre-Carboniferous strata. Though its absence from A-854 might be attributable to solution during chert diagenesis, the genus is known from bedded cherts and has been recovered quite frequently, though in poor preservation, from other Alaskan chert residues examined during the present study.

The very rare and poorly preserved conodonts of A-854 indicate a Late Devonian (prelatest Famennian) rather than early Carboniferous age (Anita Harris, written commun., 1977). One example of *Palmatolepis* sp. (or possibly *Nothognathella* sp.) was found together with eight examples of *Polygnathus* cf. *P. webbi* Stauffer. *Palmatolepis* and *Nothognath-*

ella are restricted to the Late Devonian, as is *P. webbi*.

The radiolarians listed above appear to range from at least Late Devonian to late Tournaisian. A preliminary study of chert residues from other horizons in the Ford Lake shows that rare *Cyrtosphaeractenium* sp. indet. is still present 38 m lower in the section together with other Pylentonemidae including *Archocyrtium* (more abundant than in A-854), but *T. sicarius* may be absent at this lower level and replaced by new species, possibly of the same genus, absent from A-854.

The genera *Triaenosphaera*, *Pylentonema*, *Cyrtisphaeractenium*, and *Archocyrtium* have not previously been recorded from the Devonian, although *Archocyrtium* is known from the Middle Silurian (Deflandre, 1972a, b; Holdsworth, 1977). By the presence of relatively rich pylentonemid populations, the Ford Lake assemblages contrast markedly with other well-preserved Late Devonian radiolarian faunas. A rich fauna from the siliceous Frasnian Canol Shale, Northwest Territories, Canada, completely lacks Pylentonemidae (Holdsworth, 1977; B. K. Holdsworth, unpub. data), and, in Famennian assemblages from the Huron Member of the Ohio Shale, the family is represented only by the very rare *Formaniella cibdelosphaera* (Foreman).

The absence from Ford Lake residues of many forms known from the Canol and Ohio Shales and other Late Devonian units may be due to dissolution, but the absence from these other, better preserved assemblages of many clearly solution-resistant Ford Lake forms other than the pylentonemids, for example, *Triaenosphaera* and aff. "*Cenosphaera*" cf. "*C.*" *cabrierensis* Group, strongly suggests marked differences in the compositions of the original populations.

FIGURE 2.—"*Cenosphaera*" cf. "*C.*" *cabrierensis* Deflandre, aff. "*Cenosphaera*" cf. "*C.*" *cabrierensis* Group, and Spumellaria Family and genus indet. All $\times 150$ except as noted; *m* and *n* illustrate a single probable entactiniid species; *v* and *w* illustrate specimens possibly belonging to a single species with only two, opposed spines; *p*, *q*, *t*, *u*, and probably *w* illustrate various degrees of distortion and crushing.

a-c. "*Cenosphaera*" cf. "*C.*" *cabrierensis* Deflandre.

a. UA 2500. *b.* UA 2487. *c.* UA 2486.

d-i. Aff. "*Cenosphaera*" cf. "*C.*" *cabrierensis* Group.

d. UA 2488. *e.* UA 2482. *f.* UA 2483. *g.* UA 2484.

h. UA 2480. *i.* UA 2481.

j-w. Spumellaria Family and genus indet.

j. UA 2501. *k.* UA 2475. *l.* UA 2476. *m.* UA 2471. *n.*

UA 2502. *o.* UA 2478. *p.* UA 2499. *q.* UA 2479. $\times 100$.

r. UA 2472. *s.* UA 2473. *t.* UA 2503. *p.* UA 2474, \times

100. *v.* UA 2477. *w.* UA 2504.

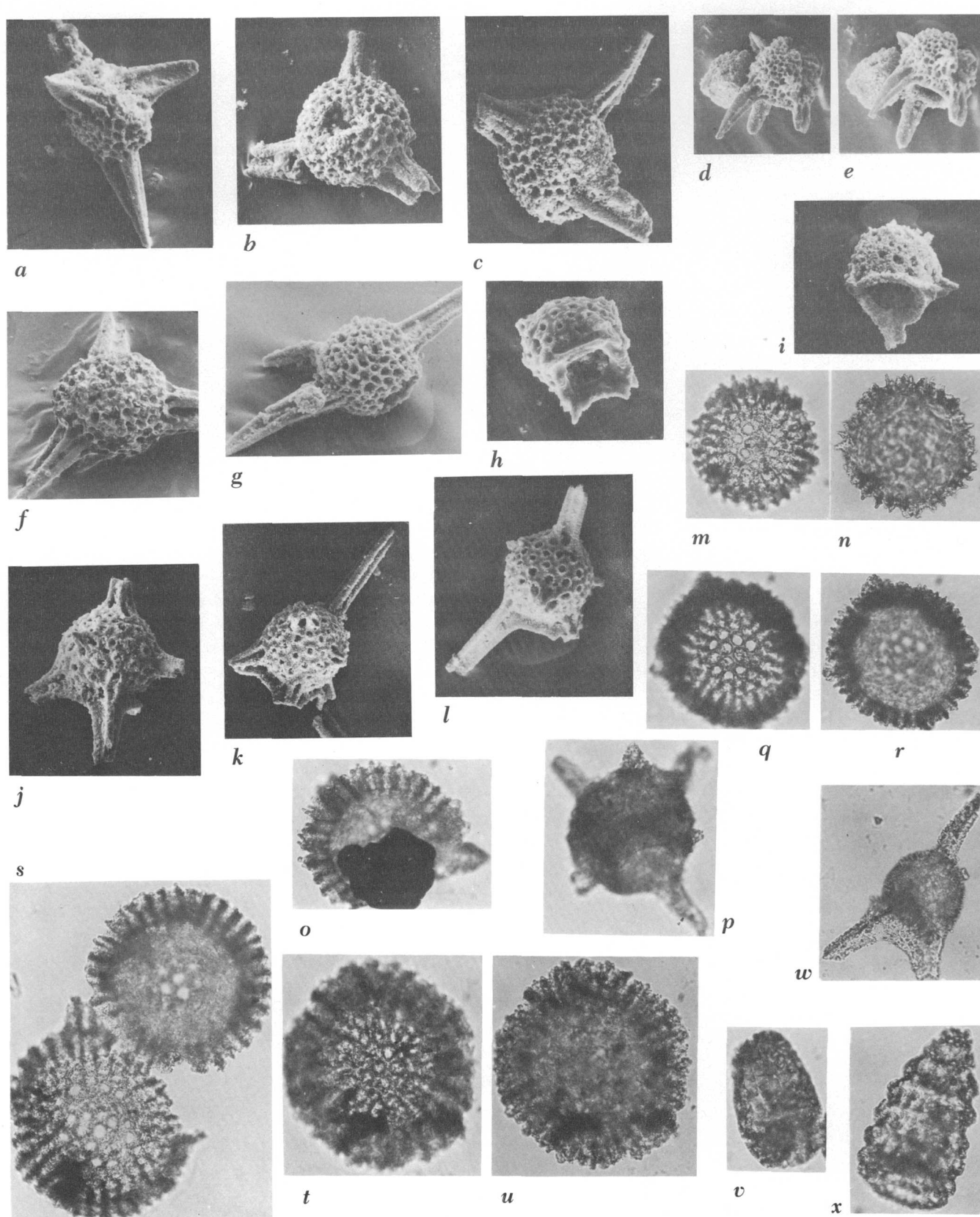


FIGURE 2

Holdsworth (1973, 1977) drew attention to the striking contrast in assemblage type that exists between the diverse and pylentonemid-rich Tournaisian radiolarian faunas of Cabrières and northwest Turkey and the usually far less diverse and pylentonemid-free faunas characteristic of central English Namurian shale goniatite bands. An even more direct contrast between these French and Turkish Tournaisian faunas from "Mediterranean-type" sequences is afforded by apparently contemporaneous, Osagean assemblages from the Sycamore Limestone, Oklahoma (Ormiston and Lane, 1976). The Sycamore faunas totally lack Pylentonemidae as well as Palaeoscenidiiae (common in the "Mediterranean" Tournaisian as well as the Canol and Ohio Shales) but possess Spongodiscidae and Phacodiscidae completely absent in all other assemblages discussed herein.

The Ford Lake Shale faunas are clearly more similar in assemblage type to those of the "Mediterranean-type" Tournaisian than to the faunas of the more clearly contemporaneous Canol and Ohio shales or the younger Sycamore Limestone. Holdsworth (1977) suggested that the extremely diverse, pylentonemid-rich faunas of southern France and Turkey reflect the influence of water derived from a closely adjacent "Tethyan" ocean; less diverse, nonpylentonemid late Paleozoic faunas existed in epicontinental seas that had more limited access to the water masses of contemporaneous open oceans. If so, perhaps the Kandik Basin in Late Devonian time was situated near the continental margin where greater oceanic influence prevailed than in areas farther inland, represented by the Canol and Ohio Shales. In the more open ocean waters of the Kandik Basin lived radiolarian faunas akin to those found in the early Carboniferous cherts of France and Turkey.

PALEONTOLOGY OF SAMPLE A-854

The Ford Lake assemblage is dominated by nonpylomate Spumellaria of originally spherical form. Most shell interiors are plugged with matrix, concealing any internal structures that may originally have been present. Some unplugged specimens are present, but, in most, an inner skeleton is absent. Such absence does not necessarily indicate an original lack of internal skeletal elements but may be due to solution. The absence of delicate external spines and truncation of major spines on many specimens also suggests strong solution of opal during chert diagenesis.

Reliable identification of many Ford Lake specimens is thus impossible, for even at the family level, a detailed knowledge of internal structure is demanded. Well-preserved late Paleozoic assemblages of nonpylo-

mate spheroidal radiolarians often are overwhelmingly dominated by Entactiniidae (in the restricted sense of Holdsworth, 1977). Members of this family are characterized by internal spicules that usually connect with major spines on the shell surface (see, for example, Foreman, 1963). In early Paleozoic assemblages, some nonspiculate (nonentactiniid) spheroidal forms are present (Fortey and Holdsworth, 1972; Holdsworth, 1977). Deflandre (1973), working with excellently preserved material, believed that at least two nonspiculate spheroidal species are present in the early Carboniferous of southern France. Allocation of a new species to the Entactiniidae requires documenting the presence of an internal spicular system as no feature of outer shell or spines is known to be diagnostic of the family. Some entactiniid species do have distinctive external features, but none of these species has been recognized in the Ford Lake assemblage; thus, the presence of Entactiniidae in the fauna, though probable, is unproven owing to the poor preservation of the material.

The relation between nonentactiniid Paleozoic spheroids and superficially similar post-Paleozoic taxa are so uncertain at present that Holdsworth (1977) united most such Paleozoic forms under the informal heading of "Palaeoactinommids." The same practice is followed in this account with respect to two Ford Lake forms having external features sufficiently similar to the nonspiculate species investigated by Deflandre (1973) as to suggest that the Ford Lake and French forms are conspecific.

The Ford Lake Shale spheroidal pylomate Radiolaria present fewer problems. All known late Paleozoic spheroidal pylomates belong to the entactiniaceid family Pylentonemidae. Again, reliable allocation to the family demands a knowledge of internal structure, but many genera and species have such distinctive external features as to allow virtually certain identification even where interiors are obscured.

Certain Ford Lake Shale forms are similar or identical to those in assemblages described from Cabrières, southern France, by Deflandre (in a large number of papers) and from the Baltalimani Formation, northwestern Turkey (Kaya, 1973; Holdsworth, 1973). In the following text, these two faunas are referred to as the "Cabrières" and the "Baltalimani" assemblages.

SYSTEMATIC DESCRIPTIONS

Subclass RADIOLARIA, Müller
 Order POLYCYSTINA, Ehrenberg (emended Reidel, 1967b)
 Suborder SPUMELLARIA, Ehrenberg
 Informal Grouping PALAEOACTINOMMIDS, Holdsworth, 1977

Diagnosis—Paleozoic spheroidal Radiolaria, sometimes pylomate, morphologically similar to the Acti-

nommidae, lacking the internal spicular system of the Entactiniacea and the distinctive lattice construction of the "Rotasphaerids."

Discussion.—Paleozoic species grouped under this heading have frequently been allocated to genera that possess post-Paleozoic type species. It is suggested that where such genera have been used for Paleozoic forms the generic names should be enclosed in quotation marks to emphasize the uncertainties which presently exist regarding phyletic relationships between Paleozoic forms of similar, often, simple, morphology. (See, for example, *Cenosphaera*, Ehrenberg, below).

Genus TRIAENOSPHAERA, Deflandre, 1973

Diagnosis.—Single spherical, reticulate lattice bearing four tetrahedrally arranged, multicostate spines.

Type species.—*Triaenosphaera sicarius* Deflandre

Discussion.—Ormiston and Lane (1976) were incorrect in suggesting that the genus possesses an internal spicule; Deflandre stressed that he could find no traces of spicule in his type material from the Cabrières assemblage.

Triaenosphaera sicarius* Deflandre, *sensu stricto

Figure 3a-c

Specimens with lattice and spine structure apparently identical with *T. sicarius* are comparatively common in the Ford Lake assemblage, though breakage frequently prevents determination of the full spine complement and symmetry. At least four specimens (UA 2457, 2458, 2459, 2462) can reliably be allocated to Deflandre's species, though UA 2457 is partly crushed. The spines of the species are highly distinctive, very broad at the base, fundamentally three-bladed but with each blade subdivided along the earlier part of its length, the spine terminating as a weakly three-bladed or unbladed rod. Edges of main and subsidiary blades are blunt, rounded, and, in at least some cases, swollen.

Triaenosphaera sicarius* Deflandre, *sensu lato

Figure 3f, g

Specimens UA 2460 and UA 2461 have pore and spine structure apparently identical with *T. sicarius* s.s.; but, in UA 2461, one spine is distinctly weaker than the other three, and, in UA 2460, no trace of a fourth spine can be found, though orientations of the three spines present are similar to the orientations of any three spines in *T. sicarius* s.s.

It is not known whether such variants occur in the Cabrières type material, but they do occur associated with *T. sicarius* s.s. in the Baltalimani assemblage. Nineteen specimens with shell and spine structure similar to *T. sicarius* s.s. were examined in the Keele University collection. In one specimen (and perhaps

a second) no trace of a fourth spine was found, and, in two specimens (and perhaps a third), the fourth spine is weaker than the other three. Thus, Ford Lake and Baltalimani populations appear to be similar, and it is reasonable to extend the definition of *Triaenosphaera* to include such populations with a minority of "aberrant" specimens.

Relationship between Triaenosphaera sicarius and Trilonche cimelia Ormiston and Lane.—Of well preserved Paleozoic species, *T. sicarius* compares most closely with the form described as "*Trilonche cimelia* sp. nov." by Ormiston and Lane (1976) from the Mississippian Sycamore Limestone, Oklahoma. They considered their new species to be close to the Middle Devonian type species, *Trilonche vetusta* Hinde, 1899. However, Nazarov (1975) showed that some Late Devonian two-shelled Entactiniidae (*Entactinosphaera* spp.) possess three of six spines preferentially developed and considered one such species so similar to *Tr. vetusta* as to justify the reallocation of Hinde's species to *Entactinosphaera*. Nazarov suggested (as had Foreman, 1963, in more general terms) that Hinde's thin-sectioned specimens failed to show the full complement of spines and internal entactiniaceid spicule, and such an argument could well apply to Hinde's two other "*Trilonche*" spp. in the same fauna.

Thus, *Trilonche* as conceived by Hinde—a two-shelled, nonspiculate spheroid with three major spines disposed in the same plane, with variants showing a fourth spine—may not actually exist in the Devonian. The Mississippian "*Tr.*" *cimelia* does, however, appear to agree broadly with Hinde's concept, an inner shell being present in at least one specimen. But the holotype figured can also be compared with *Triaenosphaera sicarius* s.l. (three-spined form), differing only in that the spines (which appear to be of similar structure to those of *T. sicarius*) are slightly weaker and apparently disposed in a single plane, whereas in *T. sicarius* no three spines occupy the same plane in either four- or three-spined morphotypes. The similarity with *T. sicarius* is underlined by the presence of a fourth spine in about 40 percent of "*Tr.*" *cimelia* specimens (A. O. Ormiston, written commun., 1977).

Marked changes in symmetry and spine number have been well documented in evolutionary lineages of Cenozoic Spumellaria (see, for example, Riedel and Sanfilippo, 1971, p. 1586), sometimes associated with loss of an inner shell (Holdsworth, 1975, p. 519). Thus, the "*Tr.*" *cimelia* population might well be viewed as either a contemporaneous variant of the Cabrières, Baltalimani, and Ford Lake *T. sicarius* populations or as a population ancestral to or descendant from such populations.

If Nazarov's (1975) reinterpretation of *Trilonche vetusta* Hinde, 1899, is correct, then *Entactinosphaera* is a synonym of Hinde's genus and in view of the doubts regarding the type material the use of "Trilonche" might usefully be abandoned as a nomen dubium. In such a case, the definition of *Triaenosphaera* might be broadened to accommodate "Trilonche" *cimelia*, which apparently lacks entactiniid characters.

Genus *CENOSPHAERA*, Ehrenberg, 1854
"CENOSPHAERA"

Diagnosis.—"Cenosphaera" is used informally for Paleozoic single shelled forms having simple pores and lacking major spines. Such usage may prove unsatisfactory because the Ford Lake assemblage contains morphotypes with and without major spines that may be phyletically closely related (see below).

"Cenosphaera" *cabrierensis* Deflandre, 1973

Deflandre, 1973, p. 1150, plate II, figs. 5-7.

"Cenosphaera" cf. "C." *cabrierensis* Deflandre

Figure 2a-c; figure 3m, n

A small number of Ford Lake specimens (for example, UA 2485, 2486, 2487) compare sufficiently well with the described Cabrières type material in lattice diameter and thickness, pore structure, and density and length of the very numerous minor spines as to suggest they belong to Deflandre's species. "C." *cabrierensis* does not, however, possess truly distinctive features, and, failing reexamination of the type material, it is not possible to be certain that Cabrières and Ford Lake morphotypes are identical. No comparable form is present amongst a collection of some 200 nonpylomate Baltalimani spheroids in the Keele University collection.

aff. "Cenosphaera" cf. "C." *cabrierensis* Group

Figure 2d-i; figure 3o-s

A few Ford Lake specimens have apparently single shells with pores and thorny surfaces similar to "C." cf. "C." *cabrierensis*, but the shells also bear very short, strong major spines (for example, UA 2488). Other more common specimens have smoother shells but with pores of similar form and density and similar short strong spines (for example, UA 2482, 2483, 2484, 2489, 2490, 2491, 2492). In other larger, more rare specimens, one spine is much longer (for example, UA 2480) and more than one such longer spine may be present (for example, UA 2481). In some cases, these longer spines are multibladed at the base, the structure being rather similar to that seen in *T. sicarius*.

A feature of aff. "C." cf. "C." *cabrierensis* Group is the considerable thickness of the shell wall in larger specimens. Smaller specimens of diameters comparable to those of "C." *cabrierensis* and "C." cf. *cabrierensis* (140-150 μm), have shell thicknesses roughly comparable with these forms, about 14-16 μm . Two specimens of 160- μm diameter show thicknesses of about 18 μm and about 24 μm compared to about 16 μm for "C." cf. "C." *cabrierensis* at 160- μm diameter and 20 μm for this form at 170- μm diameter. But the largest aff. "C." cf. *cabrierensis* Group specimens (190-240 μm), have shell thicknesses of about 30-35 μm . A single completely spineless, nonthorny specimen (UA 2494), "Cenosphaera" sp. (fig. 3t, u), of 220- μm diameter has a thickness of about 32 μm .

In the absence of direct information on original internal structure, the allocation of this group to the Palaeoactinommids rather than the Entactiniidae is tentative, but shell diameter to thickness ratios of less than 10 to 1, which seem to characterize the group, are uncommon in known, nonspongy late Paleozoic Entactiniidae, which usually display considerably thinner reticulate shells (see, for example, data in Foreman, 1963) even at a relatively large diameter. Figured specimens of *Entactinosphaera foremanae* (Ormiston and Lane, 1976, plate 1, figs. 3, 4) appear to have ratios of 13.6 to 1 and 12.3 to 1 at outer shell diameters of 231.6 and 278.2 μm , respectively, though the failure to demonstrate an inner spicular system in this species leaves its entactiniid nature in some doubt. A few apparent entactiniid Late Devonian species included by Nazarov (1975) in his genus *Astroentactinia* do have shell thicknesses comparable

FIGURE 3.—All $\times 150$ except as noted.

- a-c. *Triaenosphaera sicarius* Deflandre s.s.
 a. UA 2457. b. UA 2458. c. UA 2459.
- d, e. *Pylentonema antiqua* Deflandre s.l. UA 2468.
 f. *Triaenosphaera sicarius* Deflandre s.l. UA 2461.
 g. *Triaenosphaera sicarius* Deflandre s.l. UA 2460.
 h. Aff. *Cyrtisphaeractenium mendax* Deflandre. UA 2463.
- i-l. *Cyrtisphaeractenium mendax* Deflandre.
 i. UA 2466. j. UA 2497. k. UA 2465. l. UA 2464.
- m, n. "Cenosphaera" cf. "C." *cabrierensis* Deflandre. UA 2485.
- o. Aff. "Cenosphaera" cf. *cabrierensis* Deflandre. UA 2489.
- p. ?*Pylentonema* sp. cf. *P. antiqua* Deflandre s.s. UA 2469. $\times 200$.
- q-s. Aff. "Cenosphaera" cf. "S." *cabrierensis* Deflandre Group q, r. UA 2491. s. UA 2492.
- t, u. "Cenosphaera" sp. UA 2494.
- v. *Radiolaria incertae sedis*. UA 2498. $\times 200$.
- w. *Archocyrtium* Deflandre sp. nov. UA 2470. $\times 200$.
- x. *Radiolaria incertae sedis*. UA 2493. $\times 200$.

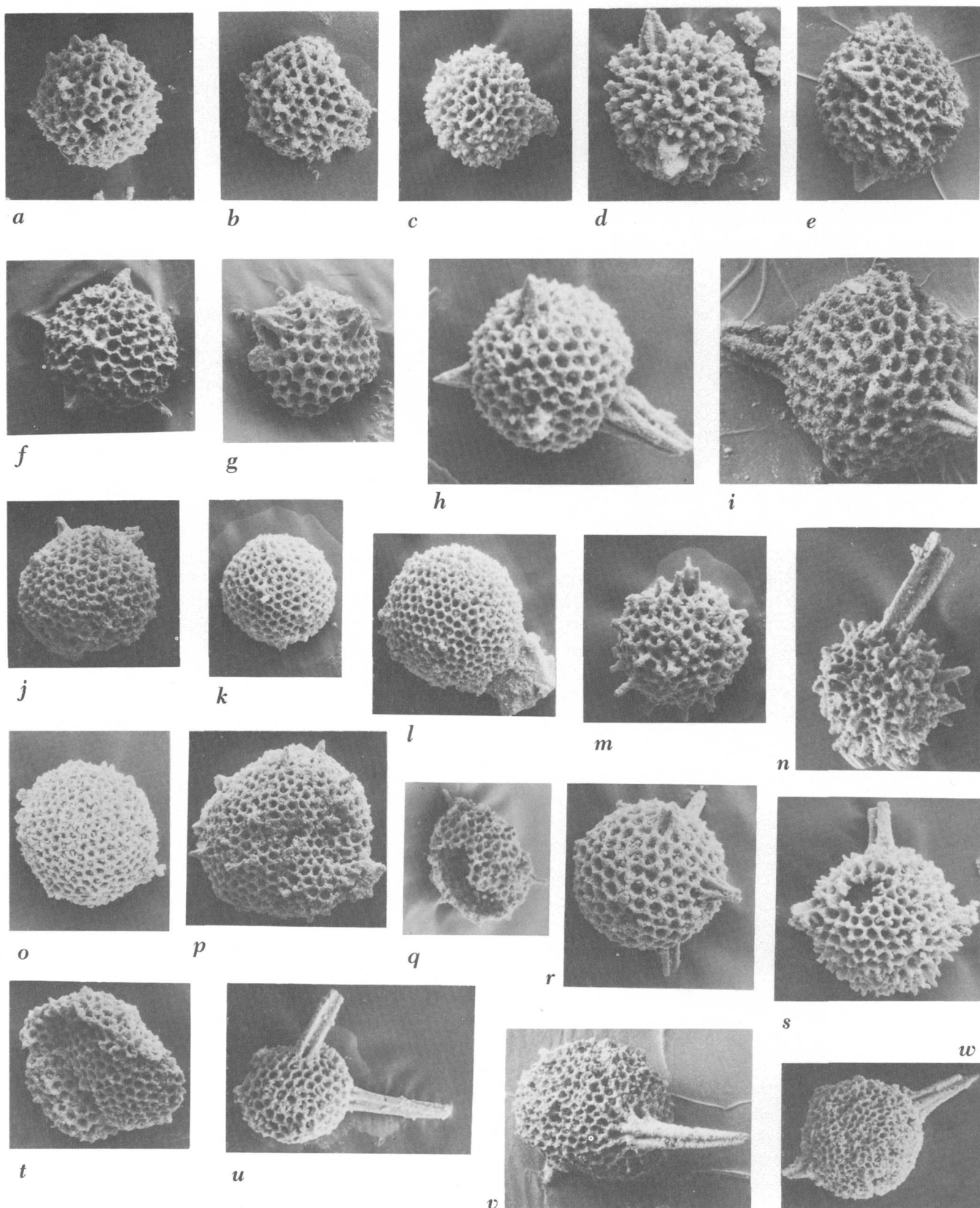


FIGURE 3

to those of Ford Lake specimens, but similarities in structure between the larger spines of aff. "C." cf. *cabrierensis* Group and those of *T. sicarius* may support a nonentactiniid allocation.

Genus *Sphaerozoum*, Meyen, 1834

In a number of previous studies of radiolarians in thin sections of late Paleozoic cherts, small tri- and multiradiate shapes have been described and interpreted as the detached spicules of *Sphaerozoum* spp. (see, for example, Hinde and Fox, 1895; Davis 1947). No such isolated spicules occur in the Ford Lake residue nor, to the writers' knowledge, have spicules of such form appeared in any Paleozoic radiolarian assemblage completely separated from its matrix. It should be noted, however, that if transverse sections were cut along the length of a *T. sicarius* spine or one of the larger spines of aff. "C." cf. "C." *cabrierensis* Group a set of shapes would result that are remarkably similar to those of the lobed and unlobed "spicules" figured by Hinde and Fox (1895, pl. 25, fig. 1a-g) and by Davis (1947, figs. 2, 3a-c). The lobed and swollen-rayed "spicules" of Davis are particularly significant as his chert specimens came from the Baltalimani Formation (see Kaya, 1973), which is known to contain *T. sicarius*. Sections of such complex, highly solution-resistant spines may well account for some at least of the records of late Paleozoic *Sphaerozoum* spp.

SPUMELLARIA Family and genus indeterminable

Figure 2j-w

Many Ford Lake spumellarian specimens have comparatively well preserved lattice exterior and spines, but their external features cannot be reliably compared to any known entactiniid or palaeoactinomiid species. Classification of such forms is presently impossible.

One of the more distinctive Ford Lake forms has relatively large pores, numerous very strong by-spines and an indeterminable number of three-bladed main spines (for example, UA 2471, 2502; fig. 2m, n) and appears to be similar to the more spinose variant of *Entactinia herculea* Foreman from the Famennian Ohio Shale. The Ford Lake form differs in that it does not seem to have the six, strong, equally developed main spines of *E. herculea*. It may be that the Ford Lake form is closer to members of an undescribed Baltalimani *Entactinia* population containing individuals with one or more of the six main spines weakly developed. In any case, these Ford Lake forms and certain other forms (fig. 2r, s, u) are probably entactiniids.

A species with only two opposed spines is represented by UA 2504 and UA 2477 (fig. 2v, w); the former appears to have been strongly crushed. Far more common are spheroids with very small, regular, hexagonal or subhexagonal pores, sometimes lacking spines and sometimes with short, weak, rodlike spines, often more or less crushed (fig. 2j-l, o-q, t).

Superfamily ENTACTINIACEA, Riedel, 1967a

Diagnosis.—Paleozoic Radiolaria with a spicule of four or more rays, point- or bar-centered, constituting the main part of the skeleton or incorporated within a latticed or spongy shell, nearly spherical, with or without pylome. Shell very rarely tubular, pylomate, and rarely (and doubtfully) conical, pylomate.

Discussion.—The diagnosis is that of Riedel's (1967a) Family Entactiniidae, but the use of "Entactiniidae" is now restricted to nonpylomate forms (Holdsworth, 1977). Nazarov, Popov, and Apollonov (1975) and Nazarov (1975) extended the definition of the Entactiniidae to include early Paleozoic forms in which the innermost skeleton is a small "polyhedron," but this practice is not followed herein.

**Family PYLENTONEMIDAE, Deflandre, 1963, emended
Holdsworth, 1977**

Diagnosis (emended herein).—Entactiniacea with single, nearly spherical, latticed (extremely rarely spongy) shell, occasionally with more than one shell, the outermost of which displays an actual or incipient pylome with differentiated rim connected to one or more of the main spines. A perforate tubular or conical extension associated with pylome is lacking.

Genus PYLENTONEMA, Deflandre, 1963, diagnosed herein

Diagnosis.—Pylentonemidae with outer shell spherical, pores numerous, closely spaced, simple; pylome circular, surrounded by well-developed, but very shallow, circular, unornamented rim. Pylome net (*sensu* Holdsworth, 1973) absent. Pylome rim connecting with one or more of three tricostulate main spines disposed around and adjacent to pylome. Four other tricostulate spines present, none of which approximates to an "apical" spine. Inner spicular system of seven rays arising from the ends of short median bar, each ray connecting with a main spine, the bar and proximal ends of rays sometimes enclosed by small, spherical, inner lattice.

Type species.—*Pylentonema antiqua* Deflandre, 1963.

Discussion.—*P. antiqua* is the only valid described species of this genus.⁴ In 1963, Deflandre described

⁴ Nazarov, Papov, and Apollonov (1975) assigned two pylomate Ordovician species to the genus, but the internal and external structure of these forms differs so radically from the *P. antiqua* holotype that assignment to *Pylentonema* appears unwarranted nor can they be viewed as Entactiniacea (Holdsworth, 1977).

only the holotype from the Cabrières assemblage, but he provided no formal generic diagnosis and the genus could be understood only in terms of this single specimen. The holotype possesses a weak inner lattice enclosing the central part of the spicular system. But Deflandre (1972a, footnote 4) indicates that, among Cabrières specimens of "*Pylentonema*," the holotype of *P. antiqua* may be unique in displaying this inner shell. The diagnosis provided above takes account of the fundamental features of the *P. antiqua* holotype but is broad enough to include within the genus (as was apparently Deflandre's intention) morphotypes lacking an interior shell as well as morphotypes known from the Baltalimani assemblage which differ considerably in their spine development from the *P. antiqua* holotype (see below).

Pylentonema antiqua* Deflandre, 1963, *sensu stricto
(Acanthopyle antiqua nomen nudum Deflandre, 1960)

Deflandre, 1960, plate 1, figure 14. Deflandre, 1963, p. 3981–3984, figures 1–5.

?*Pylentonema* sp cf. *Pylentonema antiqua* Deflandre s.s.

Figure 3p

A single Ford Lake specimen (UA 2469) of 110-μm diameter agrees in all determinable respects with the *P. antiqua* holotype, particularly in that all seven three-bladed spines appear to have been of approximately equal strength, but the nature of the lattice pores is not determinable. A second specimen (UA 2495) may be similar, but the shape and strength of the pylome rim are less well seen.

***Pylentonema antiqua* Deflandre s.l.**

Figure 3d–e

At least two Ford Lake specimens (UA 2467, 2468) possess pores and pylome structure similar to those of the *P. antiqua* holotype but differ markedly from it in that the apertural spines are far stronger than the nonapertural spines (some or all of which might originally have been undeveloped). It is not known whether these morphotypes occur with *P. antiqua* s.s. in the Cabrières assemblage, but a considerable range of variation characterizes *Pylentonema* in the Baltalimani fauna. Of 15 Baltalimani specimens, in 9 all visible spines are of approximately equal strength, in 5 specimens one or more nonapertural spines are noticeably weaker than the apertural spines, and in 1 specimen (TB220a) the three apertural spines are very strong, curved towards the aperture, while the three visible nonapertural spines are extremely short. This specimen is thus closely similar to UA 2468 and possibly to UA 2467. As the short-spined Baltalimani morphotype is part of a population

dominated by specimens apparently identical with the *P. antiqua* holotype and including specimens of intermediate morphology, the provisional designation "*Pylentonema antiqua, sensu lato*" seems appropriate to both the Baltalimani and the Ford Lake specimens.

Genus *CYRTISPHAERACTENIUM* Deflandre, 1972b

Diagnosis.—(Abridged from Deflandre, 1972b). Pylentonemidae with single spherical lattice. Pores large, widely spaced. Pylome wide with thickened rim bearing comblike spicular fringe, rim connected to three long tricostate spines. Four other spines, one invariably short, conical; others long, nonapical. Inner spicular system incompletely known.

Type species.—*Cyrtisphaeractenium mendax* Deflandre, 1927b. Only described species.

Discussion.—It is unfortunate that the delicate pylome "comb" is specified as a generic feature as it survives only in very well preserved specimens and is known in other Baltalimani pylentonemids with overall form very different from *Cyrtisphaeractenium* (see, for example, Holdsworth, 1973, fig. 1e). The absence of this structure is the only feature that seems to distinguish Deflandre's (1972b) monospecific genus *Pararchocystium* from *Cyrtisphaeractenium*. The seven-spined pylentonemid *Cyrtisphaeronemium* Deflandre (1972b) is more distinct, possessing one major main spine of "subapical" position and axial orientation and a deeper, spinose pylome rim. The other known seven-spined pylentonemid genera, *Pylentonema* and *Formaniella* Deflandre (1972b), differ in their weaker, shallower pylome rims.

***Cyrtisphaeractenium mendax* Deflandre, 1972b**

Deflandre, 1960, plate 1, fig. 19. Deflandre, 1972b, p. 14. Deflandre, 1972a, plate 1, figs. 5–11; plate 2, figs. 4–5; plate 3, figs. 1–6.

Figure 3i–l

Despite their poor preservation the commonest Ford Lake pylentonemid specimens undoubtedly belong to *Cyrtisphaeractenium*. Individuals of cyrtisphaeracteniid aspect constitute a population closely comparable with that previously considered to represent *C. mendax* in the Baltalimani assemblage, though "*C. mendax*" is now restricted to Ford Lake and Baltalimani specimens with only three spines incorporated into the pylome rim (see below). In many Ford Lake specimens, the large, widely spaced pores with raised, pustulelike rims, typical of *C. mendax* are clearly visible (fig. 3j). Though this pore structure is also characteristic of the monospecific genus *Cyrtisphaeronemium*, no Ford Lake specimen shows the diagnostic preferentially developed subapical, adapertural spine

of the genus or the rather deep, thin, flared "skirt" surrounding the pylome and the associated strong, rodlike subsidiary spines of *Cyrtisphaeronemium prudentigerum* Deflandre. In Ford Lake specimens, there appear always to have been two widely spaced adapertural spines of comparable strength, as in the Cabrières type material of *C. mendax*. Owing to common breakage of spines close to the lattice surface, it is difficult to demonstrate in Ford Lake material the unique, very short "conical" lateral spine of *C. mendax*, but it is probably preserved in UA 2465 and clear in UA 2497.

aff. Cyrtisphaeractenium mendax Deflandre

Figure 3*h*

The diagnosis of *Cyrtisphaeractenium* specifies the presence of only three major spines in the pylome margin, and this condition is clear in the *C. mendax* holotype (Deflandre, 1972a, pl. 1, figs. 9, 10). This is also the condition in most Ford Lake specimens (for example, UA 2466, fig. 3*i*), which compare in other respects with the species. Slight flattening of the external pylome rim between the apertural spines produces a subtriangular shape, though the outline of the pylome itself is circular. In a few specimens, however (for example, UA 2463, fig. 3*h*), a fourth spine is incorporated in the pylome rim, the outline of the external rim being subquadrangular. No such variant is described from the Cabrières assemblage, though two figured specimens (Deflandre, 1972a, pl. 1, fig. 8; pl. 2, fig. 4) suggest that a fourth spine is very close indeed to the aperture. In all other respects, such Ford Lake specimens compare with *C. mendax*. Prior to publication of the diagnosis of the species, a similar dimorphism was noted amongst Baltalimani specimens allocated to "*Cyrtisphaeractenium mendax*" (Holdsworth, 1973, p. 124). As it is now clear that the Baltalimani specimens with three-spined aperture are conspecific with *C. mendax* and the pylome "comb" is present in both Baltalimani dimorphs (though never seen in the more highly dissolved Ford Lake population), the designation "aff. *Cyrtisphaeractenium mendax*" seems appropriate for the morphotype with four-spined aperture in both assemblages.

Genus *ARCHOCYRTIUM* Deflandre, 1972b

Diagnosis.—Pylentonemidae with nearly spherical, perforate lattice and four spines. Three spines disposed around the pylome margin, the fourth apical to subapical in position. Pylome rim of variable depth, always imperforate. Internal spicular system consisting of four rays.

Type species.—*Archocyrtium riedeli* Deflandre, 1927b.

Discussion.—For practical purposes the genus can only be defined in terms of its four spines and tetrahedral form. Though an entactiniaceid spicular system is certainly present in some specimens, it is usually extremely difficult to see, and, in some species of archocyrtiid form, it may never have existed. Deflandre specified four rays in the generic diagnosis, one ray connecting with each spine, but Holdsworth (1973, p. 124) pointed out that, in some specimens of archocyrtiid form, rays can be found unassociated with spines and it would be unrealistic to exclude these from the genus.

Archocyrtium species nova

Figure 3*w*

Archocyrtium is extremely rare in locality A-854, though more common at a lower Ford Lake level. Two fragmentary specimens and a single almost complete individual (UA 2470) were found. This last can be compared with no described form but is apparently identical with a relatively large Baltalimani species represented in the Keele University Collection by specimens TB021, 077, and 090b.

Radiolaria Incertae Sedis

Figure 3*v, x*

Single specimens were recovered from the Ford Lake residue representing two forms of unknown affinities.

UA 2493 (fig. 3*x*) is a hollow, segmented cone, 160 μm long, widening continuously to an unrestricted aperture of 90- μm diameter. The apical segment is probably incomplete. The six further segments of equal length give a markedly undulose outline to the shell, the terminal segment being possibly bisected by a weak annular stricture. Internally, segments are not separated by septal partitions, but the external intersegment constrictions are strong. The shell appears totally imperforate.

UA 2498 (fig. 3*v*) is a broadly spindle-shaped, hollow shell, 130 μm long, with a maximum width of 76 μm tapering slightly to the 54- μm aperture; the apex is blunt. There are no traces of annular strictures or internal septae but strong indications of external longitudinal costae with spacing about 10 μm . The shell appears totally imperforate.

There are no Paleozoic forms known from well-preserved material with which either of these specimens can be compared, though multisegmented forms broadly similar to UA 2493 have been recorded from late Paleozoic chert thin sections and assigned to nassellarian genera (see, for example, Rüst, 1892). Confirmation of the pre-Mesozoic existence of multicystroid Nassellaria would be valuable, but UA 2493

is too poorly preserved for certain identification, and, pending further preparation of residues from sample A-854, the possibility of contamination cannot be ignored.

REFERENCES CITED

- Brabb, E. E., 1969, Six new Paleozoic and Mesozoic formations in east-central Alaska: U.S. Geol. Survey Bull. 1274-I, 26 p.
- Davis, A. G., 1947, Report, in McCallien, W. J., A note on the Devonian Kieselschiefer of the Bosphorus: Istanbul Univ. Faculte des Sciences Revue, ser. B, v. 12, p. 176-179.
- Deflandre, G., 1952, *Albaillella* nov. gen., Radiolaire fossile du Carbonifère inférieur, type d'une lignée aberrent éteinte: Acad. Sci. Paris Comptes Rendus, v. 223, p. 515-517.
- 1960, A propos du développement des recherches sur les Radiolaires fossiles: Rev. Micropaleontology, v. 2, p. 212-218.
- 1963, *Pylentonema*, nouveau genre de Radiolaire du Viséen: Sphaerellaire ou Nassellaire: Acad. Sci. Paris Comptes Rendus, v. 257, Groupe 9, p. 3981-3984.
- 1972a, Le système trabeculaire interne chez les Pylentonemides et les Popofskyellides, Radiolaires du Paleozoïque, Phylogénèse des Nassellaires: Acad. Sci. Paris Comptes Rendus, v. 274, série D, p. 3535-3540.
- 1972b, Remarques complémentaires sur la morphologie et la nomenclature de quelques genres de Radiolaires du Paleozoïque: Acad. Sci. Paris Comptes Rendus, v. 275, ser. D, p. 13-16.
- 1973, Observations et remarques sur les Radiolaires Sphaerellaires du Paleozoïque, à propos d'une nouvelle espèce, viséenne, du genre *Formaniella* Defl., parfait intermédiaire entre les Perioxoplastidies et les Pylentonemides: Acad. Sci. Paris Comptes Rendus, v. 276, ser. D, p. 1147-1151.
- Dunham, J. B., and Murphy, M. A., 1977, An occurrence of well-preserved Radiolaria from the Upper Ordovician (Caradocian), Eureka County, Nevada: Jour. Paleontology, v. 50, p. 882-887.
- Ehrenberg, C. G., 1854, Die systematische Charakteristik der neuen mikroskopischen organismen de tiefen Atlantischen Oceans für den Monatsbericht zum Drack zu übergeben, deren Verzeichniss in Monat Februar bereits mitgetheilt worden ist: Königlichen Preussische Akad. Wissenschaften Berlin, Monatsberichte, Jahrg. 1854, p. 236-250.
- Foreman, H. P., 1963, Upper Devonian Radiolaria from the Huron Member of the Ohio Shale: Micropaleontology, v. 9, p. 267-304.
- Fortey, R. A., and Holdsworth, B. K., 1972, The oldest known well-preserved Radiolaria: Soc. Paleontologia Italiana Boll., v. 10, p. 35-41.
- Foster, H. L., 1976, Geologic map of the Eagle quadrangle, Alaska: U.S. Geol. Survey Misc. Inv. Map I-922.
- Hinde, G. J., 1899, On the Radiolaria in the Devonian rocks of New South Wales: Geol. Soc. London Quart. Jour., v. 55, p. 38-64.
- Hinde, G. J., and Fox, H., 1895, On a well-marked horizon of radiolarian rocks in the Lower Culm Measures of Devon, Cornwall, and West Somerset: Geol. Soc. London Quart. Jour., v. 51, p. 609-688.
- Holdsworth, B. K., 1966, Radiolaria from the Namurian of Derbyshire: Palaeontology, v. 9, p. 319-329.
- 1969, Namurian Radiolaria of the Genus *Ceratoikiscum* from Staffordshire and Derbyshire, England: Micropaleontology, v. 15, p. 221-229.
- 1973, The Radiolaria of the Baltalimani Formation, Lower Carboniferous, Istanbul, in Paleozoic of Istanbul: Ege Universitesi Fen Fakultesi Kitaplar, ser. no. 40, p. 117-134.
- 1975, Cenozoic Radiolaria biostratigraphy: Leg 30: Tropical and equatorial Pacific: Initial Repts. Deep Sea Drilling Proj., v. 30, p. 499-537.
- 1977, Paleozoic Radiolaria: stratigraphic distribution in Atlantic Borderlands, in Stratigraphic micropaleontology of Atlantic Basin and Borderlands: Amsterdam, Elsevier Pub. Co., p. 167-184.
- Irwin, W. P., Jones, D. L., and Pessagno, E. A., Jr., 1977, Significance of Mesozoic radiolarians from the pre-Nevadan rocks of the southern Klamath Mountains, California: Geology, v. 5, p. 557-562.
- Kaya, O., 1973, The Devonian and Lower Carboniferous stratigraphy of the Istinye, Bostancı, and Bayukada Subareas, in Paleozoic of Istanbul: Ege Universitesi Fen Fakultesi Kitalpar, ser. no. 40, p. 1-35.
- Mamet, B. L., 1973, Foraminiferal biostratigraphy of the Lower Carboniferous Trakaya and Hybeliada Formations, Istanbul Region, Turkey, in Paleozoic of Istanbul: Ege Universitesi Fen Fakultesi Kitalpar, ser. no. 40, p. 117-134.
- McCallien, W. J., 1947, A note on the Devonian Kieselschiefer of the Bosphorus: Istanbul Univ. Faculté des Sciences Revue, ser. B, v. 12, p. 173-181.
- Meyen, F. J. F., 1834, Über das Leuchten des Meeres und Beschreibung einiger Polypen und anderer niederer Thiere: Kaiserl. Leopoldin.-Carolin. Akad. Naturf. Verh., v. 16, supp. 1, p. 125-162.
- Murata, K. J., and Norman, M. B., II, 1976, An index of crystallinity for quartz: Am. Jour. Sci., v. 276, no. 11, p. 1120-1130.
- Nazarov, B. B., 1975, Lower and Middle Paleozoic Radiolaria of Kazakhstan [in Russian]: Akad. Nauk. SSSR Geol. Inst. Trudy, v. 275, p. 1-202.
- Nazarov, B. B., Popov, L. E., and Apollonov, M. K., 1975, Radiolaria from the Lower Paleozoic of Kazakhstan [in Russian]: Akad. Nauk SSSR Izv. Ser. Geol., 1975, no. 10, p. 96-111.
- Ormiston, A. R., and Lane, H. R., 1976, A unique radiolarian fauna from the Sycamore Limestone (Mississippian), and its biostratigraphic significance: Palaeontographica, pt. A, Band 154, p. 158-180.
- Pessagno, E. A., Jr., 1977, Upper Jurassic Radiolaria and radiolarian biostratigraphy of the California Coast Ranges: Micropaleontology, v. 23, no. 1, p. 56-113, 12 pls.
- Pessagno, E. A., Jr., and Newport, R. L., 1972, A technique for extracting Radiolaria from radiolarian cherts: Micropaleontology, v. 18, p. 231-234.
- Peterlongo, J.-M., 1971, Le Paleozoïque ante-Houiller dans le Massif Central, in Jung, J., Symposium, Géologie, Géomorphologie et structure profonde du Massif Central, Français: Clermont-Ferrand, Plein Air Service Ed., p. 157-168.
- Riedel, W. R., 1967a, Some new families of Radiolaria: Geol. Soc. London Proc., no. 1640, p. 148-149.

- 1967b, Class Actinopoda, in *The fossil record—A symposium with documentation*: Geol. Soc. London, p. 291–298.
- Riedel, W. R., and Sanfilippo, A., 1971, Cenozoic Radiolaria from the western tropical Pacific, Leg 7: Initial Repts. Deep Sea Drilling Proj., v. 8, p. 1529–1671.
- Rüst, D., 1892, Beitrage zur Kentniss der fossilen Radiolarien aus Gesteinen der Trias und der palaeozoischen Schichten: *Palaeontographica*, v. 38, p. 107–192.
- Sando, W. J., Mamet, B. L., and Dutro, J. T., 1969, Carboniferous megafaunas and microfaunal zonation in the Northern Cordillera of the United States: U.S. Geol. Survey Prof. Paper 613-E, p. E1–E29.
- Schwartz, A., 1924, Ein Verfahren zur Freilegung von Radiolarien aus Kieselschäfen: *Senckenbergiana*, v. 6, p. 239–244.
- Stürmer, W., 1966, Das Wachstum silurischer Sphaerellarien und ihre späteren chemischen Umwandlungen: *Palaont. Zeitschr.*, v. 40, p. 257–261.

A REEXAMINATION OF THE PENNSYLVANIAN TRACE FOSSIL *OLIVELLITES*

By ELLIS L. YOCHELSON and DAVID E. SCHINDEL,¹

Washington, D.C.

Abstract.—The original interpretation of *Olivellites plummeri* Fenton and Fenton as the trace of an infaunal gastropod is reconsidered and rejected. The original slab bearing several examples of *O. plummeri* has been reexamined and reillustrated. The slab came from the type-locality of *O. plummeri* in Eastland County, Tex., and is a shallow subtidal sandstone of the Graham Formation; the sandstone, which has yielded additional specimens, is presumably a reworked delta-front deposit. *Olivellites* was also observed in the Caddo Creek Formation in Stephens County, Tex., but, to date, it has not been found elsewhere in north-central Texas. Interpretation of Paleozoic ichnofossils by analogy with modern traces is limited; behavioral characteristics may be the products of post-Paleozoic innovation. The internal morphology and path of *Olivellites* are unlike those of any modern gastropod trail, and the genus is removed from the Mollusca.

Paleozoic ichnofossil genera encompass a great diversity of forms found in a wide range of paleoenvironmental settings, yet we are aware of only three Paleozoic genera of ichnofossils that have been assigned to the Gastropoda. These are the Early Cambrian *Archaeonassa* (Fenton and Fenton, 1937a) and two Pennsylvanian taxa, *Olivellites* (Fenton and Fenton, 1937c) and *Aulichnites* (Fenton and Fenton, 1937b). We have had the opportunity to study *Olivellites plummeri* Fenton and Fenton, 1937, at its type-locality and at a previously unreported locality, and we strongly suspect that this trace fossil was not formed by a gastropod. Further, we suggest that, although many intriguing trails are formed by living gastropods, very few of them have any potential for preservation.

Acknowledgments.—We thank Dr. Christopher Durden of the Texas Memorial Museum for permitting us to examine and photograph the type-slab of *O. plummeri*. Dr. R. M. Linsley, Colgate University, Hamilton, N.Y., generously shared unpublished work with us. Fieldwork by Schindel in north-central Texas was supported by a grant from the Department of Geological Sciences, Harvard University, Cambridge, Mass.

¹ Museum of Comparative Zoology, Harvard University, Cambridge, MA 02138; present address, Room E-206, U.S. National Museum of Natural History, Washington, DC 20560.

PREVIOUS WORK

Olivellites was named in 1937 by Fenton and Fenton (1937c), and *O. plummeri* was designated as the type-species. The generic name has appeared in compendia, but we do not know of any subsequent descriptions of the species or of any addition of other species to this monotypic genus. The type-lot consists of several specimens on a single gray sandstone slab (fig. 1) collected by the late F. B. Plummer; no date of collection is reported. The slab was originally in the Texas Bureau of Economic Geology Collection, Austin, Tex., where its accession number was M19. It has since been transferred to the Texas Memorial Museum Collection at Balcones Research Center in Austin and bears the number 35681.

The original illustration that accompanied the description is a photograph of about one-third of this slab at one-half of the actual size. Subsequently, a new photograph of virtually the same part of this slab was published by Häntzschel (1962, p. W215, fig. 135, 3); it was slightly enlarged relative to the original photograph and is marked as 0.6 natural size. This same photograph was reproduced by Häntzschel in 1975 (p. W106, fig. 66, 3), but it was credited incorrectly to the 1937 publication (Fenton and Fenton, 1937c). The magnification of Häntzschel's 1975 photograph was reduced to two-thirds that of his 1962 photograph; the magnification is given as 0.48 natural size (Häntzschel, 1975, p. W106), although, as published, it is actually slightly less than 0.4 natural size. We do not know of any other illustrations of *O. plummeri*.

Segments of three separate specimens are shown in the original (Fenton and Fenton, 1937c, fig. 1) and subsequent (Häntzschel, 1962, fig. 135, 3; 1975, fig. 66, 3) photographs. To avoid any possible confusion, we here designate as the lectotype the longest of the specimens on the type-slab (see specimen indicated by arrows, fig. 1). This specimen begins in the upper right-hand corner of the photograph and meanders down the right one-half of the field of view to the bottom margin, at center. The trace then turns at a 90° angle and curves



FIGURE 1

FIGURE 1.—*Olivellites plummeri* Fenton and Fenton, original slab; Texas Memorial Museum (TMM) 35681, University of Texas Bureau of Economic Geology locality 67-T-1, Eastland County, Texas. (X 1). The lectotype is indicated by two arrows. Approximately 2 cm on the right side of the slab and 1 cm at the top of the slab are not shown.

toward the left margin of the photograph and then doubles back in a sharp turn, continuing back along its previous path.

Except for the references by Häntzschel (1962, 1975), we are unfamiliar with any additional works that describe or illustrate this genus. We know of no additional specific names used with *Olivellites*. *Aulichnites* Fenton and Fenton (1937b) was named from the Brazos River Conglomerate Member of the Garner Formation, near Millsap, Tex., and was also attributed to a gastropod. From elsewhere in north-central Texas, we have collected material similar to the type-species *A. parkerensis*. We judge that it is distinct from *Olivellites* but that, like *Olivellites*, it is not the result of gastropod activity. Powers (1922) described but did not name a presumed gastropod trail from the Pennsylvanian of West Texas. That trail does not appear to be similar to *Olivellites*, nor does it appear from his description and drawings to be the result of gastropod locomotion. Powers' material may be similar to *Aulichnites*, but we have not studied his material nor seen the outcrop area and cannot comment further.

Several trace fossils other than *Olivellites* have been loosely placed with *Scolicia* (Häntzschel, 1975, p. W106); all are assumed to be the result of gastropod activity. We suggest that these forms deserve further study.

OCCURRENCE

The holotype slab was collected by the late F. B. Plummer in Eastland County, Tex. Fenton and Fenton (1937c, p. 453) reported that the type-locality is "5 miles [8.05 km] west of Cisco and 5 miles [8.05 km] east of Eastland, Eastland County, Texas." A typographical error must have been made, as Eastland is east of Cisco. Their description of the type-locality should have read "5 miles [8.05 km] east of Cisco and 5 [8.05 km] miles west of Eastland***" (University of Texas Bureau of Economic Geology locality 67-T-1). At 8.05 km west of the Eastland County Courthouse, a low but prominent roadcut about 2 m high is present on the north side of U.S. Highway 80. This is the only obvious exposure along the road for about 1 km in either direction; we measured it to be 7.24 km east of the center of Cisco along the present highway route, which possibly has been changed since 1937. We are confident that this is the type-locality.

As indicated by Plummer on the field label, this outcrop is identified as the Wayland Shale Member of the Graham Formation, Cisco Group. Identification of this unit as Wayland is based on its stratigraphic position below the Avis Sandstone Member of the Graham Formation and above the Gunsight Limestone Member of the Graham Formation. The characteristic molluscan fauna found elsewhere in the lower part of the Wayland is lacking at this exposure. However, absence of body fossils from this roadcut is consistent with the coarse clastic nature of the upper part of the Wayland, where gray marine mudstones are replaced by more proximal deltaic sediments.

We found *Olivellites plummeri* in situ at three levels within 0.5 m in the lower half of this 2-m-high exposure (see fig. 2). This lower part is a fine- to medium-grained, gray-tan, thin-bedded, reworked marine sandstone that contains thin minor channel cut-and-fill structures, symmetrical oscillation ripple marks, and very abundant rib-and-furrow structures. These sandstones are interbedded with thin silt and shale layers which erode easily, showing the sandstone beds to be laterally persistent and slightly concave upward. This upward concavity has a period of about 2 m in the exposure and is strongly suggestive of a shallow shoreface. The sedimentary structures present at the type-locality indicate that *O. plummeri* occurred in a shallow subtidal setting where scour and fill of shifting sands were common. The only trace fossils found on the same bedding planes with *Olivellites* are simple vertical tubes, both straight and slightly curved, that have diameters of about 1 cm. Reworking of sediments in this shallow-water setting would preclude preservation of surface traces (hypichnia); thus, the animal that formed *O. plummeri* probably lived infaunally, as noted by Fenton and Fenton (1937c, p. 452).

Trace fossils are absent from the upper part of the outcrop, which consists of a 1-m-thick coarse-grained sandstone, containing high-angle crossbeds that have festoons as wide as 1.7 m; the erosional base of the sandstone has a channel outline. This channel deposit is more friable and ferruginous than the gray sandstone beds below. The specimens of *Olivellites* found in the lower part of the section appear more red stained than the type-slab and show internal features less clearly. That slab may have been collected from a part of the outcrop not as close to the hematite-rich channel, may have been excavated as an unweathered rock, or may simply differ in the character of its original cementation.

Poorly preserved specimens of *O. plummeri* were also found in the upper part of the Colony Creek Shale



FIGURE 2.—*Olivellites plummeri* at its type-locality. Individuals are visible in two sandstone beds, separated by several centimeters of shale. The length of the hammer is 28.5 cm.

Member of the Caddo Creek Formation, Canyon Group, 8 km northeast of Caddo, Stephens County, Tex. These specimens were observed on gray sandstone blocks exposed below the Home Creek Limestone Member of the Caddo Creek Formation in the bluffs above Caddo Creek on the Spitzer Ranch. The sandstone beds are exposed in a steep hillside east of a ranch road that drops sharply off the limestone dip slope, about 7.2 km (4.5 mi) by odometer from where the road turns east from Texas Park Road 33, approximately 6.4 km north of Caddo.

This rust-weathering tan sandstone is 1.0 to 1.7 m thick and erodes as blocks, unlike the Wayland Shale Member exposure described above, which erodes as slabs; the thickness and size of blocks precluded collection. Despite this difference in weathering habits, many of the sedimentary structures found in Plummer's locality are also found in this section. Thin low-angle tabular crossbeds, asymmetrical ripples, and

rip-up mud pebbles indicate that *O. plummeri* was formed in a shallow turbulent setting. Associated with *Olivellites* at this locality are abundant, simple, thin, vertical tubes about 0.5 cm in diameter and less common subhorizontal, gently curved burrows that are elliptical in cross section and about 4 cm in maximum diameter.

In this massive sandstone, *O. plummeri* undulates markedly in a vertical direction and has a relief of more than 1 cm; in contrast, the traces in thin sandstone slabs at the type-locality along U.S. Highway 80 meander only horizontally, except where an individual crosses over or through its previous path. It was not possible to determine whether these undulations in this massive rippled sandstone followed the existing contours of the original sediment surface, indicating movement at a constant depth within the substrate, or whether the organism changed its infaunal depth on these vertical excursions.

The only other reported occurrence of *Olivellites* is in the original description by Fenton and Fenton (1937c, p. 452), wherein they mentioned another slab collected by Plummer from "the Brazos River sandstones on U.S. Highway 80N west of Millsap, Texas." This slab was reported to be not as well preserved as the holotype, and no further mention was made. Possibly, this material was included by Fenton and Fenton (1937b) in their later description of *Aulichnites*. The slab was reported to be in the collections of Texas Christian University, and, at our request, Dr. Charles Rowett searched the collections but did not find it.

The units described above as being deposited in turbulent shallow subtidal environments are not uncommon in the long cyclic Pennsylvanian section of north-central Texas. However, we have found *Olivellites* at only these two localities, despite nearly 20 weeks of field observations made by Schindel in 1976 and by Yochelson and Schindel in 1977. Because many of the delta-front sheet sands and reworked marine sand bodies bear trace fossils of some kind, often in abundance, we must conclude either that *Olivellites* is rarely preserved or that the animal responsible for it was rare in this environment.

DESCRIPTION OF *Olivellites plummeri*

Observations of *O. plummeri* in north-central Texas confirm that it was formed by an animal crawling

beneath the sediment-water interface, rather than by one moving on the bottom. The organism formed its trace in fine to medium sand; the trace was commonly preserved on the upper surface of a sand layer overlain by silt or clay. The trace fossil meanders primarily in a single horizontal plane. The path of the animal tends to curve everywhere, and the longest uncurved segment observed was at the Colony Creek exposure and measured 15 cm. More characteristically, the trace winds sinuously, commonly executing hairpin turns and doubling back on itself. The sinuosity in the trace often causes it to cross its earlier path, commonly on the same horizontal plane. However, in some places, such as on the lectotype (fig. 1, at bottom center) and on a topotype (fig. 3), a trace crosses slightly above its earlier path, leaving that previous segment largely undisturbed and recognizable. We have seen no example of *O. plummeri* descending beneath its own trace.

Olivellites plummeri is distinguished by a thick medial cord and fine transverse ridges. Field observations confirm the original assertion by Fenton and Fenton (1937c) that the medial protuberance is on the upper surface of the trace. The width of the cord varies from 1.5 to 2.5 mm, and the entire raised part of the trace varies in width from 15 to 25 mm, though more commonly the width ranges from 20 to 23 mm. The cross section of the trace is a low flattened ellipse, and the

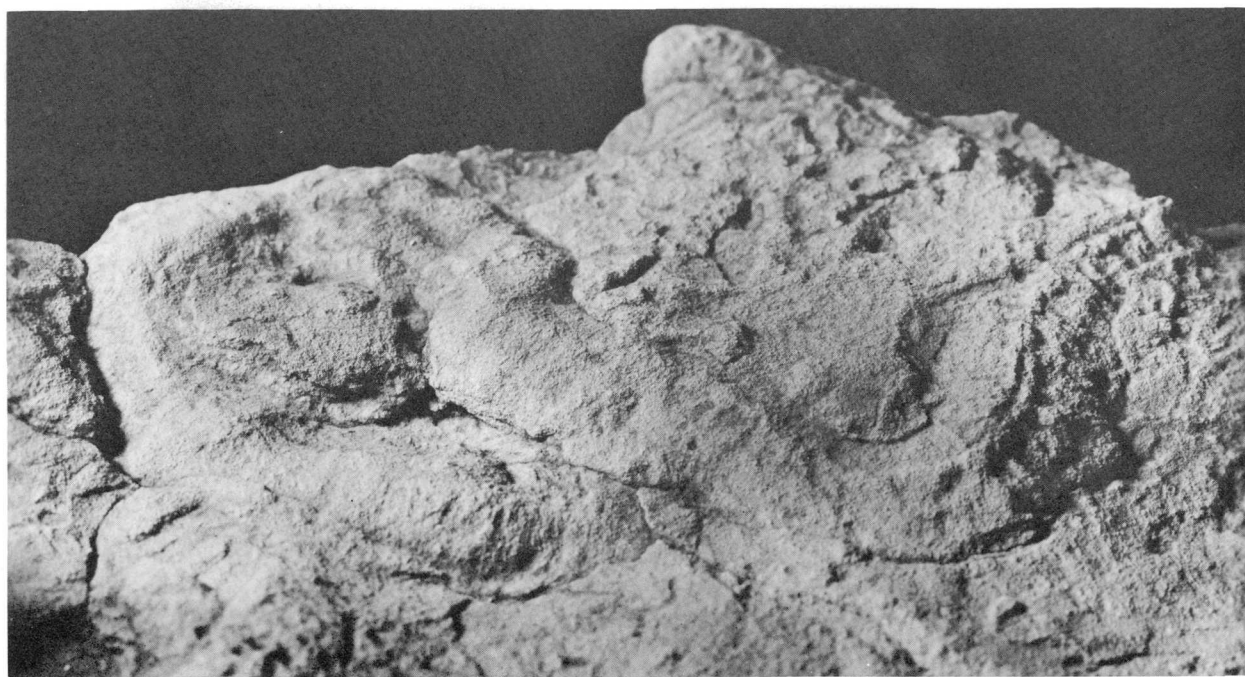


FIGURE 3.—*Olivellites plummeri* topotype in oblique view, U.S. National Museum No. 250 880 ($\times 2$). The specimen shows typical abrupt turns and a crossing. The upper surface of the slab is not flat, and the trace may be moving up the side of a ripple trough.

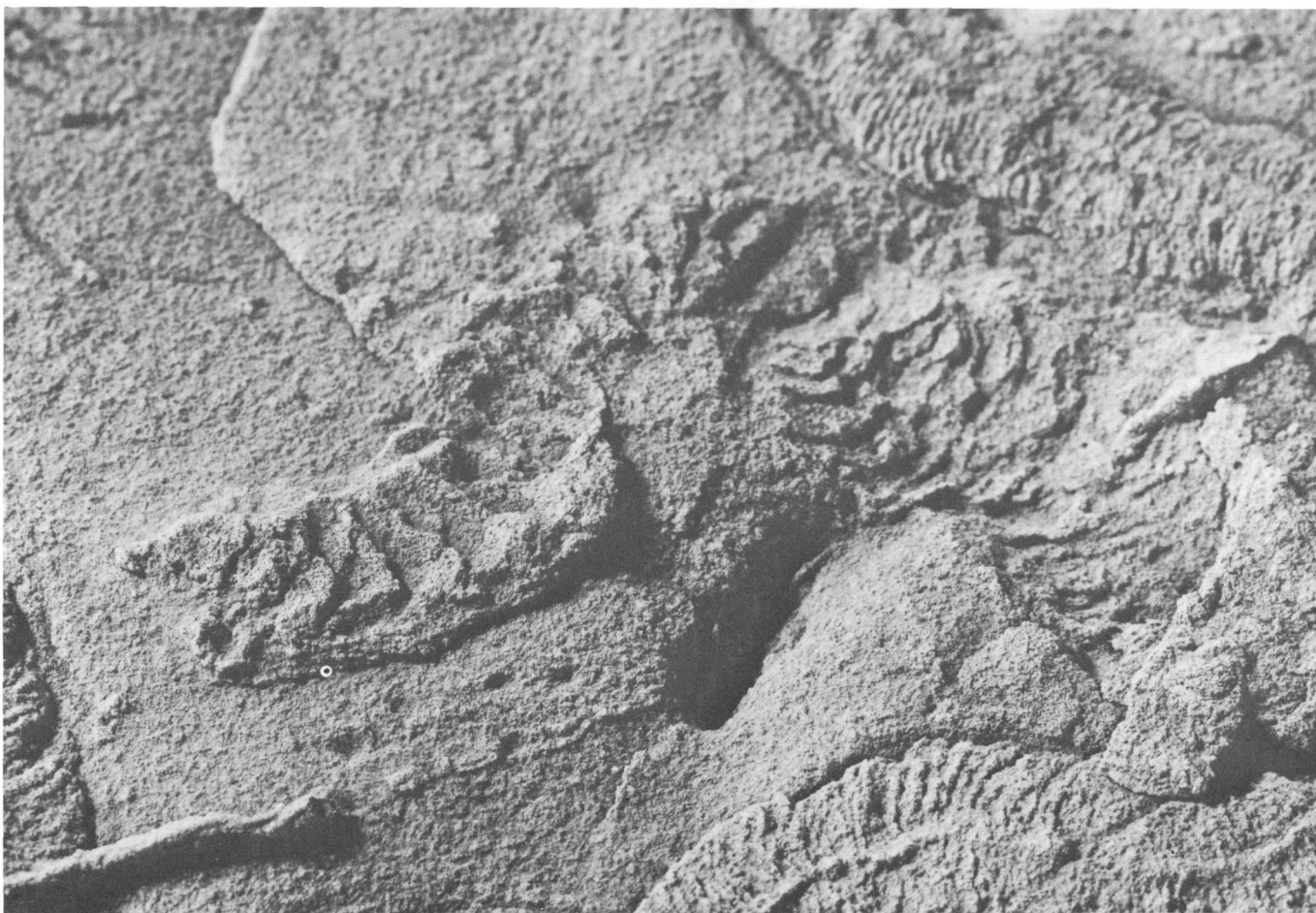


FIGURE 4.—*Olivellites plummeri*, a paralectotype, TMM 35681 ($\times 1.82$). This enlargement of a weathered specimen from the center of the original slab shows concave-up sand layers which produce transverse ridges on the upper surface of unweathered traces.

medial cord extends above the level of the highest part of the ellipse. Fine transverse ridges are the uppermost expressions of layers of sand that form the trace (see fig. 4). These sand layers are concave up, and, in contrast to their original description as "roughly vertical layers" (Fenton and Fenton, 1937c, p. 452), they approach being vertical only near the top of the trace; they are tangential to bedding near the basal surface of the specimen. The curvature of the sand layers is well shown in an oblique view of a weathered paralectotype (fig. 4). The basal surface appears featureless, bearing neither transverse ridges nor any medial depression or elevation. Thin sections of specimens collected from the type-locality show no differentiation by grain size or mineralogy between the trace and matrix.

DISCUSSION

Observations of the trace of movement formed by the living gastropod *Olivella biplicata* Sowerby sup-

plied Fenton and Fenton with a ready interpretation and, apparently, a generic name for *Olivellites*. Although this use of modern analogs in the interpretation of fossil organisms has a long tradition, we are skeptical of its application here. The trace of movement left by *Olivella* may be similar to *Olivellites*, yet this similarity does not prove, nor does it require, the existence of a Pennsylvanian snail similar to *Olivella* in form and behavior.

Fenton and Fenton (1937c, p. 452) noted that in the Elkhorn Slough area of Monterey Bay, *O. biplicata*, in feeding beneath the sand,

* * * left contorted, gently convex elevations with a sharp ridge down the center and indistinct transverse wrinkles. The convex elevation [emphasis added] was produced by the shell as a whole; the central ridge by the long siphon, which extended upward to the water. The transverse wrinkles, which were concave forward, appeared to result from side-to-side movement of the shell. The point could not be determined by digging, since water obscured all marks if the loose sand was disturbed, but it appeared that these wrinkles must be represented by a series

of irregular vertical layers in the sediment pushed behind the moving snail.

MacGinitie and MacGinitie (1949, p. 81) studied that area for years and clearly differentiated between the deeply infaunal gastropod *Polinices* and *Olivella*, which burrows “* * * just beneath the surface. As they [*Olivella*] proceed through the sand they leave a depression [emphasis added] behind them that makes a trail. When they congregate, e.g., during the breeding season, the sand or sandy mud may sometimes be a maze of tortuous lines or tracks, left by these animals.” Thus, the two reports of the trace left by *Olivella* are in conflict; Fenton and Fenton (1937c) described the trace as being an elevation that had indistinct transverse wrinkles, whereas MacGinitie and MacGinitie (1949) reported the trace as being a featureless depression.

The concave-up sand layers that form the transverse wrinkles on the surface of *O. plummeri* (fig. 4) are best interpreted as the work of an animal that piled sediment up behind it as it made forward progress through the substrate. In this interpretation, the layers are anteriorly concave, in agreement with the original description (Fenton and Fenton, 1937c, p. 452). As an epifaunal snail makes forward progress along the surface, its foot plows sediment in front of the foot and then displaces it to the sides, producing two lateral ridges separated by a groove whose width matches the width of the foot. *Olivella* moves just below the surface and seems to displace sediment around the shell; deeper infaunal gastropods such as *Polinices* move sediment over the shell as well as around it (MacGinitie and MacGinitie, 1949; R. M. Linsley, unpub. observations, 1977). None of these animals pass sand beneath the foot to produce the anteriorly concave-up sand layers present in *Olivellites*.

Two seasons of extensive field work in north-central Texas and examination of extensive collections of the U.S. Geological Survey and U.S. National Museum of Natural History have revealed no siphon-bearing Pennsylvanian gastropods compatible with an *Olivellites*-sized trace. Thus, the assertion by Fenton and Fenton (1937c) that the medial ridge of *Olivellites* was formed by a gastropod siphon extending up through the sand into the water is weak at best. This medial ridge would be more easily interpreted as a siphonal trace if it were of late Mesozoic age, when siphonate snails were common and diverse. Because it is Pennsylvanian, we are hard pressed to relate it to any particular gastropod. *Meekospira peracuta* (Meek and Worthen, 1860) has the smooth exterior surface of a potentially infaunal gastropod, yet it bears no an-

terior notch or reflexed apertural lip that would indicate the presence of a siphon, nor could its long spire make a turn as tight as that of the lectotype of *O. plummeri* (see fig. 1, lower left). A specimen of *Meekospira peracuta* that was 25 mm wide would be at least 75 mm long, yet the turn radius of the lectotype of *O. plummeri* is approximately 25 mm. We have never observed *Meekospira* 75 mm long; the largest specimens known reach only two-thirds this length.

The depressions left by the activities of gastropods in the shallow subtidal zones are rarely preserved. A rapidly drying surface of fine clay, or a scummy algal mat, quickly covered by a layer of mud, would make a suitable mold and cast pair, but far more commonly these surface traces are destroyed by waves and tides. Our observations of trails formed by living snails have convinced us that fossil representatives must be exceedingly rare. In general, most living gastropods are not found in the turbulent sand habitat indicated by the sedimentary features associated with *Olivellites*, and we have no reason to assume that Paleozoic forms lived in such an environment.

Present-day gastropod trails are rare in shallow subtidal settings, and exceptional circumstances are needed to preserve them. The path of *Olivellites* is quite unlike the trails of living gastropods. It is characterized by abrupt sharp turns and doubling back. Even the sinuous meandering of *Olivellites* would be unlike that of many gastropods (R. M. Linsley and E. L. Yochelson, unpub. observations, 1977). In contrast, gastropods on the surface commonly go from one place to another in a fairly straight line, and the turns they do make have gradual curvatures. Large siphonate forms such as *Busycon* move the shell from side to side as they test the inhalant water reaching the siphon, but the foot, upon which the shell rests, moves forward in essentially a straight path.

We suspect that the anteriorly concave-up sand layers of *Olivellites* indicate the action of an animal having ventral appendages, possibly jointed and modified for digging and packing sediment behind itself as it moves forward through the substrate. The movement of living isopods within the sand on an open beach may produce traces similar to *Olivellites*. The medial ridge might then be interpreted as the trace within the sediment of a raised dorsal ridge on a carapace rather than the trace of a soft flexible siphon.

The occurrence of *Olivellites* on the upper surfaces of sandstone layers that are overlain by shale or mudstone (see fig. 2) suggests an alternate reconstruction for the creator of the trace. If an animal traveled at a sedimentary interface and had sand below and mud

above it, its passage might be preserved only in the underlying layer. In this interpretation, such an infaunal animal could feed on the organic matter within the mud, yet still make forward progress through the more workable sand. The medial ridge of *Olivellites* would not reflect a dorsal projection as suggested by Fenton and Fenton (1937b). Rather, it would mark the ventral space between paired, paddlelike jointed appendages. As these digging appendages moved sand beneath and behind the animal, they would create anteriorly concave-up layers, separated by a ridge of sediment marking the gap between the ventrally paired appendages.

The traces of deposit feeders often turn sharply, as does the path of *O. plummeri*. Upon encountering a segment of its previous path at the sand-mud interface, an infaunal feeder might pass slightly above or below it or even through its own "wake." Our observations indicate that the creator of *O. plummeri* was capable of exercising only two of these options. The preservation of detail at these crossings is often poor, but we have seen at least two intersections in which the animal cuts through its own trace and several which indicate passage over its path (fig. 3). We have seen no examples of passage beneath the trace, suggesting that, if the above interpretation is correct, *Olivellites* avoided departure from the sand-mud interface.

According to this interpretation, *Olivellites* would have been formed by an animal about 2 cm in width and of moderate length. An elongate wormlike animal would not be expected to execute abrupt hairpin turns nor would it pass sediment backward beneath the entire length of its body.

Our aim is to remove *Olivellites* from the Gastropoda, not to reassign it. Even though we have no particular Pennsylvanian arthropod to suggest as the creator of this trace, we feel that removal of *Olivellites* from the mollusks will open the door to new investigations, possibly leading to a better understanding of the Pennsylvanian biota.

REFERENCES CITED

- Fenton, C. L., and Fenton, M. A., 1937a, Archaeonassa; Cambrian snail trails and burrows: Am. Midland Naturalist, v. 18, no. 3, p. 454-456, 1 fig., 1 pl.
- , 1937b, Burrows and trails from Pennsylvanian rocks of Texas: Am. Midland Naturalist, v. 18, no. 6, p. 1079-1084, 3 pls.
- , 1937c, Olivellites, a Pennsylvanian snail burrow: Am. Midland Naturalist, v. 18, no. 3, p. 452-453, 1 fig.
- Häntzschel, Walter, 1962, Trace fossils and problematica, in Moore, R. C., ed., Treatise on invertebrate paleontology, pt. W, Miscellanea; Conodonts, conoidal shells of uncertain affinities, worms, trace fossils and problematica: New York and Lawrence, Kans., Geol. Soc. America and Univ. Kansas Press, p. W177-W245, figs. 109-149.
- , 1975, Part W, Miscellanea, Supplement 1, Trace fossils and problematica, of Teichert, Curt., ed., Treatise on invertebrate paleontology (2d ed.): Boulder, Colo., and Lawrence, Kans., Geol. Soc. America and Univ. Kansas Press, 269 p.
- MacGinitie, G. E., and MacGinitie, Nettie, 1949, Natural history of marine animals: New York, McGraw-Hill Book Co., 473 p.
- Powers, Sidney, 1922, Gastropod trails in Pennsylvanian sandstones in Texas: Am. Jour. Sci., ser. 5, v. 3, no. 14, p. 101-107.

IOWAPHYLLUM (RUGOSE CORAL) FROM THE UPPER DEVONIAN OF ARIZONA

By WILLIAM A. OLIVER, Jr., Washington, D.C.

Abstract.—The rugose coral genus *Iowaphyllum* is uncommon but widely distributed in rocks of Devonian age. It is here reported for the first time from western North America (Late Devonian). *Iowaphyllum* is also known from the late Middle and Late Devonian of Eastern North America, but the lack of Early and early Middle Devonian species anywhere in North America leaves open the question of derivation of these forms and their relationship to Early Devonian species in Europe and Australia.

Iowaphyllum has been reported from the Lower Devonian of Czechoslovakia (Pragian and Zlichovian), Normandy (upper Siegenian), New South Wales (lower Emsian), Salair (upper Emsian or lower Eifelian); from the Middle Devonian of Kentucky and Michigan (both Givetian); and from the Upper Devonian (Frasnian) of Iowa, Belgium, Germany, and, now, Arizona. This apparently erratic occurrence has both geographic and stratigraphic interest and poses several questions: (1) Are the various species congeneric or only superficially similar? (2) If congeneric, is the apparently erratic occurrence due to an incomplete record or is it complete enough to be interpreted? and (3) If the record is reasonably complete, what accounts for the pattern? The discovery of new, well-preserved *Iowaphyllum* from Arizona serves as the vehicle for discussion of the taxonomic, stratigraphic, and biogeographic placement of the genus.

Acknowledgments.—The *Iowaphyllum* and other Arizona Martin Limestone corals described and mentioned in this paper were collected by Mrs. Gladys Nisbet, Cave Creek, Ariz. I am indebted to her for sending me the specimens, for answering innumerable questions about the source, and for permission to describe them. J. E. Sorauf, SUNY-Binghamton, later visited the J K Canyon locality and provided supplementary information. He also provided locality and stratigraphic data and specimens from Iowa. Sorauf and J. T. Dutro, Jr., critically reviewed the manuscript and made numerous helpful suggestions that have been incorporated in the published version.

IOWAPHYLLUM RELATIONSHIPS

Iowaphyllum (Stumm, 1949) has generally been placed in the Chonophyllidae (Stumm, 1949; Hill, 1956; Zheltonogova, 1960; Soshkina and others, 1962; Strusz, 1967; Oliver and Galle, 1971a, b; Coen-Aubert, 1974) although this family has been variously interpreted (compare Oliver and Galle, 1971b, p. 67, with Hill, 1956, p. F299, and either or both with Stumm, 1949, p. 47). Most of these authors have agreed on the defining characters of *Iowaphyllum* (see table 1 and following diagnosis), although Hill (written commun.) and Jell and Hill (1970, p. 7) have questioned the assignment of some species listed by Oliver and Galle (1971b, p. 81) to the genus, noting their similarity to the genus *Endophyllum* Milne-Edwards and Haime, 1851.

Endophyllum, as generally understood by authors, is different from typical *Iowaphyllum* in several size and proportion characters and in the possession of an epithelial wall in many species. These differences are summarized in table 1 and together seem to provide for usable morphologic separation, although some aphrodisoid and thamnasterioid *Endophyllum* with chonophylloid microstructure may be difficult to differentiate from *Iowaphyllum*.

Oliver and Galle (1971b, p. 81) listed described species of *Iowaphyllum*. This list is revised and updated in table 2. I now agree with Jell and Hill (1970, p. 70) that *Iowaphyllum prantli* Zheltonogova is more likely an *Endophyllum* because of its large tabularia and flattened tabulae; this form should be reinvestigated, but it is omitted from the new list. In addition, several newly recognized occurrences of *Iowaphyllum* are noted.

I conclude that *Iowaphyllum* is a recognizable chonophyllid genus (see Oliver and Galle, 1971b, p. 67-69 and 81-82, for fuller discussion of the family) and, especially, that it is distinguishable from *Endophyllum*. With the possible exception of *I. prantli* Zheltonogova, the forms assigned to *Iowaphyllum* are congeneric.

TABLE 1.—Comparison of morphology of species belonging to the genera *Iowaphyllum* and *Endophyllum*

	<i>Iowaphyllum</i>	<i>Endophyllum</i>
Form of colony	Aphroid or thamnasteroid	Phaceloid, cerioid, aphroid, or thamnasteroid.
Corallite diameter	Small; commonly < 20 mm	Large; commonly 25–45 mm.
Tabularium diameter	Small; commonly < 6 mm	Large; commonly 10+ mm.
Spacing of tabularia in colony (d^t/d)	Commonly 1 to 1½ corallite diameters (0.3–0.5).	Commonly less than corallite diameter (>0.5).
Septa	Completely dilated in dissepimentarium; vertically discontinuous in most spp.	Commonly less dilated; discontinuous.
Tabulae	Strongly arched with axial flattening or depression; upturned at margin.	Same, but broadly flattened at axis.
Microstructure	Septa composed of coarse, simple monothecanthus, one to several forming the thickness of septum.	Possibly the same, that is, chonophylloid.

TABLE 2.—List of *Iowaphyllum* species in stratigraphic order

- I. bohemicum* of Fontaine, 1977; Siegenian, Normandy.
I. cunctum (Pocta), Pragian (late Siegenian-early Emsian), Bohemia; Oliver and Galle, 1971b.
I. cabonnense Strusz, 1967; early Emsian, New South Wales.
I. bohemicum (Prantl), Zlichovian (Emsian), Bohemia; Oliver and Galle 1971a.
I. sp., Oliver, unpub. data, late Emsian (Calcaire d'Erbray), western France.
I. knotti (Davis), Givetian, Kentucky; see Stumm, 1953, 1965; needs restudy; may = *I. alpenensis* (Rominger).
I. alpenensis (Rominger), Givetian, Michigan; Stumm, 1953, and Oliver, unpub. data.
I. johanni (Hall and Whitefield), Frasnian, Iowa (Oliver and Galle, 1971a); Arizona? (see below); New Mexico (Sly Gap Formation, J. E. Sorauf, written commun., 1977).
I. multiradiata (Hall and Whitefield); Frasnian, Iowa; see discussion.
I. marginatum (Fenton and Fenton), Frasnian, Iowa; see discussion.
I. nisbeti n. sp., Frasnian, Arizona; see description below.
I. rhenanum (Schluter), Frasnian, Aachen Basin, West Germany, and Belgium; Coen-Aubert, 1974.
I. sp., Coen-Aubert, 1974, Frasnian, Belgium.

DISTRIBUTION IN TIME AND SPACE

If the various *Iowaphyllum* species listed in table 2 are phylogenetically related, as I mean to imply by stating that they are congeneric, then the most obvious gap is the complete lack of known Eifelian forms. The Siegenian-Emsian record in Europe is very good and is comparable to that of other coral genera. *Iowaphyllum cabonnense* in the Emsian of Australia is anomalous both geographically and morphologically. Congeners may have migrated between Europe and Australia parallel to the Devonian equator (Oliver, 1977, figs. 4, 13) and may yet be found in Lower Devonian rocks of intervening areas. Morphologically, the Australian species is closest to *I. alpenensis* (Givetian, Michigan), but similar morphologies are known in the Frasnian of Iowa also (see below) and complete infilling of dissepimentaria by septa may have developed several times.

Oliver (1977) discussed the history of coral faunas in the Eastern Americas Realm and showed that Give-

tian assemblages of the area were (1) endemic (originated within the area in Eifelian or earlier time), (2) cosmopolitan, or (3) invaders from western North America. Earliest known *Iowaphyllum* in the Eastern Americas Realm (Givetian) are associated with western invaders, and this is the probable origin of the eastern forms, even though no Early or Middle Devonian *Iowaphyllum* are yet known from western North America. The alternate possibilities, that *Iowaphyllum* entered eastern North America from the east or existed there in Early and early Middle Devonian time, seem less likely because of the lack of other eastern genera with such a known history. The implied gap in the record may be filled by new discoveries. Geographic distribution of Middle Devonian *Iowaphyllum* may have been restricted or individuals may have been rare. The genus did spread and become more common in the Late Devonian (Frasnian) when it is known to have occurred in western Europe and both eastern and western North America.

Iowaphyllum FROM IOWA

Stumm (1949) named *Iowaphyllum*, basing it on *Smithia johanni* Hall and Whitfield (1872) from the Upper Devonian Lime Creek Shale ("Hackberry Stage" or "Group" of authors), Hackberry Grove, Iowa. Hall and Whitfield (1872) had also described *Smithia multiradiata* from the same beds. Fenton and Fenton (1924), in a revision of the Lime Creek ("Hackberry Stage") corals, redescribed both taxa, assigning them to the genus *Strombodes*, but making the second a subspecies of *S. johanni*. They also described a third, new taxon, *Strombodes marginatus*. All three were from the upper part of the so-called "Cerro Gordo Member" ("Spirifer Zone") (stratigraphic terminology and data from J. E. Sorauf, oral commun., 1977). Stumm (1949, 1953) assigned all three taxa to his *Iowaphyllum*.

The holotype of *I. johanni* was first sectioned and illustrated by Oliver and Galle (1971a; pl. 4, figs. 1-4). The original specimens of *I. multiradiata* and *I. marginatum* are being studied (J. E. Sorauf, oral commun., 1977), but only preliminary information is available; thus, definition and separation of the Iowa taxa is not yet practical.

Study of 15 specimens of *Iowaphyllum* from the Iowa localities and stratigraphic units of the three described taxa indicates much variation within the genus. Three morphologic forms can be recognized, but two of these intergrade. This suggests that two species may be present, but much more work is needed before any decision can be made. Two of the 15 specimens have dissementaria that are almost completely filled with septal tissue containing only occasional open dissemental spaces. Thirteen specimens have more or less open dissementaria and are tentatively referred to *I. johanni* by comparison with the holotype of that species. These 13 specimens may or may not show evidence of ridges, preserved in the dissementaria and defining corallite boundaries. Because Fenton and Fenton (1924) defined *I. marginatum* as having well-defined marginal ridges and *I. johanni* as having reduced ones, it is tempting to separate my sample of 13 into these two species. They seem to intergrade, however, and the limited evidence available to me supports the assignment of all 13 to *I. johanni*. In table 3, the Iowa sample of 13 is this lot; it is termed *I. "johanni"* to avoid prejudging more definitive studies of the Iowa species now under way (J. E. Sorauf, oral commun., 1976-77).

Iowaphyllum FROM ARIZONA

Three specimens of *Iowaphyllum* are known from the Upper Devonian (Frasnian) Martin Limestone in Arizona. All were sent to me by Mrs. Gladys Nisbet; two were from J K Canyon, and one was from Haunted Canyon a few miles away (see locality data below). The two J K Canyon specimens are grossly similar to *I. "johanni"* as here discussed but have larger and more distantly spaced corallites (table 3), and the ridges preserved at the corallite margins from

locally continuous walls that define many corallites in both longitudinal and transverse sections. These specimens are so distinctive that I here assign them to a new species, *I. nisbeti*, although they may later be shown to be a geographic subspecies of *I. johanni*. The third Arizona specimen is unlike the first two and is tentatively assigned to *I. johanni*. The Arizona specimens are described in the systematic descriptions section that follows and are illustrated in figures 1-4.

SYSTEMATIC DESCRIPTIONS

Iowaphyllum Stumm

- 1949 *Iowaphyllum* Stumm, p. 50,
 1956 *Iowaphyllum* Stumm, Hill, p. 302.
 1971a *Iowaphyllum* Stumm, Oliver and Galle, p. 212-213.
 1971b *Iowaphyllum* Stumm, Oliver and Galle, p. 81-82.

Type species.—*Smithia johanni* Hall and Whitfield, 1872, p. 234, pl. 9, fig. 10; Upper Devonian (Frasnian), Lime Creek Shale, Iowa.

Diagnosis.—Massive, aphroid and thamnasteroid coralla; septa attenuate in tabularia, strongly dilated but vertically and radially discontinuous in dissementaria, often continuing across dissementaria as dilated septal ridges on top surfaces of coarse dissements. Minor septa terminate at margins of tabularia. Tabulae strongly arched axially, depressed and concave peripherally. Septa compound, composed of parallel trabeculae so that the thickness of a septum is made up of from one to several trabeculae.

Iowaphyllum nisbeti n. sp.

Figures 1a-b, 2a-e, 3a-f, 4c-e

Type specimens.—Holotype, USNM 250346; paratype, USNM 250347. Both specimens collected by Mrs. Nisbet from the Martin Limestone, J K Canyon, about 24 km west of Miami, in northeastern Pinal County, Ariz. Late Devonian, Frasnian Age.

Diagnosis.—*Iowaphyllum* in which the septal crests at corallite margins are strongly arched and vertically extended, even pointed, producing a ridge between corallites and a wall within the corallum that may be

TABLE 3.—*Tabularium diameter, axial spacing, and number of septa in Frasnian Iowaphyllum from Iowa and Arizona*

[*N₁*, sample size (colonies); *d^t*, tabularium diameter (see text explanation); *N₂*, number of tabularia measured; *OR*, observed range of colony averages; *̄*, mean of colony averages; *d^{ax}*, distance between axes of tabularia; *n*, number of major septa (measured in transverse thin sections); *N₃*, number of corallites in which counts were made. All measurements in millimeters]

	<i>N₁</i>	<i>d^t</i>			<i>d^{ax}</i>			<i>n</i>		
		<i>N₂</i>	<i>OR</i>	<i>̄</i>	<i>OR</i>	<i>̄</i>	<i>N₃</i>	<i>OR</i>	<i>̄</i>	
<i>I. "johanni"</i> , Iowa	13	1-5	3.5-5.2	4.2	8.7-14.3	11.5	4-10	13.5-23.8	17.7	
<i>I. cf. johanni</i> , Arizona	1	3	--	3.7	--	9.9	12	--	14.2	
<i>I. nisbeti</i> , Arizona	2	2, 4	5.5-5.9	5.7	14.1-14.5	14.3	6, 15	22.1-23.8	23.4	

either discontinuous or nearly continuous. This results in a pseudoceriod effect in some parts of both transverse and longitudinal sections.

Description.—The holotype colony was approximately 46 by 25 cm in diameter and 15 cm in height as measured in the field (Gladys Nisbet, written commun., 1977). Corallites on the surface of the colony, are broadly concave with raised, crested margins marking the corallite boundaries. Calices have a flat axial area (corresponding to tabularia); lower walls are distally convex but become concave near the calice margin (fig. 1). Calice depth varies from 2 to 8 mm in available specimens; shallower calices have reflexed periaxial platforms and low, gentle ridges separating corallites. Septa cross the calices as low rounded, radiating ridges.

In transverse sections (figs. 2a-e, 4d-e), the septa are radially arranged but discontinuous. Major septa number 18 to 28, averaging 22.1 and 23.8 in the two colonies (table 3). Major septa are thin and irregular in the tabularia, dilated and discontinuous in the dissepimentaria (fig. 2). Within the tabularia, they commonly meet and form an irregular structure similar to a columella. Minor septa barely enter the tabularia. Septal arrangement in tabularia tends to be bilateral (fig. 2c), but primary septa are not identifiable.

In longitudinal sections (figs. 3a-f, 4c), most space is occupied by alternating layers of dissepiments and septal crests. The septal crests arch upward and are vertically extended in positions corresponding to the surface ridges at the corallite margins. In sections, these form discontinuous or locally continuous walls between corallites. Tabularia are narrow but widely spaced (see illustrations and table 1). Tabulae are strongly arched axially but depressed peripherally so as to form a broad W-shape in section (figs. 3c, e).

Septal trabeculae are coarse, arranged subparallel to corallite axes except immediately adjacent to the tabularia where they lean toward the axes. In transverse sections, their arrangement may be uniserial (fig. 2d) or multiserial (fig. 2c, e). In longitudinal section, trabeculae are short because of the vertically discontinuous nature of the septa (fig. 3b-e).

Discussion.—*Iowaphyllum nisbeti* is characterized by its open structure and by the presence of an intercorallite ridge that forms a trabecular wall between corallites within the corallum. *I. johanni* is most similar but lacks the walls except in a very rudimentary way. In addition, *I. johanni* tabularia are smaller and more closely spaced, and there are fewer septa.

Material.—*I. nisbeti* is known only from the holotype and paratype specimens.

Iowaphyllum johanni (Hall and Whitfield)

- 1872 *Smithia johanni* Hall and Whitfield, p. 234, pl. 9, fig. 10.
 1924 *Strombodes johanni* (H. and W.), Fenton and Fenton, p. 43, pl. 15, figs. 6, 7.
 1949 *Iowaphyllum johanni* (H. and W.), Stumm, p. 50, pl. 25, figs. 1, 2 (?figs. 3, 4).
 1953 *I. johanni* (H. and W.), Stumm, cards 103-104, orig. fig. (?suppl. figs.).
 1971a *I. johanni* (H. and W.), Oliver and Galle, pl. 4, figs. 1-4.

Holotype.—New York State Museum 316. Lime Creek Shale ("Hackberry Stage"), Frasnian; Rockford, Iowa.

Diagnosis.—*Iowaphyllum* in which low ridges separate the corallites on the surfaces of colonies, but in which this feature is not, or only slightly, reflected in the internal structure.

Material studied.—Thirteen specimens, presumed to be this species, all from the area and stratigraphic position of the holotype (in addition to the holotype) were studied and compared with the Arizona specimens. Four specimens were collected by Mr. Calvin O. Levorson and deposited in the collections of the U.S. National Museum of Natural History; nine of the specimens were collected by J. E. Sorauf and are now in the collections of the Department of Geological Sciences, SUNY-Binghamton, Binghamton, N.Y.

Iowaphyllum sp. cf. *I. johanni* (Hall and Whitfield)

Figure 4a-b

Illustrated specimen.—USNM 250348; Martin Limestone, Haunted Canyon, west of Miami, Pinal County, Ariz.

Description.—A fragment of an *Iowaphyllum*, approximately 6 by 7 cm diameter, and 3 cm high, was given to Mrs. Nisbet, who in turn gave it to me for study. It lacks the distinct ridges and the internal "walls" of *I. nisbeti* and falls well within the range of morphologic variation of the studied sample of *I. "johanni"* from Iowa (table 3). Pending clarification of the taxonomy of the Iowa *Iowaphyllum*, tentative assignment to *I. johanni* seems appropriate.

LOCALITY DATA

All the described Arizona *Iowaphyllum* are from the Haunted Canyon quadrangle, located some 20 km west of Miami, Ariz. The quadrangle was geologically mapped by Peterson (1960).

USGS 9767-SD. Martin Limestone; south-southeast slope of hill 4804, NE $\frac{1}{4}$ sec. 19, T. 1 N., R. 13 E., Haunted Canyon quadrangle, Pinal County,

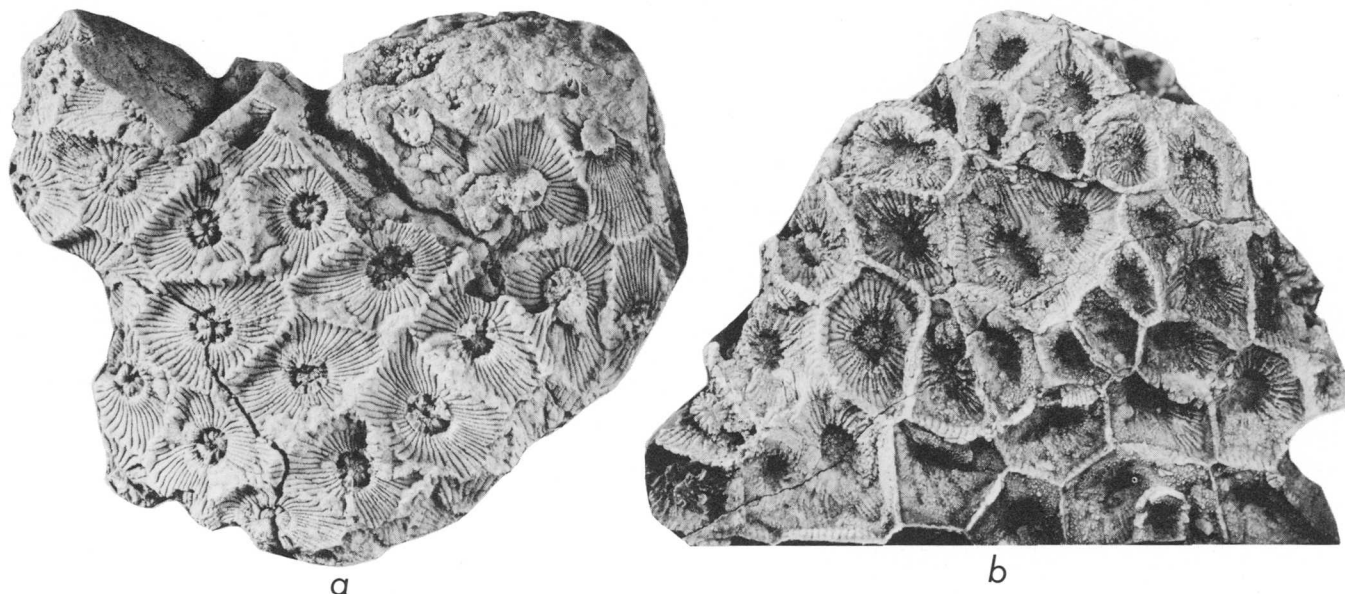


FIGURE 1.—*Iowaphyllum nisbeti* n. sp. Martin Limestone, Ariz. *a,b.* Holotype, USNM 250346. Calice views, $\times 1$.

Ariz. Hill 4804 is 2.2 km northeast of Government Hill and 3.2 km southwest of the southwest peak (4490) of J K Mountain. The canyon east of hill 4804, which continues eastward (with a road) past Mowing Machine Spring, is locally known as J K Canyon.

Iowaphyllum nisbeti was found some 100 m south-southeast and 15 to 20 m lower than the main outcrop of the coral bed at this locality, but the coral bed dips toward the *Iowaphyllum* site, and the *Iowaphyllum* is probably from a small outcrop of the same coral bed. (Gladys Nisbet, written. commun., 1977). Collected by Mrs. Nisbet.

A collection from the main outcrop of the coral bed in the Martin Limestone at this locality includes

the rugose corals *Hexagonaria* spp., *Pachyphyllum* spp., and *Tabulophyllum* spp. and the tabulates *Alveolites* sp., *Aulopora* spp., *Cladopora* sp., and *Thamnopora* sp. The collection was made by Mrs. Nisbet, and the corals were identified by Mrs. Nisbet and the author.

USGS 9768-SD. Martin Limestone: Haunted Canyon, in east central part of sec. 29, T. 1 N., R. 13 E., Haunted Canyon quadrangle, Pinal County, Ariz. *Iowaphyllum* sp. cf. *I. johanni* is from this locality, but no associated fossils are known. Presumably the specimen came from the area in Haunted Canyon mapped as Martin Limestone by Peterson, 1960. This locality is approximately 2.4 km southeast of USGS 9767-SD. The specimen was collected by Mr. Claude Bronaugh, Cave Creek, Ariz.

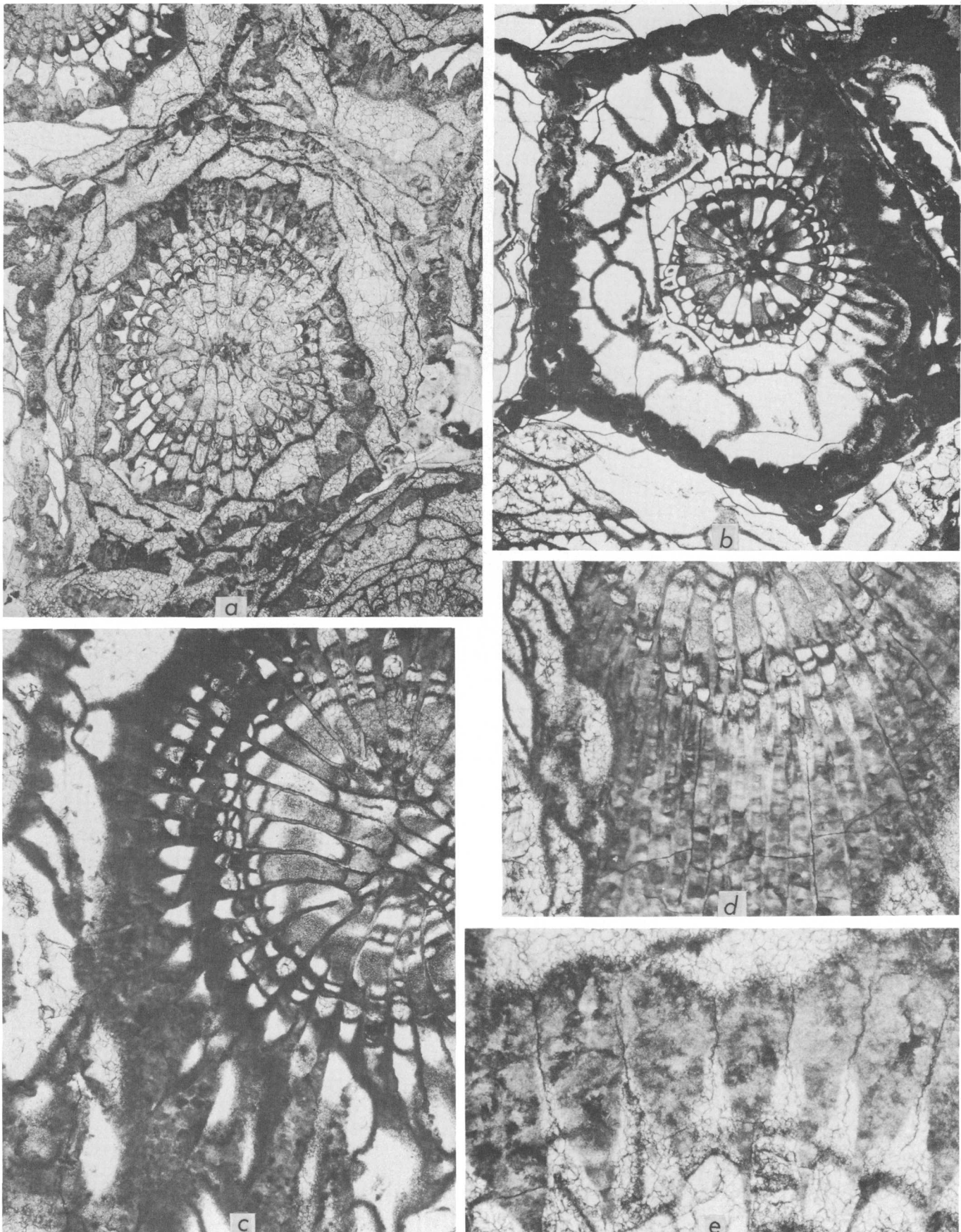


FIGURE 2.—*Iowaphyllum nisbeti* n. sp. Martin Limestone, Ariz. *a-e*. Holotype, USNM 250346. Transverse thin sections; *a* and *b*, $\times 5$; *c* and *d*, $\times 10$; *e*, $\times 25$.

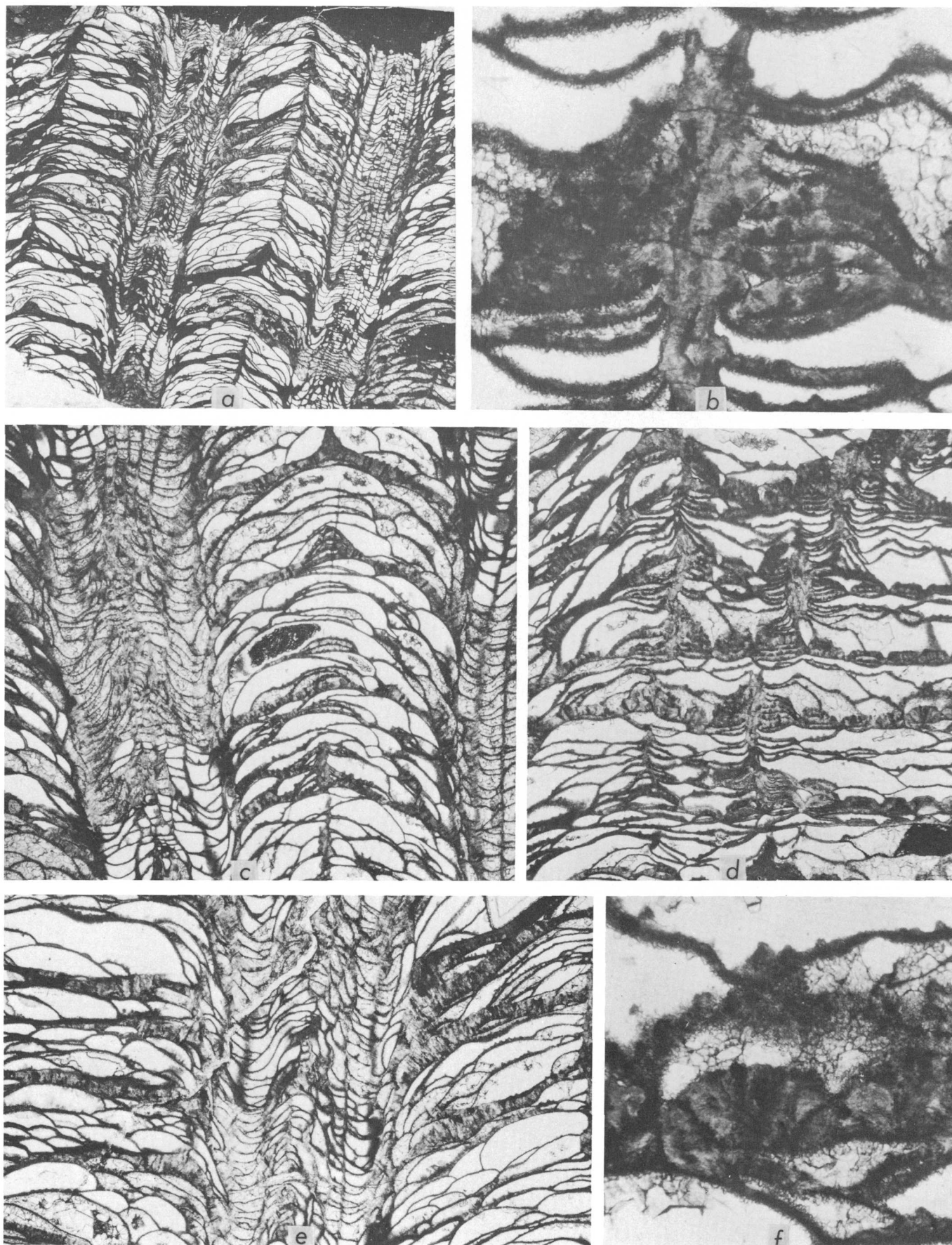


FIGURE 3.—*Iowaphyllum nisbeti* n. sp.; Martin Limestone, Ariz. a-f. Holotype, USNM 250346. Longitudinal thin sections; a, $\times 1\frac{1}{2}$; b and f, $\times 25$; c-e, $\times 5$.

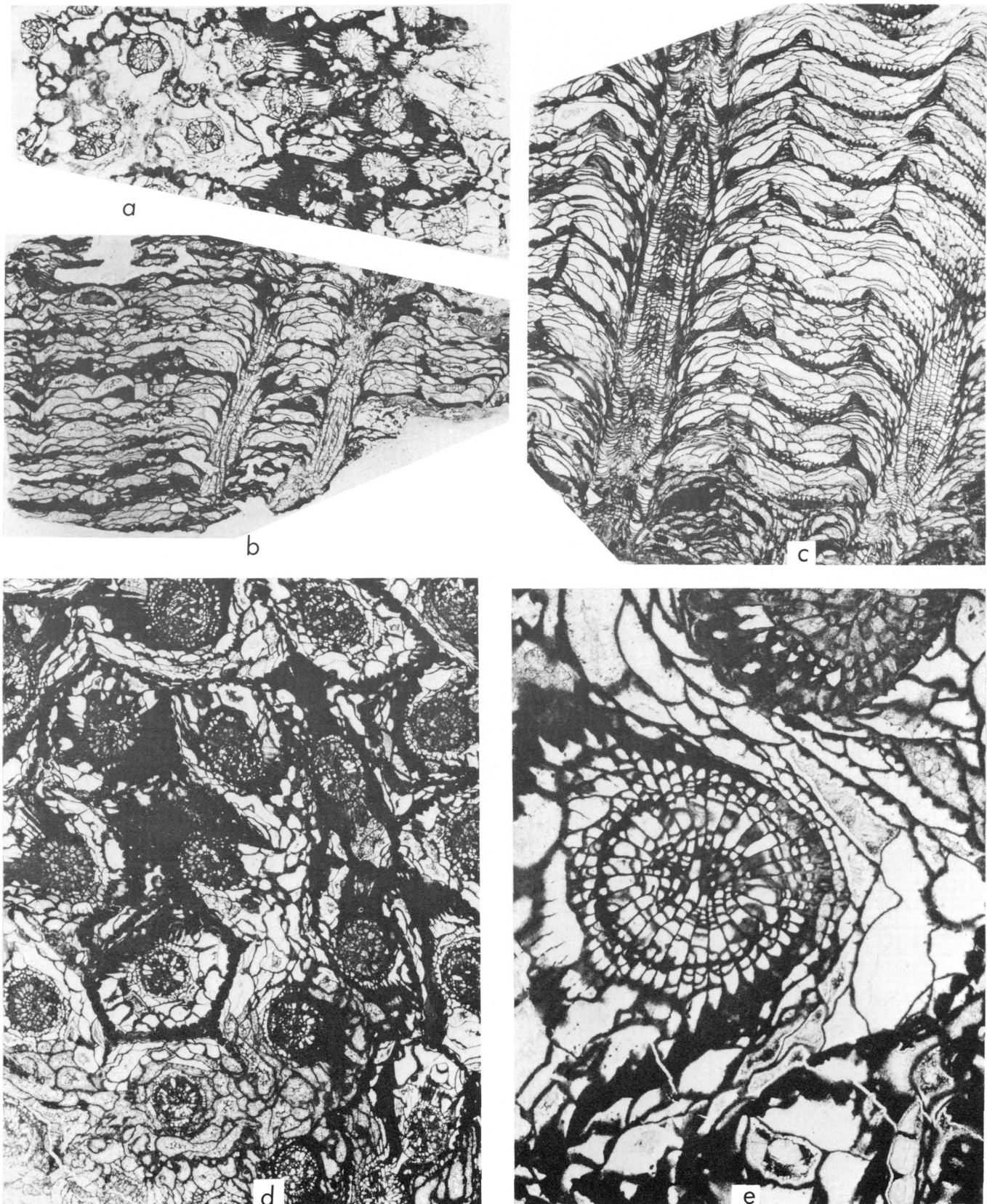


FIGURE 4.—*Iowaphyllum* spp. Martin Limestone, Arizona.
 a,b. *I.* sp. cf. *I. johanni* (Hall and Whitfield). USNM 250348.
 Transverse and longitudinal thin sections, $\times 1\frac{1}{2}$.
 c,e. *I. nisbeti* n. sp. Paratype, USNM 250347. Longitudinal

($\times 1\frac{1}{2}$) and transverse ($\times 5$) thin sections.
 d. *I. nisbeti* n. sp. Holotype, USNM 250346. Transverse thin
 section, $\times 1\frac{1}{2}$.

REFERENCES CITED

- Coen-Aubert, Marie, 1974, Representants des genres *Phillipsastraea* d'Orbigny, A., 1849, *Billingsastraea* Grabau, A. W., 1917 et *Iowaphyllum* Stumm, E. C., 1949 du Frasnien du Massif de la Vesdre et de la bordure orientale du Bassin de Dinant: Belgique Inst. Royal Sci. Nat. Bull., v. 49, 38 p.
- Fenton, C. L., and Fenton, M. A., 1924, The stratigraphy and fauna of the Hackberry Stage of the Upper Devonian: Michigan Univ. Mus. Geol. Contr. v. 1, 260 p.
- Fontaine, Henri, 1977, Decouverte du genre *Iowaphyllum* (Tetracoralliaire) dans un biostrome Eodevonien du Cotentin: Geobios, no. 10, pt. 3, p. 471-477.
- Hall, James, and Whitfield, R. P., 1872, Descriptions of new species of fossils from the Devonian rocks of Iowa: New York State Cabinet Nat. Hist., Ann. Rept. 23 [for 1873, adv. pub. 1872], p. 223-239.
- Hill, Dorothy, 1956, Rugosa, in Moore, R. C., ed., Treatise on invertebrate paleontology, pt. F, Coelenterata: Geol. Soc. America and Univ. Kansas Press, p. F233-F324.
- Jell, J. S., and Hill, Dorothy, 1970, The Devonian coral fauna of the Point Hibbs Limestone, Tasmania: Royal Soc. Tasmania, Papers and Proc. v. 104, p. 1-16.
- Oliver, W. A., Jr., 1977, Biogeography of Late Silurian and Devonian rugose corals: Palaeogeography, Palaeoclimatology, Palaeoecology, v. 22, p. 85-135.
- Oliver, W. A., Jr., and Galle, Arnost, 1971a, "Calceola" (=*Rhizophyllum*) and "Billingsastraea" (=*Iowaphyllum*) in Bohemia: [Czechoslovakia] Ústřední Ústav Geol., Věstník v. 46, p. 209-216.
- , 1971b, Rugose corals from the Upper Koněprusy Limestone (Lower Devonian) in Bohemia: Sborník Geol. Věd, Paleont. (Prague), v. 14, p. 35-106.
- Peterson, D. W., 1960 Geology of the Haunted Canyon Quadrangle, Arizona: U.S. Geol. Survey, Map GQ-128.
- Soshkina, E. D., and others 1962, Subclass Tetracoralla. Tetracorals (Rugosa), in Sokolov, B. S., ed., Osnovy paleontologii, spravochnik dlya paleontologov, i geologov SSSR; Gubki arkheotsiaty, kishechnopolostnye, chervi [in Russian]: Moscow, Akad. Nauk SSSR, v. 2, p. 286-356.
- Strusz, D. L., 1967, *Chlamydophyllum*, *Iowaphyllum*, and *Sinospongophyllum* (Rugosa) from Devonian of New South Wales: Palaeontology, v. 10, pt. 3, p. 426-435.
- Stumm, E. C., 1949, Revision of the families and genera of the Devonian tetracorals: Geol. Soc. America Mem. 40, 92 p.
- , 1953, Tetracoralla, Division 1, Unit 1F, pt. B, in Type invertebrate fossils of North America (Devonian): Wagner Free Inst. Sci., Philadelphia, cards 89-127.
- , 1965, Silurian and Devonian corals of the Falls of the Ohio: Geol. Soc. America Mem. 93, 184 p.
- Zheltonogova, V. A., 1960, in Zheltonogova, V. A., and Ivaniya, V. A., Subclass Tetracoralla (Rugosa), in Khalfina, L. L., ed., Biostratigraphy of the Paleozoic of the Sayano-Altai mountain area [in Russian]: Sibir. Nauchno-Issled. Inst. Geologii, Geofizikii, Mineral'nogo Syr'ya Trudy, v. 20, p. 360-408.



INVENTORY OF LAND USE AND LAND COVER OF THE PUGET SOUND REGION USING LANDSAT DIGITAL DATA

By LEONARD GAYDOS and WILLARD L. NEWLAND,
Moffett Field, Calif.

Abstract.—Landsat multispectral scanner digital data from four bands were analyzed using computers to produce land use and land cover information of the Puget Sound region, Wash., for use by agencies in that area. The data were first geographically registered to map coordinates. This registration enabled samples of known land cover types to be digitized from the maps. Samples of the same land cover were grouped together and then subdivided by cluster analysis into spectrally similar classes. Spectral categories were associated with specific land cover classes and used to determine spectral signatures for classification of the entire region. Reclustering and reclassification techniques were developed and then employed to minimize certain classification errors. The classified data were displayed in color using a film recorder. This color image was enlarged photographically to a 1:100 000 scale to match new base maps of the region. Although the result resembles a conventional polygonal land use and land cover map, certain image-like qualities remain and yield additional information about the landscape.

In early 1975, the National Aeronautics and Space Administration (NASA), the U.S. Geological Survey (USGS), and the Pacific Northwest Regional Commission began cooperative demonstration efforts to investigate the utility of Landsat digital data for meeting State and local land resources information needs. Four application areas (urban lands, forest lands, agricultural lands, and rangelands) were identified for study within the Pacific Northwest Land Resources Inventory Demonstration Project by the Federal, State, and local agencies. Within the urban application area, the Puget Sound region was selected as one of three test sites, along with Portland, Oreg., and Boise and surrounding Ada County, Idaho.

The primary goal of the Puget Sound project was to test the feasibility of providing a variety of regional users with land use and land cover information applicable to their local management and planning needs using Landsat multispectral scanner (MSS) digital data as the primary source material. This was to be accomplished using computer methods

for classifying the Landsat data and producing land use and land cover information in both map and statistical form. The users were also trained in selecting proper samples of land cover and in using these in land cover inventory and analysis. User groups included seven county planning agencies, the Puget Sound Council of Governments, the City of Tacoma, the Washington State Office of Community Development, and the University of Washington. Representatives of these groups met with USGS and NASA personnel early in 1975 to define objectives for the project and to formulate a technically sound work plan that would meet these objectives. One result of this cooperative effort was the 1974 inventory in map form of land use and land cover in the Puget Sound region (fig. 1, see color insert) described in this report. Land cover maps for individual counties were also produced. The land cover inventory has also been provided in statistical form for various counties, map quadrangles, and other areas specified by users.

Although the final map products depict classes commonly considered either land use or land cover (such as Residential or Forest Land, respectively), the classes distinguished from the Landsat digital data are really multispectral classes; that is, they are classes of similar multispectral reflectances. Because the data are acquired by measuring and recording light reflected from the land surface, these multispectral classes are very closely related to land cover classes. In fact, they are components of common land cover classes. By itself, a multispectral component may provide no further breakdown of a land cover category, but a number of components taken together describe a meaningful land cover class. By broadening the view of a land cover class to recognize these multispectral components, one can speak of mapping land cover using multispectral digital data. Land cover classes derived in this way can then be reinterpreted as land use classes by inferring information concerning man's ac-

tivities, just as in the interpretation of any other remotely sensed data.

Acknowledgments.—Many people have contributed to the work reported in this article. In particular, the assistance of Robert M. Ray III and his group at the Center for Advanced Computation (CAC), University of Illinois, at Urbana-Champaign, is acknowledged. Walter E. Donovan of that group completed most of the data preparation tasks and, along with Martin Ozga, maintained and extended the CAC-developed EDITOR software on which the project depended. Robert E. Slye and Donald Card of the NASA Ames Research Center provided programming support for computer processing at Ames, Calif. The planimetric accuracy of the digital data was tested by Robert E. Altenhofen of the USGS, Menlo Park. Michael McCormick of the Washington State Office of Community Development brought together and helped coordinate the activities of a large group of potential users.

RESEARCH BACKGROUND

Prior to the launch of Landsat 1 on July 23, 1972, the USGS had conducted experimental land use inventories using high-altitude aerial photographs (Wiedel and Kleckner, 1974). Soon afterwards, the USGS began investigating the prospects of using Landsat digital data for land use and land cover mapping (Ellefsen and others, 1973; Ellefsen and others, 1974). So, early in the Pacific Northwest Land Resources Inventory Demonstration Project, user agency personnel selected test sites within the Puget Sound region and USGS researchers classified Landsat digital data for those sites to produce preliminary land cover information (Hedrick and others, 1976).

The results were evaluated by user groups interested in the potential of Landsat data as a source of land resources information relevant to agricultural, range-land, and urban land management problems. These efforts created enough interest that NASA and the Project Task Force launched full-fledged demonstration projects with user participation. In addition to work on the Puget Sound project, USGS geographers provided further technical support in an inventory of irrigated lands in three test sites along the Snake River in Idaho and in an inventory of land cover in Boise and surrounding Ada County, Idaho. Other USGS researchers assisted in a land cover inventory of the Portland, Oreg., metropolitan area (Todd, 1979).

Techniques developed during this experience were applied in the Puget Sound project. Although a variety of methods and computer systems for digital processing of multispectral scanner data are now avail-

able, the USGS experience guided the methods chosen to achieve project objectives with the facilities at hand. Since 1974, the USGS has been responsible for the nationwide land use and land cover mapping and data compilation program; it is thus both a developer and a user of new techniques, such as those developed in the Puget Sound project and elsewhere, for land use and land cover mapping on a national scale (U.S. Geological Survey, 1978).

COMPUTER SYSTEMS

An image analysis system implemented on several computers was used in the Puget Sound work. The heart of the analysis system is the EDITOR (ERTS Data Interpreter and TENEX Operations Recorder) software system. The EDITOR system has been under development for the past several years by CAC, University of Illinois at Urbana-Champaign, with funding from NASA, the USGS, the U.S. Department of Agriculture, and the Advanced Research Projects Agency (ARPA), Department of Defense (Ray and others, 1975). EDITOR was developed to extend the image analysis capabilities introduced at the Laboratory for Applications of Remote Sensing (LARS), Purdue University, to more efficient processors accessible over the ARPA Network to a geographically dispersed user community (Ray, 1975).

Four computers on the ARPA Network were used in this work: A TENEX (modified DEC System PDP-10), an IBM 360/91, an IBM 360/67, and the ILLIAC IV. A CDC 7600 at NASA Ames Research Center, not on the ARPA Network, was also used. The TENEX is located at Bolt, Beranek, and Newman, Inc. (BBN) in Boston, Mass., and provides an interactive image analysis capability through EDITOR.

The IBM 360/91 at the Campus Computing Network, an ARPA Network facility at the University of California at Los Angeles, was used for geometric correction and reformatting. Because of its large core capacity, this machine was able to handle the high input-output rates needed to rotate image data efficiently for the geometric correction of an entire Landsat scene to map format. The IBM 360/67 computer at the NASA Ames Research Center was used to collect and display data processed elsewhere on the ARPA Network.

The ARPA Network's most unique and powerful component is the ILLIAC IV system located at the Ames Research Center. The ILLIAC IV is a parallel-processing computer consisting of 64 processing units; it is interfaced to the ARPA Network through an interactive TENEX system. ILLIAC IV was used for large cluster analyses and for data classification. This

computer is more than two orders of magnitude more cost-effective when using the identical algorithms first implemented on the IBM 360/67 at LARS (Ray, 1974).

The large-capacity CDC 7600 computer was used for classifying the data after statistics had been generated to form spectral signatures.

The general task of producing land cover information by classifying digital data from the Landsat four-channel MSS can be divided into four components: data preparation, data analysis, data classification, and display.

DATA PREPARATION

Image rectification

The Landsat scene (1690-18245) of June 13, 1974, was selected for the Puget Sound region study. At the time of selection, it was the most recent cloud-free scene available. A print from the scene of band 7 at a 1:500 000 scale and a USGS topographic map at a 1:250 000 scale were obtained for establishing parameters for rotating the digital data to remove skew caused by Earth rotation and for forming west-east rows and north-south columns of data cells. These tasks were accomplished by personnel at CAC.

Six well-distributed control points were identified on both the image and the map. Because the Puget Sound region has many water features, data from one of the MSS infrared bands (band 7) was used to pinpoint river bends, dams, and points of land that could also be found on the map. Coordinates for these ground control points were calculated using a data tablet digitizer and interactive EDITOR software. The map was first referenced to the digitizer coordinate system by digitizing its corners and identifying their latitude and longitude. The geographic coordinates of any other point on the map could then be determined by digitizing its position on the map and having EDITOR calculate its latitude and longitude. Geographic coordinates of row and column positions could be calculated for individual data cells, or pixels (picture elements corresponding to the instantaneous field of observation of the satellite scanner) in a similar manner.

The six control points were used to establish a least-squares linear transformation between latitude-longitude and pixel row-column coordinate systems. From this transformation, the parameters necessary for geometric rectification of the image were calculated. On the IBM 360/91, these parameters were applied to the original Landsat computer compatible tape acquired from the Earth Resources Observation Sys-

tems (EROS) Data Center. Successive rows and columns were shifted so that the pixels generated on the output tape were in a north-oriented coordinate system. No pixels were lost, replicated, or resampled.

The characteristics of the Landsat system are such that after this skew transformation, gray-scale displays of the pixels can be generated on a lineprinter at a scale of approximately 1:24 000. This provides a convenient way to relate the printout to features appearing on USGS topographic maps at that scale or to relate pixel rows and columns to geographic coordinates or UTM coordinates on some other base map (Donovan and others, 1975).

Geographic registration of images

To establish more rigorous map control, 24 control points (mostly hydrographic features) were identified on map and image within the area bounded by 47°N., 48°N., 122°W., and 123°15' W. The earlier transformation between latitude and longitude and pixel coordinates based on six control points was limited by scale. It was not possible to locate precisely a single pixel on a 1:500 000-scale print nor digitize exactly its location on a 1:250 000-scale map. The fit established was, therefore, only a first approximation, with a root mean square (RMS) error of about 240 m for rows and 230 m for columns. Even so, after image rectification, it was possible to locate pixel coordinates of a digitized latitude and longitude to within about four pixels of the correct position. For a second approximation, map locations of 24 control points within the area of greatest interest were digitized and their approximate pixel coordinates were computed. Gray-scale prints using band 7 data were then generated for blocks of 64 × 64 pixels surrounding each one of the control points.

Each gray-scale print was then matched to a 1:24 000-scale topographic map on a light table. The print was shifted into position until its features matched those of the map. The match with water bodies was especially obvious, but a match could also be made with features such as highways. Once maximum correlation was achieved, one pixel was selected as the checkpoint. The latitude and longitude of its center was digitized and matched with its row and column coordinates.

The 24 control points were then used to establish a second order least-squares polynomial fit between row and column coordinates of the pixels and latitude and longitude. The RMS in the location of these points was 50 m for pixel rows and 38 m for pixel columns. This relationship, determined by matching the loca-

tion of pixels to geographic coordinates on large-scale maps, established a second approximation of geographic control. Using EDITOR software and referring to this calibration, it was then possible in future stages of the work to determine map or data coordinates to within one pixel. The transformed tape was sent to BBN for the data analysis procedure described in the next section.

To match the final graphic product to a map projection, it was necessary to model a grid of pixels in a Universal Transverse Mercator (UTM) system and then use the least-squares linear fit to find the nearest pixel corresponding to each intersection point on the grid. This step was also done using the IBM 360/91. The step consists of resampling the data by deleting or replicating pixels to form a rectangular array fitting a UTM projection at a scale of 1:24 000 when displayed on a lineprinter or some other display device.

For one test of the geometric quality of these data, three of the four bands were displayed in false color using a Dicomod D47 image recorder. The spectral value of each pixel was displayed, one band at a time, by focusing a cathode-ray tube spot onto photographic film so that exposure and gray level varied with the spectral value. Color was achieved by exposing each band of the MSS data for the entire image successively through blue, green, and red filters. The 4- × 5-inch film transparency so exposed was evaluated for planimetric accuracy. Geographic coordinates in a Lambert conformal conic map projection were computed for 16 test pixels, while coordinates of the pixels on the film recorder product were measured in a comparator by USGS photogrammetrists. The RMS error of location differences, multiplied by 90 percent, was 201 m. This is within the 254-m National Map Accuracy Standard established for 1:500 000-scale mapping.

DATA ANALYSIS

Analysis of the data began after the skew transformation and the determination of precision geometric calibration parameters. During this phase, personnel from the user community participated in a training program conducted by USGS geographers at the NASA Ames Research Center.

Methods

The data analysis sequence followed well-known methods of multivariate statistical analysis theory (Swain, 1972). Given the reflectance values of the MSS channels, a statistical classification algorithm could be calibrated so as to classify all image pixels

according to statistical characteristics of a sample of image pixels whose identities were known. A maximum-likelihood classification algorithm was used.

Training field selection

To insure that the statistical characteristics used in the classification were valid in defining actual land covers, a large sample of training fields was established. These fields represented areas of known land cover. Ideally, training fields should be homogeneous (containing only one land cover category per field) and collectively should be representative of all land cover categories (including their spectral subtypes) in the area of study. In the Puget Sound project, members of the user community selected rectangular training fields and plotted their locations on USGS 1:24 000-scale topographic maps.

Once these training fields were identified, the process of digitizing the different cover types using the EDITOR software at the BBN TENEX began. Maps containing the training fields were registered by digitizing the four corners of each map and specifying their geographic coordinates. Then the northwest and southeast corners of each training field were digitized. By referencing the precision calibration file, pixel coordinates of each training field were calculated by EDITOR. Location of the pixels in each rectangular training field or "window" was accurate to within a distance of one pixel.

Guided cluster analysis

After all the training fields had been digitized and their corresponding pixels located, they were sorted into groups corresponding to such general land cover types as forest land, residential land, commercial or industrial land, and agricultural land. The first sort was made manually. Then the computer was employed to make a final sort based on spectral variations. Natural groupings of multispectral data from the four bands were made using a variation of the ISODATA multivariate cluster analysis algorithm (Ball and Hall, 1965). This algorithm, developed at LARS for analysis of remotely sensed data, was implemented within EDITOR by CAC.

The cluster analysis was guided by limiting the training fields to those general groupings of land cover defined by the analyst. This approach effectively targeted the clustering of the data to where it was needed most, in defining the multispectral subtypes of each land cover, rather than in scattering it over the entire range of multispectral values encountered when one tries to cluster all land covers at once.

The tape with the skew-transformed data was then read at BBN, and the data corresponding to each training field were copied onto a disk, with one disk file being used for each general land use or land cover type. Each file of multispectral data was then analyzed. The number of clusters for each general land cover group was specified by the analyst. The hope was that all spectral variations within a particular land cover type would be accounted for. In an urban area, differing materials used in construction or differing surroundings may cause very subtle diversities. In an agricultural area, the same crop may be at different stages of growth or influenced by different environmental factors. Regardless of the reason, it was important that clusters represent the spectral variations actually present in each land cover type.

Once all cluster analyses had been completed, all the pixels within each file were assigned to one cluster and both lineprinter maps and statistical information were generated. The lineprinter map for each rectangular training field window was related to known ground features. This was done by comparing the map with descriptions sent by the users and by finding each training field on available high-altitude color-infrared photographs acquired from aircraft on July 3, 1973.

Certain statistics were computed for each cluster. These were the spectral means, variances, and a measure of intercluster separability.¹ With these in hand, the analyst could determine cluster integrity. Clusters having few points or high variances were deleted. They are usually created by "contaminant" pixels, those not intended to be in the group being clustered (such as a stand of trees in a residential group), or by border pixels falling on boundaries between land cover types (such as the shoreline between land and water).

Once clustering is completed for all data files, all statistics are combined into a single file in order to inspect any conflicts between different land cover types that might have similar spectral characteristics. Such conflicts are found by comparing the separabilities between clusters. A low separability, indicating overlap between two clusters of differing land cover, is undesirable. Where such a conflict appears, it is often possible either to delete or to pool those clusters. If a cluster conflicted with two or more clusters of different land covers, it was usually deleted. If a cluster conflicted with only one cluster of a different land cover, it was usually pooled, or combined, with a cluster describing another spectral variation of the same land

cover. Both methods increased separabilities of clusters describing contrasting land covers.

DATA CLASSIFICATION

Clusters were analyzed in several iterations until a "best" set of statistics took shape. This statistics file, containing classes that had been modified by the processes of pooling and deleting, was transferred from BBN to the Ames IBM 360/67 computer over the ARPA Network. There the file was punched onto cards that could be read by the CDC 7600 computer, also at Ames. Those cards and a copy of the transformed data tape were run on the CDC 7600 to obtain a maximum-likelihood statistical classification of all pixels. Spectral reflectance values for each pixel were used as data to calculate a discriminant function for each class, and each pixel was assigned to that class for which the discriminant function was greatest.

Each land cover class was assigned a distinctive color for display on the Dicomod D47 image recorder. The Ames IBM 360/67 was used to create a three-file tape from the classification. These files control the exposure of each pixel successively through the blue, green, and red filters on the film recorder. From the resultant 4- × 5-in. film, color projection prints (8 × 10 in) are made to provide an overall look at the entire region classified.

Lineprinter maps of selected areas were also obtained for a more detailed look. Each pixel was represented by an alphanumeric symbol representing the spectral class to which it had been assigned. As was the case with the gray-scale displays, these lineprinter maps were at 1:24 000 scale and could be overlaid on USGS topographic maps at that scale.

All of the participants from the Puget Sound region evaluated the first classification attempt using the Dicomod print and lineprinter maps. Certain errors were detected. Agricultural and forest classes often appeared in urban class areas. Some urban classes appeared in agricultural class areas. Wetland classes were also confused with other classes, notably turbid water and wooded residential land.

The first step in improving upon the first classification was to identify and examine those spectral clusters that described dissimilar land cover categories. Previous versions of the clusters were inspected, and new combinations of clusters created by pooling and deleting were tried. Sometimes improvement was noticed after a small area was classified with the altered statistics; sometimes the problem only shifted because other classes were misclassified.

One successful technique used frequently was the reclustering of problem classes. In one case, for ex-

¹ Intercluster separability is described by the "Swain-Fu" distance. This is the ratio of the distance between two cluster centroids to the sum of the dispersions of the data of the two clusters. Dispersion of the data is measured in terms of ellipsoids of concentration in which the data are assumed to be normally distributed (Swain, 1972).

ample, a particular class from the first classification occurred both in wooded residential class areas and in some forested areas. Small windows containing only pixels assigned to this class were extracted from the data tape using EDITOR. Those windows containing wooded residential and forest samples were run through the clustering program separately to identify spectral signatures for each. These new clusters usually proved to be more separable spectrally than the originals and so were substituted for the latter in the revised statistics file.

After this process of redefining classes by new combinations of original clusters and reclustering, the area was classified again. Dicomod prints and line-printer maps were produced as before and evaluated by all participants. Although many problems had been solved, other misclassifications had taken on added importance as more obvious misclassifications were minimized.

At this point it was believed that as much information as possible had been extracted from the training fields by reclustering and that if further progress was to be made there would need to be a reevaluation of all information used to produce the first two classifications.

The first step in this reevaluation was to check all the training fields that had been selected by the user group. By using a Bausch and Lomb Zoom Transfer Scope, high-altitude color-infrared aerial photographs were superimposed over the training fields on the 1:24 000-scale maps. The photographs showed the true nature of the training fields, in a manner unclouded by generalization or assumption.² When the chosen training fields were examined it was found that in many cases they did not consist of the homogeneous land cover types required for determination of "clean" spectral signatures. Instead, many were too small or contained a mix of land covers. All heterogeneous training fields were improved by performing new cluster analyses of the training data. The resulting statistics file was edited once again with the addition of these new clusters from the more homogeneous training fields. The entire evaluation, reclustering, and retraining process tended to fine-tune the class signatures. In an area as extensive as the Puget Sound region, the occurrence of subtle spectral variations within the same land cover, unsampled in the training phase, was expected to occur. It was important to recognize such variation through the reclustering and retraining methodology so that the final classification

would successfully portray land cover for the entire region.

The final classification was run on the off-net NASA Ames CDC 7600 computer using the Landsat MSS digital data reformatted to the UTM projection. This classification was composed of 37 spectral clusters tentatively identified by the participants as belonging to the 13 land use or land cover classes distinguishable in the Puget Sound region by Landsat. These are shown in table 1 as they correspond to Level I and Level II classes of the USGS classification system (Anderson and others, 1976).

Though the Puget Sound classification is more detailed than Level II with respect to Agricultural Land and Forest Land categories, it falls short of the detail called for by Level II in Urban or Built-up Land categories. Differentiation of Residential from a combined Commercial-Industrial class seems feasible, however. Though some land uses can be inferred because they are associated with a distinctive land cover, others cannot. Thus, the land use class golf course or park cannot be distinguished from the land cover class pasture/grass.

The class labels in table 1 generally describe the land uses and land covers mapped using Landsat data in the Puget Sound region, though the participants realize that they have yet to describe completely the named categories. For example, no specific point of transition between "oldest growth" and "medium growth" evergreen has been proposed. A general evaluation has been made using the film recorder and lineprinter products. The consensus among the participants is that the classification does map spectrally distinctive land uses and land covers over the entire region.

TABLE 1.—*Tentative Puget Sound land use and land cover classes derived from Landsat multispectral data*

Level I	Level II	Detail
Urban or Built-up Land	Residential	/
	Commercial-Industrial	/
Agricultural Land	Cropland and Pasture	Cropland
	do	Pasture/Grass
Forest Land	Deciduous	/
	Evergreen	Oldest Growth
	do	Medium Growth
	do	Youngest Growth
Water		
Wetland	Nonforested	
Barren Land	Mixed	
(Snow)	Quarries-Transitional	

²Although in this case high-altitude imagery was available, the same task could have been accomplished, though with more difficulty, with lower altitude imagery or other ground truth.

FINAL CLASSIFICATION DISPLAY AND EVALUATION

To help the participants in their evaluation, a color print of the classification was produced at a 1:100 000 scale to match new USGS topographic maps for the Seattle and Tacoma quadrangles. The classification was displayed on an Optronics film recorder at the Jet Propulsion Laboratory in Pasadena, Calif. This system produced an image more distortion-free than that made earlier with the Dicomex film recorder.

Three black-and-white negatives, one each from film exposures through blue, green, and red filters, were composited. The composite color internegative (8×10 in) was enlarged to match as precisely as possible the water features on the 1:100 000-scale maps. Photographic paper was exposed to create prints of the classified data at a 1:100 000 scale. These prints serve as a base for dimensionally stable topographic map overlays.

Comparison of the classification display with the map overlays demonstrates a high correlation of water bodies, patterns of transportation, and residential classes. At this scale, individual pixels, though visible, also coalesce to form polygons similar to those of land use and land cover maps. The most striking aspect of this classification display is its image-like characteristic. Though the original image was generalized to the number of classes finally chosen, individual pixels were not generalized by forming polygons of any minimum mapping unit size. The pixels were mapped one by one, and, although they coalesce to form polygons, in certain areas nominal land use categories remain as heterogeneous mixtures of specific land covers.

These image-like qualities yield useful additional information about the landscape. Pixels of an area southeast of Tacoma describe residential land along roads through a patchwork of agricultural fields. This is a much truer picture of the landscape than a generalized interpretation of the area as either residential or agricultural land use.

These mixtures exist in areas of landscape complexity, such as the one noted, where several landscape elements—houses, agricultural fields, forest—all coexist. The display of the classified data as an image calls attention to these complex areas and identifies them for further investigation (Schwarz and Gaydos, 1975).

Another noticeable image-like quality is the existence of linear features not fully accounted for by the areal classification. For example, a linear transportation route (a mixture of spectral properties of pavement, bare ground, and vegetation) might be classified as a string of pixels representing a residential

area because of its spectral similarity to a combination of houses, roads, and backyards. Although "misclassified," the transportation route may be recognized immediately as a well-known freeway and hence may be useful as a landmark for aligning the classification display with a planimetric map.

Although the image is presented as a land use and land cover map, it is well to remember that the spectral values which make up the image still remain. We could have described a class, normally given a land use or land cover label, in terms of spectral values instead. In this case, the classification would be 100 percent accurate in terms of the definitions given. By interpreting spectral data as land use or land cover categories, error is introduced due to our perception and categorization of the landscape. However, once multispectral clusters have been molded to correspond as closely as possible to the proper land cover classes, misclassified pixels may correctly be regarded as spectral aberrations; that is, they are anomalous because they do not happen to possess the same spectral properties as the norm. If a pixel incorrectly classified into the evergreen class rather than the residential class had looked spectrally like the other pixels in the residential class, then it would not have been misclassified. It is only because it was somewhat different that it was classified as "evergreen," and that difference in itself may provide valuable information. Misclassified pixels may highlight areas worthy of further investigation simply because they are spectrally abnormal. This type of error, characteristic of computer classification of MSS data, is quite different from the type of errors that occur within traditional photointerpretation procedures.

ADDITIONAL TASKS

To complete the Puget Sound project, participants extended the land cover classification to include the entire Landsat scene. Where misclassifications were found within the enlarged region, the problem areas were delineated and their boundaries digitized. Near the snow line in the mountains, for example, barren rock and seasonal melting of snow altered the spectral characteristics of pixels in the forest land class so that they resembled some pixels in the urban or agricultural land classes in the lowlands. Using EDITOR, mask files stratified the data and transformed the polygon vertices to pixel coordinates. Then pixels in the problem area erroneously assigned to one class were reassigned to another using the IBM 360/67.

Polygons representing counties were also digitized. Land use and land cover information was tabulated for each county from the classification tape.

Although the project was oriented primarily to the needs of users in the Puget Sound region, an effort was also made to demonstrate the utility of its findings to other USGS land use and land cover mapping activities. To this end, an experiment in "signature extension" was undertaken. Landsat scenes acquired on the same orbit north and south of the Puget Sound scene were classified using the same 37 multispectral classes developed for classification of land use and land cover in the Puget Sound region (Gaydos, 1978).

Meanwhile, a new classification has been made using Landsat MSS data of July 1975. Although this new work is directed primarily toward further training in Landsat digital data analysis for Puget Sound participants, it also provides a data set for investigating the potential for detecting land cover change using Landsat. Copies of the classification tapes for both the 1974 and 1975 land cover classifications can be ordered through the National Cartographic Information Center. Copies of original Landsat imagery and computer compatible tapes can be ordered from the EROS Data Center.

REFERENCES CITED

- Anderson, J. R., Hardy, E. E., Roach, J. T., and Witmer, R. E., 1976, A land use and land cover classification system for use with remote sensor data: U.S. Geological Survey Professional Paper 964, 28 p.
- Ball, G. H., and Hall, D. J., 1965, ISODATA—A novel technique for data analysis and pattern classification: Menlo Park, Calif., Stanford Research Institute Technical Report, 70 p.
- Donovan, W. E., Ozga, M., and Ray, R. M., 1975, Compilation and geographic registration of ERTS multitemporal imagery: Urbana Ill., Center for Advanced Computation, University of Illinois, Document No. 52, 18 p.
- Ellefsen, Richard, Swain, Philip H., and Wray, James R., 1973, Urban land use mapping by machine processing of ERTS-1 multispectral data—A San Francisco Bay area example: West Lafayette, Ind., Purdue University Laboratory for Applications of Remote Sensing Information Note 101573, 22 p.
- Ellefsen, Richard, Gaydos, Leonard, Swain, Philip, and Wray, James R., 1974, New techniques in mapping urban land use and monitoring change for selected U.S. metropolitan areas—An experiment employing computer-assisted analysis of ERTS-1 MSS data: International Society for Photogrammetry Commission VII, Banff, Canada, Proceedings of the Symposium on Remote Sensing and Photo Interpretation, p. 51-64.
- Gaydos, Leonard, 1978, Low-cost computer classification of land cover in the Portland area, Oregon by signature extension techniques: U.S. Geological Survey Open-File Report 78-186.
- Hedrick, W. E., Cunningham, Paul, Lake, Brent, McCormick, Mike, and Shay, Ralph, 1976, Landsat—Pacific Northwest area using satellite data for planning resource management: American Institute of Planners, Practicing Planner, v. 6, no. 5, p. 18-26.
- Ray, R. M., 1974, Implementation of ILLIAC IV algorithms for multispectral image interpretation: Urbana, Center for Advanced Computation, University of Illinois, Document no. 112, p. 8.
- , 1975, Summary of ILLIAC IV-ARPA Network multispectral image processing research activities: Urbana, Center for Advanced Computation, University of Illinois, Document no. 168, 20 p.
- Ray, R. M., Ozga, Martin, Donovan, W. E., Thomas, J. D., and Graham, M. L., 1975, EDITOR—An interactive interface to ILLIAC IV-ARPA Network multispectral image processing systems: Urbana, Center for Advanced Computation, University of Illinois, Document no. 114, 15 p.
- Schwarz, D. E., and Gaydos, Leonard, 1975, Regional interpretability variations of land use using satellite data in digital and visual form: Tullahoma, University of Tennessee, Remote Sensing of Earth Resources, v. 8, p. 243-253.
- Swain, P. H., 1972, Pattern recognition—A basis for remote sensing data analysis: West Lafayette, Ind., Purdue University, Laboratory for Applications of Remote Sensing Information Note 111572, 40 p.
- Todd, William, J., 1979, Metropolitan land cover inventory using multi-seasonal Landsat data: U.S. Geological Survey Journal of Research (in press).
- U.S. Geological Survey, 1978, Yearbook 1977: p. 162-164.
- Wiedel, Joseph W., and Kleckner, Richard, 1974, Using remote sensor data for land use mapping and inventory—A user guide: U.S. Department of the Interior, Geological Survey, Interagency Report USGS-253, 60 p.; U.S. Dept. Commerce, Natl. Tech. Inf. Service, PB-242 813/4WU.

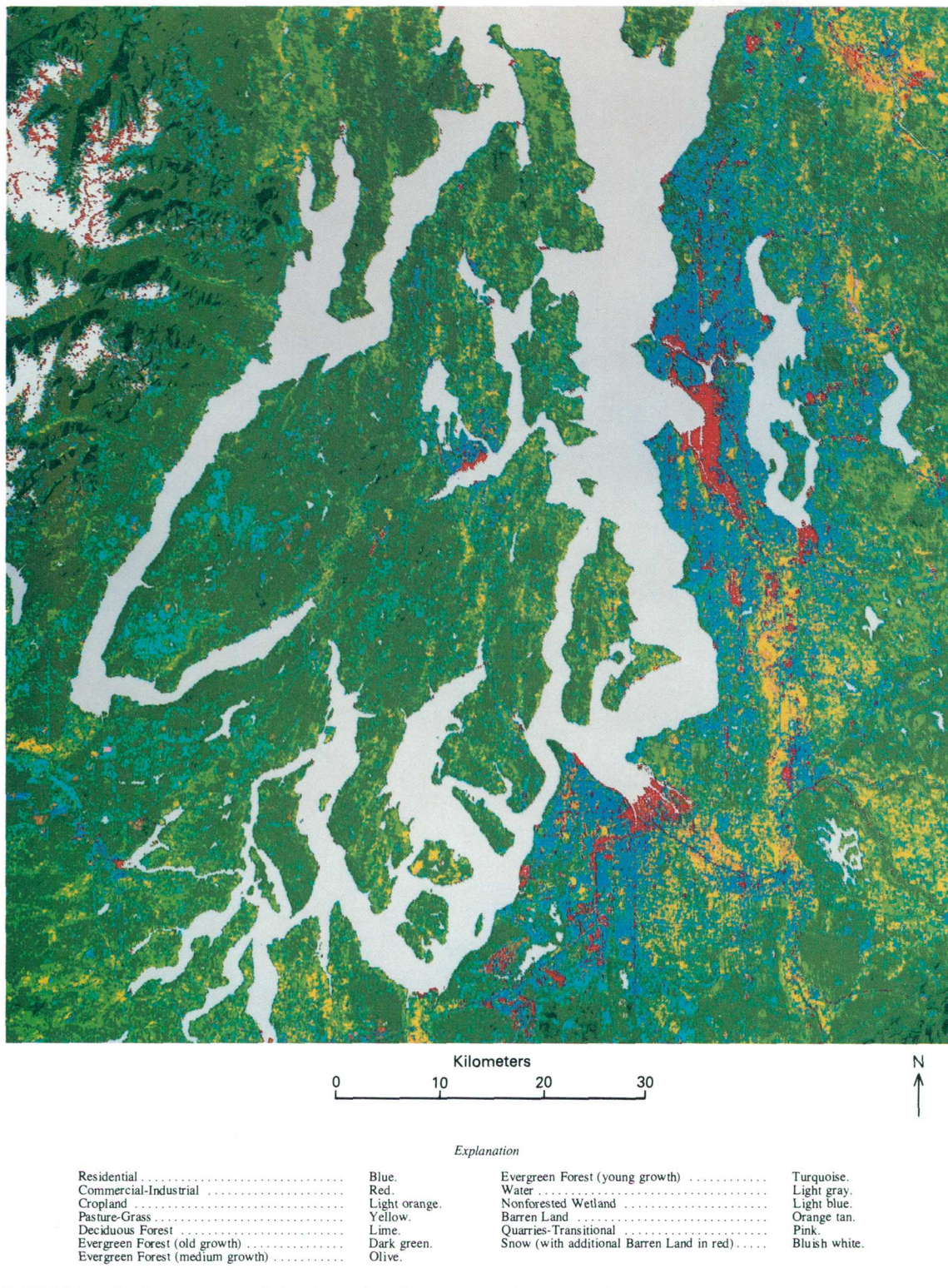


FIGURE 1.—Land cover map of the Puget Sound region, Washington, 1974. Classification was prepared by machine processing of Landsat digital data. The categories shown are statistically significant combinations of spectral classes. Some categories are difficult to recognize on the image because of the great detail at the pixel-level and the small scale and halftone reproduction of this regional-scale map. However, the exact row-and-column location of each pixel, its map coordinates, and

its spectral class and land cover class can all be retrieved from the tape. Many other maps showing other class combinations, at other scales, and with corresponding class area aggregations can also be made from the tape. Such maps have already been produced at scales of 1:100 000 and 1:250 000 for use with U.S. Geological Survey topographic maps at those scales. Class area measurements have been prepared by county and by 7.5-minute quadrangle.

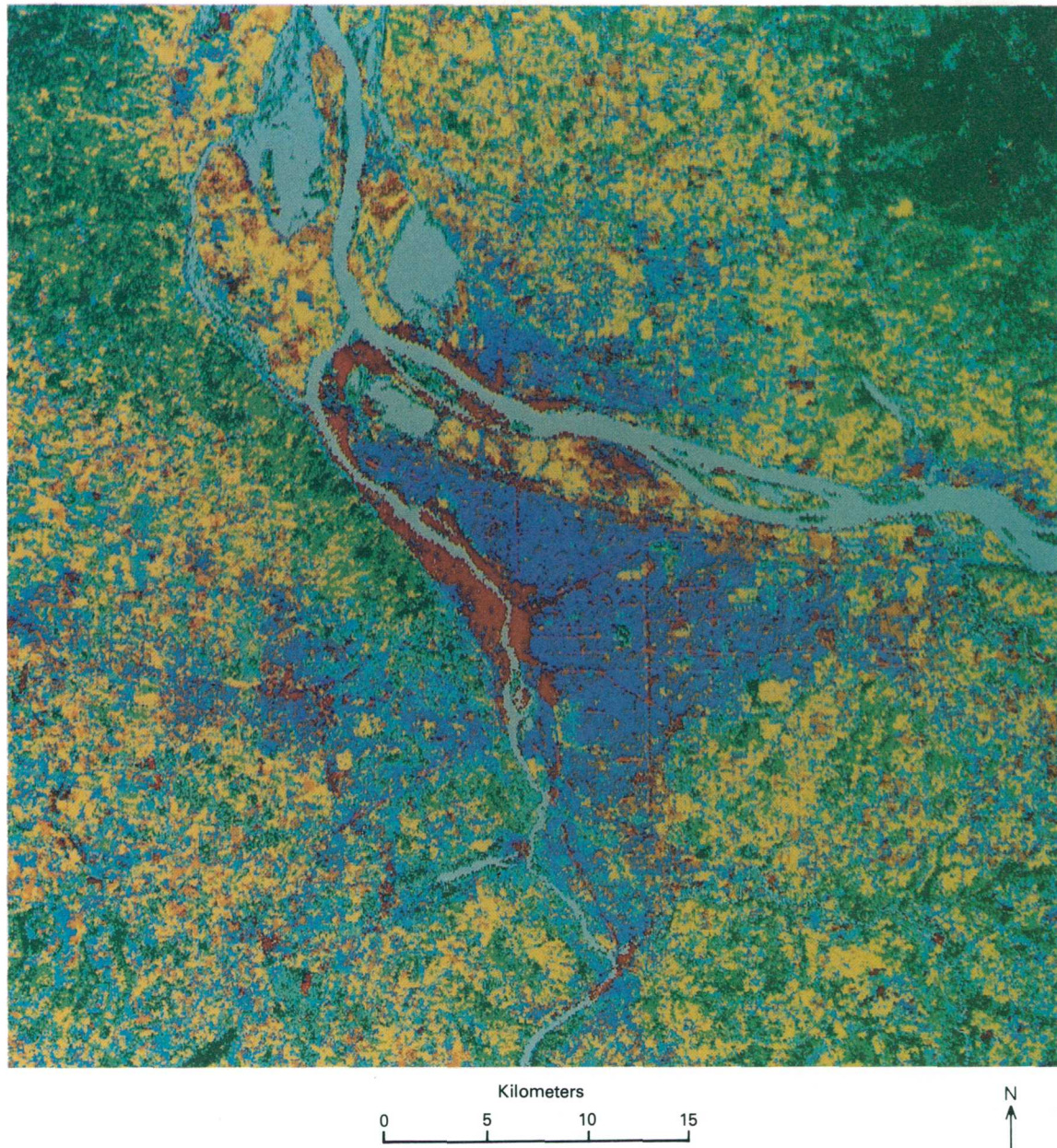


FIGURE 2.—Land cover map of the Portland area, Oregon, 1974. Classification was prepared by machine processing of Landsat digital data and by extending signatures for land cover classes from the Puget Sound region, 250 km north. The land cover classes on the Portland area map are the same as those on the

Puget Sound region map. The maps differ in appearance because the color symbol for the Quarries-Transitional category is different on the two maps, the colors for the maps were produced on different film recorders, and the maps were produced at different times.

<i>Explanation</i>			
Residential	Blue.	Evergreen Forest (medium growth)	Olive.
Commercial-Industrial	Red.	Evergreen Forest (young growth)	Turquoise.
Cropland	Light orange.	Water	Light gray.
Pasture-Grass	Yellow.	Nonforested Wetland	Light blue.
Deciduous Forest	Lime.	Barren Land	Orange tan.
Evergreen Forest (old growth)	Dark green.	Quarries-Transitional	Brown.

LOW-COST COMPUTER CLASSIFICATION OF LAND COVER IN THE PORTLAND AREA, OREGON, BY SIGNATURE EXTENSION TECHNIQUES

By LEONARD GAYDOS, Moffett Field, Calif.

Abstract.—Computer-aided techniques for interpreting multispectral data acquired by Landsat offer economies in the mapping of land cover. Even so, the actual establishment of the statistical classes, or "signatures," is one of the relatively more costly operations involved. Analysts have, therefore, been seeking cost-saving signature extension techniques that would accept training data acquired at one time or place and apply them to another. Signatures may be extended in preprocessing steps or in the classification steps that follow. In the present example, land cover classes were derived by the simplest and most direct form of signature extension: Classes statistically derived from a Landsat scene of the Puget Sound area, Wash., were applied to the adjacent Landsat scene of the Portland area, Oreg., acquired during the next 25 seconds down orbit. Many features can be recognized on the reduced-scale version of the Portland land cover map shown in this report although no statistical assessment of its accuracy is available.

The cost of classifying 5607 km² (2165 mi²) in the Portland area was less than \$0.08 per square kilometer (\$0.0788, or \$0.2041 per square mile). This and other signature extension techniques may be used not only to save money but also to complete land use and land cover mapping in other large areas where multispectral and multitemporal Landsat data are available in digital form, but other source materials are lacking.

One advantage of using sensor data from Landsat for surveys of land cover is that a large area is covered by a single scene (34 000 km²). Another advantage is that the data are in digital format. These advantages, combined with improved analytical techniques and declining processing costs (Ray, 1975), make Landsat digital data more and more attractive as a primary source for timely surveys of land cover over a large area. When the need for such a survey extends beyond a single Landsat scene, even greater analysis efficiency can be obtained through signature extension. A "signature" is a statistical characterization of the multispectral data at a given time and in a place that represents land cover categories in the area being surveyed. The hypothesis tested in the experiment reported here is that spectral signatures de-

veloped for classification of land use and land cover from one Landsat scene can be successfully applied, unaltered, to data for an adjacent scene less than 25 seconds down orbit and having a similar land cover and geographic environment.

As described in the preceding paper, land use and land cover in the Puget Sound region were mapped with the cooperation and assistance of State, regional, county, and city planning agencies by using multispectral scanner digital data acquired from Landsat-1 scene 1690-18245 on June 13, 1974 (Gaydos and Newland, 1978). U.S. Geological Survey (USGS) personnel determined the multivariate spectral signatures through interactive training, clustering, and statistics editing. They used the EDITOR analysis software developed by the Center for Advanced Computation at the University of Illinois for use on the nationwide Advanced Research Projects Agency (ARPA) network of computers (Ray and others, 1975).

Acknowledgments.—Willard Newland of USGS developed the spectral signatures for the Puget Sound region. Margaret Elliott and James Wray of the USGS planned the illustrations. The National Aeronautics and Space Administration (NASA) Ames Research Center, Moffett Field, Calif., provided computation facilities.

SIGNATURE EXTENSION PROCEDURE

An experiment was devised in which land cover signatures from a scene in the Puget Sound region were applied to Landsat data from an adjacent scene of the Portland area, which is in the same orbit. The location of these two Landsat scenes and a third scene to the north are shown in figure 1. The scenes selected for the experiment were taken on a clear day in the Pacific Northwest—June 13, 1974. Landsat scene 1690-18245 over Puget Sound was cloudless. The scene to the north (1690-18243), reaching well into British Columbia, was also clear of clouds. The scene to the

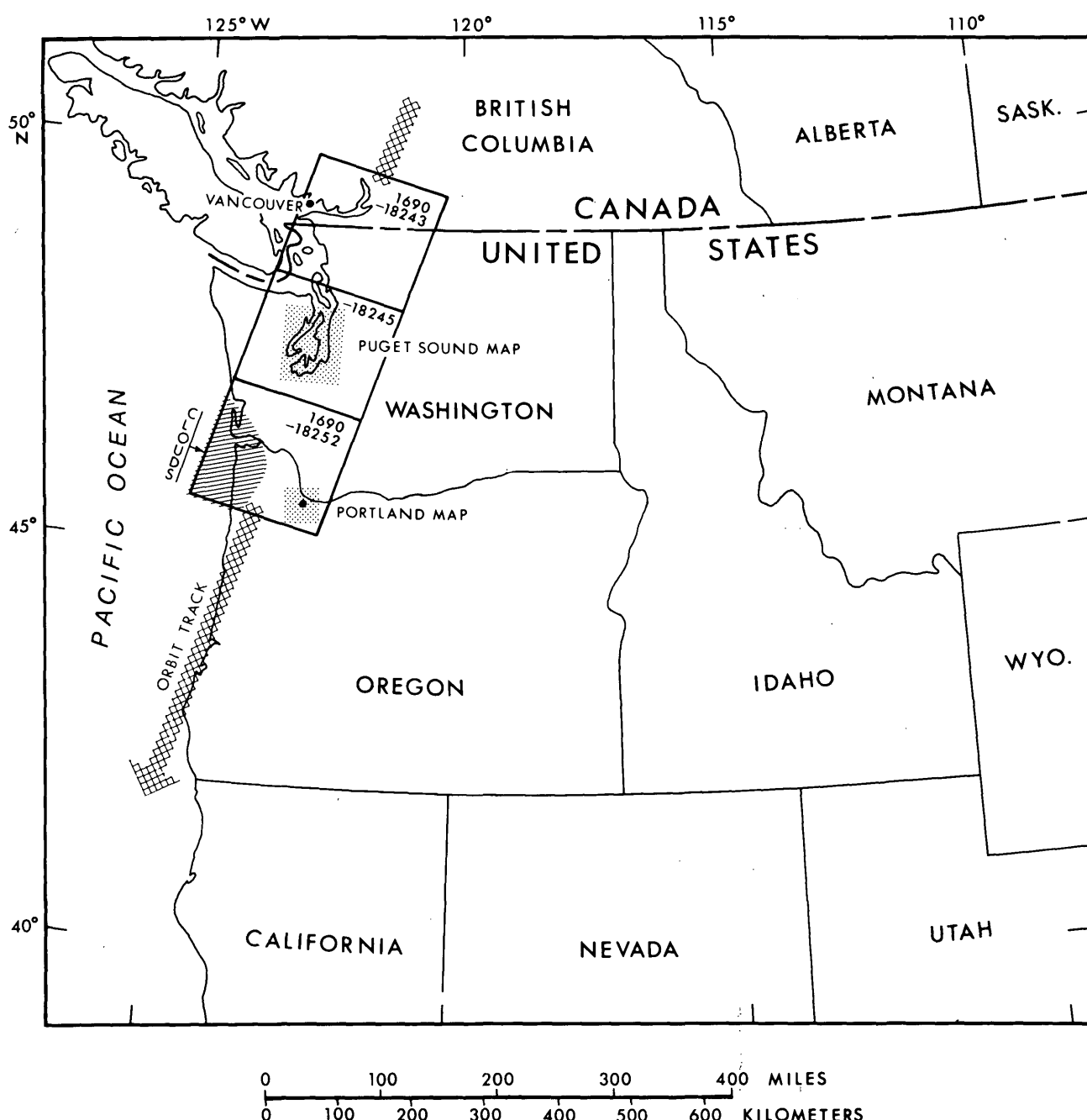


FIGURE 1.—Landsat scenes and land use and land cover maps of the Puget Sound region and Portland area. The large rectangles represent three successive Landsat scenes acquired approximately 25 seconds apart on June 13, 1974, in a southwesterly orbital pass. The small rectangles denote areas shown on land cover maps of the Puget Sound region, Wash., and Portland area, Oreg.

south (1690-18252), over Portland, was clear except for clouds covering the mouth of the Columbia River. The southeast corner of the Portland scene was chosen for the experiment. This area provided an extreme test of signature extension because it lay furthest from the Puget Sound region. The Portland area scene also included a range of land use and land cover types similar to that in the Puget Sound region.

A digital map of land cover in the Portland area produced in color by a film recorder is shown in figure 2 (see color insert). The land cover classification data can be reproduced in statistical form on tape or in map form as color or black-and-white prints at different scales.

Computer compatible tapes (CCT's) of the three scenes and photo prints of bands 5 and 7 at a scale of

1:500,000 were obtained from the EROS Data Center. Fifteen control points identifiable on both the Landsat images and the Portland 1:250,000-scale topographic map were digitized using a TI-733 remote computer terminal and a SAC GP-3 sonic digitizer that accessed

EDITOR software installed on a PDP-TENEX computer on the ARPA Network at Bolt, Baranek and Newman, Inc., Boston (fig. 3). This operation produced a first-stage geometric correction by matching line and column coordinates of data cells (picture ele-

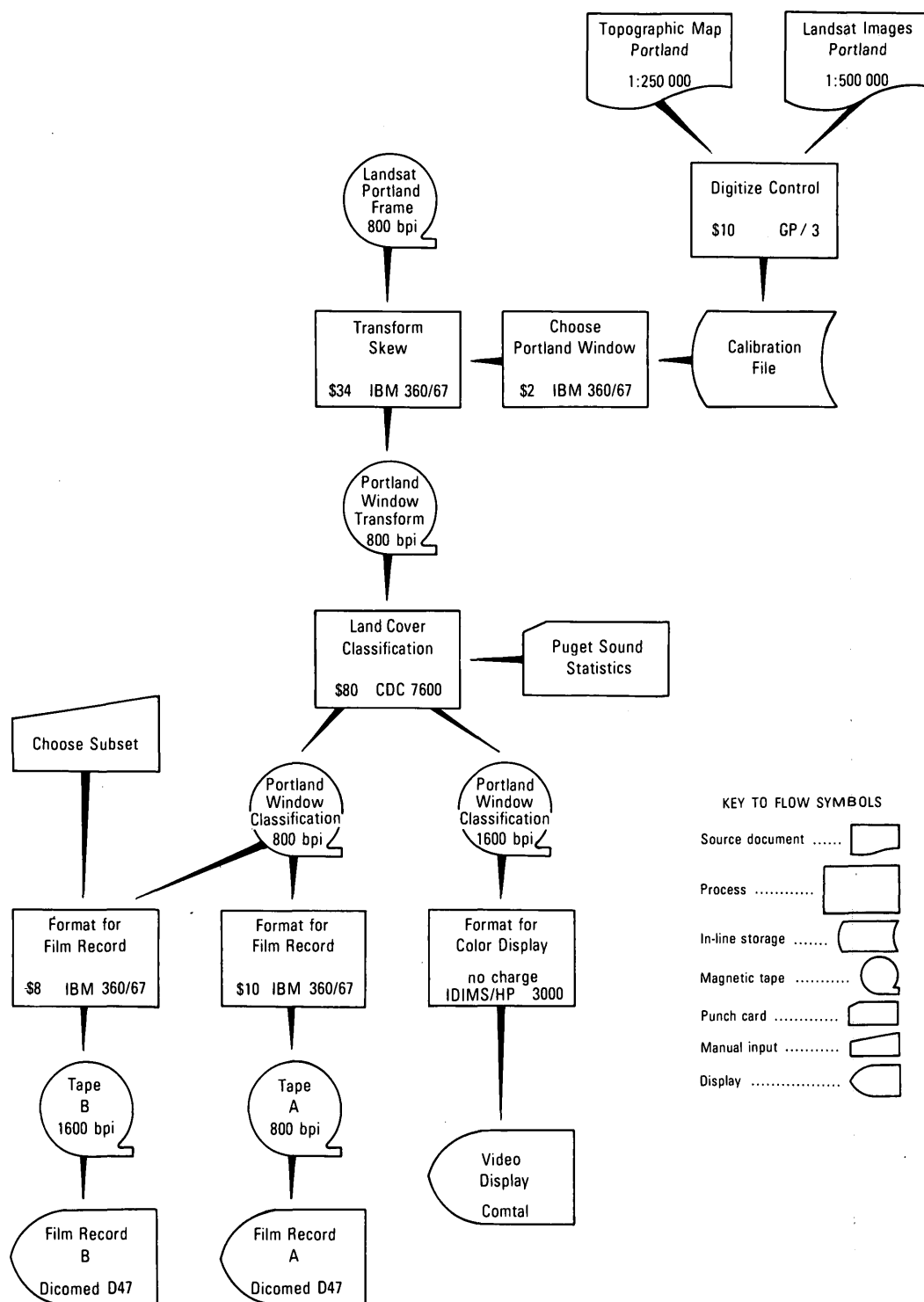


FIGURE 3.—Procedure for land cover classification of the Portland area, Oreg., by signature extension, including computation costs.

ments or "pixels") on the Landsat tape to their corresponding latitude and longitude on the topographic map. The operation also established the parameters necessary for removing skew from the digital data and rotating the data cells into west-east lines and north-south columns (Donovan and others, 1975). The skew and diagonal scan lines result from the rotation of the Earth beneath the oblique orbit of the satellite while the scanner is acquiring data.

The Calculate Coordinates Command of EDITOR was used to determine the size, in lines and columns, of the area to be transformed and its center. This command is a computer program that uses a calibration file determined from the control points to translate latitude and longitude coordinates to line and column coordinates. These coordinates were used along with the horizontal and vertical skew parameters as input to the skew-transformation software developed by the Center for Advanced Computation and installed on the IBM 360/67 computer at the NASA Ames Research Center. The original scene tapes were then read, and the "window" of lines and columns of data for just the Portland area was reformatted onto another tape. The window on this tape contained 1340 lines and 940 columns and was centered on line 918 and column 2604 of the original scene (approximately lat $45^{\circ}30' N$, long $122^{\circ}37.5' W$).

Spectral signatures from four channels of the Landsat scene of the Puget Sound region were punched on cards and used with the skew-transformed data of the Portland area. The Portland data were classified on the CDC 7600 computer at the Ames Research Center into 37 spectral classes using a maximum likelihood decision rule. The classification output was copied onto two tapes, one at 800 and the other at 1600 bits per inch (bpi) density.

The 800-bpi tape was taken to the IBM 360/67 computer at Ames where it was formatted onto yet another tape in order to display the classified data in 20 colors on the Dicomod D47 film recorder. After a Polaroid color print of the classified data had been viewed, a subset containing only 762 lines and 1024 columns of pixels was selected for expanded display. The program was rerun, and this subset was displayed again, this time using a matrix of four raster units per pixel on the film recorder. Every second line was displayed as six raster units per pixel to maintain the pixel aspect ratio and thereby to make the north-south scale equal to the west-east scale.

The 1600-bpi tape was used for interactive display of the mapped classes on the ESL IDIMS system at the Ames Research Center (Electromagnetic Systems Laboratories, 1976). The tape was copied to a disk on

the HP 3000 computer in order to view the map in color on the display screen. Trial combinations of spectral classes, land cover classes, and map symbol colors were displayed and were compared with a high-altitude color-infrared air photograph. This procedure confirmed that classification data for the Puget Sound region could be used to produce a reasonable map of land use and land cover in the Portland area. One combination of classes was selected, and the results were recorded on the color film from which figure 2 was made.

COST OF LAND COVER CLASSIFICATION

A flow diagram that describes the operations and gives the compilation costs of the land cover classification of the Portland area is shown in figure 3. Table 1 summarizes the costs of computation, labor, and materials for selected units of area. All the computer programs were run, and tapes were created in 8 work hours over 3 days elapsed time.

The costs of these operations do not include the cost of reference materials, such as aerial photographs, the cost of developing the original land cover classes for Puget Sound, or the cost of making a reproduction from the colored land cover map produced on the film recorder. Moreover, the costs do not include the expense of the second-stage geometric correction that would be needed to fit a base map to the present film-recorder map of land cover in the Portland area.

SUMMARY

Although a rigorous evaluation of the results has not yet been completed, an examination of the film recorder map products indicates that the Portland land

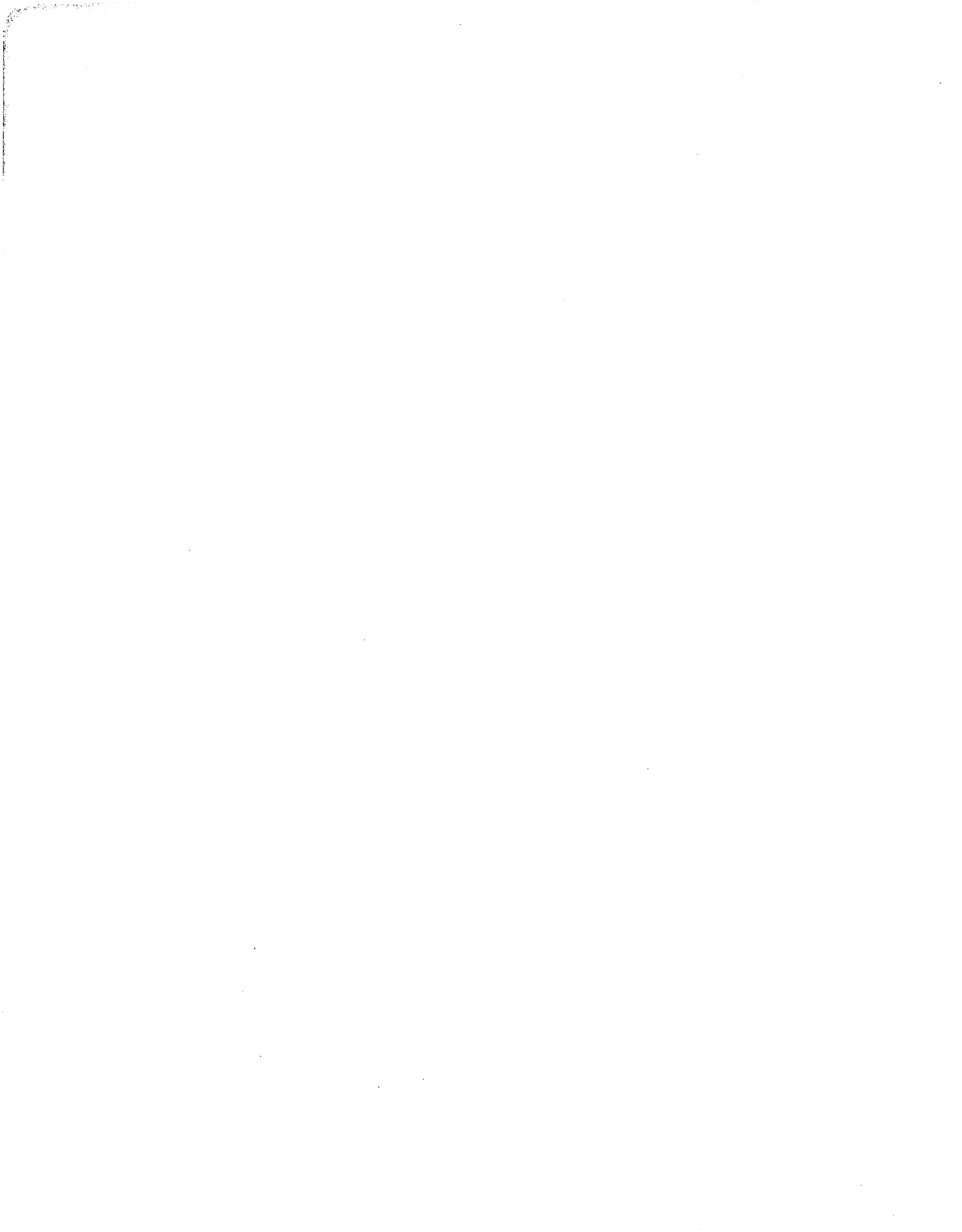
TABLE 1.—Cost of land classification in the Portland area by extension of signatures from the Puget Sound region
[Total area classified: 5607 km^2 (2165 mi^2)]

Category	Cost Total	Cost per unit area	
		Square kilometer	Square mile
Computation costs	\$144	\$0.0257	\$0.0665
Digitize control	\$10	-----	-----
Choose area	2	-----	-----
Transform skew	34	-----	-----
Classify land cover	80	-----	-----
Create film record A	10	-----	-----
Create film record B	8	-----	-----
Materials costs	242	0.0431	0.1117
Landsat tapes	200	-----	-----
Landsat prints	16	-----	-----
Topographic map	1	-----	-----
Blank tapes	25	-----	-----
Labor costs	56	0.0100	0.0259
8 hours at \$7 per hour	56	-----	-----
Grand total	442	0.0788	0.2041

cover classification is realistic and that the concept of land cover classification through signature extension down orbit (or up orbit) appears promising.

REFERENCES CITED

- Donovan, W. E., Ozga, Martin, and Ray, R. M., 1975, Compilation and geographic registration of ERTS multitemporal imagery: Urbana, University of Illinois, Center for Advanced Computation, CAC Technical Memorandum no. 52, 18 p.
- Gaydos, Leonard, and Newland, Willard, 1978, Inventory of land use and land cover for the Puget Sound Region using Landsat digital data: U.S. Geological Survey, Journal of Research, v. 6, no. 6, p. 807-814.
- Electromagnetic Systems Laboratories, 1976, Interactive digital image manipulation system (IDIMS) user manual: Sunnyvale, California, ESL, Inc., Technical Memorandum no. ESL-TM711, 261 p.
- Ray, R. M., III, 1975, Summary of ILLIAC IV—ARPA network multispectral image processing research activities: Urbana, University of Illinois, Center for Advanced Computation, CAC Doc. no. 168, 24 p.
- Ray, R. M., Ozga, Martin, Donovan, W. E., Thomas, J. D., and Graham, M. L., 1975, EDITOR—An interactive interface to ILLIAC IV—ARPA network multispectral image processing systems: Urbana, University of Illinois, Center for Advanced Computation, CAC Doc. no. 114, 28 p.



APPLICATION OF FOUR INPUT-OUTPUT MODELS FOR NUTRIENTS IN LAKE OKEECHOBEE, FLORIDA

By RONALD L. MILLER, Denver, Colo.

Abstract.—R. A. Vollenweider's (1975) nonconservative model described concentrations of nitrogen and phosphorus for 1969-70 in Lake Okeechobee, Fla., better than the models of F. Biffi in 1963, R. H. Rainey in 1967, and R. Piontelli and V. Tonolli in 1964. Vollenweider's model predicted concentrations of 1.4 milligrams per liter of total nitrogen and 0.09 mg/L of total phosphorus in the lake. The concentration of nitrogen could be approximated with conservation models but phosphorus required a nonconservative model. Unless variations in input concentrations and flow rate of the tributaries are modeled, only short-term predictions of lake concentrations can be made because of variations in inflow concentrations and because of the short time required (400 days) for the lake to be flushed by its inflow.

Interest in predictive models of lake environments has increased due to concern over eutrophication trends and to the consequential efforts to manage and to restore lakes.

The keen interest in modeling nitrogen and phosphorus concentrations in lakes stems from their role as algal "growth-limiting" nutrients. There are two approaches used to determine the "limiting" nutrient(s). In the first, the stoichiometric-limiting nutrient is determined by dividing the concentration of each available nutrient in the water by the stoichiometric requirement of algae for that nutrient. The nutrient having the lowest ratio is the limiting nutrient. In the second approach, a nutrient is considered kinetically limiting if an increase in its concentration results in a higher growth rate for the algae. In many cases, more than one nutrient is kinetically limiting. Micronutrients and even macronutrients, such as sodium and potassium ions, can be kinetically limiting. These two approaches can identify different nutrients as the limiting one(s) under certain circumstances (Verhoff, 1973). In most lakes, either nitrogen or phosphorus is the limiting nutrient.

Three fundamental concepts are required for the development of quantitative models of input-output processes in lakes. The first, and probably the most fundamental principle is the conservation of mass.

Second, the rates at which processes occur must be quantified. And third, if the conservation of more than one chemical species is considered in the model, then the stoichiometric relationship between those species during chemical transformations must be specified (Verhoff, 1973).

Vollenweider (1969) developed input-output models for nutrients in lakes analogous to models developed by Streeter and Phelps (1925) for dissolved oxygen in streams (O'Melia, 1972). Table 1 shows some of the counterparts in stream and lake models. The Streeter-Phelps-O'Conner model is more refined and generalized than Vollenweider's model, but these improvements required 35 years for development. Models of lakes, which are more complex systems than streams, can be expected to evolve into useful tools for predicting the concentrations of dissolved and suspended species (O'Melia, 1972).

PURPOSE AND APPROACH

The purpose of this work was to find, demonstrate, and evaluate lake input-output models that could be used with existing data (Joyner, 1971) for the specific case of nitrogen and phosphorus in Lake Okeechobee, Fla. Four models were selected from the literature to demonstrate different approaches that have been used for models that require only a material budget. These models form the foundation for later models, which usually are modifications of the selected models. See table 2 for a comparison of these models.

U.S. Customary units are used as a starting point only so that data can be traced more conveniently to the original source (Joyner, 1971). These data are converted to the SI units and all subsequent calculations are calculated in SI units. The term "ton" appears only as original data in U.S. Customary units. The symbols employed by authors of models were used as in the original model where feasible.

Vollenweider (1964, 1965, 1969, 1975) proposed other models. Imboden (1973) and O'Melia (1972) derived

TABLE 1.—Comparison of stream and lake models
[DO, dissolved oxygen; P, phosphorus; N, nitrogen. Data modified from that given by O'Melia (1972, table 1, p. 2-3)]

Subject of comparison	Streams	Lakes
Water-quality criteria.	Unpolluted: DO>4 mg/L. Polluted: DO<4 mg/L. (For critical period, usually summer—criteria based on fish requirements.)	Oligotrophic: P<10 µg/L and N<300 µg/L (Sawyer, 1947). Eutrophic: P>10 µg/L and N>300 µg/L. (For critical period, usually spring, before stratification—criteria based on preserving aesthetic water quality for human requirements through low productivity and so forth.)
Pollutant loading	(100 L/s)/1000 people ¹ . Consider stream characteristics (sluggish, average, rapid) ¹ .	0.2–0.5 (g/m ²)/yr phosphorus and 5–10 (g/m ²)/yr nitrogen (Vollenweider, 1968). Consider lake characteristics (depth). For example, based on observation, allowable P loading was 0.07 (g/m ²)/yr at 5-m depth and 0.60 (g/m ²)/yr at 200-m depth
Mathematical models.	$\frac{dD}{dt} = K_1 L - K_2 D$ (Streeter and Phelps, 1925). $\frac{\partial [c]}{\partial t} + V \frac{\partial [c]}{\partial x} = \frac{\partial}{\partial x} E_x \frac{\partial [c]}{\partial x} \pm \Sigma r$ (O'Conner, 1961).	$\frac{d[M_w]}{dt} = \frac{J}{Z} - (\sigma + \rho) [M_w]$ (Pointelli and Tonolli, 1964; Vollenweider, 1968).

¹ Based on observation.² Originally (4 ft³/s)/1000 people.

TABLE 2.—Comparison of models and assumptions

	Mass or concentration	Hydraulics	Conservative or nonconservative	Other assumptions
Biffi (1963)	Uses mass in lake	Uses outflow	Conservative	Constant input. Complete mixing. All parts of lake have equal probability of being flushed.
Rainey (1967)	Uses concentration	Assumes inflow equals outflow.	do	Same as those of Biffi (1963) plus the following: Precipitation equals evaporation, and the input of tributaries is separated from input of other sources.
Pontelli and Tonolli (1964).	Uses mass in lake	Uses outflow from lake.	Nonconservative. Assumes sedimentation of solute is a constant fraction of its input to lake.	Same as those of Biffi (1963).
Vollenweider (1975).	Uses concentration	Uses outflow per unit of lake surface area.	Nonconservative. Assumes sedimentation of solute is a constant fraction of mass in lake.	Do.

models that divide the lake into different layers (for stratified lakes) and redefine sedimentation in terms of flux in relation to depth. Lorenzen (1973) discussed models that consider separately the loss and release of material from sediment. The more sophisticated models have the limitation of requiring information that is not generally available and that is often difficult to

obtain even with special studies of the lake. Some of the measurements required, such as sedimentation fluxes, may be reliable only for the time and conditions studied and may add little to the accuracy of the prediction. Because Lake Okeechobee does not stratify, there was no need to subdivide the lake into layers.

The four models discussed individually in the following sections were considered indicative of the kind of information that can be obtained from input-output models that require only a material budget.

DEMONSTRATION OF MODELS AND THEIR USE

Biffi conservative model

This is the earliest and simplest model available (Biffi, 1963). The starting differential equation and two forms of the solution are

$$\frac{dx}{dt} = c - \frac{a}{b} \cdot x, \quad (1)$$

$$x = \frac{bc}{a} \left[1 - \left(1 - \frac{ax_0}{bc} \right) \cdot \exp\left(-\frac{at}{b}\right) \right], \quad (2)$$

and

$$t = \frac{b}{a} \ln\left(\frac{ax_0 - bc}{ax - bc}\right). \quad (3)$$

The steady-state solution at $t = \infty$ is

$$x_{t=\infty} = \infty = \frac{bc}{a} \quad (4)$$

and

$$t_{1/2} = \frac{b}{a} \ln 2, \quad (5)$$

where x = the amount of material in the lake at time t ,

x_0 = the amount of material in the lake at $t = 0$,

a = outflow volume (must be a rate to be consistent),

b = lake volume,

c = supply rate of material to the lake, and

t = time.

By setting $x = x_0/2$ and $c=0$, half-life (the time required for the amount of substance in the lake to decrease to one-half of the starting concentration) may be determined by solving for $t_{1/2}$ as shown in equation 5.

The assumptions made by Biffi were (1) the supply c to the lake is constant during the time studied, (2) the lake is completely mixed (the term often used is CSTR for continuously stirred tank reactor), (3) all parts of the lake have an equal probability of being flushed at all times, (4) the substance is conservative (it does not react or settle), and (5) rainfall equals evaporation (Dillon, 1974).

Application of Biffi model to Lake Okeechobee

Outflow from the lake is used to calculate the flushing effect of the lake. Any consistent set of units can

be used in this application of the model to Joyner's data (1971) for total nitrogen and total phosphorus. For nitrogen,

$$c = 22.29 \text{ ton/d} \times 9.072 \times 10^8 \text{ mg/ton}, \\ = 2.022 \times 10^{10} \text{ mg/d}, \quad (6)$$

$$a = 4966 \text{ ft}^3/\text{s} \times 2.447 \times 10^6 \text{ L} \cdot \text{s}/\text{ft}^3/\text{d}, \\ = 1.215 \times 10^{10} \text{ L/d}, \quad (7)$$

$$b = 4.02 \times 10^6 \text{ acre-ft} \times 1.234 \times 10^6 \text{ L/acre-ft}, \\ = 4.96 \times 10^{12} \text{ L}; \quad (8)$$

$$x_0 = 1.4 \text{ mg/L} \times 4.959 \times 10^{12} \text{ L} \\ = 6.9 \times 10^{12} \text{ mg, and} \quad (9)$$

$$x_\infty = bc/a = (4.96 \times 10^{12} \text{ L} \times 2.022 \\ \times 10^{10} \text{ mg/d})/(1.215 \times 10^{10} \text{ L/d}) \\ = 8.25 \times 10^{12} \text{ mg.} \quad (10)$$

x_∞ corresponds to an average concentration of 1.66 mg/L.

For phosphorus,

$$c = 5.33 \times 10^9 \text{ mg/d}, \quad (11)$$

$$a = 1.215 \times 10^{10} \text{ L/d}, \quad (12)$$

$$b = 4.96 \times 10^{12} \text{ L}, \quad (13)$$

$$x_0 = 2 \times 10^{11} \text{ mg,} \quad (14)$$

$$x_\infty = (4.96 \times 10^{12} \text{ L} \times 5.33 \times 10^9 \text{ mg/d})/1.215 \\ \times 10^{10} \text{ L/d, or} \\ = 2.18 \times 10^{12} \text{ mg.} \quad (15)$$

This corresponds to an average concentration of 0.439 mg/L.

If the input of nitrogen or phosphorus were decreased to 0, the time required for x to reach $x_0/2$ would be

$$t_{1/2} = (4.96 \times 10^{12} \text{ L}/1.215 \times 10^{10} \text{ L/d}) \times \ln 2, \text{ or} \\ = 283 \text{ d.} \quad (16)$$

Rainey conservative model

Rainey (1967), using the same assumptions as Biffi, derived an equation that differed in symbology, in the substitution of $C_1 \cdot R + Q$ for bc , and in the use of concentration instead of mass. Rainey used his model to estimate the time required to flush 90 percent of a conservative pollutant from the Great Lakes. Rainey assumed that rainfall equaled evaporation, that is, inflow equaled outflow, that the concentrations were uniform throughout the lakes (equivalent to assuming a CSTR), and that each volume increment has the same probability of being flushed from the lake. He separated tributary input from other input. In Lake Okeechobee, other input might include precipitation,

catfish bait, and back pumping from canals. Rainey's equation is

$$C_2 = C_2^0 \exp(-RT/V) + (C_1 + Q/R)(1 - \exp(-RT/V)), \quad (17)$$

where R = flow rate to and from the lake (assuming precipitation equals evaporation),

C_1 = constant concentration of input from tributaries,

C_2 = concentration of material in the lake at time = T ,

C_2^0 = concentration of material in the lake at time = 0,

Q = constant rate of material input entering lake directly,

T = time, and

V = volume of the lake.

At $T = \infty$,

$$C_2 = C_1 + Q/R. \quad (18)$$

If the material input to the lake is reduced to 0 ($C_1 = Q = 0$), the half-life of the pollutant is

$$T_{1/2} = (V/R) \ln 2. \quad (19)$$

Application of Rainey model to Lake Okeechobee

Rainey's simplifying assumption that rainfall equals evaporation implies that inflow equals outflow. To facilitate comparison with Biffi's model, the outflow was also used with Rainey's model.

For nitrogen,

$$C_2^0 = 1.4 \text{ mg/L}, \quad (20)$$

$$C_1 = [(16.60 \text{ ton/d}) \times (9.072 \times 10^8 \text{ mg/ton})] / [(1.406 \times 10^5 \text{ L/s}) \times (86400 \text{ s/d})] = 1.24 \text{ mg/L}, \quad (21)$$

$$Q = 5.69 \text{ ton/d} \times 1.050 \times 10^4 \text{ mg} \cdot \text{d/ton} \cdot \text{s, or } 5.97 \times 10^4 \text{ mg/s (from precipitation and catfish bait)}, \quad (22)$$

$$R = 4966 \text{ ft}^3/\text{s} \times 28.32 \text{ L/ft}^3 = 1.406 \times 10^5 \text{ L/s, and} \quad (23)$$

$$V = 4.96 \times 10^{12} \text{ L.} \quad (24)$$

At $T = \infty$,

$$C_2 = 1.24 + (5.97 \times 10^4 \text{ mg/s}) / (1.406 \times 10^5 \text{ L/s}), \text{ or } = 1.66 \text{ mg/L.} \quad (25)$$

For phosphorus,

$$C_2^0 = 0.04 \text{ mg/L,} \quad (26)$$

$$C_1 = 0.364 \text{ mg/L,} \quad (27)$$

$$Q = 1.05 \times 10^4 \text{ mg/s,} \quad (28)$$

$$R = 1.406 \times 10^5 \text{ L/s, and} \quad (29)$$

$$V = 4.96 \times 10^{12} \text{ L.} \quad (30)$$

At $T = \infty$,

$$C_2 = 0.364 \text{ mg/L} + (1.05 \times 10^4 \text{ mg/s}) / (1.406 \times 10^5 \text{ L/s}), \text{ or } = 0.439 \text{ mg/L;} \quad (31)$$

also for nitrogen and phosphorus,

$$T_{1/2} = (4.96 \times 10^{12} \text{ L} \times \ln 2) / (1.406 \times 10^5 \text{ L/s}), \text{ or } = 2.45 \times 10^7 \text{ s} = 283 \text{ d.} \quad (32)$$

Piontelli and Tonolli nonconservative model

Piontelli and Tonolli's model (1964) was the first to consider the loss of material through sedimentation. It is assumed that the amount of material lost to the sediment is a constant fraction of the supply of material to the lake. Their model also assumes that the lake is continuously stirred and that each volume increment has the same probability of being flushed from the lake. The equation derived from this model is

$$m_L = \mu [1 - (1 - m_L^0/\mu) \exp(-\Phi t)] \quad (33)$$

where J = constant supply of material to lake,

$$J_L = (1 - P^*)J,$$

m_L = amount of material in the lake at time = t ,

m_L^0 = amount of material in the lake at time = 0,

P^* = constant fraction of supply that is incorporated into the sediments,

q_d = rate of discharge from the lake,

t = time,

V = volume of the lake,

$\mu = J_L/\Phi$, and

Φ = flushing rate of the lake = q_d/V .

At $t = \infty$,

$$m_L = \mu. \quad (34)$$

If the input to the lake becomes 0,

$$t_{1/2} = (\ln 2)/\phi. \quad (35)$$

Application of Piontelli and Tonolli model to Lake Okeechobee

The following results were obtained using Joyner's (1971) values of N and P "trapped in lake" as values for sedimentation, for example, 3.96 and 1.90 ton/d, respectively.

For nitrogen,

$$J = 2.022 \times 10^{10} \text{ mg/d}, \quad (36)$$

$$J_L = (2.022 \times 10^{10} \text{ mg/L}) \times (1 - 0.178) = 1.66 \times 10^{10} \text{ mg/d}, \quad (37)$$

$$m_L^0 = 6.9 \times 10^{12} \text{ mg}, \quad (38)$$

$$P^* = (3.96 \text{ ton/d} \times 9.072 \times 10^8 \text{ mg/ton}) / (2.022 \times 10^{10} \text{ mg/d}), \text{ or} \\ = 0.178, \quad (39)$$

$$q_d = 1.215 \times 10^{10} \text{ L/d}, \quad (40)$$

$$V = 4.96 \times 10^{12} \text{ L}, \quad (41)$$

$$\mu = (1.66 \times 10^{10} \text{ mg/d}) / (2.45 \times 10^3 \text{ d}), \text{ or} \\ = 6.78 \times 10^{12} \text{ mg}, \quad (42)$$

$$\phi = (1.215 \times 10^{10} \text{ L/d}) / (4.96 \times 10^{12} \text{ L}), \text{ or} \\ = 2.45 \times 10^{-3}/\text{d}. \quad (43)$$

At $t = \infty$,

$$m_L = \mu = 6.78 \times 10^{12} \text{ mg}. \quad (44)$$

m_L corresponds to an average concentration of 1.36 mg/L.

For phosphorus,

$$J = 5.33 \times 10^9 \text{ mg/d}, \quad (45)$$

$$J_L = 3.61 \times 10^9 \text{ mg/d}, \quad (46)$$

$$m_L^0 = 2 \times 10^{11} \text{ mg}, \quad (47)$$

$$P^* = 0.323, \quad (48)$$

$$\mu = 1.47 \times 10^{12} \text{ mg, and} \quad (49)$$

q_d, V , and ϕ as for nitrogen.

At $t = \infty$,

$$m_L = \mu = 1.47 \times 10^{12} \text{ mg}. \quad (50)$$

m_L corresponds to an average concentration of 0.297 mg/L.

If $J = J_L = \mu = 0$ for nitrogen and phosphorus, then

$$t_{1/2} = (\ln 2) / (2.45 \times 10^{-3}/\text{d}) = 283 \text{ d}. \quad (51)$$

Vollenweider nonconservative model

Vollenweider (1975) assumed that the sedimentation rate is a constant fraction of the amount of the substance present in the lake. The equation derived from the model is

$$[m_w] = [m_w]_0 \exp [-(\rho_w + \sigma_M) (t - t_0)] \\ + [\mathbf{L}_M \{1 - \exp [-(\rho_w + \sigma_M) (t - t_0)]\}] / (\rho_w + \sigma_M). \quad (52)$$

At $t = \infty$,

$$[m_w] = \mathbf{L}_M / (\rho_w + \sigma_M), \quad (53)$$

If all input to the lake becomes 0 (all $m_i = 0$ and $\mathbf{L}_M = 0$), then

$$t_{1/2} = (\ln 2) / (\rho_w + \sigma_M), \quad (54)$$

where $[m_i]$ = concentration of tributary i ,
 $[m_w] = M_w/V$ = mean concentration in the lake,

$M_{w,0}$ = amount of substance in the lake at time $= 0$,

q_s = outflow from lake per unit of lake surface area,

S = rate of sedimentation

t = time,

V = volume of the lake,

V_i = flow rate of tributary i ,

Z = mean lake depth,

$\mathbf{L}_M = \sum V_i [m_i]/V$ = loading rate per unit volume,

$\rho_w = q/Z$ = discharge height, and

$\sigma_M = S/M_w$ = constant coefficient of sedimentation.

Application of Vollenweider model to Lake Okeechobee

The values of S used in equations 58 and 68 are equivalent to Joyner's (1971, tables 9 and 10) nitrogen and phosphorus "trapped in lake," respectively. The value of q_s was calculated from the sum (4979 ft³/s) of the outflows (Joyner, 1971, table 9) and the lake area (720 mi²) (Joyner, 1971, p. 12).

For nitrogen

$$M_{w,0} = 6.9 \times 10^{12} \text{ mg}, \quad (55)$$

$$[m_w]_0 = 1.4 \text{ mg/L}, \quad (56)$$

$$q_s = (1.218 \times 10^7 \text{ m}^3/\text{d}) / (1.9 \times 10^9 \text{ m}^2), \\ = 6.4 \times 10^{-3} \text{ m/d}, \quad (57)$$

$$S = 3.96 \text{ ton/d} \times 9.072 \times 10^8 \text{ mg/ton},$$

$$= 3.59 \times 10^9 \text{ mg/d}, \quad (58)$$

$$V = 4.96 \times 10^{12} \text{ L}, \quad (59)$$

$$Z = 2.66 \text{ m}, \quad (60)$$

$$\mathbf{L}_M = (22.29 \text{ ton/d} \times 9.072 \times 10^8 \text{ mg/ton}) / (4.96 \times 10^{12} \text{ L}),$$

$$= 4.08 \times 10^{-3} \text{ mg/L/d}, \quad (61)$$

$$\rho_w = (6.4 \times 10^{-3} \text{ m/d}) / (2.66 \text{ m}) \\ = 2.4 \times 10^{-3}/\text{d}, \quad (62)$$

$$\sigma_M = (3.59 \times 10^9 \text{ mg/d}) / (6.9 \times 10^{12} \text{ mg}), \text{ or}$$

$$= 5.2 \times 10^{-4}/\text{d}. \quad (63)$$

At $t = \infty$,

$$[m_w]_\infty = L_M / (\rho_w + \sigma_M) = 1.4 \text{ mg/L.} \quad (64)$$

If the input = 0 at $t = 0$,

$$\begin{aligned} t_{\frac{1}{2}} &= (\ln 2) / (2.4 \times 10^{-3}/d + 5.2 \times 10^{-4}/d), \text{ or} \\ &= 240 \text{ d.} \end{aligned} \quad (65)$$

For phosphorus,

$$M_{w,0} = 2 \times 10^{11} \text{ mg,} \quad (66)$$

$$[m_w]_0 = 0.04 \text{ mg/L,} \quad (67)$$

$$S = 1.72 \times 10^9 \text{ mg/d,} \quad (68)$$

$$L_M = 1.08 \times 10^{-3} \text{ mg/L/d,} \quad (69)$$

$$\sigma_M = 9 \times 10^{-3}/d, \quad (70)$$

V, Z, q_s , and ρ_w as for nitrogen.

At $t = \infty$,

$$[m_w]_\infty = 0.09 \text{ mg/L.} \quad (71)$$

If the input = 0 at $t = 0$, then

$$t_{\frac{1}{2}} = 60 \text{ d.} \quad (72)$$

DISCUSSION

The predictions from each model using Joyner's data are summarized in table 3. In addition to the concentrations predicted when time equals infinity and the half-life, table 3 contains the model predictions for 365 days and the ratio of concentration at 365 days to the concentration at infinity to show how rapidly the models approach their final value (conc_∞).

Rainey's model gave predictions that were identical to those of Biffi's model except for a difference in the number of significant figures.

According to Joyner (1971), 18 percent of the nitrogen entering the lake is "trapped" in the sediments. The two conservative models (Biffi and Rainey) predicted nitrogen concentrations in the lake that are about 18 percent higher than the predictions of the two nonconservative models (Piontelli and Tonolli and Vollenweider). Both of the nonconservative models produced similar predictions for nitrogen which is the same as the average concentration of the lake during the study period (1.4 mg/L as N). The similar be-

havior of the two nonconservative models may be due to one of the following two reasons: the quantity of nitrogen lost to the sediments (18 percent) is too low to produce a significant difference in the model predictions or the chemical form and behavior of nitrogen is such that either model can be used to describe its behavior.

For phosphorus, the two nonconservative models differed significantly from each other and from the conservative models. The predicted concentrations of the two conservative models were approximately 11 times greater than the average concentration found (0.04 mg/L as P) during the study period; Piontelli and Tonolli's model yielded a value seven times greater, but Vollenweider's value was only two times greater. The difference between the values predicted by the conservative model (0.439 mg/L) and the observed average value for the period of study (0.04 mg/L) demonstrates the nonconservative behavior of phosphorus. The difference (230 percent) between Piontelli and Tonolli's model and Vollenweider's model points out that Piontelli and Tonolli's assumption (sedimentation is proportional to the input of material to the lake) does not model the behavior of phosphorus in the lake as well as Vollenweider's assumption (sedimentation is proportional to the amount of material in the lake).

The two conservative models and Piontelli and Tonolli's model predict a half-life ($t_{\frac{1}{2}}$) of 283 days to flush one-half of the material from the lake if all phosphorus and nitrogen input to the lake ceased. Piontelli and Tonolli's model behaves as a conservative model in the calculation of half-life because sedimentation is proportional to input, which is assumed to be 0 for this calculation. Vollenweider's model results in shorter half-lives for nitrogen (-18 percent) and for phosphorus (-79 percent) than those predicted only on the basis of hydraulic flushing of the lake as in the other models. This difference results because Vollenweider's term σ_M (the constant coefficient of sedimentation) is retained in the equations used to calculate $t_{\frac{1}{2}}$ (eqs 65 and 72).

The ratio of the predicted concentration at 365 days to the predicted concentration at time infinity (conc_{365}

TABLE 3.—Comparison of model data

Model	Total nitrogen as N				Total phosphorus as P			
	Conc _∞ (mg/L)	Conc ₃₆₅ (mg/L)	Conc ₃₆₅ Conc _∞	t _½ (days)	Conc _∞ (mg/L)	Conc ₃₆₅ (mg/L)	Conc ₃₆₅ Conc _∞	t _½ (days)
Biffi -----	1.66	1.55	0.934	283	0.439	0.276	0.629	283
Rainey -----	1.66	1.55	.934	283	.439	.28	.64	283
Piontelli and Tonolli -----	1.36	1.35	.993	283	.297	.19	.64	283
Vollenweider nonconservative -----	1.4	1.4	1.0	240	.09	.09	1	60

$/conc_{\infty}$) shown in table 3 demonstrates that with Vollenweider's model phosphorus reaches its final concentration in less than 365 days. This rapid approach to $conc_{\infty}$ is due, in part, to the small change in concentration required to reach $conc_{\infty}$. With Piontelli and Tonolli's model, the nitrogen concentration reaches 99.3 percent of $conc_{\infty}$ in 365 days. This is because essentially no concentration change was required (1.4 to 1.36 mg/L) to reach the final value. Using their model, phosphorus concentrations are predicted to reach 64 percent of $conc_{\infty}$ in 365 days as a result of the large concentration change predicted (0.04 to 0.297 mg/L). The two conservative models (Biffi's and Rainey's) behaved similarly to Piontelli and Tonolli's model.

Due to the high ratio of inflow rate to lake volume (at the average inflow rate during the study period, the quantity of the inflow equaled the lake volume in about 400 days), these models can not be used to make long-term predictions of lake concentrations unless the input concentrations and flow rates are modeled far enough into the future to provide data for the lake models.

Of the four models investigated, Vollenweider's model best describes the behavior of nitrogen and phosphorus in Lake Okeechobee. His assumption that sedimentation is proportional to the amount of material in the lake is a more realistic assumption than assuming either conservative behavior (Biffi or Rainey) or the proportionality of sedimentation to quantity of input (Piontelli and Tonolli). Joyner's data tend to support this because the average lake concentration of phosphorus never approached the high values predicted by the other models during the study period (January 1969-July 1970).

It is important to understand that many hydrologic, physical, chemical, and biological factors have been ignored by these simple models. In reality, a lake with several tributaries and several outflows may behave quite differently than a continuously stirred tank reactor. Water flows along the path of least resistance from tributaries to outlets. The inflow rates vary considerably with time so that there will be pulses of nutrients and water into the lake. In Lake Okeechobee, there are the added complications of the outflows being artificially controlled by gates and of the reversal of flow of nutrient-rich drainage water from agricultural lands south of the lake. Inasmuch as 25 percent of the total nitrogen and 16 percent of the total phosphorus load comes from rainfall, modeling attempts must include water and nutrient input from rainfall.

In spite of the many factors that were ignored, Vollenweider's (1975) nonconservation model provided a reasonable short-term prediction of nitrogen and

phosphorus concentrations. It should be noted that water and nutrient input rates used in these calculations were averages for a 13-month period. In addition, the sedimentation term was used to average and incorporate all nutrient losses during the period of data collection.

CONCLUSIONS

Meaningful long-term predictions of total nitrogen and total phosphorus concentrations in Lake Okeechobee cannot be made unless the flow rates of tributaries and the concentration of nutrients in the inflow are modeled. This is due to large fluctuation of inflow rates and large fluctuations in inflow concentrations coupled with the short residence time of water in the lake (about 400 days during Joyner's study); that is, the lake responds relatively rapidly to changes in inflow concentrations.

The average nitrogen concentration could be approximated (about 18 percent high) with a conservative model, but phosphorus required a nonconservative model. Vollenweider's (1975) model described the input-output behavior of nutrients in Lake Okeechobee better than the models of Biffi (1963), Rainey (1967), and Piontelli and Tonolli (1964).

REFERENCES CITED

- Biffi, F., 1963, Determinazione del fattore tempo come caratteristica del potere di autodepurazione del Lago d'Orta in relazione ad un inquinamento costante: *Ist. Veneto Sci., Lettere ed Arti Atti, Cl. Sci. Mat. e Nat.*, v. 121, p 131-136.
- Dillon, P. J., 1974, A critical review of Vollenweider's nutrient budget model and other related models : *Water Resources Bull.*, v. 10, no. 5, p. 969-989.
- Imboden, D., 1973, Limnologische transport-und nährstoffmodelle: *Schweizer. Zeitschr. Hydrologie.*, v. 35, p. 29-68.
- Joyner, B. F., 1971, Appraisal of chemical and biological conditions of Lake Okeechobee: *U.S. Geol. Survey Open-File Rept. 71-006*, 90 p.
- Lorenzen, M. W., 1973, Predicting the effects of nutrient diversion on lake recovery, in Middlebrooks, E. J., Falkenborg, D. H., and Malony, T. E., eds., *Modeling the eutrophication process*: Utah State Univ., p. 205-210.
- O'Conner, D. J., 1961, Oxygen balance of an estuary: *Am. Soc. Civil Engineers, Trans.*, v. 126, p. 556-576.
- O'Melia, C. R., 1972, An approach to the modeling of lakes: *Schweizer Zeitschr. Hydrologie*, v. 34, p. 1-33.
- Piontelli, R., and Tonolli, V., 1964, Il tempo di residenza delle acque lacustri in relazione ai fenomeni di arricchimento in sostanze immesse, con particolare riguardo al Lago Maggiore: *Ist. Italiano Idrobiologia, Mem.*, v. 17, p. 247-266.
- Rainey, R. H., 1967, Natural displacement of pollution from the Great Lakes: *Sci.*, v. 155, p. 1242-1243.
- Streeter, H. W. and Phelps, E. B., 1925, A study of the pollution and natural purification of the Ohio River, pt. 3, Factors concerned in the phenomena of oxidation and reaeration; *U.S. Public Health Service, Bull.* 146, 75 p.

- Verhoff, F. H., 1973. A note on fundamental modeling principles and algal limiting nutrients *in* Middlebrooks, E. J., Falkenborg, D. H., and Maloney, T. E., eds., Modeling the eutrophication process: Utah State Univ., p. 213.
- Vollenweider, R. A., 1964. The correlation between the area of inflow and lake budget: German Limnological Conf., Lunz.
- 1965, Materiali ed idee per una idrochimica delle acque insubriche: Ist. Italiano Idrobiologia, Mem., v. 19, p. 213-286.
- 1968, The scientific basis of lake and stream eutrophication, with particular reference to phosphorus and nitrogen as eutrophication factors: Office for Economic Co-operation and Development, Paris, Tech. Rept. DAS/CSI/68, 27, p. 1-182.
- 1969, Möglichkeiten und Grenzen elementarer Modelle der Stoffbilanz von Seen: Archiv. Hydrobiologie, v. 66, p. 1-36.
- 1975, Input-output models with special reference to phosphorus loading concept in limnology: Schweizer Zeitschr. Hydrologie, v. 37, p. 53-84.

RECONNAISSANCE FOR MICROBIAL ACTIVITY IN THE MAGOOTHY AQUIFER, BAY PARK, NEW YORK, FOUR YEARS AFTER ARTIFICIAL RECHARGE

By E. M. GODSY and G. G. EHRLICH,
Menlo Park, Calif.

Prepared in cooperation with the Nassau County Department of Public Works

Abstract.—Tertiary-treated sewage effluent was injected into the Magothy aquifer at Bay Park, Long Island, N.Y., between 1968 and 1973. In 1977, the microbial flora in water samples from the injection well and from three nearby wells were surveyed. Differences in the composition of the microbial flora among the four wells were found. A bacterial community dominated by facultative and obligate anaerobes, including two *Clostridium* species and methanogenic bacteria, was found at a well 6.1 m from the injection well. By contrast, except for isolation of *Clostridium sphenoides* from a well 30 m away, only obligate aerobes and facultative anaerobes were found in water from the injection well and the 30 m well. Only a small number of obligate aerobes were found in samples from a well 61 m away. These results suggest that nutrients in the recharge water formed an organically enriched zone to at least a distance of 6.1 m from the point of injection but not as far as 61 m. Extensive pumping at the end of the injection program apparently removed exogenous nutrients near the injection well.

Between 1968 and 1973, the U.S. Geological Survey, in cooperation with the Nassau County Department of Public Works, conducted a series of tests to determine the feasibility of injecting tertiary-treated sewage effluent into the Magothy aquifer at Bay Park, Long Island, N.Y. (figure 1). A series of 13 tests using reclaimed water and 6 tests using city water was made. A detailed description of the last test and a comprehensive bibliography of published reports covering various aspects of the program is given by Vecchioli and others, (1975).

To recapitulate briefly, effluent from the secondary-sewage treatment plant at Bay Park was given tertiary treatment consisting of chemical coagulation, dual-media filtration, passage over activated carbon, and chlorination. Nitrogen species were not removed. Water from the tertiary-treatment plant was injected

into the Magothy formation through a well screened at 127 to 146 m below land surface. The injection stratum consists of fine to medium sand and thin beds of coarse sand. Some silt and clay are also present; lignite occurs as disseminated particles and layers. Pyrite and marcasite are also present.

At the conclusion of each injection episode, water was pumped from the injection well until pretest water-quality conditions were restored in the vicinity of the injection well. In general, 50 percent more water was pumped out than was injected.

According to Vecchioli, Bennett, Pearson, and Cerillo (1974), the native water is slightly acidic and has a dissolved solids concentration of 25 milligrams per liter. It is devoid of dissolved oxygen and has an Eh of 0 to -100 millivolts. The reclaimed water contains almost 400 mg/L of dissolved solids. The COD (chemical oxygen demand) of the reclaimed water was typically about 10 mg/L, whereas the native water had virtually no COD. In most tests, the residual chlorine content of the reclaimed water was near 2.5 mg/L. Geochemical reactions occurring during the exchange of these waters were considered by Ragone (1977).

Mats of organic and inorganic particulate matter formed near the well bore-aquifer interface during injection (Ehrlich and others, 1972). In the absence of inhibitors, microbial growth occurred in these filter mats, showing that nutrients are present in the injected reclaimed water. Microbial growth in the filter mat was suppressed by maintaining residual chlorine levels of about 2.5 mg/L in the injectant.

The persistence of chlorine in the injectant was relatively short. Ehrlich, Ehlke, and Vecchioli (1972)

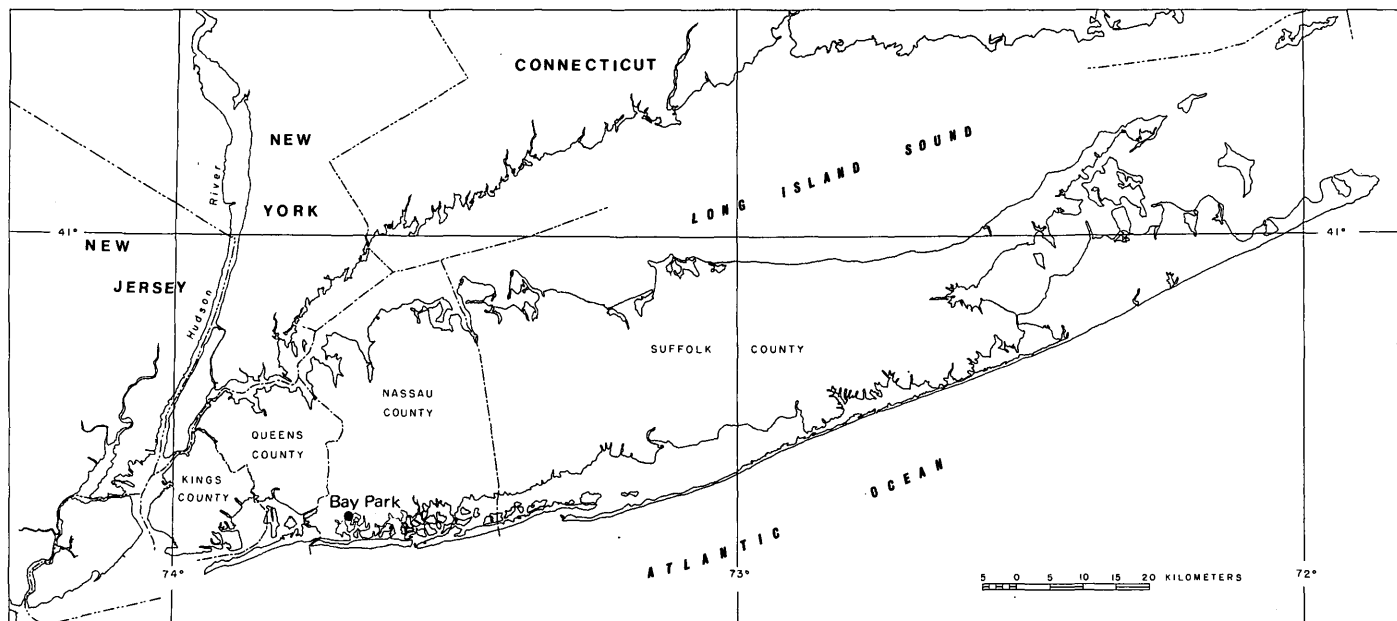


FIGURE 1.—Location of recharge site, Bay Park, Long Island, N.Y.

found that residual chlorine disappeared from chlorinated injectant in less than 48 h after entering the aquifer. This suggests that microbial growth could occur in the formation at a distance from the injection well if nutrients to support such growth were available.

In the 16th recharge test, reclaimed water with a COD concentration of 22 mg/L was injected (in all other tests, the COD was near 10 mg/L). Ku, Vecchioli, and Ragone (1975) found that only 207 out of 494 kg of COD originally injected was recovered in the repumped water. Lost constituents were assumed to be sorbed on clay and lignite in the formation or by entrapment of solid particles in the aquifer pores.

Some evidence for new microbial growth in the formation during artificial recharge was given by Ehrlich, Ehlke, and Vecchioli (1972), who found sulfate-reducing bacteria in samples from an observation well 6.1 m from the injection well during and after the seventh recharge test. John Vecchioli (oral commun., 1977) also found sulfate-reducing bacteria at this same observation well during the 19th recharge test. Neither set of observations was decisive because sulfate-reducing bacteria could be part of the indigenous microflora of the undisturbed aquifer.

There were no indications during any injection test of significant losses of hydraulic conductivity anywhere in the formation except near the well screen. Thus, any microbial growth that might have appeared did not cause significant pore blocking.

Although hydrologic measurements did not give any evidence of new microbial growth in the formation at a distance from the injection well and microbiologic evidence was inconclusive, we still suspected that some microbial growth may have occurred because significant amounts of potential nutrients were retained in the formation after redevelopment. To confirm this, microbial flora in pumped water samples from the injection well and three nearby observation wells were identified. Because the aquifer is normally under reducing conditions, we expected that active microbial communities adapted to these conditions would be dominated by anaerobes. Therefore, a special effort was made to find the types of microbes commonly found in anaerobic environments where organic matter is decomposing. The presence of such microbial communities would give strong evidence for organic enrichment of the formation, particularly if a different type of microbial flora was found at places relatively undisturbed by the earlier artificial recharge experiments.

METHODS

Location of observation wells, relative to the injection well is shown in figure 2. Wells sampled in this study were N7884 (the injection well), N7886 (6.1 m from the injection well), N7890 (30 m from the injection well) and N8022 (61 m from the injection well). In the following commentary, N7884 will be called the injection well, N7886 will be called the 6.1-m well, N7890 will be called the 30-m well, and N8022

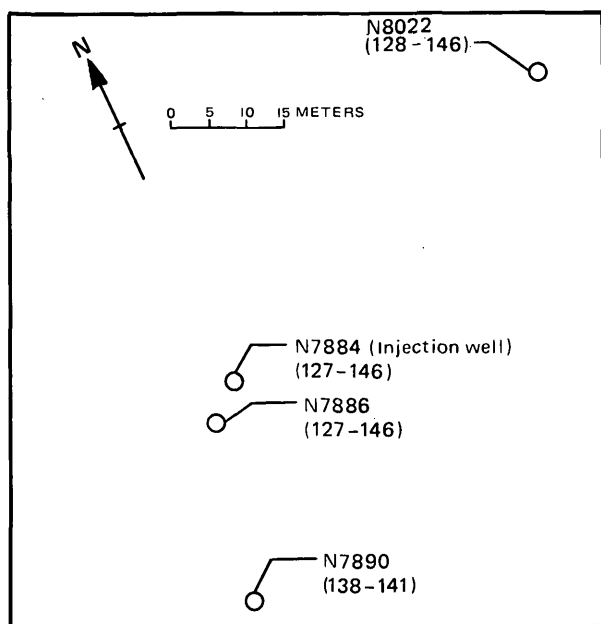


FIGURE 2.—Location of selected observation wells in relation to recharge well at Bay Park, Long Island, N.Y., sewage treatment facility. N is local well number; number in parentheses is depth of screened interval below land surface, in meters.

will be called the 61-m well. Samples were taken from each well on four consecutive days. Water was pumped until a minimum of two times the volume of the well casing had been removed before the sample was collected.

Samples for aerobic organisms were collected from the pump discharge stream in sterile glass bottles. Samples for anaerobes were collected in the following way: A length of gum rubber tubing was connected to the pump discharge pipe and coiled into a descending loop to eliminate air bubbles in the line. A small area was sterilized by swabbing with a 95-percent ethanol saturated cotton swab. One end of a double-ended syringe needle removed from a Vacutainer holder needle (Becton-Dickinson, Rutherford, N.J.) was inserted through the tubing in the sterile area. Following this, the other end of the needle was pushed through the septum of an evacuated, sterile, 100-milliliter serum bottle assembly, which, prior to evacuation, had contained an oxygen-free atmosphere of CO₂. The assembly consisted of a serum bottle capped with a butyl-rubber stopper held in place by an aluminum crimping band.

Aerobic and facultative anaerobic bacteria in 1.0 mL and larger samples were isolated by filtering measured volumes of samples through 0.45-μm Millipore membrane filters. Exposed filters were placed on plate-count agar (American Public Health Association

and others, 1976, p. 893) and incubated at 30°C. Spread plates using 0.1-mL portions of the water sample, and decimal dilutions thereof using solidified standard methods agar, were prepared. Filters and plates were incubated at 30°C and examined for colony development after 24 and 48 h.

Material from well-developed colonies on membrane filters and plates were picked and streaked onto triple sugar-iron agar slants (BBL, Division of Becton, Dickinson and Co., Cockeysville, Md.).

Facultative anaerobic bacteria were classified to genus and species using the Minitek Miniaturized Microorganism Differentiation System (BBL, Division of Becton, Dickinson and Co., Cockeysville, Md.).

Anaerobic bacteria counts were determined by the roll tube method using PRAS (prereduced anaerobically sterilized) PYG (peptone-yeast extract glucose) agar as described by Holdeman and Moore (1972). Water samples of 50 and 10 mL were tested for the presence of anaerobic bacteria by mixing with an equal volume of double-strength PRAS-PYG broth and observing for growth after 48 h at 30°C. Obligate anaerobes were classified to genus and species by the methods described by Holdeman and Moore (1972).

Iron-reducing bacteria were determined by multiple tube procedures in PRAS medium containing, per liter: glucose, 5.0 g; yeast-extract (Difco) 1.0 g; ammonium sulfate, 0.1 g; magnesium sulfate, heptahydrate, 0.2 g; potassium phosphate, dibasic (K₂HPO₄), 0.01 g; and anhydrous ferric oxide (Fisher Scientific), 20 g. The pH was adjusted to 7.0. Inoculated samples were incubated for 7 d at 30°C. Cultures were centrifuged at ×3000 gravity for 10 min, and the supernatant was withdrawn. Fe²⁺ was determined in the supernatant by the bipyridine method described by Brown, Skoustad, and Fishman (1970). Results were recorded as positive when the soluble iron concentration in the supernatant exceeded 5 mg/L.

Denitrifying bacteria were determined by multiple tube procedures using citrate-asparagine broth as described by Alexander (1965).

Sulfate-reducing bacteria were determined by multiple-tube procedures using PRAS sulfate API broth (Difco, Detroit, Mich.).

Methanogenic bacteria were determined by the presence of methane in the head space above the following medium patterned after that of Bryant, Tzeng, Robinson, and Joyner (1971), which contained: sodium formate, 2 mg/L; sodium acetate, 2 mg/L; potassium phosphate, dibasic (K₂HPO₄), 9 mg/L; hemin solution, 5 mL/L; vitamin solution of Wolin, Wolin, and Wolfe (1963), 10 mL/L; mineral solution, 490 mL/L; resazurin solution, 4 mL/L; volatile acid solution,

2 mL/L; and distilled water, to 1 L. The pH was adjusted to 7.0.

Hemin solution was prepared as follows: 5.6 g of potassium hydroxide was dissolved in 500 mL of distilled water and was mixed with 500 mL of 95 percent ethanol, and 0.1 g hemin was added (Eastman Organic Chemicals, Rochester, N.Y.) and was shaken until dissolved.

Mineral solution contains; potassium phosphate, monobasic (KH_2PO_4), 0.45 mg/L; ammonium chloride, 0.45 mg/L; magnesium chloride, 0.07 mg/L; calcium chloride, dihydrate, 0.06 mg/L; trace metal solution of Wolin, Wolin, and Wolfe (1963), 0.25 mg/L; and distilled water, to 1 L.

Resazurin solution was prepared as follows: 0.025 g resazurin (Eastman Organic Chemicals, Rochester, N.Y.) was dissolved in 10 mL of 95-percent ethanol and was diluted to 100 mL with distilled water.

Volatile acid solution was prepared by mixing equal volumes of isobutyric acid, 2-methylbutyric acid, isovaleric acid, and valeric acid (all obtained from Eastman Organic Chemicals, Rochester, N.Y.).

Ingredients were mixed and boiled under a CO_2 atmosphere following guidelines given for preparation of PRAS media by Holdeman and Moore (1972). Ten milliliters was dispensed into aluminum seal tubes (Bellco Glass, Vineland, N.J.) under a stream of an oxygen-free mixture of H_2-CO_2 (1:1), stoppered with aluminum seal stoppers (Bellco Glass, Vineland, N.J.) and crimped aluminum bands, and autoclaved at 121°C at 1.05 kilograms per square centimeter (15 psi) for 15 min.

Using sterile hypodermic syringes, 0.35 mL of a sterile saturated solution of CO_2 in 0.8-percent sodium carbonate solution and 0.18 mL of sterile 1.25-percent cysteine-hydrochloride-1.25-percent sodium sulfide solution (pH=10) were added to each tube of sterile medium prepared as directed above. Samples of 50 and 10 mL were mixed with equal volumes of double-strength medium in serum bottles capped with aluminum seal stoppers and aluminum crimping bands. Inoculated tubes were incubated under a pressurized atmosphere consisting of a 1:1 mixture of H_2-CO_2 as recommended by Balch and Wolfe (1976).

The presence of methane in the gas phase was determined after 4 weeks by gas chromatography using an Infotronics Model 15-C3 chromatograph equipped with thermal conductivity detectors and a 2.4-m \times 6-mm aluminum column filled with 150- to 200-mesh Poropak Q (Waters Associates, Inc., Framingham, Mass.). The column was operated at 50°C with helium at 40 cubic centimeters per minute as the carrier gas.

Total iron, Fe^{2+} , and pH were determined in the field by procedures outlined by Brown, Skougstad, and Fishman (1970). Analyses for COD were done at the U.S. Geological Survey Laboratory at Atlanta, Ga.

RESULTS

It was observed that media containing resazurin, a colorimetric oxidation-reduction indicator ($E^\circ = -51$ mV, at pH 7.0), remained colorless when mixed with water from the 6.1-m well indicating that the Eh of this water was less than -51 mV. By contrast, resazurin-containing media became pink when mixed with water from other wells indicating that these waters were more oxidized than water from the 6.1-m well. Native water from the Magothy aquifer is devoid of dissolved oxygen and has a slightly negative Eh with values ranging from 0 to -100 mV (Vecchioli and others, 1974).

Samples from the injection, the 30-m, and the 61-m wells did not have any characteristic odor. Samples from the 6.1-m well had a faint musty odor.

pH, Fe^{2+} , and COD values measured in samples collected during this study are given in table 1.

Native water samples taken in 1967 before the injection testing program began were slightly acidic, with pH values between 5 and 6 and Fe^{2+} concentrations between 0.1 and 0.3 mg/L (Vecchioli and others, 1974). pH values of the samples collected on the first day were within this range, but, except for samples from the 6.1-m well, pH values of subsequent samples were somewhat lower than this. Fe^{2+} con-

TABLE 1.—Results of analyses of water samples from the Magothy aquifer during microbiological reconnaissance, July 19–22, 1977

Date	Injection well N7884	Well and distance from injection well		
		N7886 6.1 m	N7890 30 m	N8022 61 m
pH				
7-19-77	9.4	5.8	5.5	5.2
7-20-77	4.3	5.1	4.8	4.6
7-21-77	5.2	5.2	4.8	4.6
7-22-77	3.7	5.2	4.9	4.5
Iron concentration (Fe^{2+}), in milligrams per liter				
7-19-77	0.5	1.7	0.5	0.2
7-20-77	0.1	0.7	0.6	0.2
7-21-77	0.1	0.7	0.5	0.4
7-22-77	0.2	0.2	0.6	0.4
Chemical oxygen demand (COD), in milligrams per liter				
7-19-77	15	90	20	25
7-20-77	10	25	30	30
7-21-77	35	35	15	15
7-22-77	15	35	35	20

TABLE 2.—*Bacterial count data*
[Bacterial count, in colonies per 100 mL]

Date	Injection well N7884		Well and distance from injection well					
	Standard plate count	Roll tube count	Standard plate count	Roll tube count	Standard plate count	Roll tube count	Standard plate count	Roll tube count
7-19-77	3×10^4	<10	5×10^4	6×10^6	5×10^8	1×10^9	1×10^6	<10
7-20-77	4×10^3	8×10^2	1×10^4	7×10^3	5×10^8	2×10^2	2×10^2	<10
7-21-77	1×10^4	5×10^2	1×10^4	3×10^5	3×10^4	1×10^2	1×10^2	<10
7-22-77	7×10^3	2×10^2	1×10^4	2×10^3	6×10^4	<10	8×10^3	<10

centrations in water from the 6.1-m and 30-m wells were generally higher than those found in 1967.

COD of water samples collected during this study were higher than previously found in the native water, which was near 0, and in reclaimed water, which was about 9 mg/L.

Obligate aerobic and facultative anaerobic bacteria counts are given in table 2. Values were generally within the range of 5×10^3 to 5×10^4 colonies per 100 mL in samples from the injection, the 6.1-m and the 30-m wells. Results from the 61-m well, during the first three days, were less than 10^3 colonies 100 mL, but approached the value for the other wells on the fourth day.

Material from a number of well-isolated colonies on the membrane filters and agar plates was picked and inoculated on and into the butt of a triple sugar-iron agar slant. Facultative anaerobic bacteria that fermented sugars with production of acid show a characteristic acidic reaction in this medium. Obligate aerobes and facultative anaerobes which do not ferment sugars, such as denitrifiers, do not produce a characteristic acid reaction in the medium. This simple procedure separates the bacteria growing on the total count plates into two classes, obligate aerobes and glucose fermenting facultative anaerobes. Results are given in table 3.

Facultative anaerobes were found only on plates derived from 6.1-m well samples and were not isolated from samples of water from the injection, the 30-m, or the 61-m wells. Thus, although the bacterial density was about the same in all the samples, the percentage of facultative anaerobic bacteria in the 6.1-m well samples was much higher than in samples from other wells.

Facultative and obligate anaerobic bacterial counts determined by the roll tube method (Holdeman and Moore, 1972), given in table 2, were higher for the 6.1-m well samples than for the other wells. Anaerobic bacteria were not detected in samples from the 61-m well.

TABLE 3.—*Distribution of obligate aerobes and facultative anaerobes among colonies of test specimens as shown by standard plate count*

Date	Well	Number of colonies tested	Number of colonies showing acid reaction	Number of colonies showing alkaline reaction
7-21-77	Injection	9	0	9
7-22-77	do	23	0	23
7-21-77	6.1-m	65	63	2
7-22-77	do	46	44	2
7-21-77	30-m	13	0	13
7-22-77	do	23	0	23
7-21-77	61-m	2	0	2
7-22-77	do	24	0	24

Anaerobically incubated PRAS-PGY broth cultures were examined by phase contrast microscopy. Cultures from the 6.1-m well contained a mixture of large and small, motile and nonmotile asporogenous rods. There was an abundance of large club-shaped, sporogenous rods, which are characteristic of members of the obligate anaerobic genus *Clostridium* in these samples. Samples from the injection and the 30-m wells contained large and small, motile and nonmotile rods, but sporogenous rods were not seen in any of the samples.

Portions of anaerobically incubated PRAS-PYG broth cultures from the injection, the 6.1-m and the 30-m wells were heated at 80°C for 10 min. Vegetative cells are killed during this heat treatment, but bacterial spores remain viable and germinate when placed in a suitable growth medium (Holdeman and Moore, 1972). When dilutions of the heat-treated broth cultures were inoculated into PRAS-PYG agar roll tubes, outgrowth occurred only with samples from the 6.1-m well. Pure cultures were obtained for 12 colonies on the last dilution. All were large ($3.0\text{--}5.0 \times 0.6\text{--}1.0 \mu\text{m}$) rods with subterminal oval spores and were identified as *Clostridium bifermentans*.

Dilutions of PRAS-PYG broth cultures which had not been heat treated were inoculated into PRAS-PYG agar roll tubes. After good growth had occurred, well-isolated colonies were picked and streaked on

tryptic soy agar slants. After aerobic incubation, growth had occurred for all isolates from the injection well samples (15 out of 15) and for all isolates from the 30-m well (4 out of 4); therefore, all isolates from these two wells were facultative anaerobic bacteria.

Enumeration of denitrifying bacteria using citrate-asparagine broth, as described by Alexander (1965), was attempted. Growth occurred in all 1.0-mL samples and in some of the 0.1-mL samples from the injection, the 6.1-m, and the 30-m wells. Growth was not observed in samples from the 61-m well.

When growth occurred, an acid reaction was recorded instead of the usual alkaline reaction or alkaline reaction with gas. Two different organisms were isolated from these cultures; *Enterobacter cloacae*, a facultatively anaerobic bacterium commonly found in soil and water samples, was isolated from the injection, the 6.1-m, and the 30-m wells. The second bacterium, isolated from only the 6.1-m and the 30-m wells, was identified as *Clostridium sphenoides*. *C. sphenoides*, is an obligately anaerobic bacterium commonly found in soil, sewage, and water samples (Walther and others, 1977). The most probable numbers of iron-reducing bacteria found in the samples are given in table 4.

A good correlation was found between the concentrations of soluble iron (table 1) and the count of iron-reducing bacteria. Ragone, Vecchioli, and Ku (1973) found high concentrations of soluble iron in water pumped from the formation after test RW10 when an appreciable pause had occurred between the end of injection and complete redevelopment. They suggested that colloidal iron oxide carried into the filter mat with the injectant was reduced by bacterial action. It is of interest to note that Ottow and Glathe (1973) reported that members of the genera *Bacillus*, *Pseudomonas*, and *Clostridium* and of the family Enterobacteriaceae can effect the reduction of ferric oxide with the production of soluble Fe^{2+} . *C. bifermentans* and *C. sphenoides* isolated from water from the 6.1-m and the 30-m wells were found to re-

duce iron oxides when inoculated into tubes of PRAS-prepared iron-reducing bacteria test medium and processed as described above.

Sulfate-reducing bacteria were not found in any of the water samples collected during this study. This contrasts with earlier findings of Ehrlich, Ehlke, and Vecchioli (1972), who found them in water samples taken from the 6.1-m well shortly after the end of a 33-day injection test, and of John Vecchioli (oral. commun., 1977), who found sulfate reducing bacteria in samples from the 6.1-m well during the final injection test (RW13).

A possible explanation for this discrepancy is as follows. During injection, reclaimed water having a SO_4^{2-} concentration of 160 mg/L (Vecchioli and others, 1975) along with particulate and soluble nutrients was introduced to the formation. After conclusion of the injection phase, the well was redeveloped by pumping out a volume of water equal to about three times the volume of water injected into the well. During this phase, sulfate-rich reclaimed water was displaced by sulfate-poor native water (SO_4^{2-} concentration = 4 mg/L) that moved toward the well. In this new environment, the sulfate-reducer population would soon deplete the available sulfate, and, in the absence of suitable nutrients, the sulfate-reducer population would then decline to low levels as observed in this study.

Methane gas was detected in the head space of all tubes inoculated with either 10 or 1.0 mL of water from each of the four 6.1-m well samples. The methanogen count is estimated to be in the range of 10^2 to 10^3 organisms/100 mL. During incubation, the methanogen test medium gradually became slightly turbid. Microscopic examination after 30 d revealed many small rod-shaped bacteria resembling members of the genus *Methanobacterium* (Zeikus, 1977).

Methane gas was not detected in tubes of medium inoculated with water from the other wells, indicating the virtual absence of methanoegnic bacteria at those sites.

DISCUSSION AND CONCLUSION

It is well known that microbes can decompose organic matter in anaerobic environments. Zeikus (1977) has referred to these situations as anaerobic organotrophic ecosystems. The rumen and gastrointestinal tracts of certain animals, flooded soils, sediments under fresh and marine waters, and sewage sludge digestors are common examples of anaerobic organotrophic ecosystems. Ground waters also provide suitable conditions for the establishment of anaerobic orangotrophic ecosystems, and the existence of anaerobic ecosystems in oil-field brines is well known (Davis, 1967).

TABLE 4.—Most probable number of iron-reducing bacteria in 100 mL of water collected during reconnaissance study

Date	Injection well N7884	Well and distance from injection well		
		N7886 6.1 m	N7890 30 m	N8022 61 m
7-19-77	<1	$\ast 10^6$	<1	<1
7-20-77	<1	10^4	10^2	<1
7-21-77	<1	10^4	<1	<1
7-22-77	<1	10^4	10^3	<1

* Fe^{2+} concentrations greater than 5 mg/L in the test broth solutions.

The pathways of transformation and types of products generated during degradation of organic substances under anaerobic conditions are varied, but methane and CO₂ are frequently the major products. In these ecosystems, methanogens are the terminal organisms of the food chain. Acetate, H₂ and CO₂ are the major nutrients for methanogens. Therefore, for the successful operation of the food chain, complex organic materials must first be converted into simpler substances such as CO₂, H₂, and volatile fatty acids by facultative and obligate anaerobes. Methanogens then use these products. In places where sulfate is abundant, sulfate-reducers are also active, sometimes to the exclusion of methanogens (Zeikus, 1977).

Several other reductions can also occur in anaerobic ecosystems. Reduction of nitrate to N₂O and N₂, reduction of hydrated ferric oxides to Fe²⁺, and reduction of manganic oxide to Mn²⁺ are sometimes observed.

The bacterial community found near the 6.1-m well contained all the physiological groups required to effect the anaerobic conversion of biotransformable material to methane and CO₂. In particular, a large proportion of these organisms were facultative anaerobic bacteria. Increased levels of Fe²⁺ were observed in the 6.1-m well along with an increased population to support iron oxide reduction, which is also indicative of an anaerobic environment. Nitrate reducers were not found.

Two species of obligately anaerobic organotrophic bacteria, *C. bifermentans* and *C. sphenoides*, isolated and identified from the 6.1-m well; H₂, CO₂, butyrate, and acetate are among the metabolic products of *C. bifermentans* and *C. sphenoides*. Finally, the presence of methanogenic bacteria demonstrates that the entire suite of bacteria found in a typical anaerobic organotrophic ecosystem is present near the 6.1-m well.

There was some evidence for an anaerobic/organotrophic ecosystem near the 30-m well; *C. sphenoides* was isolated from citrate asparagine broth, and iron-reducing bacteria were found in two of the four water samples. Methanogenic bacteria were not detected however.

The failure to find obligate anaerobes and the virtual absence of iron reducers and methanogenic bacteria in injection well samples was surprising. Earlier results had shown that significant populations of bacteria including obligate anaerobic sulfate reducers develop near the injection well in the post-injection period before redevelopment. It was, therefore, expected that the microbial community near this well would be most clearly indicative of organic enrichment. Apparently, the final redevelopment after the 19th recharge test which included treatment with hydro-

chloric acid and removal of about 4×10⁸ L of water had effectively cleared this region of nutrients so that the characteristic organisms could not develop.

The virtual absence of anaerobic organisms at the 61-m well suggests that anaerobically assimilable nutrients did not reach this area. It is possible, however, that the water at the 61-m well may have contained some compounds such as fermentation products that could be degraded under aerobic conditions. The small amount of oxygen that diffused through the well shaft may have supported the small population of aerobes found near this well.

We assume that the microbial communities in the formation are mostly contained in adherent films and that the cells found in the pumped water samples were dislodged from those films and entrained in the water moving toward the well bore. It is further assumed that the number of cells dislodged will be proportional to the total biomass and that the rate of dislodgement will be proportional to the velocity of water moving past the films. Once entrained, the movement of cells through the formation will be impeded by sorption and exclusion effects. Water samples will therefore, contain a larger proportion of cells from microbial communities near the well bore relative to the number of cells from more distant communities on a biomass to biomass basis. In other words, microbial communities from near the well screen will be overrepresented in the pumped water samples relative to more distant communities. Because of these complications, it does not appear to be feasible to relate cell counts to biomass, so we shall not attempt to do so.

One important assumption made above is that all of the important microbial types in the formation near the well will appear in the pumped water samples. The significant differences in the composition of the microbial flora between the wells are, therefore, suggestive of real differences in the quality of the ground water at these points. COD values (table 1) indicate organic enrichment of the aquifer up to and past the 61-m well but do not indicate any differences among the sampled areas. Consideration of microbial ecology shows that penetration of microbial nutrients was confined to much shorter distances.

In summary, a microbial community with species composition similar to those found in anaerobic environments where organic matter is decomposing was found near the 6.1-m well and, to a lesser extent, near the 30-m well. Communities near the injection and the 61-m wells were not composed of microbial types that would be expected in an anaerobic heterotrophic ecosystem.

Because preinjection testing had indicated that the native water was virtually free of organic matter, it is apparent that nutrients to support the observed communities must have been derived from injection of tertiary-treated sewage effluent during the period 1968-73. It is interesting to note, in conclusion, that signs of organic enrichment were evident 4 years after the last injection test had been completed.

REFERENCES CITED

- Alexander, Martin, 1965, Denitrifying bacteria, in Methods of soil analysis, pt. 2, Chemical and microbiological properties: Madison, Wisc., American Society of Agronomy, p. 1484-1486.
- American Public Health Association, American Waterworks Association, and Water Pollution Control Federation, 1976, Standard methods for the examinations of water and wastewater, (14th. ed.): New York, American Public Health Association, 1193 p.
- Balch, W. E., and Wolfe, R. S., 1976, New approach to the cultivation of methanogenic bacteria—2-mercaptoethane sulfonic acid (HS-COM)-dependent growth of *Methanobacterium ruminantium* in a pressurized atmosphere: Applied and Environmental Microbiology, v. 32, p. 781-791.
- Bryant, M. P., Tzeng, S. F., Robinson, I. M., and Joyner, A. E., Jr., 1971, Nutrient requirements of methanogenic bacteria, in Pohland, F. G., ed., Anaerobic biological treatment processes: American Chemical Society, Washington, D. C., Advances in Chemistry, Series 105, p. 23-40.
- Brown, Eugene, Skougstad, M. W., and Fishman, M. J., 1970, Methods for collection and analysis of water samples for dissolved minerals and gases: U.S. Geological Survey Techniques of Water-Resources Investigations, book 5, chap. A-1, 160 p.
- Davis, J. B., 1967, Petroleum microbiology: Amsterdam, Elsevier Publishing Co., 604 p.
- Ehrlich, G. G., Ehlke, T. A., and Vecchioli, John, 1972, Microbiological aspects of ground water recharge-injection of purified chlorinated sewage effluent at Bay Park, Long Island, New York, in U.S. Geological Survey Research 1972: U.S. Geological Survey Professional Paper 800-B, p. B241-B245.
- Holdeman, L. V., and Moore, W. E. C., 1972, Anaerobe laboratory manual, (2d. ed.): Virginia Polytechnic Institute and State University, Blacksburg, Va., 130 p.
- Ku, H. F. H., Vecchioli, John, and Ragone, S. E., 1975, Changes in concentration of certain constituents of treated waste water during movement through the Magothy Aquifer, Bay Park, New York: U.S. Geological Survey Journal of Research, v. 3, p. 89-92.
- Ottow, J. G. G., and Galthe, H., 1973, Pedochemie und Pedomikrobiologie hydromorpher boden. Merkmale, Voraussetzungen und Ursache der Eisenreduktion: Chemie der Erde, v. 32, p. 1-44.
- Ragone, S. E., 1977, Geochemical effects of recharging the Magothy Aquifer, Bay Park, New York, with tertiary-treated sewage: U.S. Geological Survey Professional Paper 751-D, 22 p.
- Ragone, S. E., Vecchioli, John, and Ku, H. F. H., 1973, Short-term effect of injection of tertiary-treated sewage on the concentration of iron in water in the Magothy Aquifer, Bay Park, New York, in Preprints of Second International Symposium on Underground Waste Management and Artificial Recharge, New Orleans, 1973: American Association of Petroleum Geologists, v. 1, p. 273-290.
- Vecchioli, John, Bennett, G. D., Pearson, F. J., Jr., and Cerrillo, L. A., 1974, Geohydrology of the artificial recharge site at Bay Park, Long Island, New York: U.S. Geological Survey Professional Paper 751-C, 29 p.
- Vecchioli, John, Oliva, J. A., Ragone, S. E., and Ku, H. F. H., 1975, Wastewater reclamation and recharge, Bay Park, N. Y.: Proceedings of the American Society of Civil Engineering, Journal of the Environmental Engineering Division, v. 101, no. GE2, Proceedings Paper 11232, p. 201-214.
- Walther, R., Hippe, H., and Gottschalk, G., 1977, Citrate a specific substrate for the isolation of *Clostridium sphenoides*: Applied and Environmental Microbiology, v. 33, p. 955-962.
- Wolin, E. A., Wolin, M. J., and Wolfe, R. S., 1963, Formation of methane by bacterial extracts: Journal of Biological Chemistry, v. 238, p. 2882-2886.
- Zeikus, J. G., 1977, The biology of methanogenic bacteria: Bacteriological Reviews, v. 41, p. 514-541.

ANNUAL INDEX TO VOLUME 6

Journal of Research of the U.S. Geological Survey

[Issue number precedes colon: page number follows colon]

SUBJECT INDEX

A

- absolute age** *see also* geochronology; isotopes
absolute age—dates
 granite: Granite of Rosalie Peak, a phase of the 1700-million-year-old Mount Evans Pluton, Front Range, Colorado 4:447
 — Potassium-argon ages of basement rocks from Saint George Island, Alaska 4:435
 igneous rocks: Age and composition of igneous rocks, Edna Mountain Quadrangle, Humboldt County, Nevada 6:727
 pyroclastics: Holocene pyroclastic-flow deposits from Shastina and Black Butte, west of Mount Shasta, California 5:611
 rhyolite: Blue Ribbon Lineament, an east-trending structural zone within the Pi-oche mineral belt of southwestern Utah and eastern Nevada 2:175
 — Pleistocene rhyolite of the Mineral Mountains, Utah; geothermal and archaeological significance 1:133
 volcanic rocks: Comendite (peralkaline rhyolite) and basalt in the Mitu Group, Peru; evidence for Permian-Triassic lithospheric extension in the central Andes 4:453
 — Galiuro Volcanics, Pinal, Graham, and Cochise counties, Arizona 1:115
 — Radiometric ages of some Cretaceous and Tertiary volcanic and intrusive rocks in South-central Arizona 4:439
Alaska—geochronology
 Paleogene: Potassium-argon ages of basement rocks from Saint George Island, Alaska 4:435
Alaska—geomorphology
 volcanic features: A tuya in Togiak Valley, Southwest Alaska 2:193
Alaska—geophysical surveys
 seismic surveys: Refraction studies between Icy Bay and Kayak Island, eastern Gulf of Alaska 5:625

- Alaska—mineralogy**
 ring silicates: Ferroaxinites from the Feather River area, northern California, and from the McGrath and Russian Mission quadrangles, Alaska 5:603
- Alaska—paleontology**
 Radiolaria: Upper Devonian radiolarians separated from chert of the Ford Lake Shale, Alaska 6:775
- aluminum—geochemistry**
 complexes: Studies of hydroxyaluminum complexes in aqueous solution 3:325
- Andes—tectonophysics**
 plate tectonics: Comendite (peralkaline rhyolite) and basalt in the Mitu Group, Peru; evidence for Permian-Triassic lithospheric extension in the central Andes 4:453
- Antarctica—petrology**
 intrusions: Igneous and metamorphic petrology of the southwestern Dana Mountains, Lassiter Coast, Antarctic Peninsula 1:95
- Arizona—geochemistry**
 Tertiary: Galiuro Volcanics, Pinal, Graham, and Cochise counties, Arizona 1:115
- Arizona—geochronology**
 Cretaceous: Radiometric ages of some Cretaceous and Tertiary volcanic and intrusive rocks in South-central Arizona 4:439
 Oligocene: Radiometric ages of some Cretaceous and Tertiary volcanic and intrusive rocks in South-central Arizona 4:439
- Arizona—paleontology**
 Coelenterata: Iowaphyllum (rugose coral) from the Upper Devonian of Arizona 6:797
- Arizona—petrology**
 igneous rocks: Galiuro Volcanics, Pinal, Graham, and Cochise counties, Arizona 1:115
- Atlantic Coastal Plain—environmental geology**
 ecology: Accuracy and consistency comparisons of land use and land cover maps made from high-altitude photographs and Landsat multispectral imagery 1:23
 land use: Accuracy and consistency comparisons of land use and land cover maps made from high-altitude photographs and Landsat multispectral imagery 1:23
 — An evaluation of errors in mapping land use changes for the Central Atlantic Regional Ecological Test Site 3:339
 maps: Accuracy and consistency comparisons of land use and land cover maps made from high-altitude photographs and Landsat multispectral imagery 1:23
 — An evaluation of errors in mapping land use changes for the Central Atlantic Regional Ecological Test Site 3:339
- Atlantic Coastal Plain—geophysical surveys**
 remote sensing: Accuracy and consistency comparisons of land use and land cover maps made from high-altitude photographs and Landsat multispectral imagery 1:23
- Atlantic Coastal Plain—paleobotany**
 biogeography: New Paleogene pollen species from the Gulf and Atlantic coastal plains 5:691
- Atlantic Coastal Plain—sedimentary petrology**
 weathering: Origin of two clay-mineral facies of the Potomac Group (Cretaceous) in the Middle Atlantic States 2:203
- Atlantic Ocean—oceanography**
 sediments: Heavy-mineral variability in the Baltimore Canyon trough area 2:215
- automatic data processing—economic geology**
 mineral exploration: Porphyry copper exploration model for northern Sonora, Mexico 1:51

automatic data processing—environmental geology

cartography: An "optimal" filter for maps showing nominal data 2:161
digital techniques: Inventory of land use and land cover of the Puget Sound region using Landsat digital data 6:807
 — Low-cost computer classification of land cover in the Portland area, Oregon, by signature extension techniques 6:815

automatic data processing—general

cartography: Use of a remote computer terminal during field checking of Landsat digital maps 4:511

automatic data processing—geophysical surveys

remote sensing: Remote-sensing methods for monitoring surface coal mining in the northern Great Plains 2:149

automatic data processing—sedimentary petrology

environmental analysis: Discrimination of fluvial and eolian deposits by number-frequency analysis of sediments of sand through silt size from a point bar, Rio Puerco, New Mexico 4:499

B**barite** *see also under economic geology under Nevada***Basin and Range Province—structural geology**

tectonics: Geometry and rates of change of fault-generated range fronts, North-central Nevada 5:637

Bering Sea—tectonophysics

plate tectonics: Potassium-argon ages of basement rocks from Saint George Island, Alaska 4:435

biogeography *see also under paleobotany under Atlantic Coastal Plain; Gulf Coastal Plain; see also under paleontology under North America***brines—properties**

thermochemical properties: Models for calculating density and vapor pressure of geothermal brines 2:247

British Columbia—stratigraphy

Miocene: Late Miocene mollusks from the Queen Charlotte Islands, British Columbia, Canada 5:677

C**California—geochronology**

Holocene: Holocene pyroclastic-flow deposits from Shastina and Black Butte, west of Mount Shasta, California 5:611

California—mineralogy

ring silicates: Ferroaxinites from the Feather River area, northern California, and from the McGrath and Russian Mission quadrangles, Alaska 5:603

California—petrology

igneous rocks: Fusion of granodiorite by basalt, central Sierra Nevada 4:459
metamorphism: Metamorphic forsterite and diopside from the ultramafic complex at the Tuolumne River, California 1:73

California—stratigraphy

Cretaceous: Paleomagnetic evidence for a Late Cretaceous deformation of the Great Valley Sequence, Sacramento Valley, California 3:383

Mesozoic: Significance of age relations above and below Upper Jurassic ophiolite in The Geysers-Clear Lake region, California 6:715

Pleistocene: Pleistocene history of volcanism and the Owens River near Little Lake, California 3:395

California—structural geology

neotectonics: Trenches across the 1906 trace of the San Andreas Fault in northern San Mateo County, California 3:347

tectonics: Paleomagnetic evidence for a Late Cretaceous deformation of the Great Valley Sequence, Sacramento Valley, California 3:383

Canada *see also Atlantic Coastal Plain; British Columbia; Rocky Mountains*

carbon—isotopes

C-13/C-12: Stable isotope studies of bedded barite at East Northumberland Canyon in Toquima Range, central Nevada 2:221

Carboniferous—paleontology

Ostracoda: Tribolbina Latham, 1932, an Early Carboniferous through Permian palaeocopid Ostracode genus 5:663

chemical analysis—techniques

sample preparation: Spectrochemical determination of submicrogram amounts of tungsten in geologic materials 2:259

— Spectrophotometric determination of tungsten in rocks by using zinc-dithiol 6:697

clastic rocks *see under sedimentary rocks***clastic sediments** *see under sediments***clay mineralogy—areal studies**

Atlantic Coastal Plain: Origin of two clay mineral facies of the Potomac Group (Cretaceous) in the Middle Atlantic States 2:203

coal *see also under economic geology under Montana*

Coelenterata—Rugosa

Devonian: Iowaphyllum (rugose coral) from the Upper Devonian of Arizona 6:797

Colorado—geochronology

Proterozoic: Granite of Rosalie Peak, a phase of the 1700-million-year-old Mount Evans Pluton, Front Range, Colorado 4:447

Colorado—petrology

intrusions: Petrology of the Precambrian intrusive center at Lake George, southern Front Range, Colorado 1:81

continental shelf *see also under oceanography under Pacific Ocean***copper** *see also under economic geology under Mexico; Nevada***copper—genesis**

mechanism: Pressure gradients and boiling as mechanisms for localizing ore in porphyry systems 6:745

Cretaceous *see also under geochronology under Arizona; see also under stratigraphy under California***crust** *see also under tectonophysics under Idaho***crystal chemistry** *see also crystal growth; minerals***crystal chemistry—oxides**

avicennite: Occurrence and formation of avicennite, Tl_2O_3 , as a secondary mineral at the Carlin gold deposit, Nevada 2:241

crystal chemistry—ring silicates

axinite: Ferroaxinites from the Feather River area, northern California, and from the McGrath and Russian Mission quadrangles, Alaska 5:603

crystal growth *see also crystal chemistry; minerals***crystal growth—silicates**

forsterite: Metamorphic forsterite and diopside from the ultramafic complex at the Tuolumne River, California 1:73

crystal growth—sulfides

phase equilibria: Differentiation of the sulfides in the Basal Zone of the Stillwater Complex, Montana 4:473

crystal structure *see also crystal chemistry; minerals***crystal structure—ring silicates**

axinite: Ferroaxinites from the Feather River area, northern California, and from the McGrath and Russian Mission quadrangles, Alaska 5:603

D**deformation** *see also geophysics***Devonian** *see also under stratigraphy under Nevada***diagenesis** *see also sedimentation***diastrophism** *see orogeny***E****earthquakes** *see also engineering geology; see also under seismology under Midwest***Eastern Hemisphere** *see also Antarctica; Atlantic Ocean***ecology** *see also under environmental geology under Atlantic Coastal Plain***engineering geology** *see also ground water; mining geology***engineering geology—materials, properties**

sandstone: Hydrochemistry and hydrodynamics of injecting an iron-rich pickling liquor into a dolomitic sandstone; a laboratory study 1:1

environmental geology *see also* engineering geology
epeirogeny *see also* orogeny
Europe *see also* the individual nations

F**faults—displacements**

normal faults: Dating Quaternary faults in the southwestern United States by using buried calcic paleosols 3:369

faults—effects

observations: Trenches across the 1906 trace of the San Andreas Fault in northern San Mateo County, California 3:347

faults—systems

grabens: Time relation of the Watchung Basalt flows to the faulting in the Newark Graben 3:391

fission-track dating *see under* geochronology**Florida—hydrogeology**

hydrology: Application of four input-output models for nutrients in Lake Okeechobee, Florida 6:821

fluid inclusions—geologic thermometry

hydrothermal fluids: Wood River mining district, Idaho; intrusion related lead-silver deposits derived from country rock source 5:579

fluid inclusions—temperature

ore-forming fluids: Pressure gradients and boiling as mechanisms for localizing ore in porphyry systems 6:745

fossil man—distribution

artifacts: Pleistocene rhyolite of the Mineral Mountains, Utah; geothermal and archaeological significance 1:133

fossils *see appropriate fossil group***G**

genesis of ore deposits *see* mineral deposits, genesis

geochemistry—processes

dissolution: Uranium in waters and aquifer rocks at the Nevada Test Site, Nye County, Nevada 4:489

oxidation: Recognition of oxidized sulfide minerals as an exploration guide for uranium 4:483

precipitation: Factors contributing to the formation of ferromanganese nodules in Oneida Lake, New York 2:231

redox: Iron in water near wastewater lagoons in Yellowstone National Park, Wyoming 3:319

geochemistry—properties

physicochemical properties: Studies of hydroxylaluminum complexes in aqueous solution 3:325

solubility: Solubility of high soluble salts in aqueous media; Part 1, NaCl, KCl, CaCl₂, Na₂SO₄, and K₂SO₄ solubilities to 100°C 6:701

thermochemical properties: Models for calculating density and vapor pressure of geothermal brines 2:247

geochronology *see also* absolute age**geochronology—fission-track dating**

plutonic rocks: Radiometric ages of some Cretaceous and Tertiary volcanic and intrusive rocks in South-central Arizona 4:439

geochronology—methods

paleosols: Dating Quaternary faults in the southwestern United States by using buried calcic paleosols 3:369

geochronology—surveys

rhyolite: Pleistocene rhyolite of the Mineral Mountains, Utah; geothermal and archaeological significance 1:133

geochronology—tephrochronology

pyroclastic flows: Holocene pyroclastic-flow deposits from Shastina and Black Butte, west of Mount Shasta, California 5:611

geologic hazards *see also* under environmental geology under Midwest; Pacific Coast

geologic hazards—floods

mapping: Accuracy of flood mapping 4:515

geomorphology *see also* glacial geology**geomorphology—fluvial features**

rivers: Structural control of the Cumberland River and its ancestral channels at Flat Lick, Kentucky 3:359

geomorphology—landform evolution

drainage systems: Pleistocene history of volcanism and the Owens River near Little Lake, California 3:395

fronts: Geometry and rates of change of fault-generated range fronts, North-central Nevada 5:637

geomorphology—volcanic features

tuyas: A tuya in Togiak Valley, Southwest Alaska 2:193

geophysical surveys *see* seismic surveys under geophysical surveys under Alaska

geophysics *see also* engineering geology**geophysics—theoretical studies**

brines: Models for calculating density and vapor pressure of geothermal brines 2:247

Georgia—environmental geology

land use: Accuracy of selected land use and land cover maps in the Greater Atlanta region, Georgia 2:169

maps: Accuracy of selected land use and land cover maps in the Greater Atlanta region, Georgia 2:169

geosynclines *see also* orogeny**geotechnics** *see* engineering geology

geothermal energy *see also* under economic geology under Utah

geothermal energy—production

theoretical studies: Models for calculating density and vapor pressure of geothermal brines 2:247

glacial geology *see also* geomorphology**glacial geology—glacial features**

grooves: Giant glacial grooves at the north end of the Mission Range, Northwest Montana 4:425

glacial geology—glaciation

erosion: A tuya in Togiak Valley, Southwest Alaska 2:193

glaciation *see under* glacial geology**grabens** *see under* systems under faults

granite *see also* under granite-granodiorite family under igneous rocks

Greece—paleontology

Ostracoda: Tribolbina Latham, 1932, an Early Carboniferous through Permian palaeocarpid Ostracode genus 5:663

ground water *see also* hydrology**ground water—surveys**

Indiana: Hydraulic characteristics of the White River streambed and glacial-outwash deposits at a site near Indianapolis, Indiana 2:273

Michigan: Three-dimensional finite-difference model of ground-water system underlying the Muskegon County wastewater disposal system, Michigan 3:307

Missouri: Relationship between hydrology and bottomland vegetation in the Ozark Mountains of Missouri 3:299

Nevada: Uranium in waters and aquifer rocks at the Nevada Test Site, Nye County, Nevada 4:489

New York: Impact of sewerage systems on stream base flow and ground-water recharge on Long Island, New York 2:263

— Reconnaissance for microbial activity in the Magathy Aquifer, Bay Park, New York, four years after artificial recharge 6:829

Wyoming: Iron in water near wastewater lagoons in Yellowstone National Park, Wyoming 3:319

Gulf Coastal Plain—paleobotany

biogeography: New Paleogene pollen species from the Gulf and Atlantic coastal plains 5:691

gymnosperms—Coniferales

ecology: Conductive heat flows in research drill holes in thermal areas of Yellowstone National Park, Wyoming 6:765

H

heat flow *see also* under geophysical surveys under Wyoming

helium—abundance

soils: Helium in soil gases of the Roosevelt Hot Springs known geothermal resource area, Beaver County, Utah 5:563

Holocene *see also* under geochronology under California

hydrogeology *see also* ground water; hydrology

hydrology *see also* ground water

hydrology—rivers and streams

tracer experiments: Preliminary evaluation of the floating dome method of measuring reeration rates 4:547

hydrology—surveys

Florida: Application of four input-output models for nutrients in Lake Okeechobee, Florida 6:821

Indiana: Hydraulic characteristics of the White River streambed and glacial-outwash deposits at a site near Indianapolis, Indiana 2:273
Missouri: Relationship between hydrology and bottomland vegetation in the Ozark Mountains of Missouri 3:299
New York: Determination of runoff coefficients of storm-water-basin drainage areas on Long Island, New York, by using maximum-stage gages 1:11
— Factors contributing to the formation of ferromanganese nodules in Oneida Lake, New York 2:231
— Impact of sewerage systems on stream base flow and ground-water recharge on Long Island, New York 2:263
— Infiltration from tributary streams in the Susquehanna River basin, New York 3:285
Susquehanna River: Definition of regional relationships between dissolved solids and specific conductance, Susquehanna River basin, Pennsylvania and New York 4:541
Wyoming: Iron in water near wastewater lagoons in Yellowstone National Park, Wyoming 3:319

I**ichnofossils—morphology**

interpretation: A reexamination of the Pennsylvanian trace fossil Olivellites 6:789

Idaho—economic geology

lead: Wood River mining district, Idaho; intrusion related lead-silver deposits derived from country rock source 5:579

silver: Wood River mining district, Idaho; intrusion related lead-silver deposits derived from country rock source 5:579

Idaho—tectonophysics

crust: Regional gravity and magnetic anomalies in the eastern Snake River plain, Idaho 5:553

igneous rocks *see also* magmas; metamorphic rocks; metasomatism; phase equilibria

igneous rocks—alteration

melting: Fusion of granodiorite by basalt, central Sierra Nevada 4:459

igneous rocks—andesite-rhyolite family

rhyolite: Pleistocene rhyolite of the Mineral Mountains, Utah; geothermal and archaeological significance 1:133

igneous rocks—geochronology

petrology: Galiuro Volcanics, Pinal, Graham, and Cochise counties, Arizona 1:115

igneous rocks—granite-granodiorite family

granite: Granite of Rosalie Peak, a phase of the 1700-million-year-old Mount Evans Pluton, Front Range, Colorado 4:447

igneous rocks—plutonic rocks

composition: Age and composition of igneous rocks, Edna Mountain Quadrangle, Humboldt County, Nevada 6:727

petrology: Petrology of the Precambrian intrusive center at Lake George, southern Front Range, Colorado 1:81

igneous rocks—ultramafic family

ophiolite: Significance of age relations above and below Upper Jurassic ophiolite in The Geysers-Clear Lake region, California 6:715

igneous rocks—volcanic rocks

age: Radiometric ages of some Cretaceous and Tertiary volcanic and intrusive rocks in South-central Arizona 4:439

genesis: Comendite (peralkaline rhyolite) and basalt in the Mitu Group, Peru; evidence for Permian-Triassic lithospheric extension in the central Andes 4:453
geochemistry: Chemistry of Tertiary volcanic rocks in the Eldorado Mountains, Clark County, Nevada, and comparisons with rocks from some nearby areas 3:409

inclusions *see also* fluid inclusions**Indiana—hydrogeology**

ground water: Hydraulic characteristics of the White River streambed and glacial-outwash deposits at a site near Indianapolis, Indiana 2:273

industrial minerals *see also under* economic geology *under* Pacific Coast

intrusions—age

absolute age: Potassium-argon ages of basement rocks from Saint George Island, Alaska 4:435

intrusions—mechanism

stress: Hypothesis; many earthquakes in the central and southeastern United States are causally related to mafic intrusive bodies 1:41

intrusions—plugs

contact: Fusion of granodiorite by basalt, central Sierra Nevada 4:459

intrusions—plutons

age: Granite of Rosalie Peak, a phase of the 1700-million-year-old Mount Evans Pluton, Front Range, Colorado 4:447

complexes: Age and composition of igneous rocks, Edna Mountain Quadrangle, Humboldt County, Nevada 6:727

petrology: Igneous and metamorphic petrology of the southwestern Dana Mountains, Lassiter Coast, Antarctic Peninsula 1:95

— Petrology of the Precambrian intrusive center at Lake George, southern Front Range, Colorado 1:81

Invertebrates *see also* Coelenterata; Ichnofossils; Mollusca; Ostracoda; Radiolaria

iron—abundance

water: Iron in water near wastewater lagoons in Yellowstone National Park, Wyoming 3:319

iron—geochemistry

precipitation: Factors contributing to the formation of ferromanganese nodules in Oneida Lake, New York 2:231

isotope dating *see* absolute age

isotopes *see also* absolute age; geochronology

isotopes—barite

analysis: Stable isotope studies of bedded barite at East Northumberland Canyon in Toquima Range, central Nevada 2:221

isotopes—ratios

polymetallic ores: Wood River mining district, Idaho; intrusion related lead-silver deposits derived from country rock source 5:579

isotopes—thermal waters

radioactive isotopes: Natural radioactivity in geothermal waters, Alhambra Hot Springs and nearby areas, Jefferson County, Montana 4:529

K**Kentucky—geomorphology**

fluvial features: Structural control of the Cumberland River and its ancestral channels at Flat Lick, Kentucky 3:359

Kentucky—sedimentary petrology

sedimentary rocks: Petrographic differentiation of depositional environments of sandstones of the Pennsylvanian Breathitt Formation, northeastern Kentucky and southwestern West Virginia 5:593

L**land use** *see also under* environmental geology

under Atlantic Coastal Plain; Georgia; Montana; Oregon; Washington

land use—management

floodplains: Accuracy of flood mapping 4:515

land use—maps

cartography: An “optimal” filter for maps showing nominal data 2:161

lava *see also* igneous rocks; magmas

lava—age

Pleistocene: Pleistocene history of volcanism and the Owens River near Little Lake, California 3:395

Triassic: Time relation of the Watchung Basalt flows to the faulting in the Newark Graben 3:391

lava—composition

chemical composition: Comendite (peralkaline rhyolite) and basalt in the Mitu Group, Peru; evidence for Permian-Triassic lithospheric extension in the central Andes 4:453

lava—petrology

lava flows: Galiuro Volcanics, Pinal, Graham, and Cochise counties, Arizona 1:115

lead *see also under* economic geology *under* Idaho

lunar studies *see* Moon

M

magmas *see also* igneous rocks; intrusions; lava

magmas—differentiation

plutons: Petrology of the Precambrian intrusive center at Lake George, southern Front Range, Colorado 1:81
sulfides: Differentiation of the sulfides in the Basal Zone of the Stillwater Complex, Montana 4:473

man, fossil *see* fossil man

manganese—geochemistry

precipitation: Factors contributing to the formation of ferromanganese nodules in Oneida Lake, New York 2:231

maps *see also under* environmental geology under Atlantic Coastal Plain; Georgia; Pacific Coast

maps—cartography

automatic data processing: Use of a remote computer terminal during field checking of Landsat digital maps 4:511

floodplains: Accuracy of flood mapping 4:515

Mars—geomorphology

erosion features: Morphology of chasma walls, Mars 5:651

mathematical geology *see also* automatic data processing

Mesozoic *see also under* geochronology under Nevada; *see also under* stratigraphy under California

metals *see also* aluminum; iron; manganese; molybdenum; tungsten; *see also under* economic geology under Utah

metamorphic rocks *see also* igneous rocks; metamorphism; metasomatism

metamorphic rocks—metasedimentary rocks

petrology: Igneous and metamorphic petrology of the southwestern Dana Mountains, Lassiter Coast, Antarctic Peninsula 1:95

metamorphism—contact metamorphism

intrusions: Igneous and metamorphic petrology of the southwestern Dana Mountains, Lassiter Coast, Antarctic Peninsula 1:95

metamorphism—P-T conditions

mineral assemblages: Metamorphic forsterite and diopside from the ultramafic complex at the Tuolumne River, California 1:73

metamorphism—thermal metamorphism

effects: Fusion of granodiorite by basalt, central Sierra Nevada 4:459

metasomatic rocks—serpentinite

petrography: Metamorphic forsterite and diopside from the ultramafic complex at the Tuolumne River, California 1:73

metasomatism—materials

granodiorite: Fusion of granodiorite by basalt, central Sierra Nevada 4:459

metasomatism—processes

serpentinitization: Metamorphic forsterite and diopside from the ultramafic complex at the Tuolumne River, California 1:73

Mexico *see also* Gulf Coastal Plain

Mexico—economic geology

copper: Porphyry copper exploration model for northern Sonora, Mexico 1:51

— Porphyry-type metallization and alteration at La Florida de Nacozari, Sonora, Mexico 1:59

Mexico—structural geology

tectonics: Porphyry copper exploration model for northern Sonora, Mexico 1:51

Michigan—engineering geology

waste disposal: Three-dimensional finite-difference model of ground-water system underlying the Muskegon County wastewater disposal system, Michigan 3:307

Midwest—environmental geology

geologic hazards: Hypothesis; many earthquakes in the central and southeastern United States are causally related to mafic intrusive bodies 1:41

Midwest—seismology

earthquakes: Hypothesis; many earthquakes in the central and southeastern United States are causally related to mafic intrusive bodies 1:41

mineral deposits, genesis—controls

geochemical controls: Pressure gradients and boiling as mechanisms for localizing ore in porphyry systems 6:745

structural controls: Blue Ribbon Lineament, an east-trending structural zone within the Pioche mineral belt of southwestern Utah and eastern Nevada 2:175

— Porphyry copper exploration model for northern Sonora, Mexico 1:51

mineral deposits, genesis—polymetallic ores

ore-forming fluids: Wood River mining district, Idaho; intrusion related lead-silver deposits derived from country rock source 5:579

mineral deposits, genesis—processes

hydrothermal processes: Implications of the petrochemistry of palladium at Iron Canyon, Lander County, Nevada 1:107

— Porphyry-type metallization and alteration at La Florida de Nacozari, Sonora, Mexico 1:59

syngensis: Stable isotope studies of bedded barite at East Northumberland Canyon in Toquima Range, central Nevada 2:221

mineral exploration—geochemical methods

trace elements: Spectrochemical determination of submicrogram amounts of tungsten in geologic materials 2:259

mineral exploration—ore guides

uranium: Iron-titanium oxide minerals and associated alteration phases in some uranium-bearing sandstones 6:707

— Recognition of oxidized sulfide minerals as an exploration guide for uranium 4:483

mineral exploration—remote sensing
ore guides: Porphyry copper exploration model for northern Sonora, Mexico 1:51

mineral prospecting *see* mineral exploration

minerals *see also* crystal chemistry; crystal growth; crystal structure

minerals—experimental studies

properties: Solubility of high soluble salts in aqueous media; Part 1, NaCl, KCl, CaCl₂, Na₂SO₄, and K₂SO₄ solubilities to 100°C 6:701

minerals—framework silicates, zeolite group

chabazite: Chabazite in siliceous tuffs of a Pliocene lacustrine deposit near Durkee, Baker County, Oregon 4:467

minerals—oxides

avcennite: Occurrence and formation of avcennite, Ti₂O₃, as a secondary mineral at the Carlin gold deposit, Nevada 2:241

experimental studies: Studies of hydroxyl-aluminum complexes in aqueous solution 3:325

limonite: Recognition of oxidized sulfide minerals as an exploration guide for uranium 4:483

occurrence: Iron-titanium oxide minerals and associated alteration phases in some uranium-bearing sandstones 6:707

minerals—ring silicates

axinite: Ferroaxinites from the Feather River area, northern California, and from the McGrath and Russian Mission quadrangles, Alaska 5:603

minerals—sheet silicates, clay minerals

occurrence: Origin of two clay-mineral facies of the Potomac Group (Cretaceous) in the Middle Atlantic States 2:203

minerals—silicates

forsterite: Metamorphic forsterite and diopside from the ultramafic complex at the Tuolumne River, California 1:73

minerals—sulfates

barite: Stable isotope studies of bedded barite at East Northumberland Canyon in Toquima Range, central Nevada 2:221

minerals—sulfides

crystal growth: Differentiation of the sulfides in the Basal Zone of the Stillwater Complex, Montana 4:473

mining geology—methods

remote sensing: Remote-sensing methods for monitoring surface coal mining in the northern Great Plains 2:149

Miocene *see also under* stratigraphy under British Columbia

Mississippian *see also* Carboniferous

Missouri—hydrogeology

hydrology: Relationship between hydrology and bottomland vegetation in the Ozark Mountains of Missouri 3:299

Mollusca—faunal studies
Miocene: Late Miocene mollusks from the Queen Charlotte Islands, British Columbia, Canada 5:677

molybdenum—genesis
mechanism: Pressure gradients and boiling as mechanisms for localizing ore in porphyry systems 6:745

Montana—economic geology
coal: Remote-sensing methods for monitoring surface coal mining in the northern Great Plains 2:149

Montana—environmental geology
land use: Remote-sensing methods for monitoring surface coal mining in the northern Great Plains 2:149

Montana—geomorphology
glacial geology: Giant glacial grooves at the north end of the Mission Range, Northwest Montana 4:425

Montana—geophysical surveys
remote sensing: Remote-sensing methods for monitoring surface coal mining in the northern Great Plains 2:149

Montana—hydrogeology
springs: Natural radioactivity in geothermal waters, Alhambra Hot Springs and nearby areas, Jefferson County, Montana 4:529

thermal waters: Natural radioactivity in geothermal waters, Alhambra Hot Springs and nearby areas, Jefferson County, Montana 4:529

Montana—petrology
magmas: Differentiation of the sulfides in the Basal Zone of the Stillwater Complex, Montana 4:473

Moon—surface properties
brightness: Spectral gradient of lunar radiobrightness; heat flow or volume scattering? 4:505

mud volcanoes *see also* volcanology

N

Neogene *see also under* geochronology *under* Utah

neotectonics *see also under* structural geology *under* California; New Mexico

Nevada—economic geology
barite: Stable isotope studies of bedded barite at East Northumberland Canyon in Toquima Range, central Nevada 2:221

copper: Implications of the petrochemistry of palladium at Iron Canyon, Lander County, Nevada 1:107

palladium: Implications of the petrochemistry of palladium at Iron Canyon, Lander County, Nevada 1:107

Nevada—geochemistry
isotopes: Stable isotope studies of bedded barite at East Northumberland Canyon in Toquima Range, central Nevada 2:221

trace elements: Implications of the petrochemistry of palladium at Iron Canyon, Lander County, Nevada 1:107

uranium: Uranium in waters and aquifer rocks at the Nevada Test Site, Nye County, Nevada 4:489

volcanic rocks: Chemistry of Tertiary volcanic rocks in the Eldorado Mountains, Clark County, Nevada, and comparisons with rocks from some nearby areas 3:409

Nevada—geochronology
Mesozoic: Age and composition of igneous rocks, Edna Mountain Quadrangle, Humboldt County, Nevada 6:727

Nevada—geomorphology
landform evolution: Geometry and rates of change of fault-generated range fronts, North-central Nevada 5:637

Nevada—mineralogy
oxides: Occurrence and formation of avocennite, Tl_2O_3 , as a secondary mineral at the Carlin gold deposit, Nevada 2:241

Nevada—stratigraphy
Devonian: Stable isotope studies of bedded barite at East Northumberland Canyon in Toquima Range, central Nevada 2:221

Nevada—structural geology
tectonics: Blue Ribbon Lineament, an east-trending structural zone within the Piñon mineral belt of southwestern Utah and eastern Nevada 2:175

New Jersey—stratigraphy
Triassic: Time relation of the Watchung Basalt flows to the faulting in the Newark Graben 3:391

New Mexico—sedimentary petrology
sediments: Discrimination of fluvial and eolian deposits by number-frequency analysis of sediments of sand through silt size from a point bar, Rio Puerco, New Mexico 4:499

New Mexico—structural geology
neotectonics: Dating Quaternary faults in the southwestern United States by using buried calcic paleosols 3:369

New York—geochemistry
nodules: Factors contributing to the formation of ferromanganese nodules in Oneida Lake, New York 2:231

New York—hydrogeology
ground water: Impact of sewerage systems on stream base flow and ground-water recharge on Long Island, New York 2:263

— Reconnaissance for microbial activity in the Magathy Aquifer, Bay Park, New York, four years after artificial recharge 6:829

hydrology: Definition of regional relationships between dissolved solids and specific conductance, Susquehanna River basin, Pennsylvania and New York 4:541

— Determination of runoff coefficients of storm-water-basin drainage areas on Long Island, New York, by using maximum-stage gages 1:11

— Infiltration from tributary streams in the Susquehanna River basin, New York 3:285

noble gases *see also* helium

nodules—ferromanganese composition
genesis: Factors contributing to the formation of ferromanganese nodules in Oneida Lake, New York 2:231

nonmetals *see also* sulfur

North America *see also* Atlantic Coastal Plain; Gulf Coastal Plain; Mexico; Rocky Mountains

North America—paleontology
biogeography: Late Miocene mollusks from the Queen Charlotte Islands, British Columbia, Canada 5:677

Northern Hemisphere *see also* Atlantic Ocean; North America; Pacific Ocean

O

Oligocene *see also under* geochronology *under* Arizona

ophiolite *see under* ultramafic family *under* igneous rocks

ore guides *see under* mineral exploration

Oregon—environmental geology
land use: Low-cost computer classification of land cover in the Portland area, Oregon, by signature extension techniques 6:815

Oregon—mineralogy
framework silicates, zeolite group: Chabazite in siliceous tuffs of a Pliocene lacustrine deposit near Durkee, Baker County, Oregon 4:467

orogeny—absolute age
Laramide Orogeny: Radiometric ages of some Cretaceous and Tertiary volcanic and intrusive rocks in South-central Arizona 4:439

Ostracoda—Paleocopida
Carboniferous: Tribolbina Latham, 1932, an Early Carboniferous through Permian palaeocopid Ostracode genus 5:663

oxides *see under* minerals

oxygen—isotopes
O-18/O-16: Stable isotope studies of bedded barite at East Northumberland Canyon in Toquima Range, central Nevada 2:221

P

Pacific Coast—economic geology
industrial minerals: Chabazite in siliceous tuffs of a Pliocene lacustrine deposit near Durkee, Baker County, Oregon 4:467

Pacific Coast—environmental geology
geologic hazards: Holocene pyroclastic-flow deposits from Shastina and Black Butte, west of Mount Shasta, California 5:611

maps: Inventory of land use and land cover of the Puget Sound region using Landsat digital data 6:807

Pacific Coast—tectonophysics
plate tectonics: Significance of age relations above and below Upper Jurassic ophiolite in The Geysers-Clear Lake region, California 6:715

Pacific Ocean *see also* Bering Sea

Pacific Ocean—oceanography

continental shelf: Refraction studies between Icy Bay and Kayak Island, eastern Gulf of Alaska 5:625

paleoecology—Mollusca

Miocene: Late Miocene mollusks from the Queen Charlotte Islands, British Columbia, Canada 5:677

Paleogene *see also* *under* geochronology under Alaska

paleomagnetism—Cretaceous

California: Paleomagnetic evidence for a Late Cretaceous deformation of the Great Valley Sequence, Sacramento Valley, California 3:383

paleotemperature *see* geologic thermometry under fluid inclusions

Paleozoic *see also* Carboniferous; Permian

palladium—abundance

rocks: Implications of the petrochemistry of palladium at Iron Canyon, Lander County, Nevada 1:107

palynomorphs—miospores

Paleogene: New Paleogene pollen species from the Gulf and Atlantic coastal plains 5:691

Pennsylvania—hydrogeology

hydrology: Definition of regional relationships between dissolved solids and specific conductance, Susquehanna River basin, Pennsylvania and New York 4:541

Pennsylvanian *see also* Carboniferous

Permian—paleontology

Ostracoda: Tribolbina Latham, 1932, an Early Carboniferous through Permian palaeocpid Ostracode genus 5:663

Peru—geochemistry

trace elements: Comendite (peralkaline rhyolite) and basalt in the Mitu Group, Peru; evidence for Permian-Triassic lithospheric extension in the central Andes 4:453

petrology—nomenclature

plutons: Granite of Rosalie Peak, a phase of the 1700-million-year-old Mount Evans Pluton, Front Range, Colorado 4:447

Phanerozoic *see also* Carboniferous; Permian

phase equilibria—sulfides

interpretation: Differentiation of the sulfides in the Basal Zone of the Stillwater Complex, Montana 4:473

phosphorus—abundance

thermal waters: Phosphorus in hydrothermal waters of Yellowstone National Park, Wyoming 6:755

planetology *see also* Mars; Moon

Plantae *see also* gymnosperms; ichnofossils; palynomorphs

plate tectonics *see also* *under* tectonophysics under Andes; Bering Sea; Pacific Coast

Pleistocene *see also* *under* geochronology under Utah; *see also* *under* stratigraphy under California

plutons *see under* intrusions

Proterozoic *see also* *under* geochronology under Colorado

R

radioactive dating *see* absolute age

Radiolaria—biostratigraphy

correlation: Significance of age relations above and below Upper Jurassic ophiolite in The Geysers-Clear Lake region, California 6:715

Radiolaria—faunal studies

Devonian: Upper Devonian radiolarians separated from chert of the Ford Lake Shale, Alaska 6:775

regional geology *see* areal geology

remote sensing *see also* *under* geophysical surveys under Atlantic Coastal Plain; automatic data processing; Montana

remote sensing—automatic data processing

cartography: Use of a remote computer terminal during field checking of Landsat digital maps 4:511

rhyolite *see* *under* andesite-rhyolite family under igneous rocks

ring silicates *see under* minerals

Rocky Mountains—hydrogeology

springs: Phosphorus in hydrothermal waters of Yellowstone National Park, Wyoming 6:755

S

sandstone *see also* *under* clastic rocks under sedimentary rocks

sedimentary rocks *see also* *under* sedimentary structures; sedimentation; sediments

sedimentary rocks—clastic rocks

sandstone: Iron-titanium oxide minerals and associated alteration phases in some uranium-bearing sandstones 6:707

— Petrographic differentiation of depositional environments of sandstones of the Pennsylvanian Breathitt Formation, northeastern Kentucky and southwestern West Virginia 5:593

sedimentary rocks—properties

permeability: Hydrochemistry and hydrodynamics of injecting an iron-rich pickling liquor into a dolomitic sandstone; a laboratory study 1:1

sedimentary structures *see also* sedimentary rocks; sediments

sedimentary structures—biogenic

structures

ichnofossils: A reexamination of the Pennsylvanian trace fossil Olivellites 6:789

sedimentary structures—planar bedding structures

bars: Discrimination of fluvial and eolian deposits by number-frequency analysis of sediments of sand through silt size from a point bar, Rio Puerco, New Mexico 4:499

sedimentary structures—secondary

structures

nodules: Factors contributing to the formation of ferromanganese nodules in Oneida Lake, New York 2:231

sedimentation—environment

streams: Discrimination of fluvial and eolian deposits by number-frequency analysis of sediments of sand through silt size from a point bar, Rio Puerco, New Mexico 4:499

sediments *see also* sedimentary rocks; sedimentary structures; sedimentation

sediments—clastic sediments

grain size: Discrimination of fluvial and eolian deposits by number-frequency analysis of sediments of sand through silt size from a point bar, Rio Puerco, New Mexico 4:499

lithofacies: Origin of two clay-mineral facies of the Potomac Group (Cretaceous) in the Middle Atlantic States 2:203

volcanic ash: Chabazite in siliceous tufts of a Pliocene lacustrine deposit near Durkee, Baker County, Oregon 4:467

sediments—composition

mineral composition: Heavy-mineral variability in the Baltimore Canyon trough area 2:215

seismic surveys *see under* geophysical surveys under Alaska

seismology *see also* engineering geology

silicates *see under* minerals

silver *see also* *under* economic geology under Idaho

slope stability *see also* engineering geology; geomorphology

soils—surveys

New Mexico: Dating Quaternary faults in the southwestern United States by using buried calcic paleosols 3:369

solubility *see under* properties under geochemistry

South America *see also* Andes; Peru

South Carolina—paleobotany

palynomorphs: New Paleogene pollen species from the Gulf and Atlantic coastal plains 5:691

Southern Hemisphere *see also* Antarctica; Atlantic Ocean; Pacific Ocean

Southwestern U.S.—geochronology

methods: Dating Quaternary faults in the southwestern United States by using buried calcic paleosols 3:369

spectrometry *see* spectroscopy

spectroscopy—techniques

sample preparation: Spectrochemical determination of submicrogram amounts of tungsten in geologic materials 2:259

— Spectrophotometric determination of tungsten in rocks by using zinc-dithiol 6:697

springs *see also* ground water; *see also under* hydrogeology under Montana; Rocky Mountains

standard materials—analysis

tungsten: Spectrophotometric determination of tungsten in rocks by using zinc-dithiol 6:697

sulfates *see under* minerals

sulfides *see under* minerals

- sulfur—abundance**
soils: CS₂ and COS in soil gases of the Roosevelt Hot Springs known geothermal resource area, Beaver County, Utah 5:571
- sulfur—isotopes**
S-34/S-32: Stable isotope studies of bedded barite at East Northumberland Canyon in Toquima Range, central Nevada 2:221
- sulphur** *see* Sulfur

T

- tectonics** *see also* faults; orogeny; *see also under* structural geology *under* Basin and Range Province; California; Mexico; Nevada; Utah
- tephrochronology** *see under* geochronology
- Tertiary** *see also under* geochronology *under* Western U.S.
- Texas—paleontology**
ichnofossils: A reexamination of the Pennsylvanian trace fossil Olivellites 6:789
- thermal waters** *see also under* hydrogeology *under* Montana; Utah; Wyoming
- trace elements** *see under* geochemical methods *under* mineral exploration; *see under* geochemistry *under* Nevada; Peru
- Triassic** *see also under* stratigraphy *under* New Jersey
- tungsten—analysis**
spectroscopy: Spectrochemical determination of submicrogram amounts of tungsten in geologic materials 2:259
— Spectrophotometric determination of tungsten in rocks by using zinc-dithiol 6:697

U

- underground water** *see* ground water
- United States** *see also* the individual states and regions
- uranium** *see also under* economic geology *under* Western U.S.
- uranium—abundance**
ground water: Uranium in waters and aquifer rocks at the Nevada Test Site, Nye County, Nevada 4:489
- uranium—exploration**
ore guides: Recognition of oxidized sulfide minerals as an exploration guide for uranium 4:483

- Utah—economic geology**
geothermal energy: Pleistocene rhyolite of the Mineral Mountains, Utah; geothermal and archeological significance 1:133

- metals*: Blue Ribbon Lineament, an east-trending structural zone within the Pi-oche mineral belt of southwestern Utah and eastern Nevada 2:175

- Utah—geochronology**
absolute age: Pleistocene rhyolite of the Mineral Mountains, Utah; geothermal and archeological significance 1:133
Neogene: Blue Ribbon Lineament, an east-trending structural zone within the Pi-oche mineral belt of southwestern Utah and eastern Nevada 2:175

- Pleistocene*: Pleistocene rhyolite of the Mineral Mountains, Utah; geothermal and archeological significance 1:133
surveys: Pleistocene rhyolite of the Mineral Mountains, Utah; geothermal and archeological significance 1:133

- Utah—hydrogeology**
thermal waters: CS₂ and COS in soil gases of the Roosevelt Hot Springs known geothermal resource area, Beaver County, Utah 5:571
— Helium in soil gases of the Roosevelt Hot Springs known geothermal resource area, Beaver County, Utah 5:563

- Utah—structural geology**
tectonics: Blue Ribbon Lineament, an east-trending structural zone within the Pi-oche mineral belt of southwestern Utah and eastern Nevada 2:175

V

- Vertebrata** *see also* fossil man; ichnofossils
- volcanic features** *see under* geomorphology
- volcanism** *see under* volcanology
- volcanoes** *see under* volcanology
- volcanology—volcanism**
age: Pleistocene history of volcanism and the Owens River near Little Lake, California 3:395
— Time relation of the Watchung Basalt flows to the faulting in the Newark Graben 3:391
- igneous activity*: Age and composition of igneous rocks, Edna Mountain Quadrangle, Humboldt County, Nevada 6:727
- subglacial environment*: A tuya in Togiak Valley, Southwest Alaska 2:193

volcanology—volcanoes

- California*: Holocene pyroclastic-flow deposits from Shastina and Black Butte, west of Mount Shasta, California 5:611

W**Washington—environmental geology**

- land use*: Inventory of land use and land cover of the Puget Sound region using Landsat digital data 6:807
— Low-cost computer classification of land cover in the Portland area, Oregon, by signature extension techniques 6:815

waste disposal *see also under* engineering geology *under* Michigan; *see also under* environmental geology *under* Wyoming**waste disposal—industrial waste**

- experimental studies*: Hydrochemistry and hydrodynamics of injecting an iron-rich pickling liquor into a dolomitic sandstone; a laboratory study 1:1

waste disposal—liquid waste

- experimental studies*: Studies of hydroxylaluminum complexes in aqueous solution 3:325

weathering *see also under* sedimentary petrology *under* Atlantic Coastal Plain**West Virginia—sedimentary petrology**

- sedimentary rocks*: Petrographic differentiation of depositional environments of sandstones of the Pennsylvanian Breathitt Formation, northeastern Kentucky and southwestern West Virginia 5:593

Western Hemisphere *see also* Atlantic Ocean; North America; Pacific Ocean**Western U.S.—economic geology**

- uranium*: Iron-titanium oxide minerals and associated alteration phases in some uranium-bearing sandstones 6:707

Western U.S.—geochronology

- Tertiary*: Age and composition of igneous rocks, Edna Mountain Quadrangle, Humboldt County, Nevada 6:727

Wyoming—environmental geology

- waste disposal*: Iron in water near wastewater lagoons in Yellowstone National Park, Wyoming 3:319

Wyoming—geophysical surveys

- heat flow*: Conductive heat flows in research drill holes in thermal areas of Yellowstone National Park, Wyoming 6:765

Wyoming—hydrogeology

- thermal waters*: Phosphorus in hydrothermal waters of Yellowstone National Park, Wyoming 6:755

AUTHOR INDEX

A

- Addicott, W. O. 5:677
 Allison, C. 6:775
 Alt, J. N. 3:347
 Anderson, J. J. 2:175
 Anderson, R. E. 3:409
 Anderson, R. S. 1:81
 Aronson, D. A. 1:11
 Aruscavage, P. 6:697

B

- Banks, N. G. 4:439
 Bayer, K. C. 5:625
 Bersillon, J. L. 3:325
 Bigelow, R. C. 5:563
 Bonilla, M. G. 3:347
 Bowman, H. R. 4:453
 Brown, D. W. 3:325
 Brown, F. H. 1:133
 Bruns, T. R. 5:625
 Bryant, B. 4:447
 Burkham, D. E. 4:515

C

- Calk, L. C. 4:459
 Campbell, E. Y. 6:697
 Carlson, R. R. 1:107
 Clyne, M. A. 6:701
 Coonrad, W. L. 2:193
 Cox, E. R. 3:319
 Creasey, S. C. 1:115
 Cunningham, C. G. 5:745

D

- Dean, W. E. 2:231
 Denton, E. H. 5:563
 Dickson, F. W. 2:241
 Dingman, R. J. 1:1
 Dockter, R. D. 4:439
 Dodge, F. C. W. 4:459
 Doe, B. R. 5:579
 Duffield, W. A. 3:395

E

- Ehrlich, G. G. 6:829
 England, A. W. 4:505
 Erd, R. C. 5:603
 Erickson, R. L. 6:727
 Evans, S. H., Jr. 1:133

F

- Faust, G. T. 3:391
 Fiessinger, F. 3:325
 Fitzpatrick-Lins, K. 1:23; 2:169; 3:339

- Fleck, W. B. 3:307
 Flores, R. M. 5:593
 Force, L. M. 2:203
 Francis, F. S. 1:1
 Frederiksen, N. O. 5:691
 Friedman, I. 1:133

G

- Gaydos, L. 6:807, 815
 Ghosh, S. K. 2:231
 Godsy, E. M. 6:829
 Goldhaber, M. B. 4:483; 6:707
 Grimes, D. J. 2:259
 Gude, A. J., III. 4:467
 Guptill, S. C. 2:161

H

- Haas, J. L., Jr. 2:247
 Hall, W. E. 5:579
 Harms, T. F. 5:571
 Harvey, E. J. 3:299
 Hedge, C. E. 4:447
 Hem, J. D. 3:325
 Hietanen, A. 5:603
 Hinkle, M. E. 5:563, 571
 Hoare, J. M. 2:193
 Hodgen, L. D. 3:347
 Holdsworth, B. K. 6:775
 Hopkins, D. M. 4:435
 Hutchinson, C. F. 4:511

I

- Izett, G. A. 1:133

J

- Janzer, V. J. 4:529
 Johnson, G. R. 4:505
 Jones, D. L. 6:775

K

- Knebel, H. J. 2:215
 Knox, W. D. 4:541
 Krieger, M. H. 1:115

L

- Leinz, R. W. 2:259
 Leonard, R. B. 4:529
 Lindsey, D. A. 2:175
 Lipman, P. W. 1:133; 2:175
 Lucchitta, B. K. 5:651
 Lystrom, D. J. 4:541

M

- Mabey, D. R. 5:553
 Machette, M. N. 3:369
 Macke, D. L. 4:499
 Mamula, N., Jr. 2:149
 Mankinen, E. A. 3:383
 Marsh, S. P. 6:727
 Mattick, R. E. 5:625
 McDonald, M. G. 3:307
 McKeown, F. A. 1:41
 McLaughlin, R. J. 6:715
 Megard, F. 4:453
 Mehnert, H. H. 1:133; 2:175
 Meyer, W. 2:273
 Miller, C. D. 5:611
 Miller, R. L. 6:821
 Moncure, G. K. 2:203
 Morgan, B. A. 1:73

N

- Naeser, C. W. 1:133; 4:439
 Nash, W. P. 1:133
 Newell, W. L. 3:359
 Newland, W. L. 6:807
 Noble, D. C. 4:453

O

- Oliver, W. A., Jr. 6:797

P

- Page, N. J. 1:107; 4:473
 Pessagno, E. A., Jr. 6:715
 Plafker, G. 5:625
 Pluhowski, E. J. 2:263
 Poole, F. G. 2:221
 Potter, R. W., II. 2:247; 6:701
 Priego de Wit, M. 1:59

R

- Radtke, A. S. 2:241
 Ragone, S. E. 1:1
 Raines, G. L. 1:51
 Randall, A. D. 3:285
 Reynolds, R. L. 4:483; 6:707
 Rice, D. D. 3:359
 Rinella, F. A. 4:541
 Robinove, C. J. 4:511
 Rosholt, J. N. 4:489
 Rowley, P. D. 1:133; 2:175
 Rye, R. O. 2:221; 5:579

S

- Schindel, D. E. 6:789
 Shawe, D. R. 2:221

Shepard, R. G. 4:499
 Sheppard, R. A. 4:467
 Silberman, M. L.... 4:435, 439, 453; 6:727
 Simon, F. O. 4:473
 Skelton, J. 3:299
 Slack, J. F. 2:241
 Smith, G. I. 3:395
 Sohn, I. G. 5:663
 Spinello, A. G. 2:263
 Stauffer, R. E. 6:755
 Stephens, D. W. 4:547

T

Theodore, T. G. 1:59, 107
 Thompson, J. M. 6:755
 Twichell, D. C. 2:215

V

Vennum, W. R. 1:95
 Venuti, P. E. 1:107

W

Wallace, R. E. 5:637
 White, D. E. 6:765
 Witkind, I. J. 4:425
 Wobus, R. A. 1:81

Y

Yochelson, E. L. 6:789

Z

Zielinski, R. A. 4:489

ANNOUNCEMENT

**DIRECT-MAIL SALES OF
USGS OPEN-FILE REPORTS
By the
U.S. Geological Survey**

Purpose of Program

- To furnish microfiche or paper-duplicate copies of open-file reports from a single, centrally located facility.
- To provide faster order-filling service to the public for copies of open-file reports.
- To increase the availability of earth-science information to the scientific community.

Order USGS Open-File Reports From:

Open-File Services Section, Branch of Distribution, U.S. Geological Survey, Box 25425, Federal Center, Denver, CO 80225. (Telephone: 303-234-5888.)

Price information will be published in the monthly listing "New Publications of the Geological Survey."

This facility will stock open-file reports only. Please do not mix orders for open-file reports with orders for any other USGS products. Checks or money orders, in exact amount for open-file reports ordered, should be made payable to U.S. Geological Survey. Prepayment is required.

Order by series and number (such as Open-File Report 77-123) and complete title.

Inquiries concerning this new program should be sent to the address given above.

CESSATION OF PUBLICATION OF THE JOURNAL OF RESEARCH OF THE U.S. GEOLOGICAL SURVEY

We wish to announce that the "Journal of Research of the U.S. Geological Survey" will cease publication with this issue (vol. 6, no. 6). The Superintendent of Documents will refund money for any issues owed to subscribers.



RECENT PUBLICATIONS OF THE U.S. GEOLOGICAL SURVEY

The following books may be ordered from the Branch of Distribution, U.S. Geological Survey, 1200 South Eads Street, Arlington, VA 22202 (an authorized agent of the Superintendent of Documents, Government Printing Office). Prepayment is required. Remittances should be sent by check or money order payable to U.S. Geological Survey. Give series designation and number, such as Bulletin 1368-A, and the full title. Prices of Government publications are subject to change. Increases in costs make it necessary for the Superintendent of Documents to increase the selling prices of many publications offered. As it is not feasible for the Superintendent of Documents to correct the prices manually in all the previous announcements and publications stocked,

the prices charged on your order may differ from the prices printed in the announcements and publications.

In addition to the publications mentioned below, other professional papers, water-supply papers, bulletins, circulars, single copies of the periodical "Earthquake Information Bulletin," maps, and items of general interest, such as leaflets, pamphlets, and booklets, are available at the above address. All new Survey publications are listed in a free monthly catalog, "New Publications of the Geological Survey"; to subscribe, send name and address to U.S. Geological Survey, 329 National Center, Reston, VA 22092. (Some reports that are now out of print at the Superintendent of Documents can also be obtained at the Branch of Distribution address.)

Professional Papers

- P 628. The tectonics of North America—A discussion to accompany the tectonic map of North America scale 1:5 000 000, by P. B. King. 1969. 94 p. \$3. (Reprint.)
P 813-E. Summary appraisals of the nation's ground-water resources—California region, by H. E. Thomas and D. A. Phoenix. 1976. p. E1-E51; plate in pocket. \$3. (Reprint.)
P 813-F. Summary appraisals of the nation's ground-water resources—Texas-Gulf region, by E. T. Baker, Jr., and J. R. Wall. 1976. p. F1-F29; plates in pocket. \$2.45. (Reprint.)
P 813-J. Summary appraisals of the nation's ground-water resources—Great Lakes region, by W. G. Weist, Jr. 1978. p. J1-J30. \$1.50.
P 813-M. Summary appraisals of the Nation's ground-water resources—Hawaii region, by K. J. Takasaki. 1978. p. M1-M29. \$1.50. (Supersedes Open-File Report 77-825.)
P 899. The karst landforms of Puerto Rico, by W. H. Monroe. 1976. 69 p.; plate in pocket. \$3.25. (Reprint.)
P 993. Historic ground failures in northern California triggered by earthquakes, by T. L. Youd and S. N. Hoose. 1978. 177 p.; plates in pocket. \$5.25.
P 1003. Effects of urbanization on streamflow and sediment transport in the Rock Creek and Anacostia River basins, Montgomery County, Maryland, 1962-74, by T. H. Yorke and W. J. Herb. 1978. 71 p.; plates in pocket. \$2.50.
P 1045. Computer-aided estimates of concentrating-grade iron resources in the Negaunee iron-formation, Marquette district, Michigan, by W. F. Cannon, S. L. Powers, and N. A. Wright. 1978. 21 p. \$1.30.
P 1050. Geological Survey research 1977. 1977 (1978). 411 p. \$6.

Bulletins

- B 1131. Geology and mineral deposits of the Turtle Lake quadrangle, Washington, by G. E. Bechart and P. L. Weis. 1963. 73 p.; plates in pocket. \$3.50. (Reprint.)

- B 1401. Rapid analysis of silicate, carbonate, and phosphate rocks—revised edition, by Leonard Shapiro. 1975. 76 p. \$2.40. (Reprint.)
B 1438. Understanding natural systems—A perspective for land-use planning in Appalachian Kentucky, by W. L. Newell. 1978. 50 p. \$1.90.
B 1443. Feasibility and cost of using a computer to prepare landslide susceptibility maps of the San Francisco Bay region, California, by E. B. Newman, A. R. Paradis, and E. E. Brabb. 1978. 27 p.; plate in pocket. \$2.
B 1448. Geology of the Juazohn quadrangle, Liberia, by R. G. Tysdal. 1978. 39 p. \$1.60.
B 1449. Geology of the Buchanan quadrangle, Liberia, by R. G. Tysdal. 1978. 31 p. \$1.40.
B 1452. Thermodynamic properties of minerals and related substances at 298.15 K and 1 bar (10^5 pascals) pressure and at higher temperatures, by R. A. Robie, B. S. Hemingway, and J. R. Fisher. 1978. 456 p. \$4.75.

Water-Supply Papers

- W 2045. Fluvial sediment in Ohio, by P. W. Anttila and R. L. Tobin. 1978. 58 p. \$2.30. (Supersedes Open-File Report 76-575.)
W 2046. Calibration of a mathematical model of the Antelope Valley ground-water basin, California, by T. J. Durbin. 1978. 51 p.; plates in pocket. \$7.25. (Supersedes Open-File Report 76-833.)
W 2053. Evaporation and radiation measurements at Salton Sea, California, by A. M. Sturrock, Jr. 1978. 26 p. \$1.30. (Supersedes Open-File Report 77-74.)

Techniques of Water-Resources Investigations

- TWI 1-D1. Water temperature-influential factors, field measurement, and data presentation, by H. H. Stevens, Jr., J. F. Ficke, and G. F. Smoot. 65 p. \$1.60. (Reprint.)
TWI 3-C1. Fluvial sediment concepts, by H. P. Guy. 55 p. \$2.50. (Reprint.)
TWI 4-A2. Frequency curves, by H. C. Riggs. 15 p. \$1.20. (Reprint.)

**U.S. GOVERNMENT
PRINTING OFFICE
PUBLIC DOCUMENTS DEPARTMENT
WASHINGTON, D C 20402**
OFFICIAL BUSINESS
PENALTY FOR PRIVATE USE \$300

FOURTH-CLASS MAIL
POSTAGE & FEES PAID
USGS
PERMIT No. G23